INVESTIGATIONS ON THE SOFT COMPUTING TECHNIQUES IN SHUNT ACTIVE FILTERS

A THESIS

Submitted in partial fulfilment of the
requirements for the award of the degree
of
DOCTOR OF PHILOSOPHY
in
ELECTRICAL ENGINEERING

by

KISHORE KUMAR PEDAPENKI

DEPARTMENT OF ELECTRICAL ENGINEERING
INDIAN INSTITUTE OF TECHNOLOGY ROORKEE
ROORKEE – 247667 (INDIA)

JUNE 2016

INDIAN INSTITUTE OF TECHNOLOGY ROORKEE
ROORKEE

CANDIDATE'S DECLARATION

I hereby certify that the work which is being presented in this thesis entitled **INVESTIGATIONS ON THE SOFT COMPUTING TECHNIQUES IN SHUNT ACTIVE FILTERS** in partial fulfilment of the requirements for the award of the Degree of Doctor of Philosophy and submitted in the Department of Electrical Engineering of the Indian Institute of Technology Roorkee is an authentic record of my own work carried out during a period from July 2010 to May 2016 under the supervision of Prof. S.P.Gupta, Emeritus Fellow and Dr. Mukesh Kumar Pathak, Associate Professor, Department of Electrical Engineering, Indian Institute of Technology Roorkee.

The matter presented in this thesis has not been submitted by me for the award of any other degree of this or any other Institute.

(**KISHORE KUMAR PEDAPENKI**)

This is to certify that the above statement made by the candidate is correct to the best of our knowledge.

(Mukesh Kumar Pathak)
Supervisor

(S.P.Gupta)
Supervisor

Date: _____

The Ph.D. Viva-Voce Examination of **Mr. KISHORE KUMAR PEDAPENKI** Research Scholar, has been held on……..

Signature of Supervisors

Signature of External Examiner

Chairman, DRC

Head of the Department

ABSTRACT

Electric loads constitute fairly large number of power electronic converters due to ever increasing demand of controller driven electric systems. The conversion of electric power by the power electronic converters introduces harmonics. As harmonics has higher frequency (integral multiple of fundamental), they may interfere with the communication lines and introduce unwanted noise. The other effects of harmonics are additional losses and heating in motors, capacitors, and transformers. Harmonics can interference with motor controllers. Additionally, the power converters draw reactive power during controlled operation which put extra reactive power burden on the supply system.

The tuned inductor and capacitor filters connected across supply can be used to compensate for the source current harmonics. These passive filters however, suffer from the problem of fixed compensation, large size and detuning due to aging of passive elements. They also suffer from exciting unwanted resonance conditions. The power capacitors are also used for improving the power factor by meeting reactive power demand. Traditional methods of static VAR compensation, such as fixed capacitors or thyristor capacitor controlled reactors and thyristor switched capacitors have the problem that the VAR generated or absorbed is in proportion to energy storage capacity of inductor or capacitor or both. The size of these elements has to be increased considerably with the increase in VAR compensation. This twin problem of reactive power compensation and the harmonic injection has been receiving lot of attention and has led to development of different methods of adjustable and dynamic compensation, which came to be known as active power filters. The active power filter has the ability to mitigate harmonics and perform reactive power compensation for non-linear as well as dynamically changing loads. They offer high quality solution for power quality problems with much lower size of passive components and emancipation from detuning due to aging of passive elements.

In this work, the shunt active filter has been considered for mitigating the harmonics and for compensating the reactive power. A two level inverter is used for implementation of shunt active filter. The unit voltage template method is used to get the unit waveform of the source voltage by dividing each phase voltage with its maximum value so that the wave has the unit amplitude at supply frequency. The error signal between the DC capacitor voltage of the inverter and the reference voltage is processed in a voltage controller. The output signal of controller is multiplied by the unit voltage wave to get the reference current waveform for the source phase currents. The actual phase current is sensed to obtain the current error, which is processed in a current controller to generate the required signals to drive the inverter switches. The performance of shunt active power filter has been investigated with following voltage controllers, one at a time:

1. Proportional Integral Controller
2. Fuzzy Logic Controller
3. Neural Network Controller
4. Neuro Fuzzy Controller

In proportional integral (PI) controller, the proportional and integral gains have been determined corresponding to the lowest value of total harmonic distortion (THD) for a given non-linear load setting. With change in load setting, the PI controller parameters need to be tuned again to get lowest THD. It is also seen that continuing with same PI controller parameters for wide variation of non linear load gives highly suboptimal results. The option of varying PI controller parameters for each load setting is not feasible. On the other hand, the artificial intelligence (AI) controllers perform this operation automatically and give the lowest value of total harmonic distortion under any load condition.

Fuzzy logic voltage controller is implemented in present work to address this issue. It employs Mamdani method of fuzzy inference system. Here, the triangular membership function is chosen. For defuzzification, centroid method is used as it takes the centre of the gravity, the densest area of the crisp values. Rule base is formed on the basis of a number of membership functions which is taken as seven.

Neural networks are simplified models of the biological nervous system and therefore have drawn their motivation from the kind of computing performed by a human brain. Once appropriately trained, the network can be utilized for effective use in solving unknown or untrained instances of the problem. The Back-Propagation algorithm has been used for training neural network based voltage controller investigated in this work.

One of the most researched forms of hybrid systems is neuro fuzzy controller. Neural networks and fuzzy logic represent two distinct methodologies to deal with uncertainty. Neural networks can model complex non-linear relationships and are appropriately suited for classification phenomenon into predetermined classes. On the other hand, the precision of outputs is quite often limited and does not give zero error but only minimization of least squares of errors. Also, the training data has to be chosen carefully to cover the entire range over which the different variables are expected to change. Fuzzy logic systems address the imprecision of inputs and outputs directly by defining them using fuzzy sets and allow for a greater flexibility in formulating system descriptions at the appropriate level of detail. Neuro fuzzy systems which are an integration of neural networks and fuzzy logic, have demonstrated the potential to extend the capabilities of systems beyond either of these technologies when applied individually.

The simulation results for a non-linear load, represented by a three-phase fully controlled bridge rectifier feeding a series connected R-L load, are obtained for steady state and transient conditions. Performance is investigated for (a) balanced load (b) unbalanced load

and (c) step change in load. The firing angle of rectifier is varied to represent wide variation of non linear load. The simulation results are obtained in terms of waveforms of load current, compensating current, source current and source voltage under above mentioned loading conditions. These simulations are carried out using voltage controllers based on PI, fuzzy logic, neural network and neuro fuzzy logic.

For investigations with PI controller, the controller gains are determined for given source voltage and load setting. The gains so determined, are not modified when a change in load settings is considered. Three settings of load are considered corresponding to firing angle of rectifier at 0, 30° and 60°. In each case, the value of series connected R-L at output of the rectifier are so adjusted that the power drawn from the source is 1kVA. The performance of active power filter under various controllers is calculated from the THD of the compensated source current and the fundamental power factor. For PI controller, the simulation results show that the source current THD increases when the firing angle is varied from 0 to 60º.

The fuzzy logic voltage controller based shunt active power filter is designed for voltage error, change in error and the corresponding output. The simulation results again show that the source current THD increases when the firing angle is varied from 0 to 60º, but there is an improvement over PI controller case.

A two layered feed forward network is used in this work for neural network with sigmoid hidden neurons and linear output neurons with twenty hidden neurons. The simulation results show that the source current THD increases when the firing angle is varied from 0 to 60º. The results here are improved over that of the PI voltage controller case and also the fuzzy logic voltage controller case.

In neuro fuzzy voltage controller case, seven triangular membership functions are used from fuzzy side and Back-Propagation method is used from the neural network side with three epochs. The simulation results show that the source current THD increases when the firing angle is varied from 0 to 60º. These results are a further improvement over the PI voltage controller case, the fuzzy logic voltage controller case and also neural network based voltage controller case. The reactive power drawn by the load is highest at α=60°. However, in all above investigation, it is observed that the compensated source current has a fundamental power factor of almost unity.

In order to further verify the above simulation studies of voltage controllers, a laboratory prototype of shunt active power filter has been developed. The experimental results have been limited to a case of non linear rectifier load with α=0. A three phase diode bridge rectifier has been taken for the testing purpose. The switching devices used in the prototype are MOSFETs. The driving signals are processed in a MATLAB Simulink based program by the d'SPACE 1104 kit. Two types of controllers used in experimental work are PI and fuzzy logic controller. The waveforms of load current, compensating current, source current, source

voltage and DC capacitor voltage are recorded for both steady state and transient conditions. Source current THD is also obtained in each case. The harmonics generated by this rectifier are found to be mitigated by the two-level inverter based active power filter.

ACKNOWLEDGEMENTS

I take this opportunity to express my sincere gratitude towards my respected supervisors Prof. S.P. Gupta, Emeritus Professor and Dr. Mukesh Kumar Pathak, Associate Professor, Department of Electrical Engineering, Indian Institute of Technology Roorkee for their proficient and enthusiastic guidance, advice and encouragement, which were the constant source of inspiration for the completion of this research work and for critically examining the thesis write up.

Their painstaking support and exhaustive involvement in preparation of manuscript, conduction of the experimental investigations and simulation studies are gratefully acknowledged. I sincerely appreciate their pronounced individualities, humanistic and warm personal approach, which has given me strength to carry out this research work on steady and smooth course. I humbly acknowledge a lifetime's gratitude to them.

I express my deep sense of gratitude to the Head, Electrical Engineering Department, Indian Institute of Technology Roorkee, for providing the excellent laboratory and computing facilities of the department for this research work. My sincere thanks are also due to my SRC chairman Prof. Pramod Agarwal, my SRC internal expert Dr. Sumit Ghatak Choudhuri and my SRC external expert Dr. Bulusu Anand for extending moral support and technical discussions as and when required during the research work.

I acknowledge my sincere gratitude to the Ministry of Human Resources Development (MHRD), Govt. of India for providing financial support during work.

I am thankful to the technical staff of the Power Quality lab and other staff members of the workshop and stores for their timely cooperation and needful help.

I thankfully appreciate and acknowledge my indebtedness to my friends and research scholars Dr. Jayaram Nakka, Dr. Tirupathi Raju Kanumuri, Dr. D. Sreenivasarao, Dr. Durga Sukumar, Dr. Rakesh Mourya, Dr. Giribabu, Dr. Jatin Patel, Dr. Rajesh Patel, Dr. Venkata Ramana Naik, Dr. Aurobinda Panda, Dr. Suresh Dhanawath, Mr Sidharth, Mr. Y. Srinivasa Rao, Mr. Sukanta Haldar, Mr. Vadhtya Jagan, Mr. Janardhana Rao and Mr. Raveendhra for their cooperation and moral support during my stay at Roorkee.

Thanks are also due to all those who helped me directly and indirectly for the completion of the work.

My special, sincere, heartfelt gratitude and indebtedness are due to my parents, Sri. Sivunnaidu and Smt. Vijaya Lakshmi for their constant encouragement and blessings. My heartiest gratitude to my sister, Smt. Swarna Latha and my brother in law, Sri. Reddi Rama Krishna Murthy Naidu, my nephews Mr. Gowtham and Mr. Chaitanya for their endless support, encouragement and patience, which helped to concentrate on my research.

I am lucky to get the helping hands from my wife Padmini. Even though she has missed me a lot during my work, she waited patiently for the completion of the research

work. I appreciate her for the kind support extended. No words can adequately express my gratitude to her.

I am proud to humbly dedicate this research work to my parents.

May all praise be to Almighty, the most beneficent, and the most merciful!

Kishore Kumar Pedapenki

CONTENTS

LIST OF FIGURES

LIST OF TABLES

LIST OF ACRONYMS

AC	Alternating Current
ADALINE	Adaptive Linear Neuron
ANFIS	Artificial Neuro Fuzzy Inference System
APF	Active Power Filter
BP	Back-Propagation
CHB	Cascaded H Bridge
DC	Direct Current
DSP	Digital Signal Processor
FLC	Fuzzy Logic Controller
GA	Genetic Algorithm
IEEE	Institute of Electrical & Electronics Engineers
IGBT	Insulated Gate Bipolar Transistor
IRP	Instantaneous Reactive Power Theory
MLI	Multilevel Inverter
MLP	Multi Layer Perceptron
MOSFET	Metal Oxide Semiconductor Field-effect Transistor
NN	Neural Network
PF	Power Factor
PI	Proportional and Integral
PLL	Phase Locked Loop
PWM	Pulse width Modulation
RMS	Root Mean Square
SRF	Synchronous Reference Frame
THD	Total Harmonic Distortion
TS	Takagi-Sugeno Fuzzy Inference System
VSI	Voltage Source Inverter
UPQC	Unified Power Quality Conditioner

LIST OF SYMBOLS

v_s	Three-phase source voltage
I_{sa}, i_{sb} and i_{sc}	Three-phase source currents
i_{La}, i_{Lb} and i_{Lc}	Three-phase load currents
i_{ca}, i_{cb} and i_{cc}	Three-phase compensating currents
$i_{sa,ref}$, $i_{sb,ref}$ and $i_{sc,ref}$	Three-phase reference currents
V_m	Maximum source voltage
m_a	Amplitude modulation index
m_f	Frequency modulation index
L_C	Coupling inductor of inverter
V_{dc}	DC link voltage
C_{dc}	DC link capacitor
$V_{dc,ref}$	DC link reference voltage
k_p, k_i	Proportional and integral gains

1.1 Overview

Recently, there has been spurt in use of power electronic converters both in industrial as well as in domestic applications. These power electronic systems present highly non-linear characteristics. Some of the small power domestic electrical appliances like television sets and computers, multiple low-power diode rectifiers, and microwave ovens draw much distorted currents. These non-linear loads lead to generation of current/voltage harmonics and draw reactive power and are the cause for poor power quality in ac power lines. It is desirable that the converter draws sinusoidal currents from the distribution network.

The increase in non linearity causes undesirable features like low system efficiency and poor power factor. It also causes power quality disturbance to other consumers and interference in nearby communication networks. Shunt passive filters consisting of tuned LC elements and/or high-pass filters have been used to suppress the harmonics, and power capacitors have been employed to improve the Power Factor (PF) at the utility/mains. They have the limitations of fixed compensation and large size and can also excite resonance conditions. The active power filter is now seen as a viable alternative over the passive filters to compensate for harmonics and reactive power requirements of the non-linear load.

1.2 Harmonics

A harmonic [7] can be defined as a sinusoidal component of a periodic wave having a frequency that is an integral multiple of the fundamental frequency. Harmonics can be thought of, therefore, as voltages and/or currents having frequencies which are some multiple of the fundamental frequency. Typical harmonics for a 50 Hz three phase with quarter wave symmetric voltage/ current waveforms are the fifth (250 Hz), the seventh (350 Hz), and the eleventh (550 Hz). Fig. 1.1(a) depicts a 50 Hz sinusoid representative of the fundamental voltage and current waves found in power systems. The sinusoid has a peak value of 1.0 pu. Similarly, Fig. 1.1(b) shows a 250 Hz sinusoid (referred to as a fifth harmonic) with a peak value of 0.2 pu. The two sinusoids differ in frequency and magnitude. Fig. 1.1(c) illustrates the wave shape resulting from the addition of Fig. 1.1(a) and (b). The resulting wave shape is quarter wave symmetric and distorted by the presence of a harmonic. Generally an electrical system is plagued with non sinusoidal wave shapes, as in Fig. 1.1(c). According to Fourier theory, any periodic waveform deviating from a constant amplitude sinusoidal wave contains harmonics which are integral multiples of the fundamental frequency. The harmonics of a distorted periodic waveform can therefore be represented by a Fourier series.

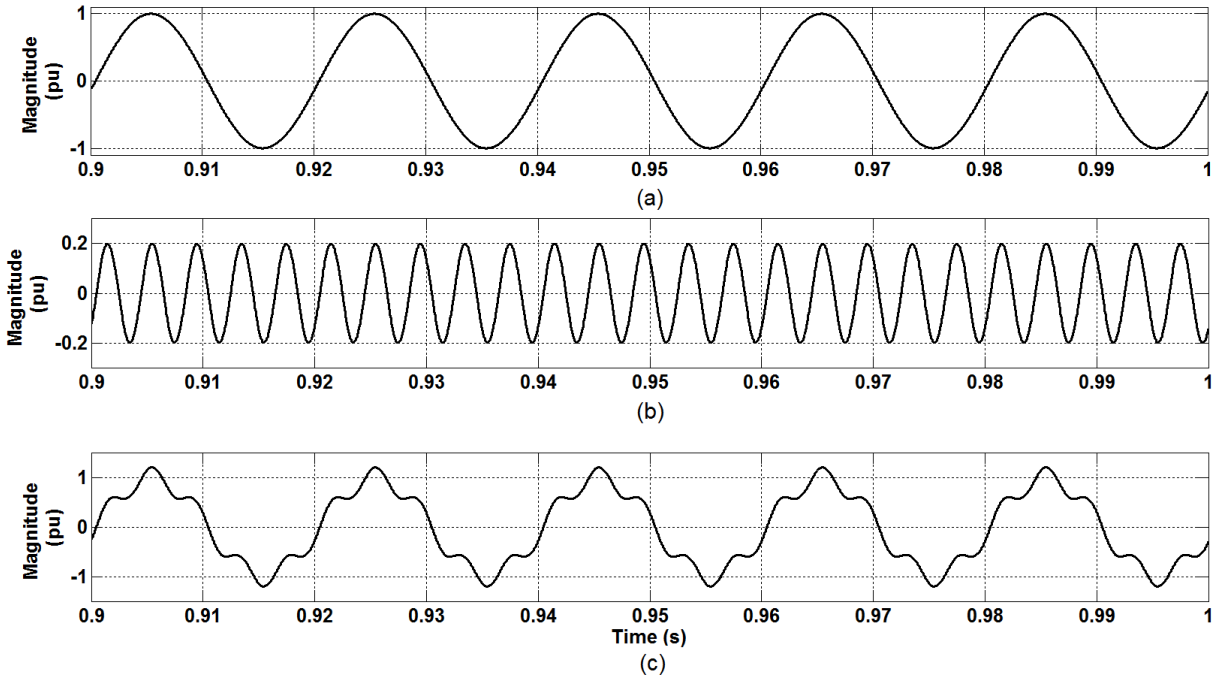

Fig. 1.1 (a) 50 Hz (fundamental) signal, (b) 250 Hz (fifth harmonic) signal, (c) Total signal of fundamental and fifth harmonic

1.2.1 Causes of Harmonics

In the past, ac motor driven dc generators, known as motor-generator sets, provided the energy to motors and loads requiring dc power [7]. The advent of low-cost solid-state electronics made modern forms of static power conversion possible against the bulky and expensive rotating machines system. Static rectifiers and drives began to replace the older methods of conversion [1]. Solid-state rectification is drawing non-sinusoidal currents and reactive power from supply mains. These system problems became especially noticeable whenever the solid-state converter unit and/or its load represented a substantial portion of the total system power requirements.

At first, the most noticeable system problem was the poor power factor associated with phase-controlled static rectification. Economics and system voltage regulation call for mandatory improvement in the power factor. This was usually accomplished with the addition of shunt power factor correction capacitors. Further, due to presence of harmonics in voltage/ current waveforms, the application of capacitor banks created other system problems. These problems involved the interaction of harmonic voltages and currents with power factor correction capacitors. In the presence of harmonics, equipment such as computers, communication systems, and controllers may respond incorrectly to normal inputs, not respond at all, or give false outputs.

1.2.2 Effects of harmonics

Power system problems such as communication interference, heating, and solid-state device malfunctions are the direct result of harmonics. These problems are categorized and listed below.

1.2.2.1 Communication Interference

Magnetic coupling between electrical power circuits and communication circuits can cause what is known as communication interference. The amount of interference will depend upon the magnitude of the induced current (or voltage), frequency**,** and the extent of the magnetic (electrostatic) coupling.

1.2.2.2 Heating

It is common to refer to heating as copper loss. By using superposition, the total losses due to fundamental and harmonic currents can be expressed as a sum of the individual harmonic losses.

$$I^2R = I_{50Hz}^2R + I_{250Hz}^2R + I_{350Hz}^2R + \cdots$$

Since most AC equipment ratings are based on 50 Hz losses, the addition of the harmonic loss components requires de-rating the equipment. It can be seen that they add to the total amount of heating.

1.2.3 Harmonic measurements and analysis

A device for user-adjustable on-line automatic data-gathering and analysis either was not yet available or existed only in semi portable and highly sophisticated form.

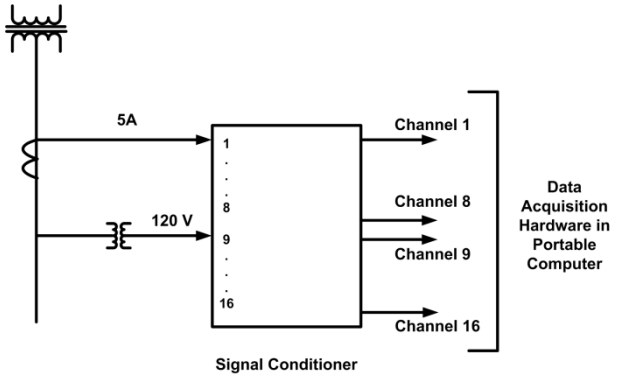

Fig. 1.2 Line diagram of data acquisition system

The first link between the system and the recorded data is the instrument transformer. It is important to use instrument transformers with a flat frequency response throughout the range of frequencies under consideration. Next is the customized signal conditioner. The purpose of this device is to take a signal from potential or current sensors and convert it to an acceptable input voltage level for the data-acquisition hardware.

1.3 Reactive Power

Power factor is defined as the ratio of real power to apparent power. This definition is often mathematically represented as kW/kVA, where the numerator is the active (real) power and the denominator is the apparent power.

1.3.1 Causes of low power factor

Most of the loads have inductive nature. So, they contribute lagging power factor. Transformers at substations have lagging power factor because they draw magnetizing current which causes total current to lag behind the voltage thereby decreasing the power factor. The Synchronous motor, rotating converter and other commutator motors can work at leading power factor thereby improving the power factor. Arc Lamps, arc furnaces with reactors and fault limiting reactors work at low lagging power factor.

1.3.2 Effects of low power factor

1.3.2.1 Effects on Alternators

Let the voltage and current ratings of an alternator be 500 V and 1000 A respectively. Then the KVA rating of the alternator is

$$\frac{V \times I}{1000} = \frac{500 \times 1000}{1000} = 500KVA$$

At Unity PF, load supplied = 500*1 = 500 KW

At 0.6 PF, load supplied = 500*0.6 = 300 KW

The full load rating of the alternator is decreased to 300 KW from 500 KW, although the voltage and current are at rated values. Similar to Alternators, at low power factor, KW capacity of the transformer, transmission lines etc. are also decreased.

1.3.2.2 Effects on Transmission Lines

In order to carry the same power from sending end to receiving end, the transmission lines has to carry more current at low power factor. To achieve this, the conductor size of the transmission line has to be increased, which increases cost of the transmission lines and the copper losses, which in turn reduces the efficiency of the power system. Similarly, cross sectional area of bus bar and contact surface of switchgears must be enlarged for the same power to be delivered at low power factor.

1.3.3 Measurement of Reactive Power

The waveforms of voltage and current of a typical network are shown in Fig. 1.3 with a phase angle Φ between them. Instantaneously, the power is the product of voltage and current.

$$Power(p) = Voltage(v) \times Current(i)$$

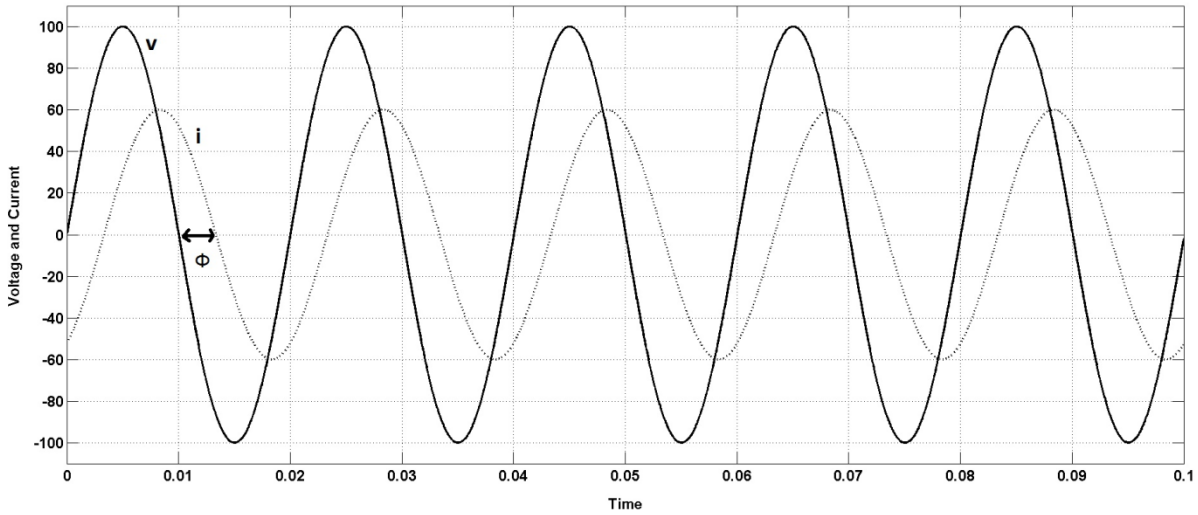

Fig. 1.3 Voltage, current and phase difference between them

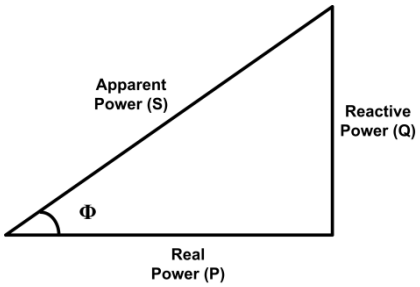

Fig. 1.4 Power triangle

According to Fig. 1.4 we can write the following equations for the real, reactive and apparent powers.

Real Power (P) = VI cosΦ

Reactive Power (Q) = VI sinΦ

where V and I are the RMS Values of voltage and current respectively.

Apparent Power (S)

$$S = \sqrt{P^2 + Q^2}$$

Therefore,

$$P = S \times \cos\Phi$$

Hence,

Power Factor,

$$\cos\Phi = \frac{P}{S}$$

Reactive Power,

$$Q = S \times \sin\Phi = P \times \tan\Phi$$

1.4 Classification of Power Filters

To mitigate the problems of harmonics and reactive power, power filters are employed in the network. The effectiveness of a filter depends on number of factors. As such, wide range of power filters has evolved over the years.

A classification of power filters [24] is presented below, followed by brief description.

According to nature of filtering

According to nature of filtering, there are two types of filters:

1) Passive Filters
2) Active Filters

According to Topology

According to topology of filters, there are four types of active filters:

1) Series active filters
2) Shunt active filters
3) Combination of active and passive filters (Hybrid Filter)
4) Combination of series and shunt active filters (Unified Power Quality Compensators - UPQC)

According to control parameter

According to controlled parameter, there are two types of filters:

1) Current controlled PWM shunt active filter
2) Voltage controlled PWM shunt active filter

According to supply configuration

According to supply, there are three types of active filters:

1) 2 wire (1-phase)
2) 3-wire (3-phase)
3) 4-wire (3-phase with neutral)

According to placement of filters

According to placement of filters, there are two types of active filters:

1) Active filters installed by individual customer in their own premises near load.
2) Active filters installed by utilities at the substations and /or the distribution feeders.

1.4.1 According to nature of filtering

In the past, the combination of tuned inductor and capacitor filters connected in parallel to the supply and/or high pass filters were used to compensate for the harmonics. These passive filters have the problem of fixed compensation and large size. They also suffer from exciting resonance conditions. The numbers of filters are as many as the number of harmonics to be eliminated. Power capacitors are utilized for improving the power factor by

supplying reactive power demand. Traditional methods of static VAR compensation based fixed capacitors or thyristor capacitor controlled reactors and thyristor switched capacitors have the problem that the VAR generated or absorbed is in proportion to energy storage capacity of inductor or capacitor or both. The size of these elements has to be increased considerably with the increment in VAR to be compensated.

The active power filters developed recently have ability to perform compensation of harmonics and meet reactive power demand of non-linear loads more effectively. It has been done by combining the advantages of regulated systems with a reduced rating of the necessary inductor and capacitor components.

1.4.2 According to Topology

According to topology of the filter, active filters are classified into three types, series active filter, shunt active filter and hybrid active filter which is the combination of both series and shunt active filters.

1.4.2.1 Series Active Filter

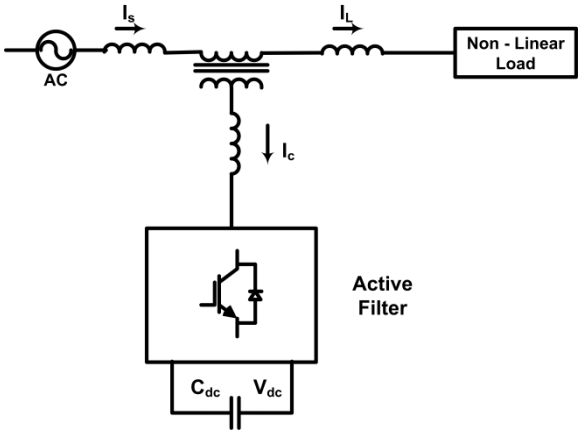

Fig. 1.5 Series active filter

Fig. 1.5 shows the basic block of a stand-alone active series filter [14]. It is connected in front of the load in series with the mains, using a matching transformer, to eliminate voltage harmonic, and to balance and regulate the terminal voltage of the load or line. It has been used to reduce negative-sequence voltage and regulate the voltage on three-phase systems. It can be installed by electric utilities to compensate voltage harmonics and to damp out harmonic propagation caused by resonance with line impedances and passive shunt compensators.

Fig. 1.6 show the principle of an active shunt filter, which is most widely used to eliminate current harmonics, reactive power compensation (also known as STATCOM), and balancing current imbalance.

1.4.2.2 Shunt Active Filter

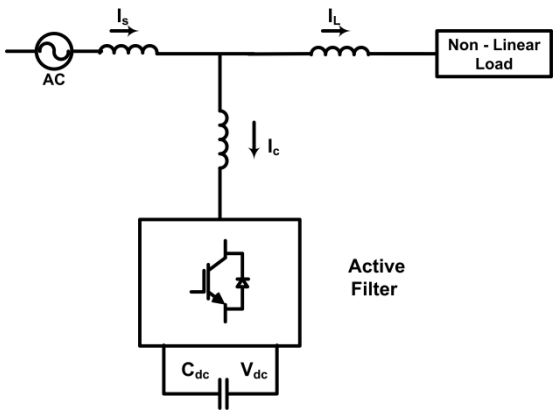

Fig. 1.6 Shunt active filter

1.4.2.3 Hybrid Filters

Fig. 1.7, Fig. 1.8, Fig. 1.9 are the three configurations of hybrid filters which are the combination of Active Series/Shunt and Passive Filters [19] .

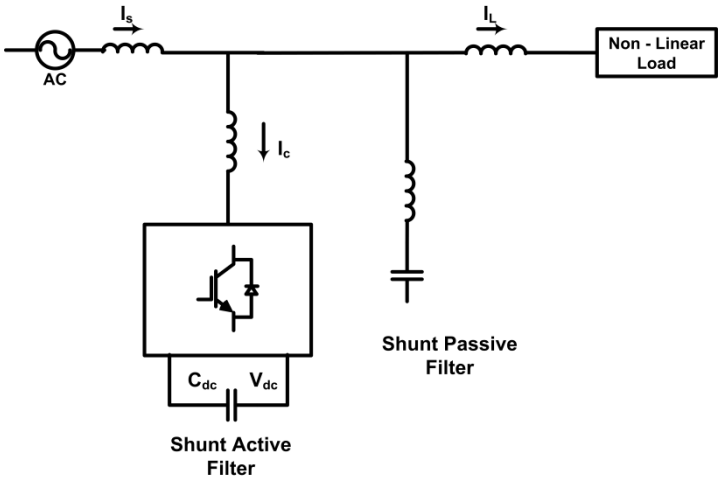

Fig. 1.7 Combination of shunt active and shunt passive filters

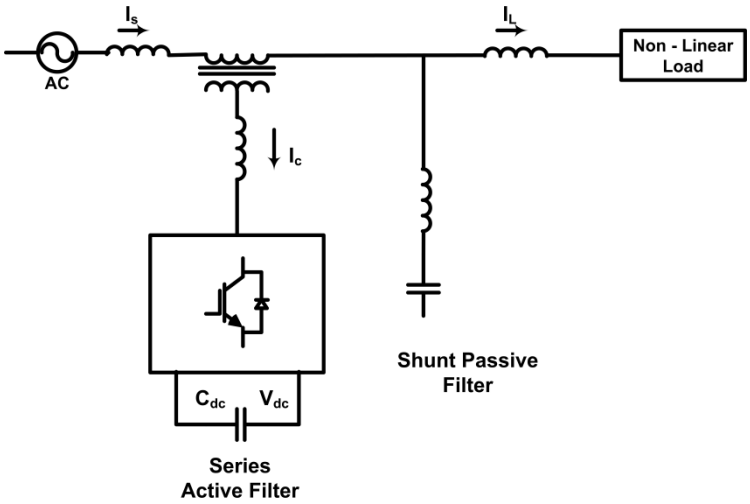

Fig. 1.8 Combination of series active and shunt passive filters

The main purpose of hybrid filters is to reduce the rating of active filter and initial cost. Fig. 1.7. is the combination of shunt active and shunt passive filters and is used for harmonic compensation or harmonic damping and for controlling reactive power.

Fig. 1.8. shows the combination of series active and shunt passive filters and is used for harmonic isolation and harmonic damping. It is quite popular as the size of active filter is reduced to 5% of load size [16]. However it is difficult to protect active filter against over currents and it does not offer reactive power control.

Fig. 1.9 shows a series active filter connected in series with shunt passive filter. It is used for harmonic damping or harmonic compensation. It is easy to protect active filter against over currents but no reactive power compensation is achieved [27].

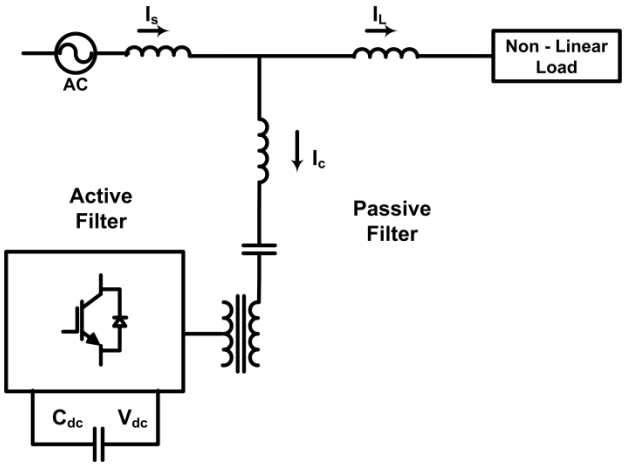

Fig. 1.9 Active filter connected in series with shunt passive filters

1.4.2.4 Unified Power Quality Conditioners (UPQC)

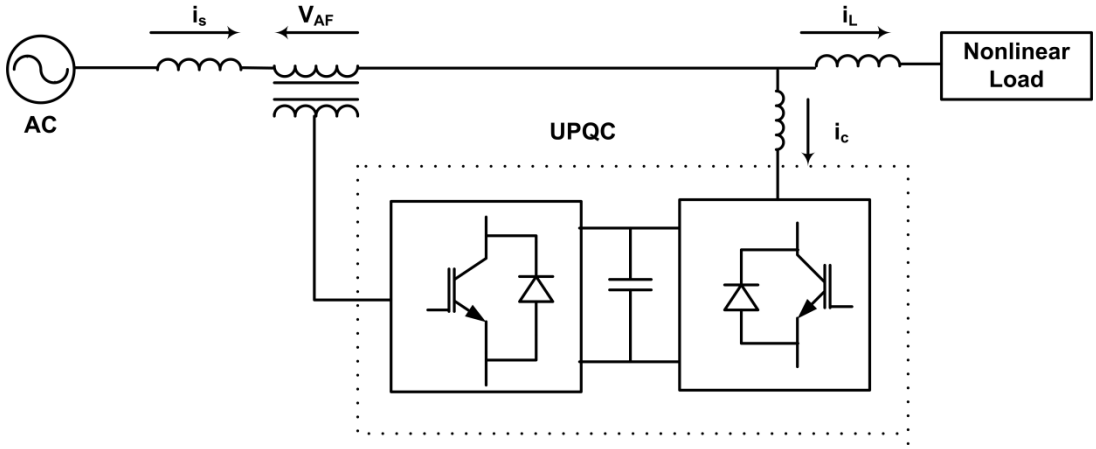

Fig. 1.10 Unified power quality conditioners

Fig. 1.10 shows a unified power quality conditioner (also known as a universal active filter), which is a combination of active shunt and active series filters [26]. The dc-link storage element (either inductor or dc-bus capacitor) is shared between two current source or voltage-source bridges operating as active series and active shunt compensators.

1.4.3 According to control parameter

According to control parameter, the filters are of two types viz. Voltage-controlled Shunt Active Power Filter (VSAPF) and Current-controlled Shunt Active Power Filter (CSAPF) as shown in Fig. 1.11 and the advantages and disadvantages of these topologies are discussed in Table 1.1.

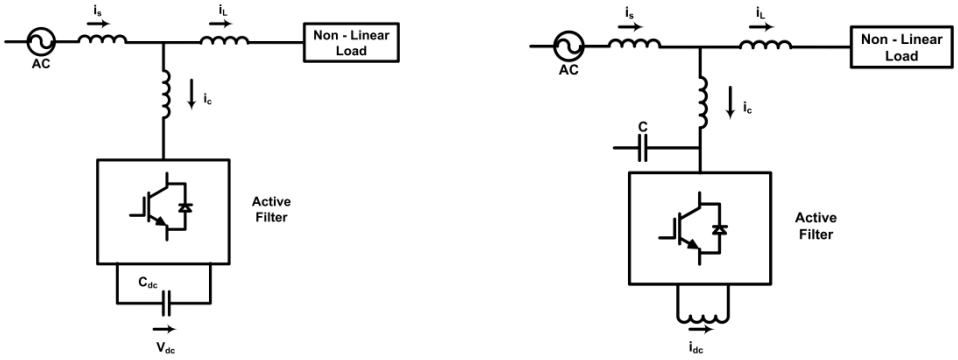

Fig. 1.11 (a) Voltage-controlled shunt active power filter (b) Current-controlled shunt active power filter

Table 1.1 Advantages and disadvantages of VSAPF and CSAPF (Fig. 1.11)

	VSAPF	**CSAPF**
Advantages	1) Effective filtering of harmonics 2) High efficiency at nominal operating point	1) Effective filtering of harmonics 2) Simple open loop current control is possible 3) High efficiency also with low power loads
Disadvantages	1) Switching ripple in the output currents 2) Power losses in ac filter 3) Low efficiency with low power loads 4) Limited lifetime of the electrolytic dc link capacitor	1) Bulky and heavy dc inductor 2) High dc link losses 3) Over voltage clamp circuit is necessary

1.4.4 According to supply configuration

1.4.4.1 Two-Wire

Two-wire (single phase) Active Filters are used for all three types i.e. series active power filter, shunt active power filter and a combination of both as unified line conditioners [3], [17]. Both converter configurations, current-source PWM bridge with inductive energy storage element and voltage-source PWM bridge with capacitive dc-bus energy storage elements, are used to form two-wire active filters circuits. Figs.1.12-1.14 shows three configurations of series active, shunt active, and a combination of both.

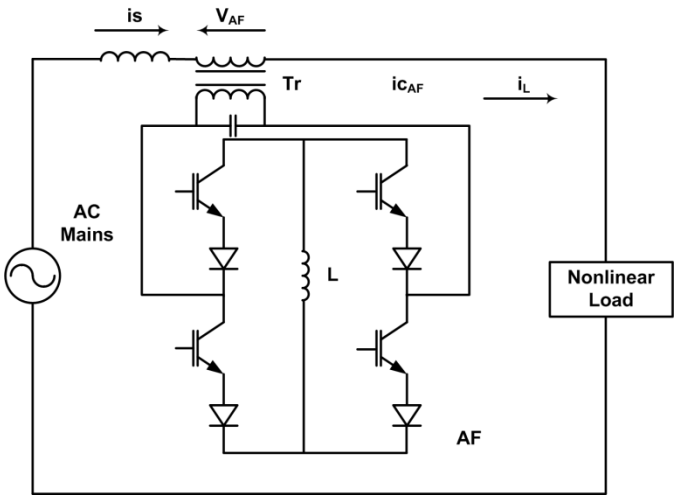

Fig. 1.12 Two wire series active filter with current source converter

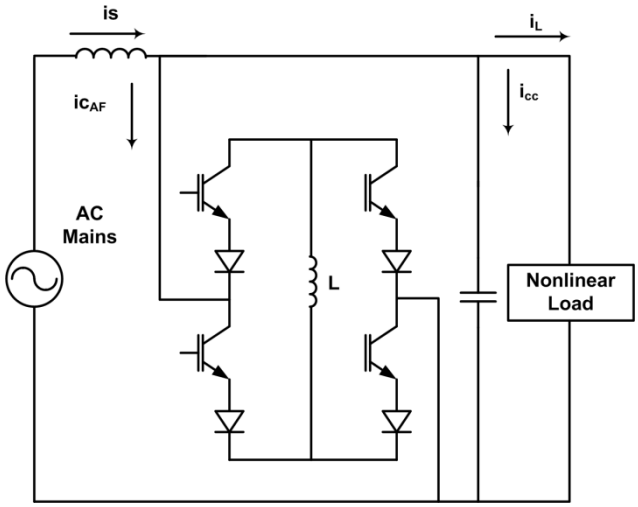

Fig. 1.13 Two wire shunt active filter with current source converter

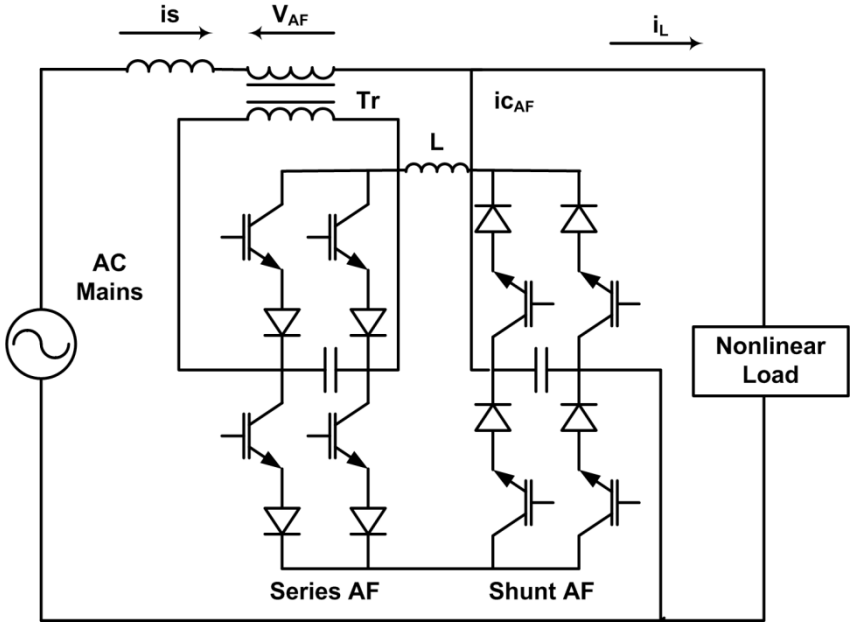

Fig. 1.14 Two wire unified power quality conditioner with current source converter

1.4.4.2 Three-Phase Three-Wire Active Filters

Three-phase three-wire non-linear loads [4], [6], such as adjustable speed drives (ASDs), are major applications of solid-state power converters and, lately, many ASDs, etc., incorporate active filters in their front-end design. All configurations, shown in Figs.1.5 -1.11, have been developed with three wires on the ac side and two wires on the dc side. Shunt active filters are developed in the current-fed type (Fig. 1.11 (a)) or voltage fed type with single-stage (Fig. 1.11 (b)) or multistep/multilevel and multi series configurations. Active series filters are developed for stand-alone mode (Fig. 1.5) or hybrid mode with passive shunt filters (Fig. 1.9). The latter (hybrid) has become quite popular as it reduces the size of power devices and cost of the overall system. A combination of active series and active shunt is used for unified power quality conditioners (Fig. 1.11) and universal filters.

1.4.4.3 Four-Wire Active Filters

A large number of single-phase loads may be supplied from three-phase mains with neutral conductor. They cause excessive neutral current, harmonic and reactive power burden, and unbalance. To reduce these problems, four-wire active filters [15], [11] have been developed as:

1) Active shunt mode with current fed and voltage fed
2) Active series mode
3) Hybrid form with active series and passive shunt mode.

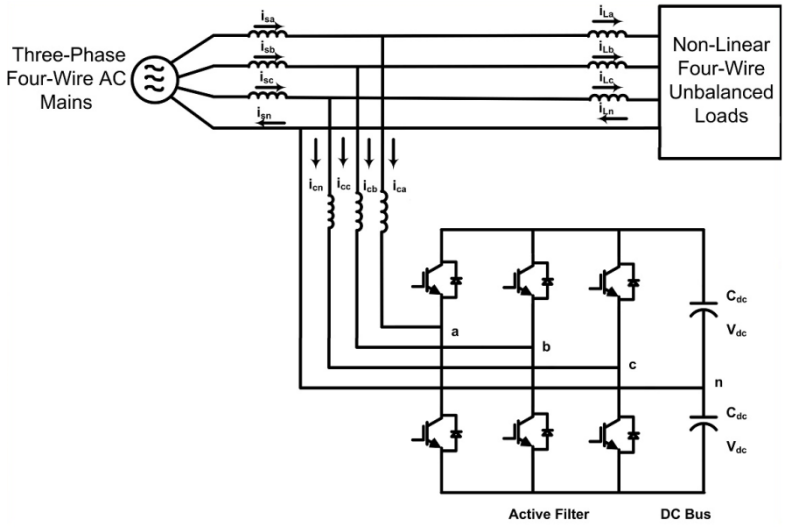

Fig. 1.15 Capacitor midpoint four-wire shunt active filter

Fig. 1.15, Fig. 1.16, Fig. 1.17 show three typical configurations of shunt active filters. The first configuration of a four-wire shunt active filters is known as the capacitor midpoint type, used in smaller ratings. Here, the entire neutral current flows through dc-bus capacitors which are of a large value. Fig. 1.16 shows another configuration known as the four-pole switch type, in which the fourth pole is used to stabilize the neutral of the active filters. The three single phase bridge configuration, shown in Fig. 1.17, is quite common and this version

allows the proper voltage matching for solid-state devices and enhances the reliability of the active filter system.

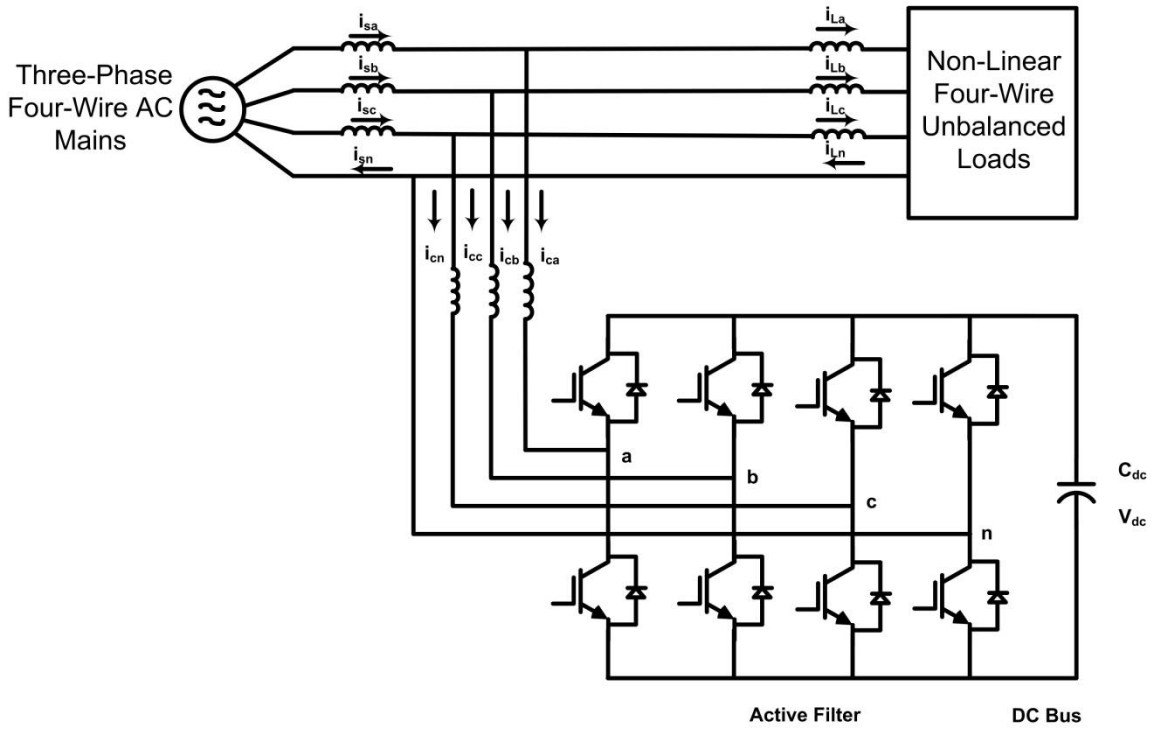

Fig. 1.16 Four-pole four-wire shunt active filter

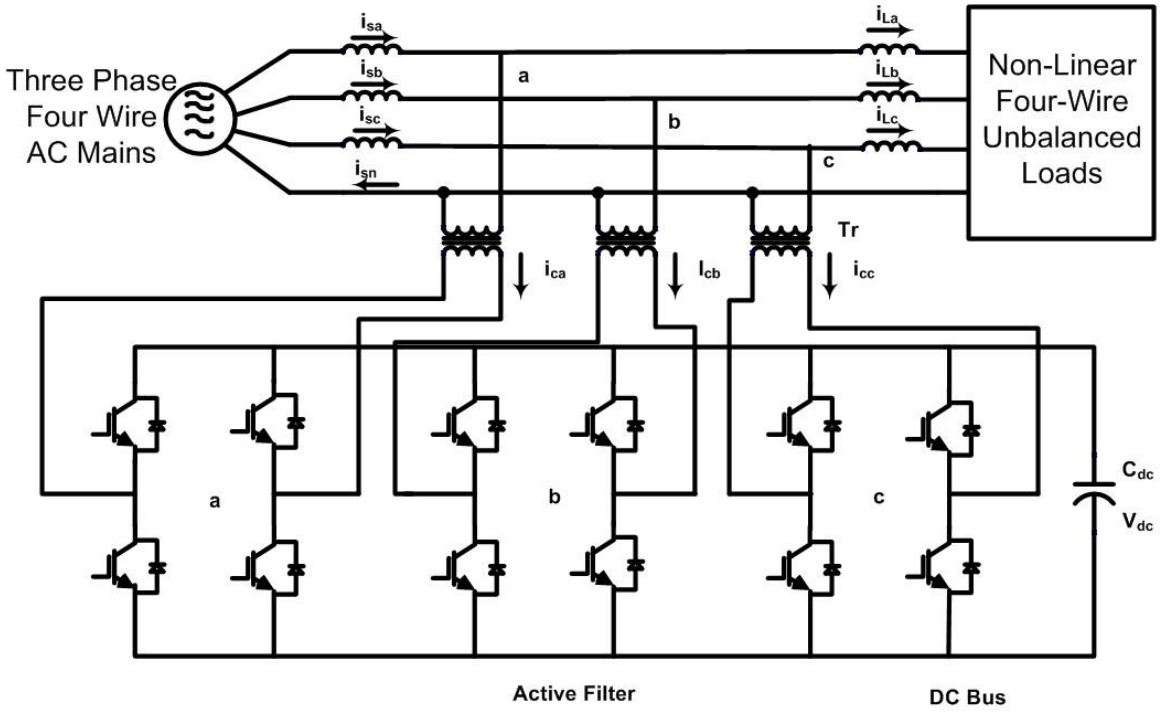

Fig. 1.17 Three bridge four wire shunt active filter

1.4.5 According to placement of filters

Both customers and utilities are responsible for installation of active power filters. Therefore, from installation point of view active power filters are classified into two groups:

1) Active filters installed by individual customer in their own premises near harmonic producing loads. The main purpose of installing active filters by individual customer is to compensate current harmonic, current imbalance and/or reactive power requirement load. Shunt active filter is normally used. Also a voltage source PWM converter based active filter is proved to be better over its counterpart current source PWM converter based active filter.

2) Active filters installed by utilities at the substations and /or the distribution feeders. The main purpose is to compensate voltage harmonics and voltage imbalance. Series active filter is normally used.

1.5 Control Strategies

There are three stages of control

1) Signal Conditioning
2) Estimation of Compensating signals
3) Generation of firing signals for switching devices of converters.

1.5.1 Signal Conditioning

In order to implement the control algorithm, online measurement of various voltage and current signals such as AC mains voltage, DC link voltage, load, source and filter currents etc. are required. These signals are also used to measure and record various parameters. Advancement and commercial availability of Hall Effect voltage and current sensors offer accurate signal conditioning. These sensors meet the requirements of high accuracy, easy installation, linearity, fast response and most important galvanic isolation. The sensed signals are sometimes filtered to remove noise due to analog and digital filters and are scaled appropriately.

1.5.2 Estimation of Compensating Signals

The estimation of the compensating signal is the most important part of the active filter control and has an impact on compensation objectives, rating of active filters and its transient and steady state performance.

Control methods of the active filters are based on instantaneous derivation of compensating commands in the form of either voltage or current signals from distorted and harmonic-polluted voltage or current signals. There are number of control methods, listed below:

- Instantaneous reactive power theory

- Synchronous d-q reference frame method
- Synchronous Detection Method
- Flux based Controller
- Notch Filter Method
- PI Controller
- Sliding Mode Controller

Out of all these methods Instantaneous active and reactive power theory is widely used. Akagi et al. [16], [4], [5] has presented the new instantaneous reactive power compensation comprising switching devices without energy storage components. It is based on three phase to two phase transformation. Instantaneous active and reactive power consumed by load is computed by transformed main voltage and distorted current signals. Harmonic active and reactive powers are extracted from instantaneous active and reactive power using low pass and high pass filters. Three phase compensating commands are obtained from the inverse transformation of harmonic active and reactive powers.

By using this method we can control the shunt, series active filters and combination of these with shunt passive filters. But this method suffers from some disadvantages. The mains voltage is assumed to be as an ideal source, which is not the case in practice. So, the performance of compensation is unsatisfactory, which is also complex in implementation and requires more hardware. Further, it is not applicable to single phase and three phase with neutral supply systems.

Watenabe et.al [10] explained physical meaning of the real and imaginary powers and physical meaning of zero sequence instantaneous power and analyzed the concepts of symmetrical and unbalanced systems but it is applicable to three phase three wire system only. Peng et al. [22] introduced instantaneous theory for three phase, four wire system with zero sequence and harmonics and also introduced generalized theory of instantaneous reactive power for three phase power system which is valid for sinusoidal or non sinusoidal, balanced or unbalanced, with or without zero sequence currents or voltages. Although these methods are widely used these have disadvantages of high cost, complex solutions and also difficult to implement for low and medium powers.

The topology is connected to the distribution system as shown in Fig. 1.18 and a current controller is implemented to force the filter currents to follow a desired reference. The current references for each of the three phases are derived by sensing the load currents and removing from their fundamental frequency components. Thus, the current references consist of the harmonic current components drawn by the load. By forcing the filter output current to follow the reference, only a fundamental frequency sinusoidal current is drawn from the source (or distribution transformer). Hence, the undesirable harmonic current components are removed from the source side of the system. In the case of the filter with the

fourth switch pole, the current reference is simply the negative sum of the three phase current references. A simple constant-hysteresis, tolerance-band controller is used in the preliminary simulations of the system and active filter, using the electromagnetic transients program**.** A constant frequency approach is preferable, both from the point of view of circuit analysis and practical implementation of the proposed system. A constant switching frequency, hysteresis-band approach**,** which maintains an essentially constant switching frequency, is being considered. To charge and maintain adequate charge on the DC-side capacitor, a PI regulator will be used to control the flow of real power from the AC-side to DC-side of the converter. Since the converter is designed only to compensate for harmonics, which do not include the fundamental, this real power transfer merely compensates for the losses in the various filter components, switches and interconnections. In a well-designed system these losses are minimal.

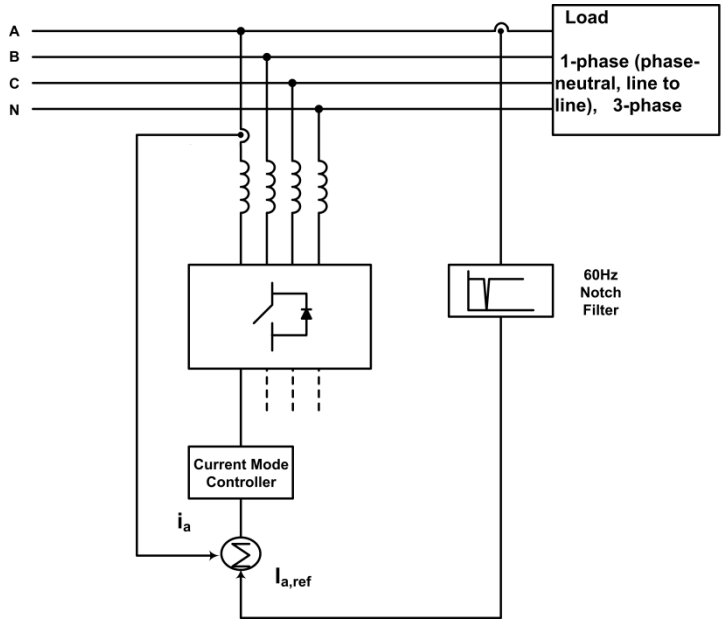

Fig. 1.18 Schematic of control strategy for three-phase, four-wire active filter

In this method the DC link voltage (VSPWM) or DC link current (CSPWM) is controlled to obtain the desired reference value and its output is equal to peak of reference current. Reference compensating currents are obtaining by multiplying the peak value by unit sinusoidal wave which is in phase with source voltage [21].

Compensating current = Reference current- Load current

It is a simple method, easy to implement for low and medium power applications and there is no need to sense the harmonic or VAR.

Bhim Singh et al. [24] introduced three phase active power filtering of harmonic current using PI controller. It has a simple control algorithm of shunt active filter for AC voltage regulator at point of common coupling, harmonic elimination, power factor improvement, load

balancing of non-linear loads using indirect current control test. In this two PI controllers used for

- Amplitude of in phase of reference supply current.
- Amplitude of quadrature component of reference supply current.

The algorithm has self supporting DC bus and reduced number of current sensors. It is observed that the voltage regulation and power factor correction to unity are two different issues and can't be achieved simultaneously. A proper combination of in phase and quadrature component gives reasonable level of performance and voltage at PCC is regulated by leading power factor.

Chatterjee et al. [26] proposed instantaneous reactive power volt ampere compensation and harmonic suppressor system without sensing reactive volt ampere demand. It does not involve any complicated control logic. It is the cycle-by-cycle reference current control mode by regulating DC link voltage. In hardware, PI and PLL (Phase Locked Loop) based sine wave generator was used to implement control algorithm.

Huang et al. [27] presented a control algorithm for three phase, three wired active filter under non ideal mains. Mains current can be effectively controlled by a simple controller. By this algorithm, the mains current become balanced and undistorted in spite of disturbances in mains and load. A sine wave generator and 120º phase shifter are used for achieving this.

All these methods are mostly for three-phase three-wire systems. But normally residential, commercial and industrial power is distributed through three phase, four wire system. In practice three-phase to neutral loads are not completely balanced. There may be an excess neutral current due to load unbalance and single phase non-linear loads [33], [8].

If loads are not balanced, there may be a significant neutral current. Three single phases connected between line and neutral are used to provide filtering which will give independent compensation in each phase but they are cumbersome and expensive.

There are number of schemes to provide filtering in three phase four wire system. Bon-Rabee [13] used a time sharing method to eliminate predetermined number of harmonic compensations. Number of controlled switches and energy storage elements are reduced but control scheme is compensation intensive and series diodes are required to direct current flow.

The schemes shown in Fig. 1.15 and Fig. 1.16 neutralize harmonic associated with loads on three phase four wire system and prevent the flow of harmonic currents in utilities neutral wire and requires no series diodes. Out of these two methods, four-switching leg topology is preferred to capacitor midpoint topology because only one dc bus is regulated unlike the midpoint capacitor method where two dc bus voltages are regulated, and the voltage/ current rating of DC side capacitor is reduced.

Thomas et al. [11] introduced three phase four wire, three leg inverter with split capacitor for harmonic compensation. Neutral current is reduced without need of additional leg. Harmonic Compensation of load is achieved by a Band Pass Filter. Chen et al. [29] proposed a new algorithm for shunt active filter for three phase, four-wire system with unbalanced, distorted source voltage and unbalanced load. In this method symmetrical component transformation is not needed. But active filter has three single phase voltage type forced commutated inverters, three single phase transformers and DC link capacitor. Direct current control is used which requires more number of current sensors. Shunt active filter based on current controlled PWM converter has been effectively used for highly non-linear loads but requires high power converter with fast switching.

Multi level inverters have the ability to improve harmonic spectrum and attain high voltage with limited maximum device rating. But, it requires complex control scheme and has poor performance/cost ratio due to large number of switches, diodes and capacitors. The voltage unbalance between different levels increases active component count in diode clamp model and increases passive element count in flying capacitor model.

Shailendra Kumar Jain [31] proposed a new control algorithm for a shunt active power filter to compensate harmonics and reactive power required by non-linear loads. If the utility voltage is distorted, active power filter (APF) allows similar level of distortion in the compensated source current. Therefore, the resultant source currents have the same waveform as that of the supply voltage. Due to similar shape of the source voltage and currents, reactive power is compensated completely. The scheme provides an additional feature of compensation of either only harmonics, or both harmonics and reactive power simultaneously, based on the capacity of the APF.

1.5.3 Generation of control signals

The third stage of control of the active filters is to generate gating signals for the solid-state devices of the active filter based on the derived compensating commands, in terms of voltages or currents. A variety of approaches, such as hysteresis-based current control, PWM current or voltage control, deadbeat control, sliding mode of current control, fuzzy-based current control, etc., are available which can be implemented either through hardware or software (in DSP-based designs) to obtain the control signals.

A hysteresis current controller derives the switching signals from the comparison of the current error with a fixed hysteresis band. Although simple and extremely robust, it usually results in variable switching frequency. This results in additional stress on the switching devices. Many improvements to original control structure have been suggested to achieve fixed modulation frequency by a variable width of the hysteresis band.

Routimo et al. [34] presented the comparison of voltage source inverter and current source inverter used as APF. The current source inverter is found better in only low load

power when compared to the voltage source inverter. The application of multiple APFs in the navy electric ships to get high power capacity and high reliability is demonstrated. It proposes the novel paralleling technique and compared with other techniques applied till date. Rajesh Gupta et al. [36] proposed the control of three-level shunt APF using frequency selective proportional plus multiple resonant controllers. Abdelaziz Zouidi et al. [37] described the voltage source inverter based three-phase shunt APF in terms of topology, modelling and control strategies. M.K. Mishra et al. [39] presented the design and dynamics of voltage source inverter. The active filter was studied under unbalanced and non linear loads supported by PSCAD simulations. Johann F. Petit et al. [40] modified the Fryze's algorithm based on classical power theories for obtaining an optimal estimation in the current reference when the utility voltage is distorted. Lucian Asiminoaei et al. [41] proposed control and parallel operation of two APFs. One active filter was used in feed forward topology to get good dynamic response and other was in feedback topology to get good steady state response.

Maria Isabel Montero et al. [42] compared all available control strategies. Bhim Singh et al. [47] proposed a T connected three level inverter based APF. The T connected transformer mitigates neutral current and the three level inverter mitigates harmonic current. Abdelmadjid Chaoui et al. [48] dealt with the design, simulation and experimentation of shunt APF. This paper also discussed the impact of parameters on signals quality. Udom Khruathep et al. [49] proposed the control algorithm based on sensing of the source voltage and source current. It was found that reactive power could be compensated and harmonic current could be reduced, compared to the results of an APF with the load current detection. Peng Xiao [51] proposed, a novel topology where two active filter inverters are connected with tapped reactors to share the compensation currents. The proposed active filter topology can also produce seven voltage levels, which significantly reduces the switching current ripple and the size of passive components.

Oleg Vodyakho et al. [52] demonstrated three-level inverter based shunt APF using LCL ripple filter. Tuhin S. Basu et al. [57] dealt with a unique combination of two inverters which may work as an APF or a STATCOM. Two inverters are switched at different frequencies. The low frequency inverter takes care of the reactive power demand of the system and makes the source current in phase with the voltage, while, the high frequency inverter mostly compensates for the harmonics. S.B. Karanki et al. [62] proposed a topology that enables DSTATCOM to have a reduced DC link voltage without any compromise on the performance. This proposed topology uses a series capacitor along with the interfacing inductor. M. F. Shousha et al. [63] proposed a time domain harmonic detection technique which is an improved a-b-c reference frame formula based upon the p-q theory with a positive sequence detector to solve the problem of bad performance of shunt APFs (SAPF)

under non-ideal mains. This method was compared with existing control methods. Yi Tang et al. [64] proposed an LCL filter based SAPF for three phase three-wire power system, together with its generalized design and control procedure. Being of higher order, the proposed SAPF provides better filtering without using large passive components.

Quoc-Nam Trinh et al. [65] presented a control scheme without a harmonic detector. The absence of the harmonic detector not only simplified the control scheme but also significantly improved the accuracy of the APF, since the control performance was no longer affected by the performance of the harmonic tracking process. Mostafa S. Hamad et al. [69] introduced an open-loop control strategy for the SAPF, which was capable of mitigating specific and predetermined harmonics and consequently achieved low total harmonic distortion. The delays were minimized or eliminated when extracting the reference current and controlling the filter current. Le Ge et al. [70] introduced two techniques for joint active disturbance rejection control (ADRC) to get good dynamic response and repetitive control (RC) to get good static response. Parag Kanjiya et al. [71] presented an optimal algorithm to control a three-phase four-wire shunt APF under non ideal supply conditions. The optimization problem aimed at maximizing the power factor subject to current harmonic constraints, had been formulated and solved mathematically using the Lagrangian formulation.

1.6 Literature Review on application of Artificial Intelligent techniques

A literature review on artificial intelligence based controllers such as fuzzy logic [73]-[152], neural network [153]-[202] and neuro fuzzy controllers [203]-[218] is presented in this section.

Juan Dixon et al. [73] demonstrated a new technology based on fuzzy logic of sensing the source currents and the dc link voltage to get the signals to drive the APF. The technique was demonstrated through simulation and hardware results. V.S.C.Ravi Raj et al. [74] presented comparison of fuzzy logic controller (FLC), PI controller and sliding mode controller and concluded that FLC performs satisfactorily in regulating the output during external disturbances. Juan W Dixon et al. [75] presented the fuzzy and PI simulation and experimental results and concluded that the fuzzy logic controller is better out of two. In this paper, the rectifier load is used as the non linear load. Reactive power and unbalanced loads can also be compensated by this method and there is no need to measure and/or calculate the harmonics and reactive power. A. Dell. Aquila et al. [76] introduced fuzzy control to achieve a very high reduction of the line current harmonic distortion.

S. K. Jain et al. [77] reported the experimental validation of the wide range of simulation study under steady state and transient states. In this paper, sensing of source currents and source voltages is employed. The comparison of controllers based on PI and FLC are reported. A. Dell' Aquilla et al. [78] aimed to minimize the APFs cost by means of a

new current reference. It was done on the single phase system with current control method. A. Dell' Aquila et al. [79] worked on single-phase systems using a microcontroller for control. The controllers used were hysteresis control and two predictive controllers. It was based on half bridge topology of APF. The experimental results were compared with simulation results. B. Mazari et al. [80] presented the fuzzy logic based controller at dc voltage error to get the reference currents and at the current error to get the signals. At the processing of current error constant fuzzy hysteresis band is used. M. Farrokhi et al. [81] introduced a new fuzzy logic based scheme for indirect current control of the shunt APF for non-linear loads current harmonics and reactive power compensation. This approach did not require to complicated signal processing for non-linear load current harmonics extraction and used in direct current control method.

B. Suresh Kumar et al. [82] worked on the three-phase four-wire systems. The paper demonstrated application of fast Fourier transform for balanced and unbalanced and variable load conditions. It helped in harmonic minimization, reactive power compensation and power factor improvement, Hocine Benalla et al. [83] used the notch filter method, consisting solely of two serial band-pass filters, for reference currents calculation, and the application of fuzzy logic for better active filter current control accuracy. This approach improved THD to 0.99% in 80 ms with fuzzy correctors compared to 1.14% in 80 ms with classical correctors. C. N. Bhende et al. [84] introduced Takagi–Sugeno (TS)type fuzzy logic controller. The advantage of the Takagi-Sugeno type fuzzy logic controller to the previously used Mamdani type fuzzy logic controller is that the latter has the limitation of large number of fuzzy sets compared to former. So the optimization of large number of coefficients increases the complexity of the controller. On the other hand, Takagi-Sugeno fuzzy controllers are quite general in that they use arbitrary input fuzzy sets, any type of fuzzy logic, and the general defuzzifier.

Brahim Berbaoui et al. [85] presented Ant colony algorithm to optimize FLC parameter. Ant colony optimization realized the optimal adjustment of the membership functions and normalization gains. The improved dynamic behaviour and performance control of ant colony algorithm was reported by the simulation results. These results are superior to traditional fuzzy controller. G.K. Singh et al. [86] proposed a simple control scheme which can compensate the line currents with unbalanced loads also. Tested over a wide range of load, the proposed method had given satisfactory results in harmonic compensation and reactive power components from utility currents. C. Benachaiba et al. [87] introduced a fuzzy regulator to improve the DC capacitor voltage response. Here, three control techniques are used. The first one is based on the PQ theory. In the second, the average power is calculated and divided equally between the three phases. The third method consists of calculating the instantaneous and average powers of the load.

C.Sharmeela et al. [88] described the design of inverter, active filter and the control strategy. The paper explained the advantages of fuzzy logic, with simulation results. Othmane Abdelkhalek et al. [89] proposed a method based on FLC with variable coefficient with the aim of shortening the rise time of the regulated condenser voltage. M.C. Ben Habib et al. [90] presented an advanced control theory based on a self tuning filter. It was applied to a three phase balanced and unbalanced power network with sinusoidal or non sinusoidal voltages and satisfactory results were obtained. This method takes into account voltage perturbation of harmonics and unbalance introduced in the power supply network. It guaranties a stable and sinusoidal load current. An Luo et al. [91] used an injection circuit on hybrid active filter. It had the ability to reduce harmonics and to improve power factor. The capacity of the APF is very low. The main advantages are to decrease the tracking error and to increase the dynamic response and robustness.

S. Saad et al. [92] introduced the multilevel APF. The advantages of multilevel APF is to improve the supply current waveform. It can also be used in high power with reduced maximum device rating. The fuzzy logic control algorithm is proposed for both current controller and the voltage controller. Ahmed A. Helal et al. [93] introduced compensation of harmonic current in three phase four wire system for both balanced and unbalanced cases. The paper used fast Fourier transform blocks to get the filtering. Soumia Kerrouche et al. [94] presented a detailed narration on fuzzy logic and the application to APF with the simulation results under steady state and step change of the load. T Narasa Reddy et al. [95] introduced a fuzzy logic controller to single phase APF which does not require accurate mathematical model, can work with imprecise inputs, can handle non-linearity and is more robust than conventional non-linear controllers. M.B.B. Sharifian et al. [96] reported the advantages of dynamic band hysteresis controller. It has the simplest technique for high speed compensation systems. It has fast current control response and inherent limiting of the peak current. The basic disadvantage of fixed band is that it results in variable switching frequency causing high switching losses. This problem can be overcome by the fuzzy hysteresis band by changing the hysteresis band to get the fixed switching frequency.

G. Jayakrishna et al. [97] used hysteresis current controlled PWM method. Synchronous d-q frame of reference is used to get the reference current signals. THDs for currents and voltage were compared with and without APF. Karuppanan P et al. [98] presented a novel PLL circuit in conjunction with Proportional Integral (PI), Proportional Integral Derivative (PID) and Fuzzy Logic controller (FLC) based shunt Active Power Line Conditioners for the current harmonics and reactive power compensation due to the non-linear/unbalanced loads. Karuppanan P et al. [99] designed the APF with hysteresis band current control and fuzzy logic based voltage controller for steady state and transient operations. A comparison of the simulation results was presented for PI and fuzzy

controllers. E. Latha Mercy et al. [100] designed APF with p-q theory with fuzzy logic controller as the voltage controller. The simulation results were reported before and after compensation.

D. A. Gadanayak et al. [101] used a Takagi-Sugeno type fuzzy logic controller to generate reference currents and novel fuzzy hysteresis band current controller to limit the maximum switching frequency. G. M. Sarhan et al. [102], introduced type 2 fuzzy logic controller. The synchronous reference frame with PI, type 1 and type 2 fuzzy logic controllers were presented for comparison. Nie-Tan control strategy was adopted instead of commonly used strategies. P Rathika et al. [103] used two fuzzy logic controllers. First one with fuzzy adaptive hysteresis band technology to get the switching signals and the second one with fuzzy logic based voltage controller to get the reference currents. Nadhir Mesbahi et al. [104] introduced the fuzzy logic controller for the three level APFs. The carrier based PWM strategy was used to derive the signals for IGBTs. Instantaneous reactive power theory was used to get the reference currents. Mikkili Suresh et al. [105] used p-q theory and id-iq theory to get the reference currents with the help of fuzzy logic controller. This can work for balanced, unbalanced and non-sinusoidal conditions. Karuppanan P et al. [106], extracted the desired reference current(s) using FLC with Phase Locked Loop algorithm. The VSI gate switching signals are derived from adaptive-hysteresis current controller. The adaptive-hysteresis controller changes the bandwidth based on instantaneous compensation current variation.

B. Suresh Kumar et al. [107] demonstrated PI, Fuzzy Logic controlled shunt APF for three-phase four-wire systems with balanced, unbalanced and variable loads. Karuppanan Pitchai Vijaya et al. [108], proposed adaptive fuzzy hysteresis current controller (HCC) which calculates the hysteresis bandwidth effectively using fuzzy logic. The bandwidth can be adjusted based on compensation current variation, which is used to optimize the required switching frequency and improves active filter substantially. Hamza Bentria et al. [109] investigated two types of control algorithms for shunt active filter. These two types of control are the notch filter and the synchronous reference algorithms to generate the references current of the compensator. Suresh Mikkili et al. [110] presented shunt APF using the p-q theory with balanced, unbalanced and non sinusoidal conditions. Simulation results established superiority of the dynamic behaviour of fuzzy logic controller over PI controller. Chennai Salim et al. [111] adopted the synchronous reference frame (SRF) detection method and the synchronous current reference (SCR) detection method to determine the compensation currents. To improve the performance of the conventional control scheme based on hysteresis controller and take advantages of intelligent techniques, fuzzy and ANN current controllers were proposed in this paper. K. Sebasthi Rani et al. [112] reported the comparison and analysis of PI and FLC results. It can also work for varying and uncertain

supply conditions. It can offer a much better dynamic response. Rathika Ponpandi et al. [113] introduced the fuzzy logic for three phase four wire four leg APF. Modified p-q theory was adopted for calculating the compensating currents. Fuzzy adaptive hysteresis band technique was applied to derive the switching signals. Karuppanan P et al. [114] used a novel adaptive hysteresis controller to get the signals for VSI. The comparison and superiority of the adaptive hysteresis controller to fixed hysteresis controller is reported.

Li Bin et al. [115] presented the controller which detects the main current and DC side capacitor voltage. Calculation method of the switch duty cycle is deducted on the basis of a mathematical model. This controller has fewer measurement, higher robustness and simpler calculation as compared to traditional controllers. Simulations verified that the APF with proposed controller can compensate the harmonics effectively. H. Kouara et al. [116] presented the comparison of the proposed fuzzy logic controller against the conventional proportional integral one through simulation results and a clear advantage of the fuzzy logic control was reported. Moreover, for identification of reference currents, multi-variable filter having the advantage of extracting harmonic voltages directly from the αβ axis. Mikkili, Suresh et al. [117] presented comparison of p-q and id-iq methods to extract reference currents and evaluation of their performance under various source conditions with PI and fuzzy logic controllers in MATLAB using Real Time Digital Simulator Hardware.

Kouara, H. et al. [118] reported a new method for identifying reference currents. It is based on p-q theory using two improvements: multi-variable filter having the advantage of extracting harmonic voltages directly from the axis and the second improvement consists of use of fuzzy logic controller to extract current harmonics components. A comparison between classical method and the new approach had been illustrated in order to find the best way to reduce network harmonic currents. Aml. F. Abdel Gawad et al. [119] presented improvement in the three phase shunt APF performance by using the fuzzy logic controller for the DC voltage regulation and by evaluation of the hysteresis band based on genetic algorithm (GA). GA and FLC are compared with the conventional methods to verify their effectiveness on the SAPF performance. B. Soujanya Yadav et al. [120], introduced fuzzy based cascaded multi-level voltage source inverter. The inverter switching signals are generated based on the triangular sampling.

Lamchich et al. [121] introduced a very simple control method to perform the identification of disturbing currents. It is formed by a DC voltage regulator and a balance between the average power of load and the active power supplied by the grid. The output current of the voltage source inverter (VSI) must track the reference current. This is done by a neural controller based on a PI-Fuzzy adaptive system as reference corrector. Panda et al. [122] presented the performance of the control strategies in terms of harmonic mitigation and DC link voltage regulation. The proposed shunt APF with different fuzzy membership

functions (Trapezoidal, Triangular and Gaussian) is able to eliminate the uncertainty in the system and achieve outstanding compensation abilities. Karuppanan,P. et al. [123] acknowledged certain errors in their earlier published paper titled ‘‘PI and fuzzy logic controllers for shunt APF—A report”. The ambiguity in bandwidth calculation of adaptive hysteresis controller and control aspects of dc-link voltage issues were addressed. The shunt APF system was investigated through extensive simulation results. Sentilnathan N et al. [124] presented a new method for harmonic and reactive power compensation with a fuzzy logic controller and a new control algorithm for APF to eliminate harmonics and compensate the reactive power of three phase diode bridge rectifier with RL load. The fuzzy logic controller was used to predict the reference current values and the firing pulses were generated using hysteresis current controller.

Benaissa, Amar et al. [125] presented a study divided in two parts. The first one dealt with the harmonic isolator which generates the harmonic reference currents. The second part focused on the generation of the switching pattern of the inverter by using a fuzzy logic controller applied and extended to a five level shunt APF. Ram Kumar PV et al. [126] incorporated the comparison of PI and fuzzy for dynamic load conditions and settling time.

Gore, Anil M. et al. [128] investigated the performance of proportional-integral (PI) and fuzzy controllers for shunt APF. Instantaneous reactive power theory (IRP) and synchronous reference frame theory (SRF) are used to generate reference current signals of filter. DC capacitor voltage is maintained constant using PI, Mamdani fuzzy and Takagi-Sugeno (TS) fuzzy controllers. Performance is analyzed using simulation of SAPF with IRP and SRF reference current generation methods with PI and fuzzy controllers. Fuzzy controller has better results compared to PI controller. TS fuzzy controller requires less number of fuzzy sets, rules and computational time compared to Mamdani fuzzy controller. Dhanavath Suresh et al. [129] introduced hybrid APF for three phase four wire system. A coupling capacitor is added to reduce the DC link voltage requirement. This method is used to reduce rating of the compensator. Sakshi Bangia et al. [130] proposed a shunt hybrid active filter by active filter connected in parallel and shunt connected three phase single tuned LC filter for 5th harmonic frequency with rectifier load. The active filtering system is based on SRF. The proposed fuzzy logic based control strategy improves active filter operation and reduces the selected harmonic contents.

Usman, Hamisu et al. [132] presented the modelling and simulation of single-phase shunt APF controlled with fuzzy logic controller to mitigate the harmonics. The proposed scheme uses MATLAB fuzzy tool box environment. Simulation results obtained by the proposed control algorithm found to satisfy within the recommended IEEE 519-1992 harmonic standard limit. Fei, Juntao et al. [133] reported an adaptive control technology and PI-fuzzy compound control technology to control an APF. AC side current compensation and

DC capacitor voltage tracking control strategy are discussed and analyzed. Model reference adaptive controller for the AC side current compensation is derived and established based on Lyapunov stability theory; proportional and integral (PI) fuzzy compound controller is designed for the DC side capacitor voltage control. The adaptive current controller based on PI-fuzzy compound system is compared with the conventional PI controller for APF.

Salim, Chennai et al. [134] presented a control strategy based on the synchronous reference frame detection method that gives a good performance particularly if the source voltage is unbalanced or distorted. The new control scheme proposed in this work is based on fuzzy technique and it is designed to improve APF compensation capability by adjusting the current error based on fuzzy rule. To improve the output of three-level voltage inverter and avoid an unbalanced AC voltage waveform a neutral-point potential voltage compensator is used with a proportional integral controller to maintain dc voltage constant.

Benazir Hajira A et al. [135] presented the synchronous reference frame theory (d-q Theory) used for extracting compensated reference current for FLC. Beny, P. G et al. [136] proposed power quality improvement using shunt active filter with modified Mamdani rule based fuzzy logic controller. The fuzzy logic controller converts the real value in to fuzzy number. Parimala V et al. [137] presented the improvement of power quality in three phase four wire system with balanced and unbalanced source condition. The PI controller is used to regulate the DC link voltage. The synchronous reference frame method is used for extracting reference current. The PWM controller is used to generate gate pulses and applied to three phase VSI based shunt APF with split capacitor topology.

Aziz Boukadoum et al. [138], presented modelling and simulation of a shunt APF based on fuzzy logic controller. The Instantaneous Reactive Power Algorithm is used for extracting compensated reference harmonic current. A fuzzy logic controlled shunt APF using hysteresis band current is applied to regulate the DC capacitor voltage.x. Karvekar, Sushil [140] presented the control of Goertzel Algorithm based shunt APF with sliding mode controller. The sliding mode controller is used to regulate voltage of the capacitor used in inverter. It improves the dynamic response of the system and provides faster convergence.

P. Parthasaradhy et al. [141] presented two types of control algorithms to regulate the DC bus voltage of a high three phase shunt APF - proportional integral (PI) and fuzzy logic controllers. The synchronous reference frame phase locked loop algorithm is used to extract the harmonic reference currents. The hysteresis band method is employed to derive the switching signals of the high shunt APF. Aziz Boukadoum et al. [142] presented a novel compensation method based on fuzzy logic controller for SAPF. The principle of the Instantaneous reactive power algorithm is applied for extracting the reference compensating currents of the shunt power converter. The FLC is applied to regulate the DC capacitor voltage. The simulation results are presented and interpreted. Fahmy, A. M. et al. [143]

presented four-leg SAPF featuring reactive power compensation, line current harmonics mitigation, neutral-current reduction and system load-currents balancing. The authors proposed a hybrid controller for the four-leg SAPF: FLC for the DC-link voltage and predictive control for the grid current. The DC-link voltage FLC handles the system uncertainties and non-linearities, hence improving the transient performance.

Madhuri, N. et al. [144] presented fault tolerant SAPF using PI controller with redundancy. However in this study, FLC instead of PI controller is used to achieve better performance. Simulation results are obtained in presence of open / short circuit fault which are better in comparison with fault tolerant SAPF using PI controller. Sebasthirani, K. et al. [145] proposed a dc link control strategy based on the fuzzy logic controller. SAPF gating pulses are generated using hysteresis current controller based pulse width modulation technique. Musa S. et al. [146] presented the fuzzy logic current control technique for generation of pulse for PWM current control of the three phase inverter. A band pass filter was used in SRF for harmonics extraction. Benaissa, Amar et al. [147], introduced five-level inverter to get the advantage of low harmonic power and elimination of harmonics under distorted voltage conditions. It was based on self tuning filters. Dipen A. Mistry et al. [148], compared the PI and fuzzy logic controllers under balanced and unbalanced source with normal and increased loads. The FLC had improved results compared to PI. Suresh Mikkili et al. [151] reported the type-1 and type-2 fuzzy logic controllers with triangular membership function. This work was validated by using OPAL-RT simulator. The simulations using MATLAB and OPAL-RT were compared. R.Belaidi et al. [152] a fuzzy logic controller was developed to adjust the energy storage of the dc voltage. The reference current computation of the SAPF was based on the instantaneous reactive power (p-q) theory.

Dawei Gao et al. [153] presented a shunt APF with control method based on neural network. The proposed APF can eliminate harmonics, compensate power factor, and correct unbalanced problems simultaneously. Simulation and experimental results were given, the close agreement between the simulation and the experimental results proves the validity of the proposed control method and the feasibility of the shunt APF. Elmitwally et al. [154] presented a three-phase four-wire shunt APF for harmonic mitigation and reactive power compensation in power systems supplying non-linear loads. Three adaptive linear neurons are used to produce the desired three-phase filter current templates. Another feed forward layer neural network is used to control the output filter compensation current online. This is accomplished by producing the appropriate switching patterns. Adequate tracking of the filter reference currents is obtained by this method. The active filter injects the current required to compensate the harmonic and reactive components of the line currents. M. Rukonuzzaman et al. [155] presented the neural network based harmonic detection from the source lines. This work had been done on the single phase APF. M. Rukonuzzaman et al. [156] presented

the harmonic detection and estimation of source current by the neural network method and the signals to inverter in active filter were sent through space vector modulation technique.

Jesus R. Vazquez et al. [158] proposed the adaptive neural network to get the reference currents and multilayer feed forward network for hysteresis band comparator. J. L. Flores Garrido et al. [160] proposed two different control strategies. One of them is based on static Multi Layer Perceptron (MLP) neural network that has proved to be the most appropriate by measuring the rectangular components of the signal harmonics. The other strategy, based on dynamic MLP, permits extracting the instantaneous value of the fundamental waveform. In F. Temurtas et al. [161], feed forward and Elman's recurrent neural networks (NN) are used in detecting harmonics to improve processing speed. These can work well to detect all harmonics.

L. H. Tey et al. [162] introduced a self charging technique to regulate the DC capacitor voltage. The design concept of adaptive APF was verified by simulation results. Dubey et al. [163] presented a novel neural network controlled hybrid parallel APF. The neural network controller comprises two similar adaptive linear neurons (ADALINE), and it has been designed to extract fundamental frequency components from non sinusoidal and unbalanced currents. It has been shown that the proposed neural controller is simple, fast and accurate.

Marcelo G. Villalva et al. [165] presented an alternative method for the control of a three-phase four-wire shunt APF employing an adaptive neural network. A simple and efficient four-wire selective current compensator based on adaptive linear neural networks was studied and successfully implemented. N.B.Muthuselvan et al. [166] presented the neural based PI control applicable for APF with single phase system, which is comprised of multiple non-linear loads. The system consists of an uncontrolled rectifier and ac controller as a non-linear load, with an active filter to compensate for the harmonic current injected by the load. The active filter is based on a single-phase inverter with four controllable switches forming a standard H-bridge inverter. Djaffar Ould Abdeslam et al. [167] proposed a filter based on ADALINE neural networks which are organized in different independent blocks. A neural method based on ADALINE has been introduced for the online extraction of the voltage components to recover a balanced and equilibrated voltage system, and three different methods for harmonic filtering.

Yongtao Dai et al. [168] presented the artificial neural network (ANN) current controller adapted as APF and a current controller based on modified hysteresis current control is used to generate the firing pulses. The studies have been carried out using the detail digital dynamic simulation. Maurizio Cirrincione et al. [169] structured two neural adaptive filters to get fundamental voltage and to compute the load harmonic compensation current. One notch filter is used to compute compensating current and the band filter is used to extract fundamental coupling point voltage.

Rachid Dehini et al. [171] presented a significant contribution to identification and control strategies in order to improve the shunt APF performance. The novel approach is based on intelligent neural network techniques. The performance of the proposed ANN was verified through simulation studies. Ngac Ky Nguyen et al. [172] presented two ADALINE-based schemes for identifying the harmonic currents generated by non-linear loads in power distribution systems. Each neural network method is based on formalized expressions of the active and reactive instantaneous powers. In both methods, the expressions of the instantaneous powers are learned on-line by ADALINE. The amplitude of each harmonic term is thus individually estimated with the ADALINE weights. This allows calculation of the compensating currents of an APF in real-time.

Guiying Liu et al. [173] introduced an all-function APF which can compensate harmonics, inter-harmonics, asymmetries, fundamental sequence reactive powers and so on. Its basic concept and main features are explained. To solve the problem of control for all-function APF, its intelligent control strategy and working process based on BP neural network are expounded. Vahid Dargahi et al. [174] presented investigations on multi cell converters. Implementation of flying capacitor multi cell converters (FCMC) based shunt APFs using artificial neural network is investigated in this paper. State-space representation of FCMC is also derived. Experimental results of five- level FCMC is also given in the paper. N. Gupta et al. [175] presented a design of a neural network controller to extract fundamental frequency components from non-sinusoidal and unbalanced currents. These fundamental frequency components will be used as unit templates. The APF realized by a current controlled IGBT based PWM-VSI bridges with a common dc bus capacitor. Current controller based on pulse width modulation with suitable carrier frequency is used to generate the firing pulse.

Yang Han et al. [176] proposed an effective control scheme for three-phase three-wire APF using neural-based harmonic identification scheme. To achieve improved steady state and dynamic response, the feedback control plus feed-forward control structures is utilized in the proposed control algorithms. The steady-state error minimization is achieved by the feedback loop, where the proportional integral regulators were adopted in *d*-axis and *q*-axis of the synchronous rotating reference frame synchronized with grid voltages by using the phase-locked loop. The adaptive linear combiners are utilized in the feed-forward loop, which serves the purpose of load disturbance rejection, and it significantly enhances dynamic performance of APF. Gupta Nitin et al. [177] presented a new method for harmonic and reactive power compensation with power factor improvement using an artificial neural network and a new control algorithm for APF for power quality conditioning of a variable load under non-ideal mains voltage conditions. Chennai Salim et al. [178] proposed a new APF in order to gain the advantages of the three-level inverter and artificial neural networks and to reduce the complexity of classical control schemes, a new APF configuration controlled by

two MLPNN (Multi-Layer Perceptron Neural Network) is proposed for a three level inverter. Saeideh Masjedi et al. [179] utilized the radial base neural network with three layers to mitigate harmonics. The structure of this neural network and the adaptive adjusting algorithm are presented.

Ngac Ky Nguyen et al. [180] used novel ADALINE based architecture for harmonic currents identification and on-line tracking which works in different reference frames resulting from specific currents or powers decompositions. Chennai Salim et al. [182] presented two ANN, the first one is used to replace the PWM logic controller while the second regulate the dc voltage link of the shunt active filter. Awan Uji Krismanto et al. [183] utilised the radial basis function neural network type for controlling the compensation current of shunt APF for harmonics mitigation.

Garrido et al. [184], the “dynamic multilayer perceptron” neural network has been applied to the control of an APF. The objective is developing a new suitable control technique by APF for compensation of harmonic distortion present in non-linear loads current by electric power circuits. El-Mamlou et al. [185] developed an efficient APF to estimate and compensate for harmonic distortion in an electrical power network. The developed APF control scheme is based on a double proportional feedback controller and a single-phase voltage source half-wave bridge inverter. Zahira, R. et al. [186] dealt with many control schemes for reference current generation such as p-q theory, dead beat controller, adaptive control, neuro fuzzy, wavelet control, sliding mode control, delta-sigma modulation, vector control, SFX control, repetitive control etc. for improving the steady state and dynamic performance of APF. S. Janpong et al. [187] presented the review paper based on the study on the application of Neural Networks on shunt APF. It first explains the harmonics and shunt active filters then moves to the application of Neural Networks, the architectures of neural networks.

Sahu, Laxmi Devi et al. [188] presented the hybrid filter comprising both passive filter and the APF. This work was based on the simulation study for the variable loads and the unbalanced supply. The extraction of the source voltages and currents was done by the neural network method. Zeng et al. [189] compared various methods of harmonic detection and developed the adaptive algorithm. The control strategy is based on the optimal voltage space vector hysteresis current. Simulation study showed that the selection method and control strategy are good for filtering. Menda VV Appalanaidu et al. [190] used neural network as the detection and current controller. The detection of load and compensation currents and source voltages are necessary to use this neural network. The application, design and simulation results are reported in this paper. Almaita et al. [191] explained background on harmonic detection and current control methods. In this paper, the radial neural network is used.

Campanhol, L. B. G et al. [192] presented a method based on artificial neural network, which was used to obtain the reference currents for harmonic current suppression and reactive power compensation in a shunt APF applied to three-phase four-wire system. Ponnusamy Thirumoorthi et al. [193] presented two soft computing techniques, fuzzy logic and neural network to design a new control scheme for switching a shunt APF. These control schemes consists of three control loops, namely a voltage loop, current loop and reference generation loop. Ramchandra, N. et al. [194], the ANN-based controller is designed and trained offline using data from the conventional PI controller. The performances of ANN and PI controller are studied and compared for Unified Power Quality Conditioner using simulations. Bhattacharya Avik et al. [195] used predictive and adaptive neural network to get the compensated currents. The simulation and experimental validations were reported to support the work for balanced and unbalanced loads for three phase three wire system. Nguyen, Ngac Ky et al. [196] demonstrated that the ADALINE learning process allows the compensation schemes to be well suited for online adaptive compensation. Digital implementations of the identification schemes are performed and their effectiveness is verified by experimental studies.

Fei, Juntao et al. [198] proposed adaptive neural network strategy to achieve the asymptotical stability of the APF system. The parameters of neural network are adaptively updated to achieve the desired tracking task. Qasim, Mohammed et al. [199] presented a phase-locking control scheme based on artificial neural networks for APF. The proposed phase locking was achieved by estimating the fundamental supply frequency and by generating a phase-locking signal. Geetha Mathiyalagan et al. [200] presented a single phase shunt APF and ANN is used to extract current and voltages of the supply. Mohammed Qasim et al. [201] presented the analysis of performance, limitations and advantages of adaptive linear neuron and feed forward multi layer neuron and compared many aspects supported by both simulations and experimental studies. Mahajan Vasundhara et al. [202] presented a fuzzy logic controller for voltage error and another fuzzy logic controller for current controller to get the PWM signals and the neural network for getting the reference currents. The work was supported by both simulations and experimental results for a five level inverter used as APF.

Bayindir K. Cagatay et al. [203] presented two control schemes one with fuzzy logic controller and another with hierarchical neuro fuzzy. A new switching development scheme is introduced in this paper. Husev Oleksandr et al. [204] proposed a new control scheme with neuro fuzzy regulator for parallel APFs. Mridul Jha et al. [205] presented a neuro fuzzy controller based APF for three phase four wire system. This paper explained the fuzzy controller and neuro controller and the control strategy used in this work. The P-Q theory was used in this work.

G. Nageswara Rao et al. [206] presented a neuro fuzzy application for five-level APF with D-Q reference frame theory. Level shifted PWM technique was adopted to investigate the performance of Cascaded H-bridge (CHB) inverter, The advantages of CHB inverter are low harmonic distortion, reduced number of switches and suppression of switching losses. Bett, N. K. et al. [207] used a hybrid filter, a passive filter in parallel with a shunt active filter that is controlled by an adaptive Neuro-Fuzzy inference system (ANFIS) controller. The current compensation is much better in this hybrid filter when compared to that of APF. Zahira, R. et al. [208] presented various control techniques in Shunt APF namely fixed frequency control, SFX Algorithm based adaptive control, delta modulation, dead beat current control, soft computing techniques. Vishnuvardhan, M. et al. [209] presented a control strategy for the unified power quality conditioner (UPQC). The main problem of UPQC is the high discharging time of DC link capacitor. To eliminate this problem an enhanced neuro fuzzy controller based UPQC is proposed in this paper. Rao, G. Nageswara et al. [210] proposed a feedback controller to separate the harmonics which are controlled by neuro fuzzy controller. In this paper a multilevel inverter was used as APF. Jayakumar K.S. et al. [211] compared the performance of PI, Fuzzy and neuro fuzzy controllers aiming to get the best THD with neuro fuzzy controller. A five level inverter was used as an APF and D-Q reference frame theory was used to get active filtering. Rajani, B. et al. [212] proposed a PI and neuro fuzzy controller for multi converter unified power quality conditioner with three phase four wire system. P-Q theory was used to perform the active filtering.

Karthik, N. et al. [213] proposed fuzzy and neuro fuzzy controllers on a cascaded multilevel inverter and compared with PI controller. Out of three, neuro fuzzy has proved as the best controller. Thulasiraman Sundar Rajan Giri et al. [214] proposed a bidirectional switch to control the voltage error and fuzzy logic controller with DC motor and three phase induction motor as the loads. Weike Yuan et al. [215] a fuzzy neural network and genetic algorithm based predictive control was adopted in this work. The fuzzy neural network was employed to predict the future harmonics compensating current in order to make predictive control accurate and compact. The genetic algorithm was used to optimize model parameters. Mehta, Dharmik N. et al. [216] designed a single phase full bridge FPGA model. To speed up the operation fuzzy logic with neural network trained data was used. Xilinx ISE program and Model Sim were employed to synthesis VHDL code for the neuro fuzzy system used in FPGA. Rajan, GT Sundar et al. [217] proposed a bidirectional switch at the front end for improving the conduction of input current and the buck converter at the output stage of three phase rectifier for the voltage regulator. The PI, fuzzy logic and the neuro fuzzy controllers were used in this work. B.Venkata siva et al. [218] proposed the instantaneous active and reactive power theory for shunt APF. The performance of conventional PI is

compared with artificial neural network based PI controller and Particle swarm algorithm based PI controller.

1.7 Scope of the work and Author's Contribution

Applications of power electronic converters are increasing day by day in converting and controlling the huge electrical power. They has led to the injection of harmonic currents and drawing the reactive power from the supply mains. The generation of current harmonics leads to further degradation in source voltage and generation of more harmonics. Owing to these problems, the devices used in the consumer ends will get affected and they are underutilized. APF is the viable solution for these problems. It is able to compensate the reactive power, neutral current and input current balancing in addition to mitigation of harmonics.

There are many topological and control methodologies in APF as discussed in the literature review. Various configurations of APF are proposed to compensate current and voltage harmonics as well as compensation of reactive power, neutral current, voltage flicker, current and voltage unbalance and voltage regulations. Series APFs are proposed for voltage related problems such as compensation of voltage harmonics, voltage unbalance, voltage regulation and flicker etc. whereas shunt APFs are preferred for current related problems such as compensation of current harmonics, unbalance, reactive power etc. and are recommended to be installed at the customer's end.

Improvement in high power self commutating switching devices like IGBT and GTO used in power circuit of active power circuit and control techniques have attracted the attention of researchers in this field. A voltage source PWM converter based APF has more advantages over its counterpart viz. lightweight, high efficiency and low cost. The controlling part of this system is how to generate the reference current to produce the PWM signals. Many control techniques used to derive the harmonics and reactive volt ampere requirement of the load. This is difficult to estimate the reference currents especially in the area of low and medium power applications. The easier method by sensing line currents is used in this work.

Now-a-days the soft computing techniques are used to implement the design of the controller and to get the better transient response. The soft computing techniques used in this work and also hybrid systems combining soft computing techniques like fuzzy logic, neural networks, and genetic algorithm are effective in solving the wide variety of real world problems. For example, while neural networks are good at recognizing patterns, they are not good at explaining how they reach their decisions. Fuzzy logic systems, which can reason with imprecise information, are good at explaining their decisions but they cannot automatically acquire the rules they use to make those decisions. These limitations have been a central driving force behind the creation of intelligent hybrid systems where two or

more techniques are combined in a manner that overcomes the limitations of individual technique. Hybrid systems are also important when considering the varied nature of application domains. The use of intelligent hybrid systems is growing rapidly with successful applications in many areas including process control, engineering design, financial trading, credit evaluation, medical diagnosis, and cognitive simulation.

The main contributions made in this work are as follows

1) Design, development and investigations on three-phase shunt active power filter for harmonic mitigation and reactive power compensation with a novel neuro fuzzy based controller. Extensive simulations are carried out with balanced / unbalanced non linear load at varying level of reactive power demand.
2) The active power filter has also been tested with PI, fuzzy logic and neural network based controllers.
3) A prototype active power filter has been developed in laboratory to validate the simulated investigations.

1.8 Organization of the Thesis

The thesis is organized in eight chapters. The overview of all the chapters is as follows:

A brief overview of power quality, problems such as harmonics, reactive power compensation, classification of filters, control strategies and the detailed literature review on fuzzy logic, neural network and neuro fuzzy based controllers for shunt active power filter are presented in **Chapter 1.**

The survey of voltage and current harmonics before application of active power filter has been conducted to know the existing harmonics in the system with 1kVA load. The solution with PI controller covering the basics and implementation in MATLAB is reported. The simulations for different loads with balanced and unbalanced nature are studied. The performance is investigated during transient and steady state conditions, which is presented in **Chapter 2**.

Introduction of fuzzy logic controller and its implementation in MATLAB is presented in **Chapter 3**. The simulations results for different loads with balanced and unbalanced loads are studied. The performance is investigated during transient and steady state conditions.

Introduction of neural network based controller and its implementation in MATLAB is presented in **Chapter 4**. The simulations results for different loads with balanced and unbalanced loads are studied. The performance is investigated during transient and steady state conditions.

Introduction of neuro fuzzy controller and its implementation in MATLAB is presented in **Chapter 5**. The simulations results for different loads with balanced and unbalanced loads are studied. The performance is investigated during transient and steady state conditions.

Chapter 6 presents selected experimental results for different loads in transient and steady state conditions.

Comparison of all the simulation results of PI, fuzzy logic, neural network and neuro fuzzy based controllers are presented and through exhaustive tabulations and graphical representations for the various parameters. The comparison is also done between the hardware and simulation results in **Chapter 7**.

Chapter 8 summarises the important conclusions of the work and states the scope for future research. List of references are listed at the end.

2.1 Types of Controllers

In control system, a controller has a key role to play in regulating a control parameter in accordance with an input signal with desired accuracy. A variety of controllers have been developed over time which can broadly be classified in two categories:

a. Conventional controllers
b. Unconventional controllers

The conventional controllers such as proportional (P), proportional integral (PI), proportional derivative (PD) and proportional integral derivative (PID) controllers perform according to a well defined transfer function and produce corresponding quality of output. The unconventional controllers such as fuzzy, neuro and neuro fuzzy controllers are based on artificial intelligence where knowledge of a precise mathematical model is generally not required.

Many industrial processes are non-linear and thus difficult to describe mathematically. However, it is known that good non-linear processes can be satisfactory controlled using PID controllers provided that controller parameters are tuned well. Practical experience shows that this type of control has a lot of sense, since it is simple and based on three basic behavior types: proportional (P), integral (I) and derivative (D). PID controller and its different types such as P, PI and PD controllers are today basic building blocks in control of various processes. Inspite of their simplicity, they are used to solve complex control problems, especially when combined with different functional blocks, filters (compensators or correction blocks), selectors etc. It is expected that it will be a backbone of many complex control systems.

2.2 Conventional Controllers

PID controllers use three basic types or modes: P - proportional, I - integral and D - derivative. While proportional and integral modes are also used as single control modes, a derivative mode is rarely used on its own in control systems. Combinations such as PI and PD control are very often used in practical systems. The brief description of these controllers is given below:

2.2.1 On-Off Controller:

The output of on-off controller is shown in Fig. 2.1.

$$u(t) = U_{max}; \forall\ e(t)>0$$
$$= U_{min}; \forall\ e(t)<0$$

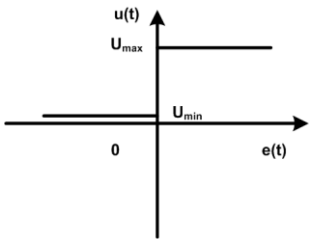

Fig. 2.1 Output characteristics of system with on-off controller

Where

e(t) = control error (for unit feedback)

u(t) = control signal (controller output)

Control signal u(t) can have only two possible values, high U_{max} or low level U_{min}, depending on whether error is positive or negative. Assuming that process (controlled plant) has a positive static gain, high-level control signal will cause increase in controlled variable value. The main idea in this type of control with only two control levels is to achieve desired value of the controlled variable in shortest possible time.

An inadequacy in this type of control is that the control signal tends to oscillate which may cause control variable to oscillate around desired value. Sometimes there is no remedy for this problem. On-off controller is very simple, since there are only two possible control signal values, no matter what is the value of control error. Process is forced to oscillate since u(t) is never zero (it is either U_{max} or U_{min}). The only way to avoid these forced oscillations is to diminish gain for small values of control error e(t). That can be achieved by introducing a proportional mode which will be active for certain values of control error.

2.2.2 Proportional (P) Controller:

The P controller eliminates the output oscillations caused in on - off controller but it does have a steady state error. Its characteristics are shown in Fig. 2.2., and transfer function is shown in Fig. 2.3.

$u(t) = U_{max}$; $\forall\ e(t) > e_0$

$= U_0 + K\ e(t)$; $\forall\ -e_0 < e(t) < e_0$

$= U_{min}$; $\forall\ e(t) < e_0$

Where U_0 = Amplitude of control signal when control error is zero.

K = P controller gain for nominal area $e(t) < |e_0|$

The relation between control signal and control error inside $e(t) < |e_0|$ is $u(t) = u_0 + K\ e(t)$ and the control error is $e(t) = (u(t)-U_0)/K$.

For properly designed control system the steady state error should be zero. With a P controller the zero steady state error is obtained when $K = \infty$ or $u(t) = U_0$. With $K = \infty$, the P controller is changed to on-off controller and the forced oscillations again come into picture. For $u(t) = U_0$, P controller cannot stabilize higher order processes.

Large control gain K gives

1) Smaller Steady state error, i.e. better reference following
2) Faster dynamics, i.e. broader signal frequency band of the closed loop system and large sensitivity with respective to measuring value.
3) Smaller amplitude and phase margin.

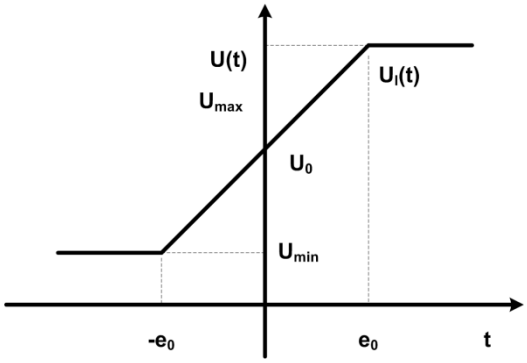

Fig. 2.2 Output characteristics of the system with P controller

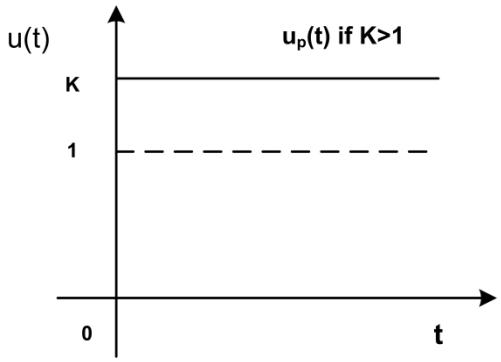

Fig. 2.3 Transfer characteristics of the system if P controller is applied if K>1

2.2.3 Proportional and Integral (PI) Controller:

The following equation represents the control process in a PI controller:

$$u(t) = K\left[e(t) + \frac{1}{T_i}\int_0^t e(T)dT \right]$$

Where:

T_i = integral time constant of PI controller.

$K_i = K/T_i$ is called reset mode. Integral control is also sometimes called reset control.

The transfer function of the integrator and PI controller are shown in Fig. 2.4 and Fig. 2.5, respectively. The output of the controller is a line with K_i as the slope. The integrator shows that the output starts from zero as in Fig. 2.4 and the PI controller shows that the output starts from the value K which is the gain of proportional controller as this is the combined effect of the P and I controllers.

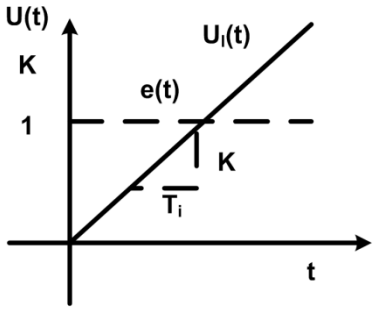

Fig. 2.4 Transfer function of Integrator

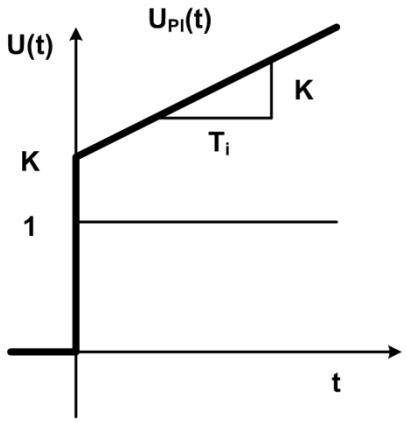

Fig. 2.5 PI Controller transfer function

The name comes from the term "manual reset" which marks a manual change of operating point or of "bias" U_0 in order to eliminate error. PI controller performs this function automatically. If control signal of P controller in proportional area is compared with PI controller outputs signal it can be seen that constant signal U_0 is replaced with signal proportional with the area under error curve:

$$U_0 = \left[\frac{K}{T_i} \int_0^t e(T)dT \right]$$

The fact that U_0 is replaced with an integral allows PI controller to eliminate steady state error. On the other hand, P controller cannot eliminate steady state error since it does not have any algorithm that would allow for the controller to increase control signal in order to increase controlled variable. It can be concluded that PI controller will eliminate forced oscillations and steady state error resulting in operation of on-off controller and P controller respectively. However, introducing integral mode has a negative effect on speed of the response and overall stability of the system. PI controllers are very often used in industry, especially when speed of the response is not an issue.

2.3 Choice of Controllers

1. On-off controller

- There is no need to tune any parameters.
- As no storage elements are present there is no need to maintain it.
- It is used in Home appliances, like refrigerators, washers etc. And also temperature controller in building.

2. P Controller

- It is used to get large gain to improve steady state error.

3. PI Controller

- It is used when fast response of the system is not required
- It produces large disturbance and noise during operation of the process.
- It is used if there is only one energy storage in process.
- It is used when there is a large transportation delays in the system.

The PI controller is a better controller for avoiding oscillations and the steady state error but it adversely affects on speed of the response and the stability of the system. These two features are improved in a PID controller. However, in power electronic applications, the switching frequency of the switching pulses is generally very high and using PID controller creates noise and disturbances. In general for the power electronic applications, therefore the PI controller is found more favourable.

The procedure of selecting the proportional and integral constants is explained in Appendix A.

2.4 Description of System and Its Model

The basic principle of compensation in the APF is described in this section in detail.

Let us consider

$i_s(t)$ is the instantaneous source current,

$i_L(t)$ is the instantaneous load current, and

$i_c(t)$ is the instantaneous compensating current

From Fig. 2.6, according to Kirchhoff's current law, the instantaneous currents can be related as

$$i_s(t) = i_L(t) - i_c(t)$$

Let the instantaneous source voltage be $v_s = V_m \sin \omega t$

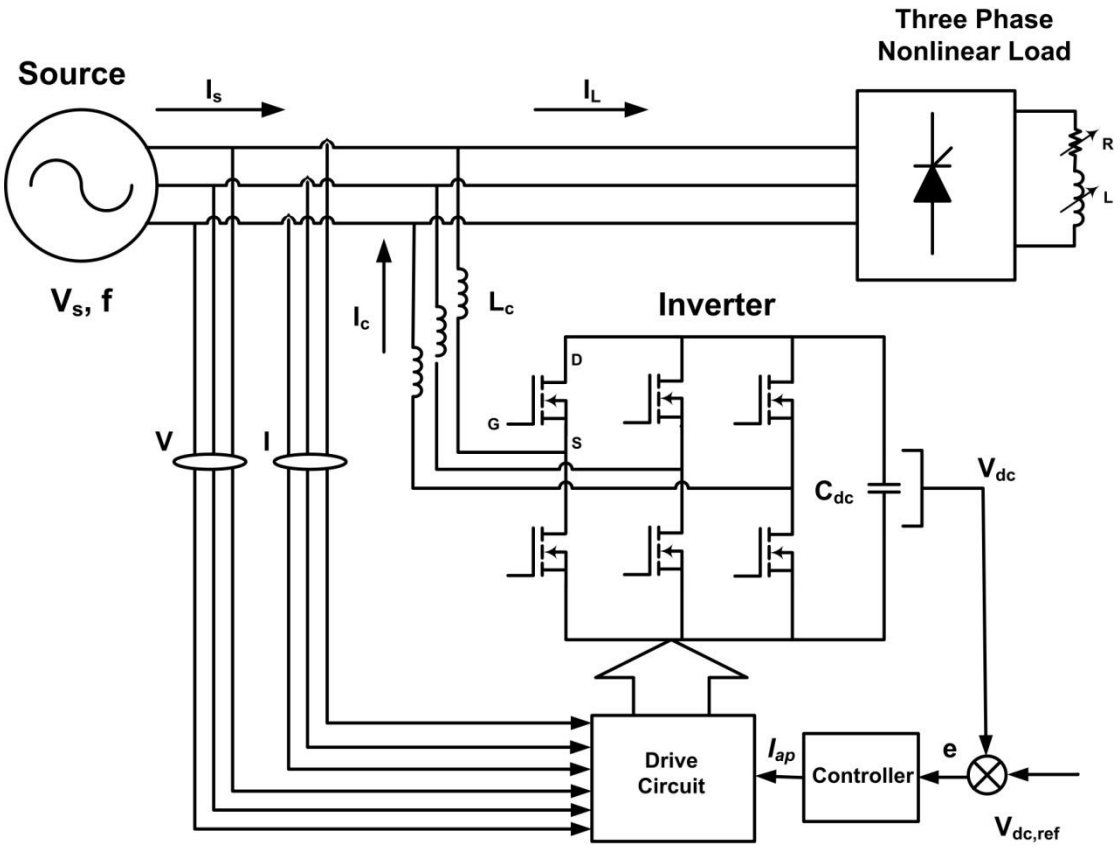

Fig. 2.6 Schematic diagram of shunt active power filter

For a non-linear load the load current can be divided into two parts, one is the fundamental component and second one is the harmonic component and can be written as

$$i_L(t) = \sum_{m=1}^{\infty} I_m \sin(m\omega t + \phi_m) = I_1 \sin(\omega t + \phi_1) + \sum_{m=2}^{\infty} I_m \sin(m\omega t + \phi_m)$$

The instantaneous load power can be given in terms of source voltage and load current as

$$p_L(t) = v_s(t) \times i_L(t)$$

$$= V_m I_1 \sin^2 \omega t \times \cos\phi_1 + V_m I_1 \sin\omega t \times \cos\omega t \times \sin\phi_1$$

$$+ V_m \sin\omega t \times \sum_{m=2}^{\infty} I_m \sin(m\omega t + \phi_m) \qquad (2.1)$$

$$= p_{re}(t) + p_{rec}(t) + p_{har}(t)$$

From Equation (2.1), real (fundamental) power is drawn by the load

$$p_{re}(t) = V_m I_1 \sin^2 \omega t \times \cos\phi_1 \qquad (2.2)$$

From Equation (2.1), the fundamental source current is

$$i_s(t) = \frac{p_{re}(t)}{v_s(t)} = I_1 \cos\phi_1 \sin\omega t = I_{sm} \sin\omega t$$

Where $I_{sm} = I_1 \cos\phi_1$

Also there are some switching losses in the PWM converter. Hence, the source must supply a small overhead for the capacitor leakage and converter switching losses in addition to the real power of the load.

Hence, total peak current supplied by the source

$$\boldsymbol{I}_{sp} = \boldsymbol{I}_{sm} + \boldsymbol{I}_{sL}$$

If the active filter provides the total reactive and harmonic power, then $i_s(t)$ will be in phase with the source voltage and will be sinusoidal. The active filter then must provide the following compensation current:

$$i_c(t) = i_L(t) - i_s(t)$$

Hence, for the accurate and instantaneous compensation of reactive and harmonic power, it is necessary to calculate $i_c(t)$. This will be considered as reference current.

Estimation of Reference Source Current

The peak value of the reference current I_{sp} can be estimated by controlling the dc side capacitor voltage. The ideal compensation requires the main current to be sinusoidal and in phase with the source voltage irrespective of nature of the load current. The desired source currents after compensation [4] can be given as

$$i_{sa,ref} = I_{sp} \sin \omega t$$

$$i_{sb,ref} = I_{sp} \sin(\omega t - 120^{\circ})$$

$$i_{sc,ref} = I_{sp} \sin(\omega t + 120^{\circ})$$

where $I_{sp} = I_{sm} + I_{sL}$ is the amplitude of the desired source current. Since this current is in phase with the source voltage, one only needs to know the magnitude (and not phase angle) of desired source current.

Fig. 2.7 gives simulink model of shunt APF. The use of PI type of controller [12] requires that its gain and time constant be fine tuned for a given load. The system consists of a three phase supply feeding a rectifier fed RL load (non-linear load). The APF block contains the two level inverter using MOSFETs as switching devices. There are six MOSFETs and they are controlled by the signals which are provided by the Control Circuit block. The Inverter provides compensating current I_c which is added to load current I_L to obtain near sinusoidal and in phase source current I_s. The prevailing value of V_{dc} is compared with the reference value $V_{dc,ref}$. The error is processed in a controller and appropriate drive command for the inverter is obtained from the drive circuit corresponding to the prevailing source currents and voltages.

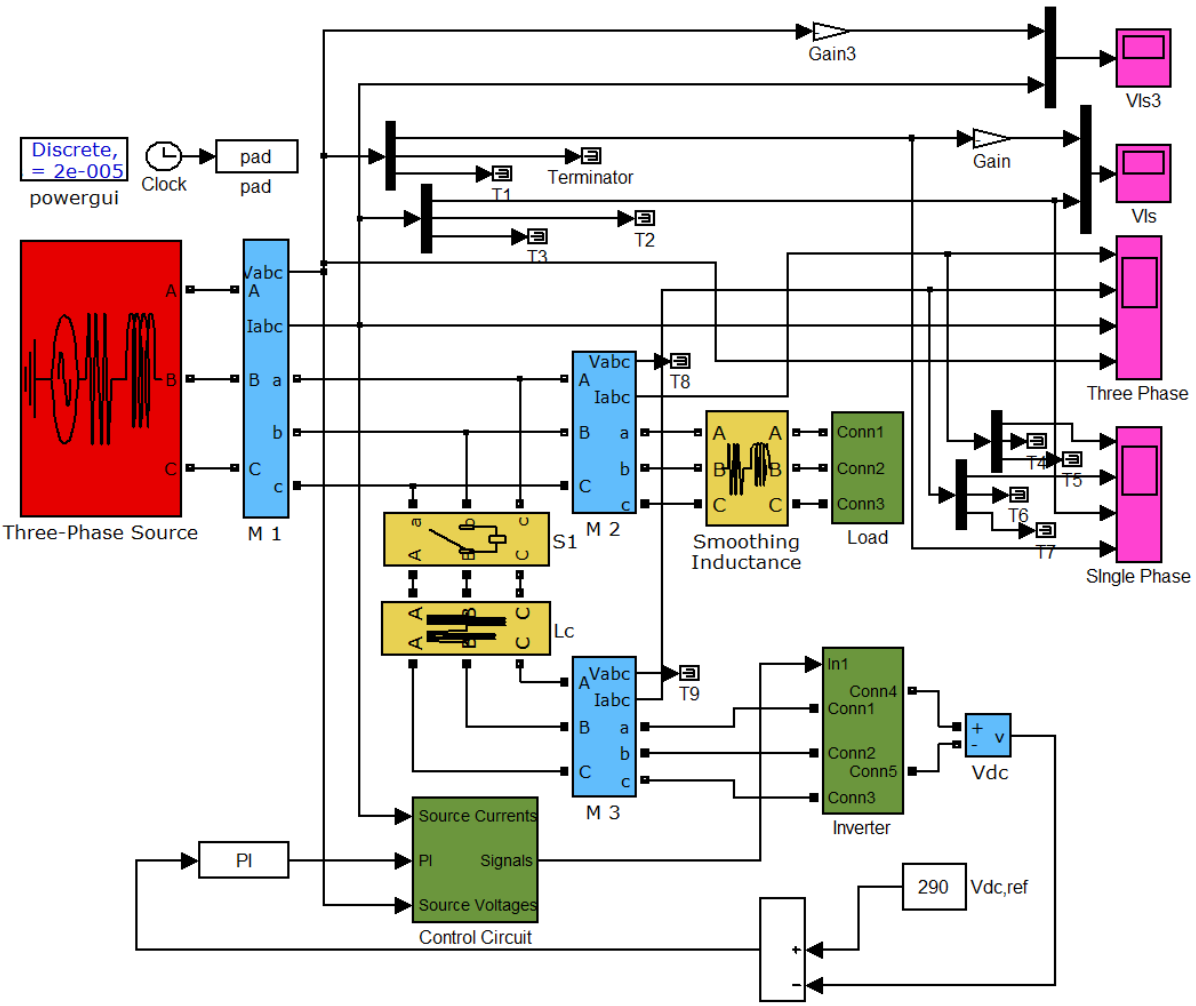

Fig. 2.7 Simulation diagram of shunt active power filter

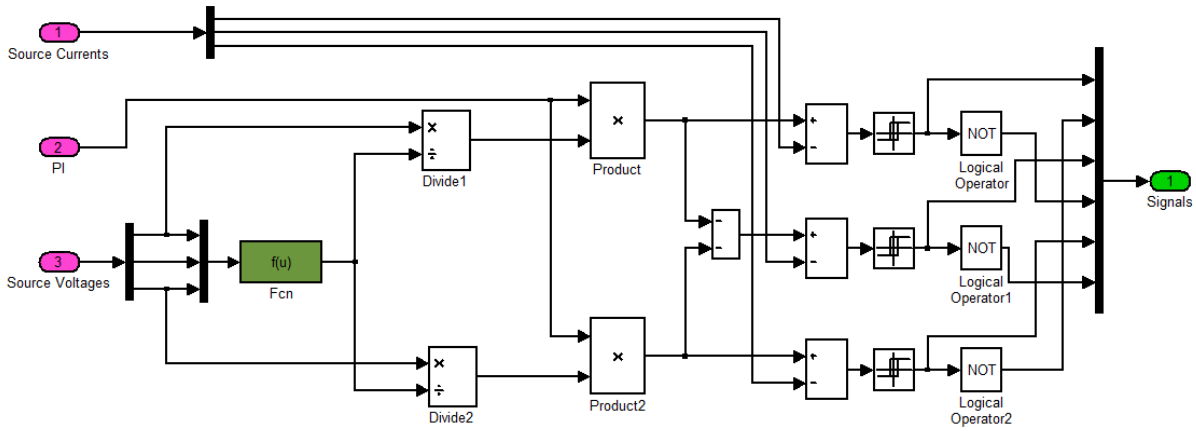

Fig. 2.8 Drive Circuit

Fig. 2.8 shows the detailed drive circuit. The drive circuit shows the details of obtaining the gating signals for inverter switches. The output of peak detection block (Fcn) is logged to the peak phase voltage. Each phase voltage is divided by this peak value to get the unit voltage template. This is multiplied with the output of the multiplier to get the current signal corresponding to the shape of voltage and having magnitude of output of Controller. This will

be the reference signals to compare with sensed current signals from supply mains. This is given to hysteresis controller to get the signals. Here the numbers 1 to 6 are the corresponding signals to each device in the inverter.

Design of Power Circuit of APF

Design of a power circuit includes three main parameters [10]:

1. Filter inductor (L_c)
2. DC side capacitor (C_{dc}), and
3. Reference value of dc side capacitor voltage ($V_{dc,ref}$)

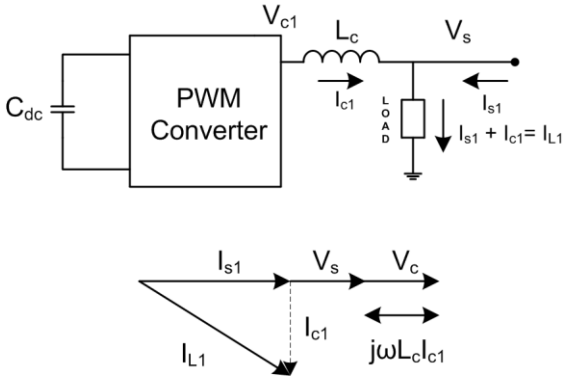

Fig. 2.9 Design of APF

Selection of L_c and $V_{dc,ref}$

From Fig. 2.11 we can conclude that

$$V_{c1} = V_s + j\omega L_c I_{c1}$$

$$jI_{c1} = \frac{V_{c1} - V_s}{\omega L_c}$$

$$|I_{c1}| = \frac{V_{c1} - V_s}{\omega L_c}$$

The 3-phase reactive power delivered from the APF is as follows

$$Q = 3V_s I_{c1} = 3V_s \frac{(V_{c1} - V_s)}{\omega L_c} \qquad (2.3)$$

Where,

Q = Three phase reactive power delivered from the APF.

V_s = Supply voltage

I_{c1} = Fundamental compensating current

V_{c1} = Fundamental Output voltage of inverter

L_c = Inductance of filter inductor

This shows that the active filter can compensate the reactive power only when $V_{c1} \rangle V_s$. Ripple Attenuation Factor is the ratio of Harmonic compensating current and rated fundamental compensating current.

$$Rip.Att.Fac. = \frac{I_{char}}{I_{c1}} \tag{2.4}$$

Table 2.1 Generalized harmonics of V_{LL} for a large and odd m_f [29]

Order of Harmonic (h)	m_a	
	0.8	1.0
Fundamental	0.490	0.612
$m_f \pm 2$	0.135	0.195
$m_f \pm 4$	0.005	0.011
$2m_f \pm 1$	0.192	0.111
$2m_f \pm 5$	0.008	0.020
$3m_f \pm 2$	0.108	0.038

The harmonic compensating current is represented as

$$I_{char}\left(m_f \omega\right) = \frac{V_{char}(m_f \omega)}{m_f \omega L_c} \tag{2.5}$$

Where

$I_{char}\left(m_f \omega\right)$ = Harmonic compensating current

$V_{char}(m_f \omega)$ = Harmonic compensating voltage

m_f = Frequency modulation ratio of the PWM converter

If the PWM converter is assumed to operate in the linear modulation mode ($0 \le m_a \le 1$), the amplitude modulation factor m_a is expressed as [9].

$$m_a = \frac{\sqrt{2}V_{c1}}{V_{dc}/2} \tag{2.6}$$

Hence, Voltage across capacitor, $V_{dc} = 2\sqrt{2}V_{c1}$ for m_a = 1.

From Equation (2.3) the value of I_{c1} can be calculated. By using equation (2.4) and Table 2.1 the values of I_{char} and V_{char} can be calculated. By substituting these values in equation (2.5) the value of L_c can be calculated. By substituting the value of L_c in equation (2.3) one can get V_{c1} and hence $V_{dc,ref}$.

Design of the dc side capacitor (C_{dc})

The design of dc side capacitor is based on the principle of instantaneous power flow. The selection of C_{dc} is governed by reducing the voltage ripple. As per the specification of peak-to-peak voltage ripple ($V_{dcr,p-p}$) is

$$V_{dcr,p-p} = \frac{\pi I_{c1,rated}}{\sqrt{3}\omega C_{dc}}$$

The dc side capacitor C_{dc} can be found as

$$C_{dc} = \frac{\pi I_{c1,rated}}{\sqrt{3}\omega V_{dcr,p-p}} \quad (2.7)$$

From the above equations and specifications the Shunt Active Filter's Compensating Inductance (L_c) and Capacitance (C_{dc}) are computed as 6mH and 4800μF.

Finally we can make an m file to find out the system parameters of an APF with name as getL is

```
function Lc = getL(f,Vs,RAF,mf,Qc,Vdcr)
Lc=(3*0.388*Vs*Vs)/(2*pi*f*RAF*mf*Qc);
Vdcref=(2*sqrt(2)*((3*Vs*Vs)+(2*pi*f*Lc*Qc)))/(3*Vs)
Cdc=(pi*Qc)/(3*sqrt(3)*2*pi*f*Vs*Vdcr)
```

This programs takes supply frequency, supply voltage, ripple amplification factor, frequency modulation, reactive power compensated and the maximum peak to peak voltage ripple in dc side as the arguments from the command window and computes the values L_c, $V_{dc,ref}$ and C_{dc}.

Hysteresis Current Controller

A hysteresis controller is used to generate the gating signals to the inverter. The hysteresis band is set to run the current error between lower limit $i_{sa,Ref,L}$ and upper limit $i_{sa,Ref,U}$. Fig. 2.10 shows the base drive signals to the switching device 1. $i_{sa,ref}$ is the reference current i_{sa} is the actual current. Let the reference current $i_{sa,ref}$ is positive and the switching device 1 is on when the actual current i_{sa} is equal to the lower limit of the $i_{sa,ref}$ i.e. $i_{sa,Ref,L}$ and vice versa. The switching operation of switching devices automatically forces the actual current i_{sa} to follow the reference current $i_{sa,ref}$. The inverted signals are given to the switching device 2. This can also be explained if $i_{sa,ref}$ is negative. The hysteresis band is

tested for some values. Out of these values, the hysteresis band is finalised. The Total Harmonic Distortion (THD) for all the hysteresis band values are tried and finally observed that the total harmonic distortion corresponding to hysteresis band 0.01A is finalised.

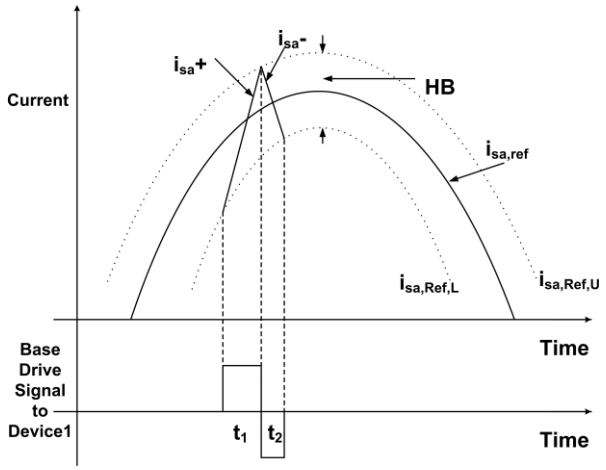

Fig. 2.10 Hysteresis controller

2.5 Results and Discussion

The simulated results of the PI controller based shunt APF are studied in this section. The load is a three phase thyristorised controlled rectifier feeding a series R-L load. Three settings of firing angle α are considered as 0, 30° and 60°. In each case, the response is obtained for following conditions:

- Active Filter is enabled with fixed and balanced load
- Step change in load, with active filter enabled
- Unbalanced load, with active filter enabled

2.5.1 Simulation results for rectifier fed RL load at α=0

The simulated results with at α=0 are given below under different conditions:

2.5.1.1 Active filter is enabled

Fig. 2.11 (a) shows the waveforms of load current, compensating current, source current and source voltage at α=0 with PI controller. In this case the values of R and L at the output of rectifier are adjusted such that the load on ac side is 1 kVA. The APF is initially disabled from t=0 to t=0.5 s. The compensating current is zero and source current is same as the load current. The source current is non sinusoidal with harmonics and is found to have THD of 30.64%. At t=0.5 s when the APF is enabled, the compensating current is applied at point of common coupling which makes the source current nearly sinusoidal unlike the load current. The THD of source current is now reduced to 2.93%. These waveforms show that after enabling, the shunt APF compensates for the reactive power demand and reduces the harmonic content in the source current. Fig. 2.11 (b) shows the waveforms of source current

and source voltage from t=0.44 s to t=0.46 s and from t=0.54 s to t=0.56 s i.e. the response of the system for one cycle before and after the enabling of APF.

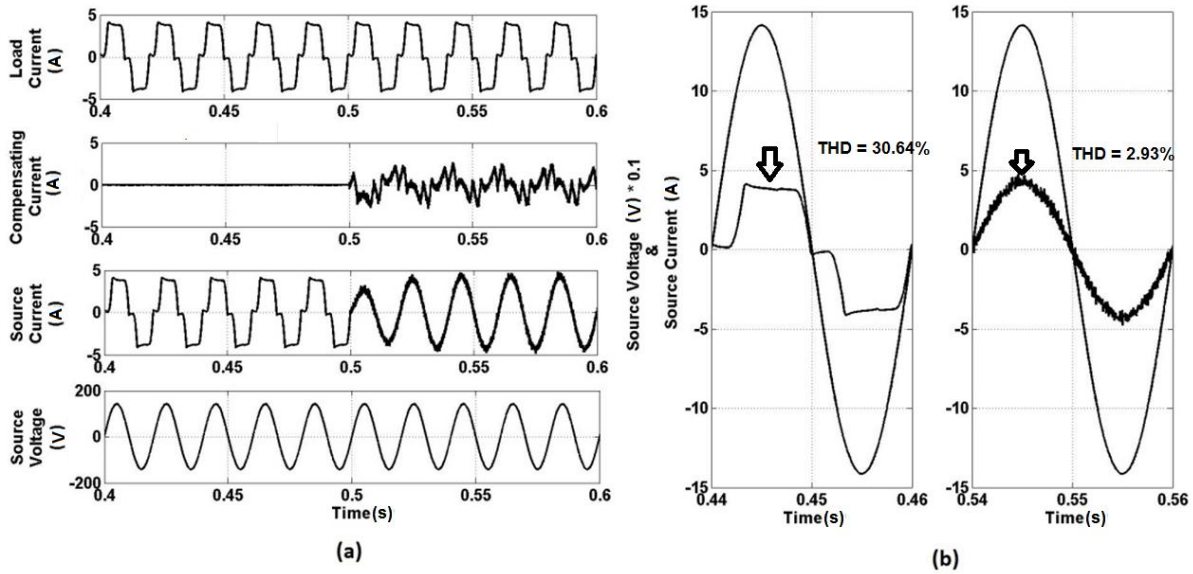

Fig. 2.11 (a) Response of active power filter at α=0 (b) Source voltage and current waveforms for one cycle before and after the enabling of active filter

2.5.1.2 Step change in load

Fig. 2.12 (a) shows the waveforms of load current, compensating current, source current and source voltage at α=0 with PI controller. Here, initially the load is 1 kVA up to t=0.5 s and at t=0.5 s the load is suddenly increased to 2 kVA (by suitable variation of R and L at the output of rectifier) and then, the load is brought back to 1kVA at t=0.7s. The amplitude of load current, compensating current and source current also increases in response to the increase in load up to t=0.7 s, then they return to previous values. The source current is again found to be nearly sinusoidal. The quality of source current is measured in terms of its THD under these loading conditions. From the FFT analysis of source current waveforms at 1 kVA and 2 kVA, the THD is 2.93% and 2.88% respectively. These waveforms show that after increment in load also, the shunt APF compensates the reactive power and reduces the harmonic content in the source current. Fig. 2.12 (b) shows the waveforms of source current and source voltage from t=0.44 s to t=0.46 s and from t=0.54 s to t=0.56 s i.e. the response of the system for one cycle before and after the step change in load of APF. Transient is completed in about two cycles without any overshoot.

2.5.1.3 Unbalanced load

Fig. 2.13 (a) shows the waveforms of load current, compensating current, source current and source voltage at α=0 with PI controller. Here, initially the load is balanced up to t=0.5 s and at t=0.5 s. Unbalance is introduced by applying a linear star connected load in

parallel to existing 1kVA load, with Ra=40 Ω, Rb=60 Ω and Rc=20 Ω. The amplitude of load current, and compensating current is also changed by application of unbalanced load. The source current is again found to be nearly sinusoidal. The quality of source current is measured in terms of its THD under these loading conditions. From the FFT analysis of source current waveforms at balanced load and unbalanced load, the THD is 2.93% and 2.73% respectively. These waveforms show that even with unbalanced load, the shunt APF compensates the reactive power and reduces the harmonic content in the source current. Fig. 2.13 (b) shows the waveforms of source current and source voltage from t=0.44 s to t=0.46 s and from t=0.54 s to t=0.56 s i.e. the response of the system for one cycle before and after the application of unbalanced load of APF. The source current becomes balanced after enabling APF even though the load is unbalanced.

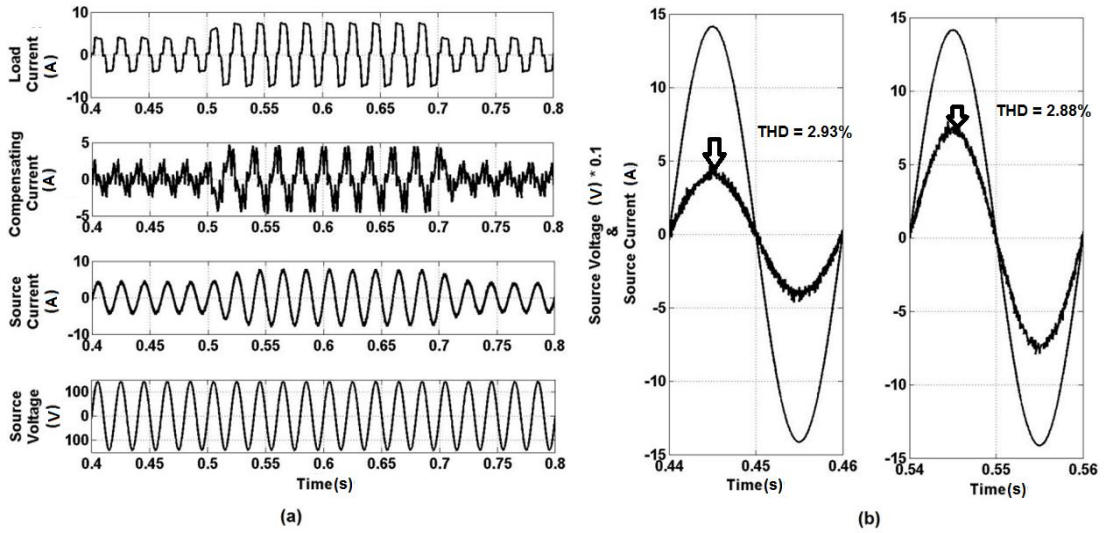

Fig. 2.12 (a) Step change in load of active power filter at α=0 (b) before and after the step change of load for one cycle each

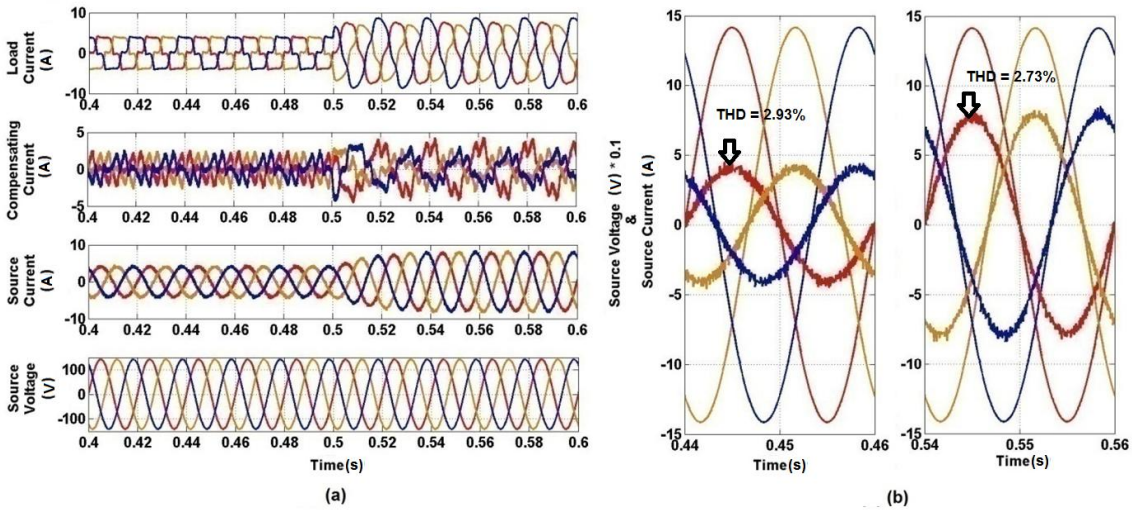

Fig. 2.13 (a) Application of an unbalanced load at t=0.5 s (I_a=5.84 A, I_b= 5.92 A and I_c=5.89 A) for α=0 (b) before and after the application of unbalanced load for one cycle each

2.5.2 Simulation results for rectifier fed RL load at α=30°

The simulated results with at α=30° are given below under different conditions:

2.5.2.1 Active filter is enabled

Fig. 2.14 (a) shows the waveforms of load current (1 kVA load), compensating current, source current and source voltage at α=30° with PI controller. The APF is initially disabled from t=0 to t=0.5 s. The compensating current is zero and source current is same as the load current. The source current is non sinusoidal with harmonics and is found to have THD of 37.57%. At t=0.5 s when the APF is enabled, the compensating current is applied at point of common coupling which makes the source current nearly sinusoidal unlike the load current. The THD of source current is now reduced to 4%. These waveforms show that after enabling, the shunt APF compensates for the reactive power demand and reduces the harmonic content in the source current. Fig. 2.14 (b) shows the waveforms of source current and source voltage from t=0.44 s to t=0.46 s and from t=0.54 s to t=0.56 s i.e. the response of the system for one cycle before and after the enabling of APF.

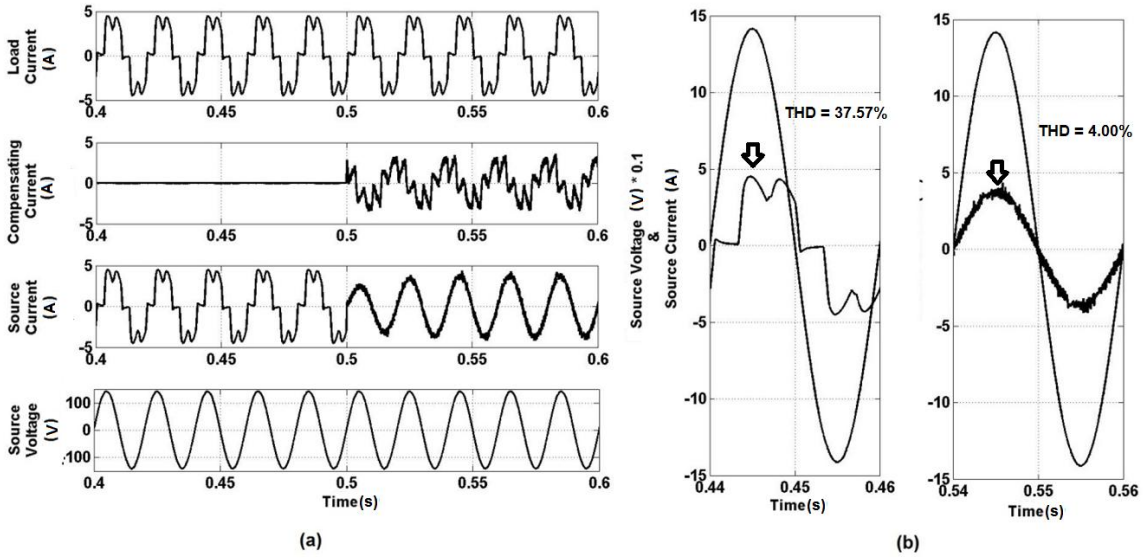

Fig. 2.14 (a) Response of active power filter at α=30° (b) Source voltage and current waveforms for one cycle before and after the enabling of active filter

2.5.2.2 Step change in load

Fig. 2.15 (a) shows the waveforms of load current, compensating current, source current and source voltage at α=30° with PI controller. Here, initially the load is 1 kVA up to t=0.5 s and at t=0.5 s the load is suddenly increased to 2 kVA and then, the load is brought back to 1kVA at t=0.7 s. The amplitude of load current, compensating current and source current also increases in response to the increase in load up to t=0.7 s, then they return to previous values. The source current is again found to be nearly sinusoidal. The quality of source current is measured in terms of its THD under these loading conditions. From the FFT

analysis of source current waveforms at 1 kVA and 2 kVA, the THD is 4% and 3.12% respectively. These waveforms show that after increment in load also, the shunt APF compensates the reactive power and reduces the harmonic content in the source current. Fig. 2.15 (b) shows the waveforms of source current and source voltage from t=0.44 s to t=0.46 s and from t=0.54 s to t=0.56 s means the response of the system for one cycle before and after the step change in load of APF. Transient is completed in about two cycles without any overshoot.

2.5.2.3 Unbalanced load

Fig. 2.16 (a) shows the waveforms of load current, compensating current, source current and source voltage at α=30° with PI controller. Here, initially the load is balanced up to t=0.5 s and at t=0.5 s. Unbalance is introduced by applying a linear star connected load in parallel to existing 1kVA load, with Ra=40 Ω, Rb=60 Ω and Rc=20 Ω. The amplitude of load current, and compensating current also changed by applying the unbalanced load. The source current is again found to be nearly sinusoidal. The quality of source current is measured in terms of its THD under these loading conditions. From the FFT analysis of source current waveforms at balanced load and unbalanced load, the THD is 4% and 3.93% respectively. These waveforms show that even with unbalanced load, the shunt APF compensates the reactive power and reduces the harmonic content in the source current. Fig. 2.16 (b) shows the waveforms of source current and source voltage from t=0.44 s to t=0.46 s and from t=0.54 s to t=0.56 s i.e. the response of the system for one cycle before and after the application of unbalanced load of APF. The source current becomes balanced after enabling APF even though the load is unbalanced.

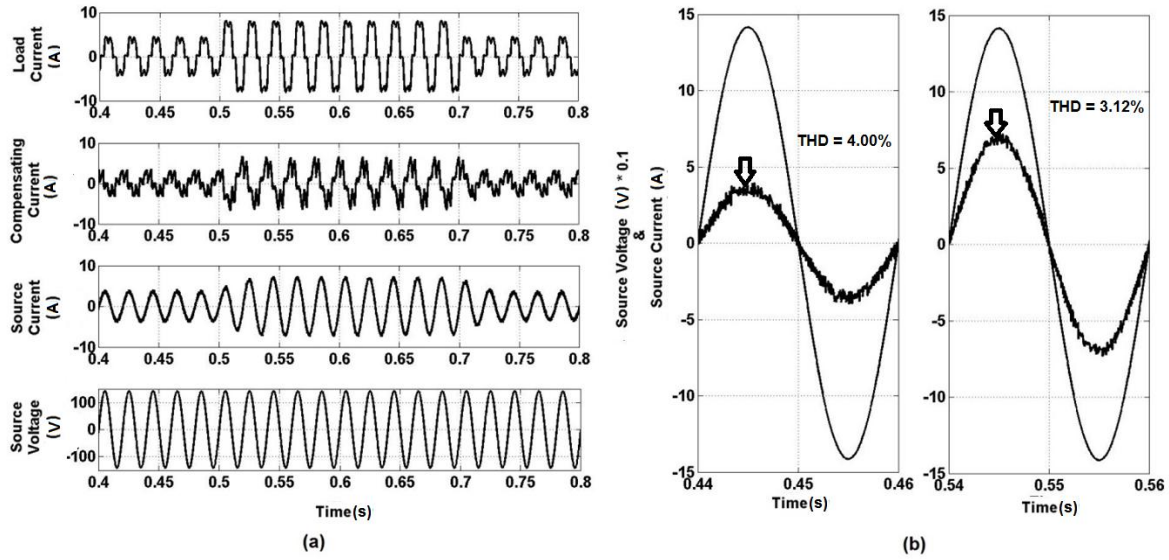

Fig. 2.15 (a) Step change in load of active power filter at α=30° (b) before and after the step change in load for one cycle each

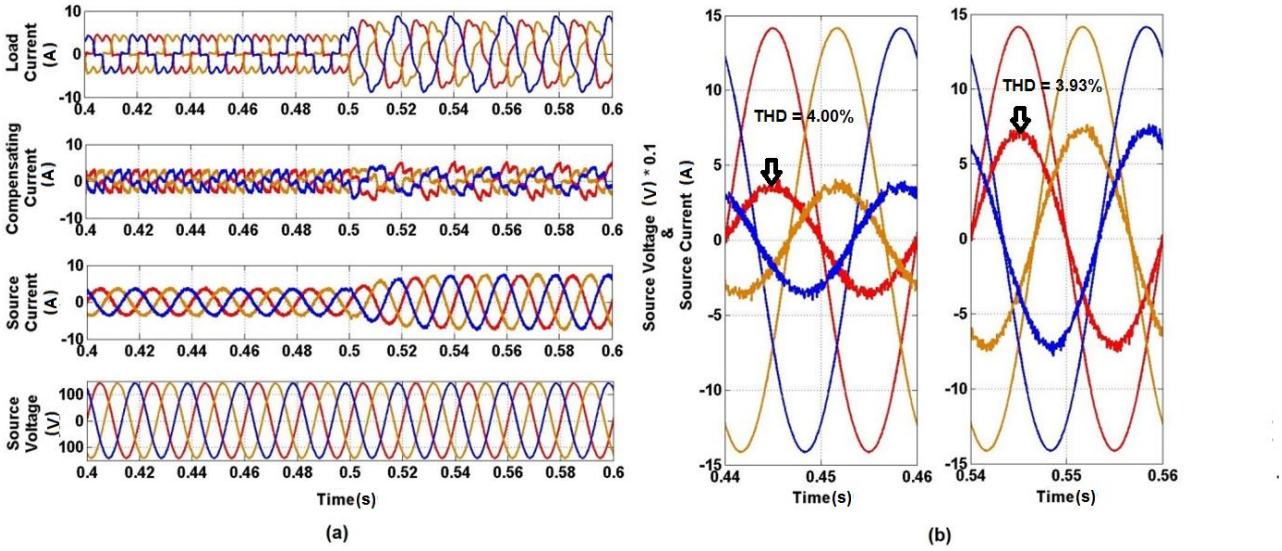

Fig. 2.16 (a) Application of an unbalanced load at t=0.5 s (I_a=4.88 A, I_b= 4.96 A and I_c=4.93 A) for α=30° (b) before and after the application of unbalanced load for one cycle each

2.5.3 Simulation results for rectifier fed RL load at α=60°

The simulated results with at α=60° are given below under different conditions:

2.5.3.1 Active filter is enabled

Fig. 2.17 (a) shows the waveforms of load current (1 kVA load), compensating current, source current and source voltage at α=60° with PI controller. The APF is initially disabled from t=0 to t=0.5 s. The compensating current is zero and source current is same as the load current. The source current is non sinusoidal with harmonics and is found to have THD of 64.36%. At t=0.5 s when the APF is enabled, the compensating current is applied at point of common coupling which makes the source current nearly sinusoidal unlike the load current. The THD of source current is now reduced to 5.97%. These waveforms show that after enabling, the shunt APF compensates for the reactive power demand and reduces the harmonic content in the source current. Fig. 2.17 (b) shows the waveforms of source current and source voltage from t=0.44 s to t=0.46 s and from t=0.54 s to t=0.56 s i.e. the response of the system for one cycle before and after the enabling of APF.

2.5.3.2 Step change in load

Fig. 2.18 (a) shows the waveforms of load current, compensating current, source current and source voltage at α=60° with PI controller. Here, initially the load is 1 kVA up to t=0.5 s and at t=0.5 s the load is suddenly increased to 2 kVA and then, the load is brought back to 1kVA at t=0.7 s. The amplitude of load current, compensating current and source current also increases in response to the increase in load up to t=0.7 s, then they return to previous values. The source current is again found to be nearly sinusoidal. The quality of

source current is measured in terms of its THD under these loading conditions. From the FFT analysis of source current waveforms at 1 kVA and 2 kVA, the THD is 5.97% and 4.37% respectively. These waveforms show that after increment in load also, the shunt APF compensates the reactive power and reduces the harmonic content in the source current. Fig. 2.18 (b) shows the waveforms of source current and source voltage from t=0.44 s to t=0.46 s and from t=0.54 s to t=0.56 s i.e. the response of the system for one cycle before and after the step change in load of APF. Transient is completed in about two cycles without any overshoot.

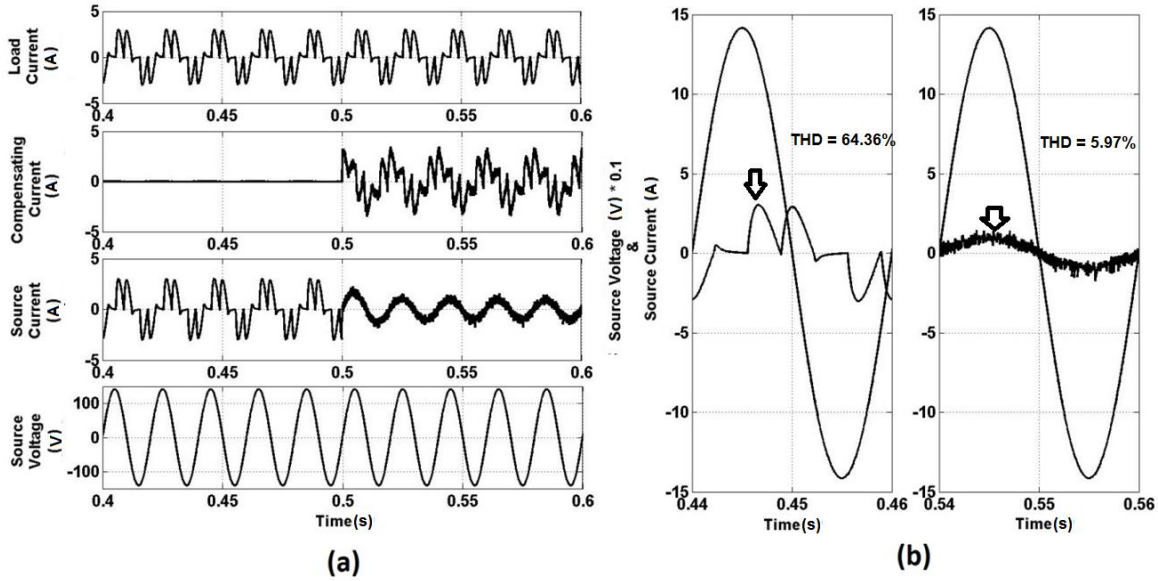

Fig. 2.17 (a) Response of active power filter at α=60° (b) Source voltage and current waveforms for one cycle before and after the enabling of active filter

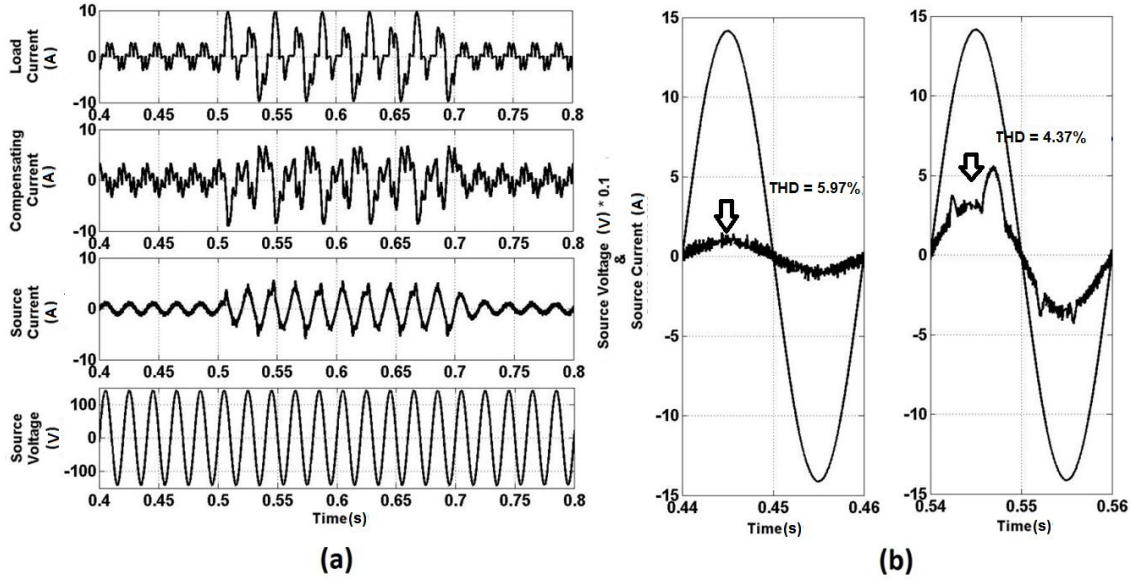

Fig. 2.18 (a) Step change in load of active power filter at α=60° (b) before and after the step change in load for one cycle each

2.5.3.3 Unbalanced load

Fig. 2.19 (a) shows the waveforms of load current, compensating current, source current and source voltage at α=60° with PI controller. Here, initially the load is balanced up to t=0.5 s and at t=0.5 s. Unbalance is introduced by applying a linear star connected load in parallel to existing 1kVA load, with Ra=40 Ω, Rb=60 Ω and Rc=20 Ω. The amplitudes of load current and compensating current are also changed by applying the unbalanced load. The source current is again found to be nearly sinusoidal. The quality of source current is measured in terms of its THD under these loading conditions. From the FFT analysis of source current waveforms at balanced load and unbalanced load, the THD is 5.97% and 5.38% respectively. These waveforms show that even with unbalanced load, the shunt APF compensates the reactive power and reduces the harmonic content in the source current. Fig. 2.19 (b) shows the waveforms of source current and source voltage from t=0.44 s to t=0.46 s and from t=0.54 s to t=0.56 s i.e. the response of the system for one cycle before and after the application of unbalanced load of APF. The source current becomes balanced after enabling APF even though the load is unbalanced.

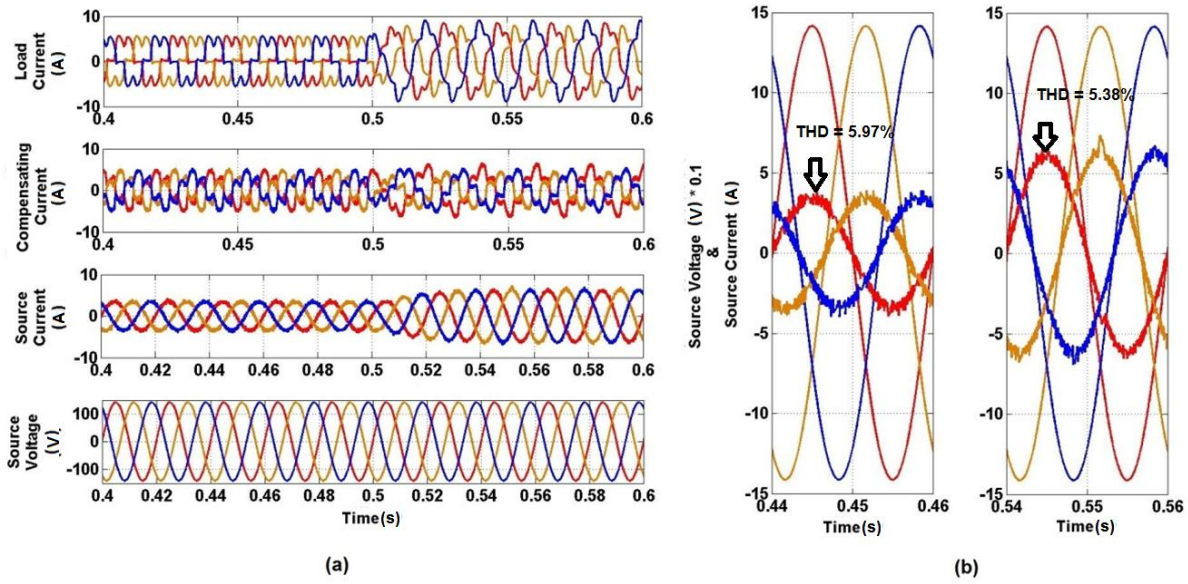

Fig. 2.19 (a) Application of an unbalanced load at t=0.5 s (I_a=3.66 A, I_b= 3.72 A and I_c=3.70 A) for α=60° (b) before and after the application of unbalanced load for one cycle each

2.6 Comparison of Simulation Response

The total harmonic distortion in source current after applying the APF is shown in table 2.2. THDs found at α=15º and 45º have also been included As per IEEE std. 519 [226], the source current THD should be lesser than 5%. As in table 2.3, the source current THD for firing angle 60° is more than 5% which is not permissible. The lower value of the source current THD can be achieved for higher firing angles by changing the proportional and integral gains of the PI controller. But, it is also not possible for changing the PI controller

parameters for each and every firing angle. So, the soft computing techniques are introduced to reduce the value of the source current THD within permissible limits of IEEE std. 519. The detailed comparison of all the source current THDs with various parameters will be discussed in Chapter 7. The corresponding graph showing the change of total harmonic distortion with respect to the firing angle is shown in Fig. 2.20. As the firing angle increases the source current total harmonic distortion also increases and crosses the permissible limit of source current THD i.e. 5% according to IEEE-std. 519.

Table 2.2 Total Harmonic Distortion for various firing angles with PI controller

S.No.	Firing angle (α in °)	Total Harmonic Distortion (THD in %)
1	0	2.93
2	15	3.25
3	30	4.00
4	45	4.35
5	60	5.97

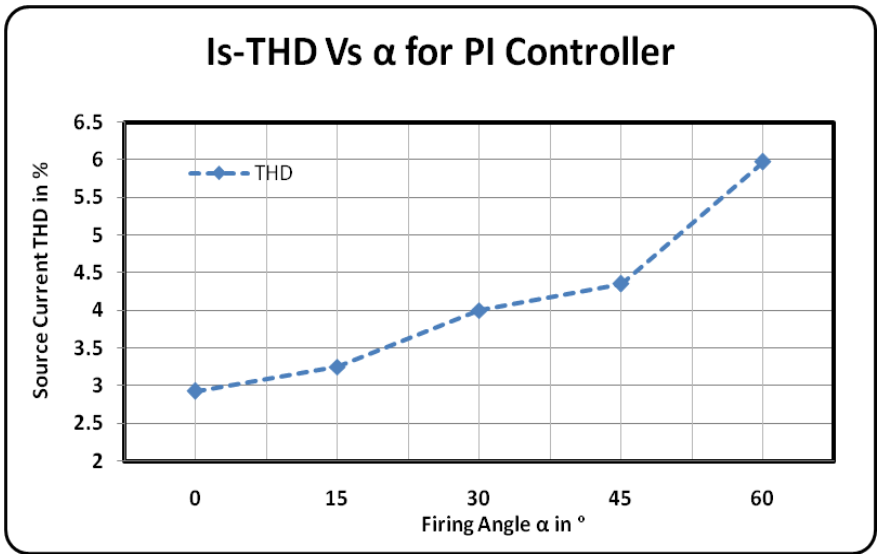

Fig. 2.20 Source current THD in percentage with respect to firing angle α in degree for PI controller

2.7 Conclusion

This chapter explained the basics of PI controller, block diagram of shunt APF, design of the parameters required for this system, simulation study of the PI controller based shunt APF. By looking at the results for different loads with various firing angles we can conclude that the PI controller based shunt APF is effective in mitigating the harmonics and compensating the reactive power. It is not good at higher firing angles as the source current total harmonic distortion crosses 5% which is not permissible according to IEEE-std. 519. For lower firing angles this method will be applicable for getting the permissible source current total harmonic distortion.

Chapter 3: FUZZY LOGIC BASED SHUNT ACTIVE POWER FILTER

3.1 Introduction

Artificial Intelligence (AI) is an area of computer science concerned with designing intelligent computer systems that exhibit the characteristics we associate with intelligence in human behaviour. However, the term intelligence is not very well defined and therefore has been less understood. Consequently, tasks associated with intelligence such as learning, intuition, creativity, and inference all seem to have been only partially understood.

The quest to comprehend, model and implement theories of intelligence, has not just registered modest success in developing techniques and methods for intelligent problem solving, but in its relentless pursuit, has fanned out to encompass a number of technologies in its fold. Some of these technologies include, but are not limited to, expert systems, neural networks, fuzzy logic, genetic algorithm and probabilistic reasoning. Of these technologies neural networks, fuzzy logic and probabilistic reasoning are known as soft computing. Probabilistic reasoning, generic algorithms, chaos are parts of learning theory.

According to Zadeh, soft computing differs from hard computing in its tolerance to imprecision, uncertainty and partial truth. Hard computing methods are predominantly based on mathematical approaches and therefore demand a high degree of precision and accuracy in their requirements. But in most of engineering problems, the input parameters cannot be determined with a high degree of precision and therefore, the best estimates of the parameters are used for obtaining solution to problems. This has restricted the use of mathematical approaches for the solution of inverse problems when compared to forward problems.

On the other hand, soft computing techniques, which have drawn their inherent characteristics from biological systems, present effective methods for the solution of even difficult inverse problems. The guiding principle of soft computing is exploiting the tolerance for imprecision, uncertainty and partial truth to achieve tractability, robustness and low cost solution.

3.2 Fuzzy Logic

Fuzzy set theory proposed in 1965 by Lotfi A.Zadeh is a generalization of classical set theory. Fuzzy logic representations founded on Fuzzy set theory, try to capture the way humans represent and reason with real world knowledge in the face of uncertainty. Uncertainty could arise due to generality, vagueness, ambiguity, chance or incomplete knowledge.

A fuzzy set can be defined mathematically by assigning to each possible individual in the universe of discourse, a value representing its grade of membership in the fuzzy set. This grade corresponds to the degree to which that individual is similar or compatible with the

concept represented by the fuzzy set. In other words, fuzzy sets support a flexible sense of membership of elements of a set.

In classical set theory, an element either belongs to or does not belong to a set and hence, such sets are termed crisp sets. But in a fuzzy set, many degrees of membership (between 0 and 1) are allowed. Thus, a membership function $\mu_A(x)$ is associated with a fuzzy set A such that the function maps every element of the universe of discourse X to the interval [0, 1].

The capability of fuzzy sets to express gradual transitions from membership ($0< \mu_A(x) \leq 1$) to non-membership ($\mu_A(x) = 0$) and vice versa has a broad utility. It not only provides for a meaningful and powerful representation of measurement of uncertainties, but also provides for a meaningful representation of vague concepts expressed in natural language.

Operations such as union, intersection, subset hood, product, equality, difference and disjunction are also defined on fuzzy sets. Fuzzy relations associate crisp sets to varying degree of membership and support operations such as union, intersection, subset hood, and composition of relations.

Just as crisp set theory has influenced symbolic logic, fuzzy set theory has given rise to fuzzy logic. While in symbolic logic, truth values true or false alone are accorded to propositions, in fuzzy logic multi valued truth values which are developed by a set of fuzzy IF-THEN rules are supported have found wide applications in real-world problems.

3.3 Fuzzy Inference System

Fuzzy inference system interlinks the fuzzy values into the crisp values and vice versa. It converts the linguistic or numerical inputs into numerical or linguistic outputs, based on the system requirement. The main parts of the fuzzy inference system are (Fig.3.1)

1. Fuzzification
2. Defuzzification
3. Decision Making Unit
4. Knowledge Base

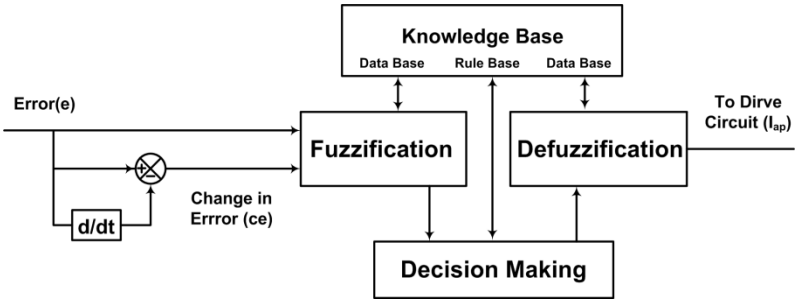

Fig. 3.1 Fuzzy Inference System

3.4 Fuzzification

Fuzziness in the fuzzy set is designed by the membership functions. There are many types of membership functions to represent an input variable. The value of membership function is in between 0 and 1. These membership functions are represented graphically. The main features of the membership functions are defined in following three properties:

1. Core,
2. Support and
3. Boundary.

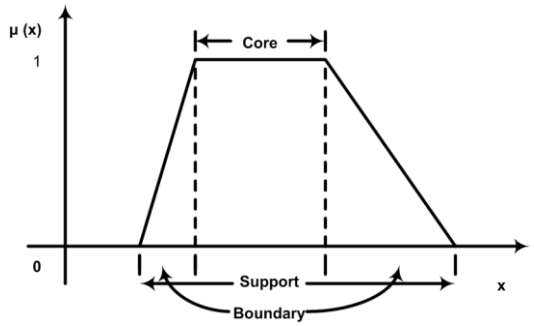

Fig. 3.2 Features of membership function

If the region of universe whose value of membership functions is 1 in the set of *P*, then this gives the core of the membership function of *P*. The elements which have membership value 1 are called elements of the core.

$$\mu_P(x) = 1$$

If the region of universe whose value of membership functions is non zero in the set of *P*, then this gives the support of the membership function of *P.* The elements which have membership value in between 0 and 1 are called elements of the support.

$$\mu_P(x) > 1$$

If the region of universe whose value of membership functions is non zero but not the full membership function, is called the boundary of the membership function of P. The elements whose membership value is a non zero but not 1 are the elements of the boundary.

$$0 < \mu_P(x) < 1$$

3.4.1 Membership Functions

1) Triangular membership function

The triangular curve is a function of a vector x, and depends on three scalar parameters *a*, *b*, and *c*, as described by

$$f(x;a,b,c)=\begin{cases}0, & x\le a\\ \dfrac{x-a}{b-a}, & a\le x\le b\\ \dfrac{c-x}{c-b}, & b\le x\le c\\ 0, & x\ge c\end{cases}$$

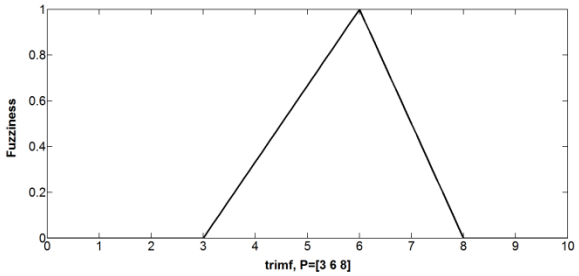

Fig. 3.3 Shape of the triangular membership function

The parameters *a* and *c* locate the "feet" of the triangle and the parameter *b* locates the peak. The Fig. 3.3 shows the shape of triangular membership function with a=3, b=6, c=8.

2) Trapezoidal membership function

The trapezoidal curve is a function of a vector, x, and depends on four scalar parameters *a*, *b*, *c*, and *d*, as described by

$$f(x;a,b,c,d)=\begin{cases}0, & x\le a\\ \dfrac{x-a}{b-a}, & a\le x\le b\\ 1, & b\le x\le c\\ \dfrac{c-x}{c-b}, & c\le x\le d\\ 0, & d\le x\end{cases}$$

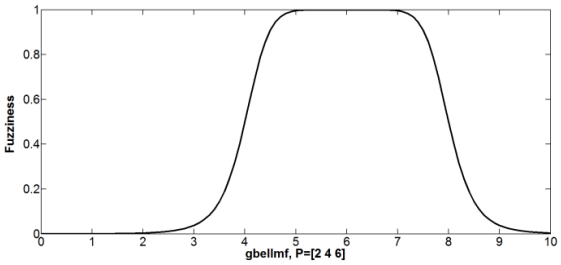

Fig. 3.4 Shape of the trapezoidal membership function

The parameters a and d locate the "feet" of the trapezoid and the parameters *b* and *c* locate the "shoulders". The Fig. 3.4 shows the shape trapezoidal membership function with a=1, b=5, c=7 and d=8.

3) Generalized bell membership function

The generalized bell function is a function of a vector x, and depends on three parameters *a*, *b*, and *c* as described by

$$f(x;a,b,c)=\frac{1}{1+\left|\dfrac{x-c}{a}\right|^{2b}}$$

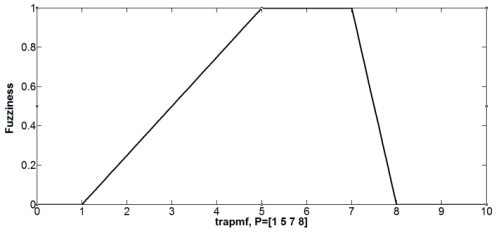

Fig. 3.5 Shape of the generalized bell membership function

where the parameter *b* is usually positive. The parameter *c* locates the center of the curve. Fig.3.5 shows the shape of gbell membership function with a=2, b=4 and c=6.

4) Gaussian membership function

The symmetric Gaussian function is a function of a vector x, and depends on two parameters a and b as given by

$$f(x;a,b) = e^{\frac{-(x-b)^2}{2a^2}}$$

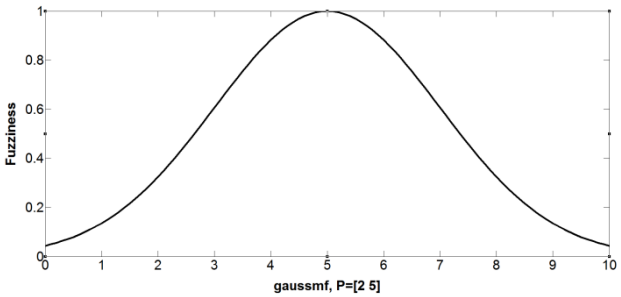

Fig. 3.6 Shape of the gaussian membership function

The Fig. 3.6 shows the shape of gauss membership function with a=2 and b=5.

Out of these membership functions, the triangular membership function is applied in present work for getting maximum fuzziness of designing the fuzzy inference system.

3.4.2 Membership Value Assignment

There are different methods of assigning membership values or functions to the fuzzy variables.

Intuition method is based on human's own intelligence and the skill of making the membership functions based on the system data and the performance. The knowledge of the linguistic variables should be known to get these membership functions.

Inference method depends on the known facts and the knowledge. It involves the knowledge of deductive reasoning.

The polling process is used to assign membership functions by rank ordering process. Preference is based on the pair wise comparison.

Angular fuzzy sets are different from other sets of fuzzy logic as it takes the coordinate description. These are applied in quantitative description of the linguistic variables known as truth table.

Neural networks are used to simulate the work just like the human brain. The given data is first converted into the training data and the testing data. The neural network is first trained with the training data and then tested with the testing data to get the perfect membership functions.

Genetic algorithm uses Darwin's theory of evolution. It is based on "the survival of existence" and the new category will come to exist while performing the reproduction, cross over and mutation of the existing category.

Inductive reasoning method can also be used to get the membership functions based on the characteristics of the system. This requires a strong data base of the input output relations. If the system is dynamic this method cannot be applicable as the relation keeps on changing.

3.5 Defuzzification

Method of converting fuzzy values, linguistic or numerical, into the crisp value or numerical is called Defuzzification. The following are different methods of defuzzification

1. Max-membership principle
2. Centroid method
3. Weighted average method
4. Mean–max membership
5. Centre of sums
6. Centre of largest area and
7. First of maxima or last of maxima

3.5.1 Max- Membership Principle

This method is also known as the height method as it converges the fuzzy values into the maximum of the entire fuzzy set.

It follows the expression as below

$$\mu(z^*) \geq \mu(z) \text{ Where } Z^* \in Z$$

This can also be represented pictorially as follows (Fig. 3.7)

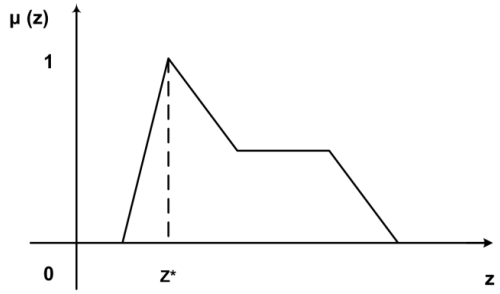

Fig. 3.7 Max- Membership Principle

3.5.2 Centroid Method

This method is also known as centre of gravity or centre of area method. This is widely used method as it takes the centre of the gravity, the mostly dense area, as the crisp value. This method is based on the expression

$$z^* = \int \frac{\mu(z) z dz}{\mu(z) dz}$$

The graphical representation is as shown in Fig. 3.8

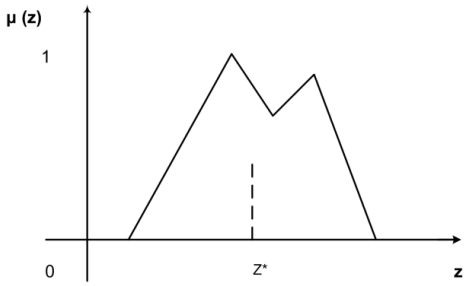

Fig. 3.8 Centroid Method

3.5.3 Weighted Average Method

This method can be used for the symmetric output membership functions only. This can be formed by weighing each membership output value with the largest membership value. The evaluated expression is

$$z^* = \frac{\sum \mu(z) z}{\sum \mu(z)}$$

The graphical representation is as shown in Fig. 3.9

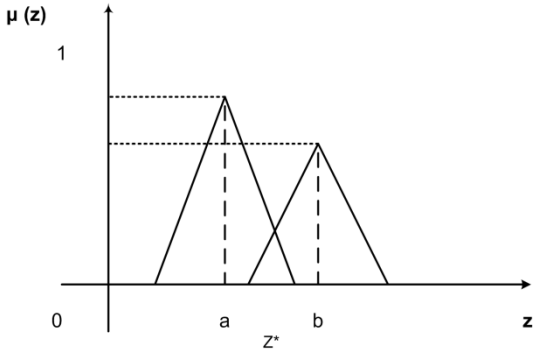

Fig. 3.9 Weighted Average Method

3.5.4 Mean- Max Method

This method is just like the Max- Membership Principle. Here it is taking the range of the maximum values unless the max- membership principle where only unique point is the maximum value. This is also known as middle of maxima method. The expression that governs this method is

$$z^* = \frac{a+b}{2}$$

The graphical representation is as shown in Fig. 3.10

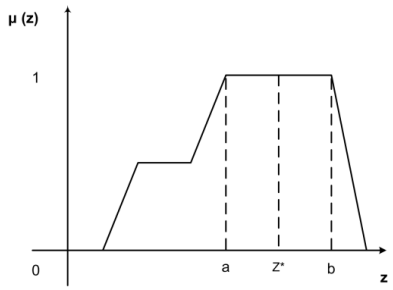

Fig. 3.10 Mean- Max Method

3.5.5 Centre of Sums Method

It involves algebraic sum of the two fuzzy sets *P1* and *P2* instead of union. The intersected area is added twice. This is like weighted average method where the highest membership value is considered.

The defuzzification value is

$$z^* = \frac{\int_2 z \sum_{k=1}^{n} \mu_{p_k}(z) dz}{\int_2 \sum_{k=1}^{n} \mu_{p_k}(z) dz}$$

The graphical representation is as shown in Fig. 3.11

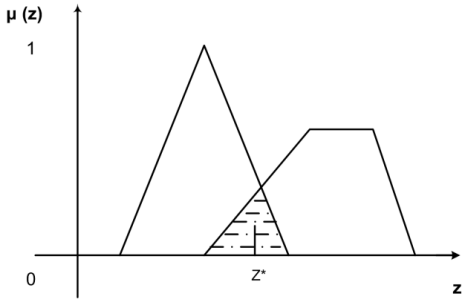

Fig. 3.11 Centre of Sums Method

3.5.6 Centre of largest area

If the fuzzy set consists of two convex sub regions then the entire convex sub region with the largest area represents the defuzzification value.

$$z^* = \frac{\int z \mu_{p_m}(z) dz}{\int \mu_{p_m}(z) dz}$$

The graphical representation is as shown in Fig. 3.12

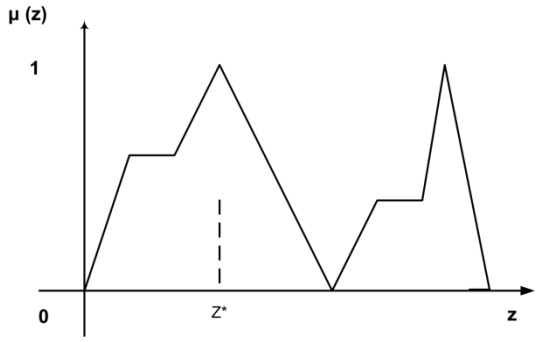

Fig. 3.12 Centre of largest area Method

3.5.7 First of Maxima or Last of Maxima

This method is based on the calculation of the all fuzzy sets used to determine the smallest membership value, with maximized degree of membership.

The evaluated formula is

Let largest height in the union is represented as $hgt(P_k)$ then it is found by

$$hgt(P_k) = \sup_{z \in Z}(\mu_{P_k}(z))$$

First of Maxima is found by

$$z^* = \inf_{z \in Z}(z \in Z / \mu_{P_k}(Z) = hgt(P_k))$$

Last of Maxima is found by

$$z^* = \sup_{z \in Z}(z \in Z / \mu_{P_k}(Z) = hgt(P_k))$$

Where inf = infirm denotes greatest lower bound

Sup = supremum denotes least upper bound

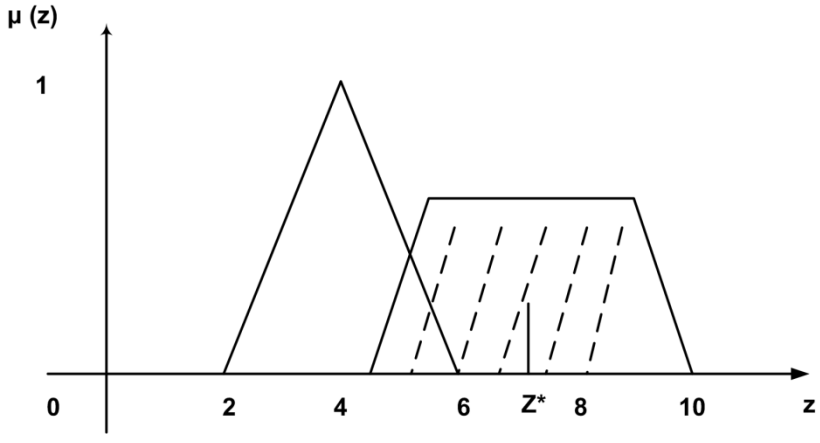

Fig. 3.13 First of Maxima or Last of Maxima Method

3.6 Implementation of fuzzy logic controller

Fig. 3.14 shows a schematic diagram used to simulate the APF using fuzzy logic controller. Here the measurement blocks are considered to measure the required voltages and currents at those places. The schematic diagram shows a fuzzy logic controller for DC link voltage control of shunt APF.

The MATLAB Simulink model of fuzzy logic controller is shown in Fig. 3.15. The fuzzy logic controller is placed in place of PI controller. The fuzzy logic controller is shown as AIC, i.e. Artificial Intelligence Controller, in Fig. 3.15. The input to fuzzy controller is the error in capacitor votage. The change in error will be the difference of the error and the unit delayed error. Error and change in error are fed to fuzzy logic controller block through the multiplexer. The fuzzy logic controller processes these signals to produce the necessary output. The final output of the fuzzy logic controller is fed to the control circuit which produces switching signals.

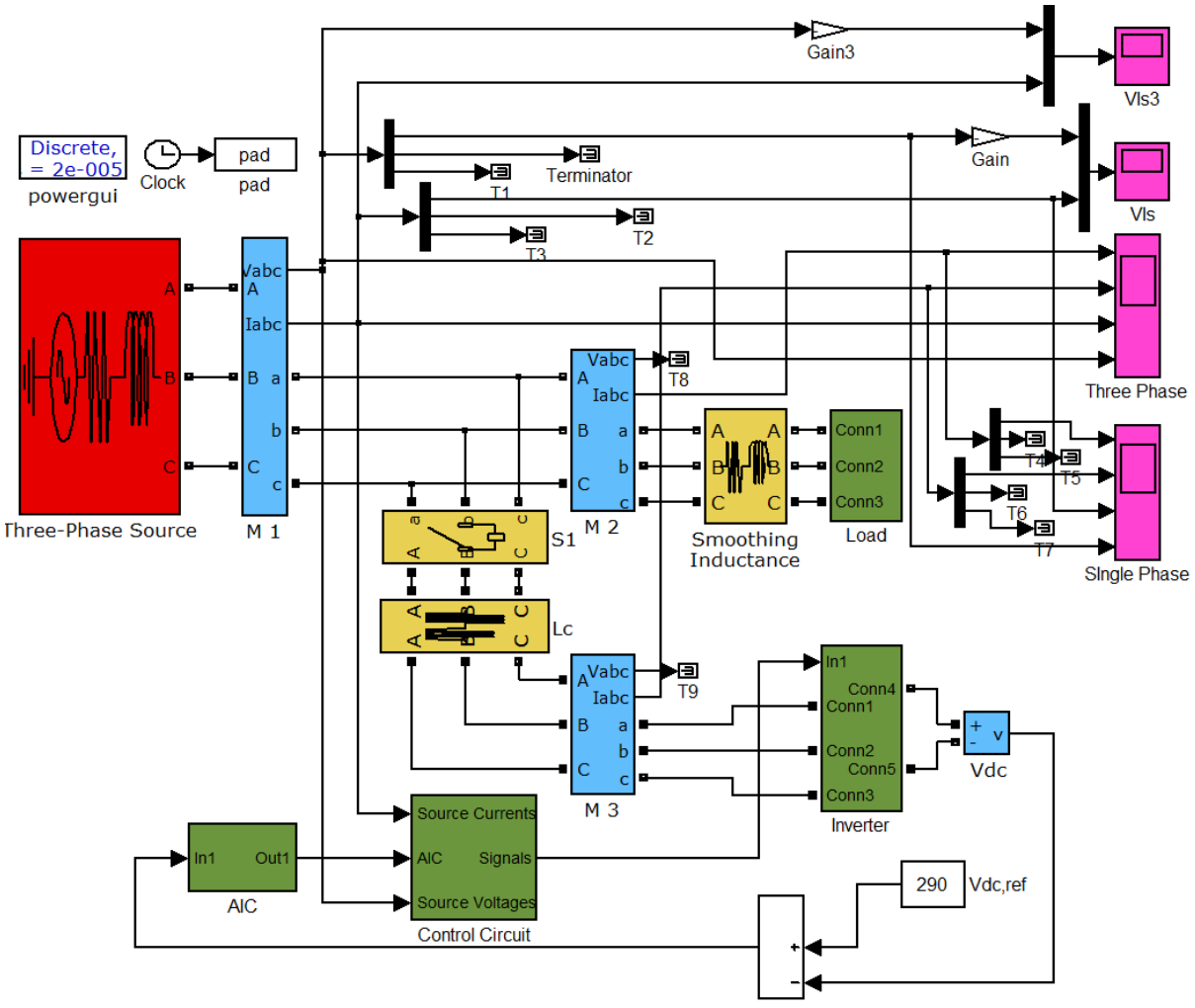

Fig. 3.14 Simulation diagram of shunt active power filter with fuzzy logic controller

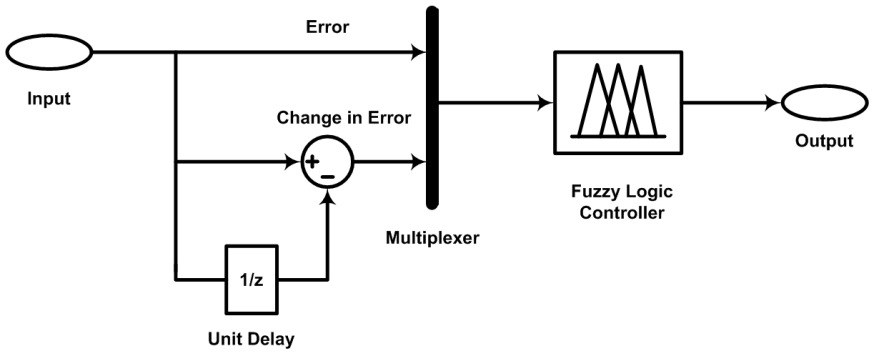

Fig. 3.15 Block diagram of the fuzzy logic controller

The fuzzy logic controller in the MATLAB is available as a Graphic User Interface. The fuzzy logic controller is configured as discussed below. The first thing is the fuzzy inference system (FIS) which has been choosen as Mamdani type as shown in Fig. 3.1. It consists of fuzzification, knowledge base, decision making and defuzzification methods. The fuzzification is done for two parameters called error and change in error. The FIS is shown in Fig. 3.16.

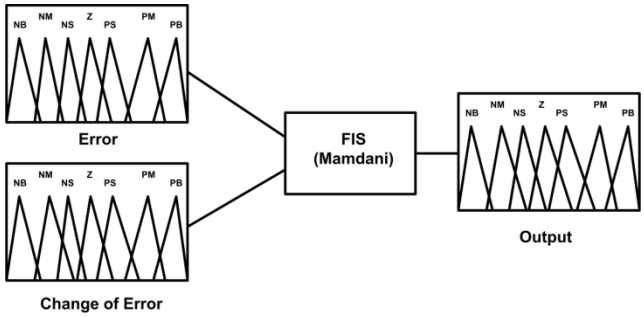

Fig. 3.16 Inputs, output and the FIS

As shown in Fig. 3.16, the input variables error and change of error and the output variables are assigned seven membership functions. The method of FIS used here is the Mamdani and that is also shown in the controller block with name as APF. The membership functions and type of membership fuctions of the input and output parameters of the FIS are shown in Fig. 3.17.

As shown in Fig. 3.17, the membership function of each parameter is the triangular membership function. Each parameter has seven membership functions named as negative big (NB), negative medium (NM), negative small (NS), zero (Z), positive small (PS), positive medium (PM) and positive big (PB). This can be done by using the section called membership value assignment. Out of seven methods of assigning membership values, intuition method is used in this work. By using the knowledge base, the values are assigned

by observing the data of the APF with the PI controller. The rules were defined as shown in Table 3.1.

The table contains the error on the left most column and the first row shows the change in error. All other letters represent the output values for the corresponding inputs of error and change in error. The defuzzification method used in this process is centroid method. Fig. 3.18 shows the surface view of the inputs and outputs. It shows the values of each parameter and their spread over in the graph in three dimensional view.The rule table can also be represented in linguistic form where the input1, input2 and output are given their respective membership linguistic assigned values as nb, nm, ns, z, ps, pm and pb as shown in Fig. 3.19.

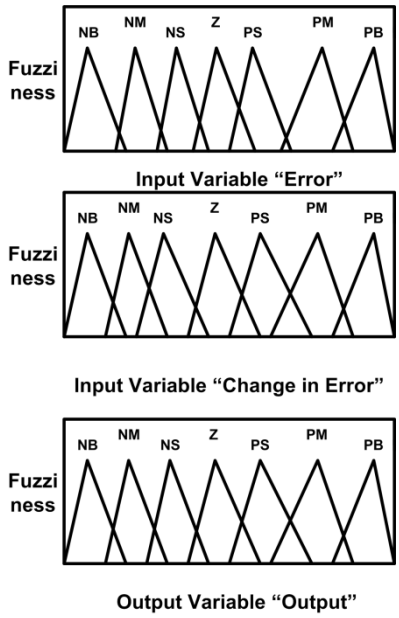

Fig. 3.17 Membership functions of inputs and output

Table 3.1 Rule Table of FIS

ce / e	NB	NM	NS	Z	PS	PM	PB
NB	NB	NB	NB	NB	NM	NS	Z
NM	NB	NB	NB	NM	NS	Z	PS
NS	NB	NB	NM	NS	Z	PS	PM
Z	NB	NM	NS	Z	PS	PM	PB
PS	NM	NS	Z	PS	PM	PB	PB
PM	NS	Z	PS	PM	PB	PB	PB
PB	Z	PS	PM	PB	PB	PB	PB

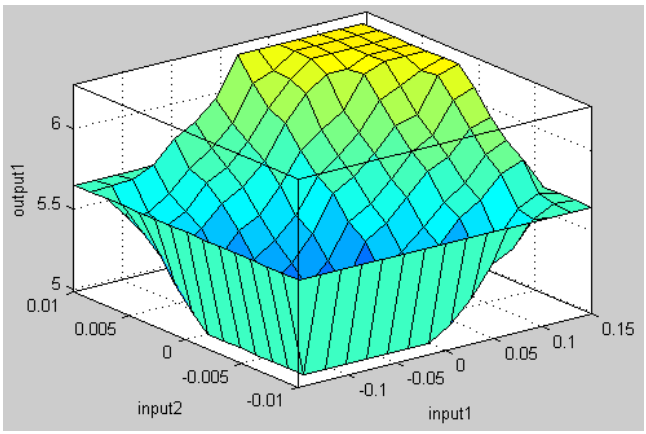

Fig. 3.18 Surface view of FIS

1. If (input1 is nb) and (input2 is nb) then (output1 is nb) (1)
2. If (input1 is nb) and (input2 is nm) then (output1 is nb) (1)
3. If (input1 is nb) and (input2 is ns) then (output1 is nb) (1)
4. If (input1 is nb) and (input2 is ze) then (output1 is nb) (1)
5. If (input1 is nb) and (input2 is ps) then (output1 is nm) (1)
6. If (input1 is nb) and (input2 is pm) then (output1 is ns) (1)
7. If (input1 is nb) and (input2 is pb) then (output1 is ze) (1)
8. If (input1 is nm) and (input2 is nb) then (output1 is nb) (1)
9. If (input1 is nm) and (input2 is nm) then (output1 is nb) (1)
10. If (input1 is nm) and (input2 is ns) then (output1 is nb) (1)
11. If (input1 is nm) and (input2 is ze) then (output1 is nm) (1)
12. If (input1 is nm) and (input2 is ps) then (output1 is ns) (1)
13. If (input1 is nm) and (input2 is pm) then (output1 is ze) (1)
14. If (input1 is nm) and (input2 is pb) then (output1 is ps) (1)
15. If (input1 is ns) and (input2 is nb) then (output1 is nb) (1)
16. If (input1 is ns) and (input2 is nm) then (output1 is nb) (1)
17. If (input1 is ns) and (input2 is ns) then (output1 is nm) (1)
18. If (input1 is ns) and (input2 is ze) then (output1 is ns) (1)
19. If (input1 is ns) and (input2 is ps) then (output1 is ze) (1)
20. If (input1 is ns) and (input2 is pm) then (output1 is ps) (1)
21. If (input1 is ns) and (input2 is pb) then (output1 is pm) (1)
22. If (input1 is ze) and (input2 is nb) then (output1 is nb) (1)
23. If (input1 is ze) and (input2 is nm) then (output1 is nm) (1)
24. If (input1 is ze) and (input2 is ns) then (output1 is ns) (1)
25. If (input1 is ze) and (input2 is ze) then (output1 is ze) (1)
26. If (input1 is ze) and (input2 is ps) then (output1 is ps) (1)
27. If (input1 is ze) and (input2 is pm) then (output1 is pm) (1)
28. If (input1 is ps) and (input2 is nb) then (output1 is nm) (1)
29. If (input1 is ps) and (input2 is nm) then (output1 is ns) (1)
30. If (input1 is ps) and (input2 is ns) then (output1 is ze) (1)
31. If (input1 is ps) and (input2 is ze) then (output1 is ps) (1)
32. If (input1 is ps) and (input2 is ps) then (output1 is pm) (1)
33. If (input1 is ps) and (input2 is pm) then (output1 is pb) (1)
34. If (input1 is ps) and (input2 is pb) then (output1 is pb) (1)
35. If (input1 is ze) and (input2 is pb) then (output1 is pb) (1)
36. If (input1 is pm) and (input2 is nb) then (output1 is ns) (1)
37. If (input1 is pm) and (input2 is nm) then (output1 is ze) (1)
38. If (input1 is pm) and (input2 is ns) then (output1 is ps) (1)
39. If (input1 is pm) and (input2 is ze) then (output1 is pm) (1)
40. If (input1 is pm) and (input2 is ps) then (output1 is pb) (1)
41. If (input1 is pm) and (input2 is pm) then (output1 is pb) (1)
42. If (input1 is pm) and (input2 is pb) then (output1 is pb) (1)
43. If (input1 is pb) and (input2 is nb) then (output1 is ze) (1)
44. If (input1 is pb) and (input2 is nm) then (output1 is ps) (1)
45. If (input1 is pb) and (input2 is ns) then (output1 is pm) (1)
46. If (input1 is pb) and (input2 is ze) then (output1 is pb) (1)
47. If (input1 is pb) and (input2 is ps) then (output1 is pb) (1)
48. If (input1 is pb) and (input2 is pm) then (output1 is pb) (1)
49. If (input1 is pb) and (input2 is pb) then (output1 is pb) (1)

Fig. 3.19 List of 49 rules of FIS

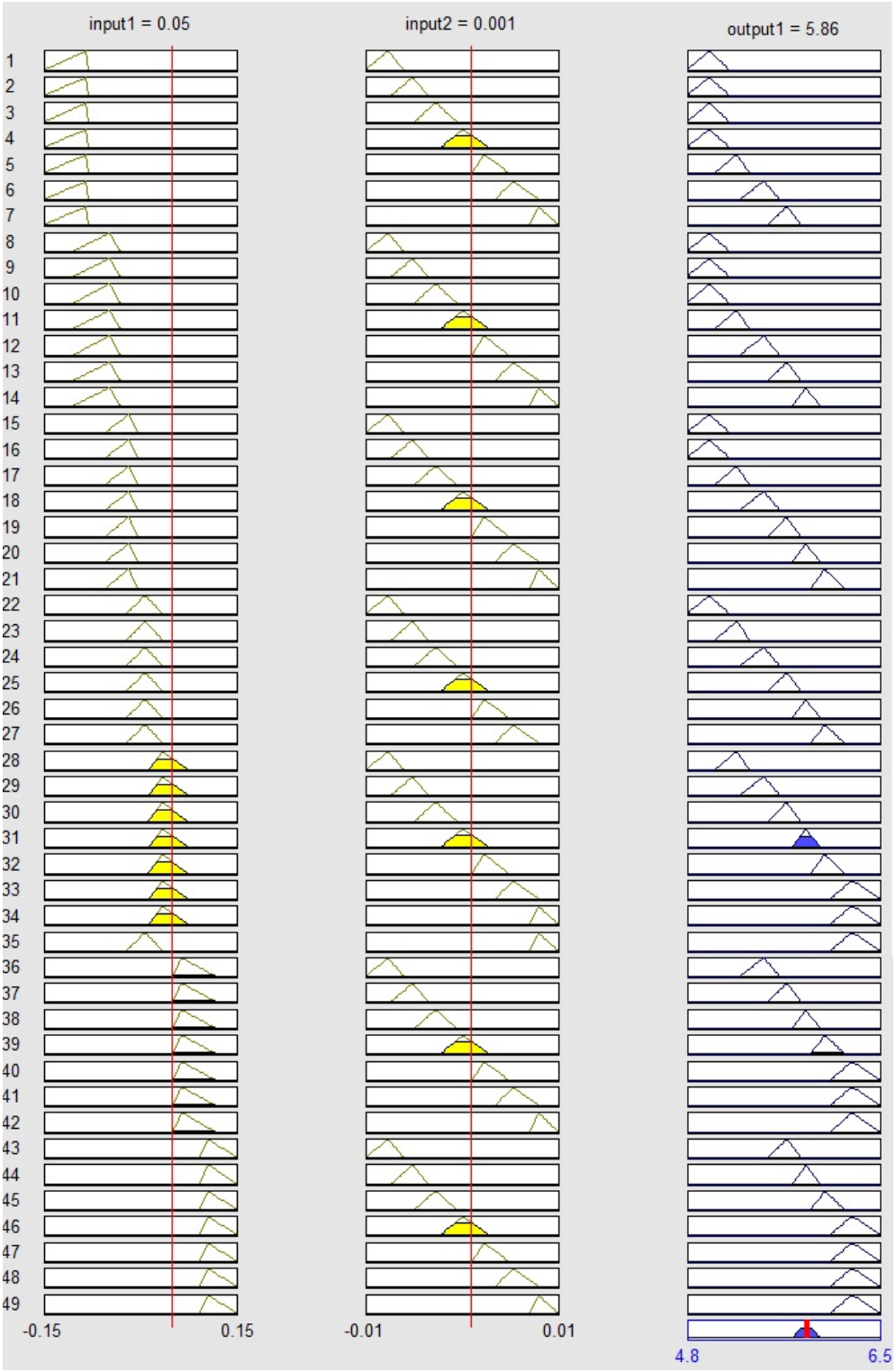

Fig. 3.20 Rule Viewer

Fig. 3.20 shows the rule viewer of FIS. It shows three vertical sets of figures which contain error, change in error and output for 49 rules. The selected value of the inputs are shown in red color. As in Fig. 3.20, the input1 called as error and the input2 called as change in error were set as 0 at red line. The min method is used to get the output of the controller from error and change in error and the max mehtod is used to get the ultimate output of the

49 rules from all individual outputs of each rule. This ultimate output is processed with defuzzification method i.e. centroid method. As in Fig. 3.20, the values taken for a study are Error = 0.05, Change in Error = 0.001 and output = 5.86. In this way within the range of error and change in error, the fuzzy inference system gives the required output. This output is the final controller output.

After setting all the range of error, change in error and output, writing the rules and the defuzzification method, the whole data is exported to workspace and saved as a .fis file. This fis file need to be called from the fuzzy logic controller block in MATLAB Simulink as shown in Fig. 3.14.

3.7 Simulation Results

The simulated results of the fuzzy logic controller based shunt APF are studied in this section. The load is a three phase thyristorised controlled rectifier feeing a series R-L load. Three settings of firing angle α are considered as 0, 30° and 60°. In each case, the response is obtained for following conditions:

- Active Filter is enabled with fixed and balanced load
- Step change in load, with active filter enabled
- Unbalanced load, with active filter enabled

3.7.1 Simulation results for rectifier fed RL load at α=0

The simulated results with at α=0 are given below under different conditions:

3.7.1.1 Active filter is enabled

Fig. 3.21 (a) shows the waveforms of load current (1 kVA load), compensating current, source current and source voltage at α=0 with fuzzy logic controller. The APF is initially disabled from t=0 to t=0.5 s. The compensating current is zero and source current is same as the load current. The source current is non sinusoidal with harmonics and is found to have THD of 30.64%. At t=0.5 s when the APF is enabled, the compensating current is applied at point of common coupling which makes the source current nearly sinusoidal unlike the load current. The THD of source current is now reduced to 2.71%. These waveforms show that after enabling, the shunt APF compensates the reactive power and reduces the harmonic content in the source current. Fig. 3.21 (b) shows the waveforms of source current and source voltage from t=0.44 s to t=0.46 s and from t=0.54 s to t=0.56 s i.e. the response of the system for one cycle before and after the enabling of APF.

3.7.1.2 Step change in load

Fig. 3.22 (a) shows the waveforms of load current, compensating current, source current and source voltage at α=0 with fuzzy logic controller. Here, initially the load is 1 kVA up to t=0.5 s and at t=0.5 s the load is suddenly increased to 2 kVA and then, the load is

brought back to 1kVA at t=0.7 s. The amplitude of load current, compensating current and source current also increases in response to the increase in load up to t=0.7 s, then they return to previous values. The source current is again found to be nearly sinusoidal. The quality of source current is measured in terms of its THD under these loading conditions. From the FFT analysis of source current waveforms at 1 kVA and 2 kVA, the THD is 2.71% and 2.65% respectively. These waveforms show that after increment in load also, the shunt APF compensates the reactive power and reduces the harmonic content in the source current. Fig. 3.22 (b) shows the waveforms of source current and source voltage from t=0.44 s to t=0.46 s and from t=0.54 s to t=0.56 s means the response of the system for one cycle before and after the step change in load of APF. Transient is completed in about two cycles without any overshoot.

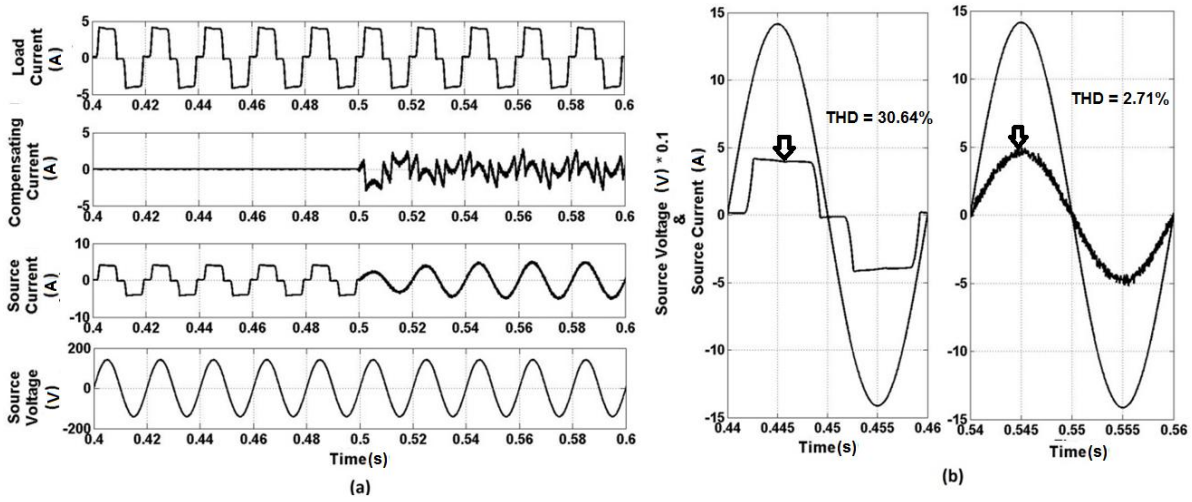

Fig. 3.21 (a) Response of active power filter at α=0 (b) Source voltage and current waveforms for one cycle before and after the enabling of active filter

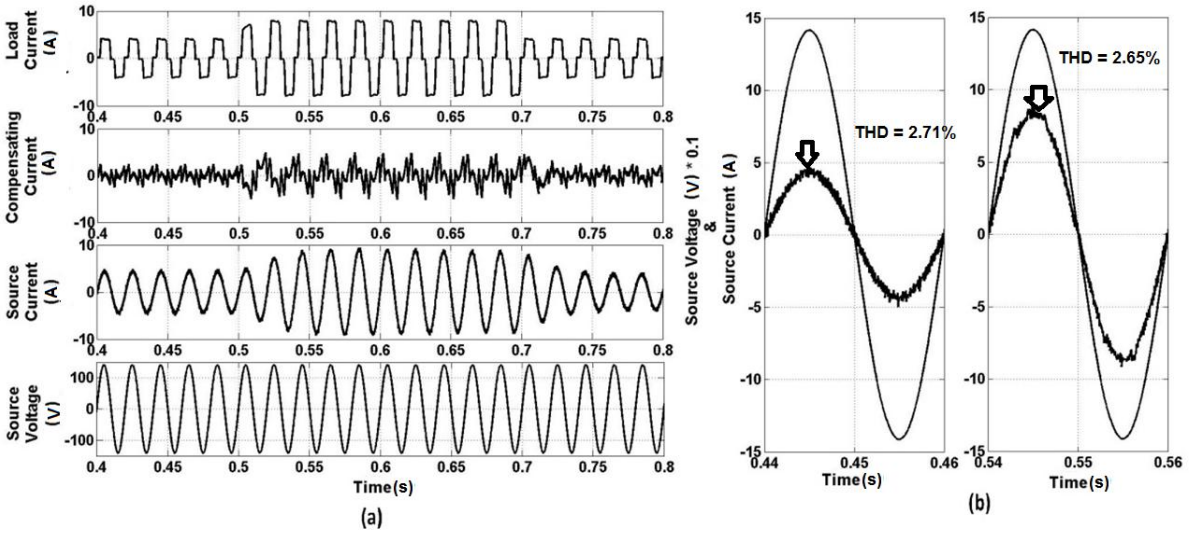

Fig. 3.22 (a) Step change in Load of active power filter at α=0 (b) before and after the step change in load for one cycle each

3.7.1.3 . Unbalanced load

Fig. 3.23 (a) shows the waveforms of load current, compensating current, source current and source voltage at α=0 with fuzzy logic controller. Here, initially the load is balanced up to t=0.5 s and at t=0.5 s. Unbalance is introduced by applying a linear star connected load in parallel to existing 1kVA load, with Ra=40 Ω, Rb=60 Ω and Rc=20 Ω. The amplitude of load current, and compensating current are also changed by applying the unbalanced load. The source current is again found to be nearly sinusoidal. The quality of source current is measured in terms of its THD under these loading conditions. From the FFT analysis of source current waveforms at balanced load and unbalanced load, the THD is 2.71% and 2.69% respectively. These waveforms show that even with unbalanced load, the shunt APF compensates the reactive power and reduces the harmonic content in the source current. Fig. 3.23 (b) shows the performance of source current and source voltage from t=0.44 s to t=0.46 s and from t=0.54 s to t=0.56 s i.e. the response of the system for one cycle before and after the application of unbalanced load of APF. The source current becomes balanced after enabling APF even though the load is unbalanced.

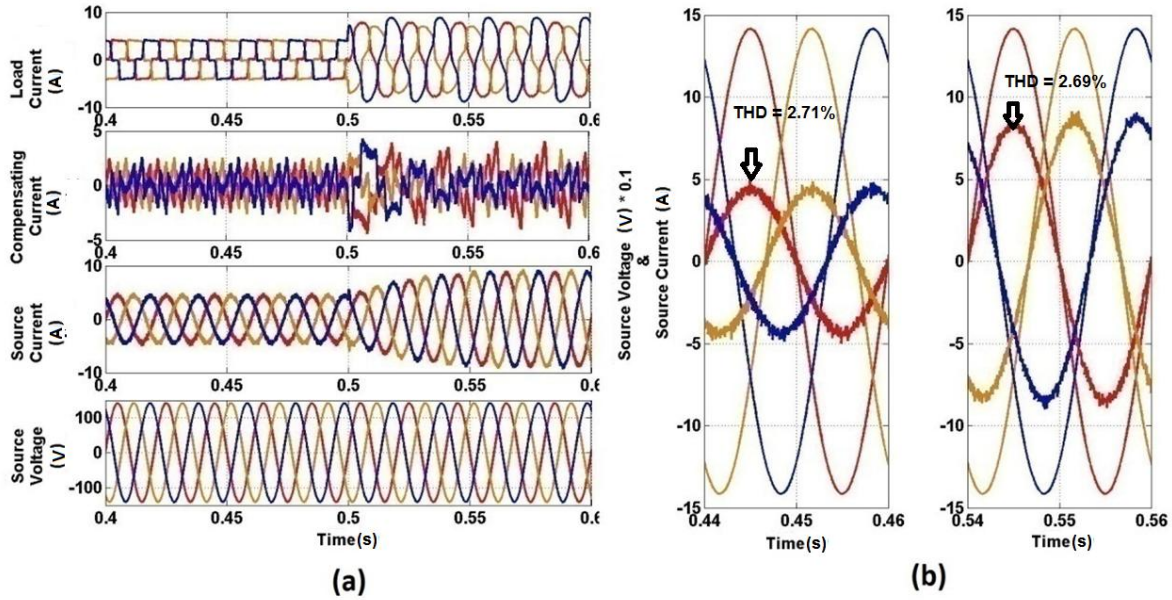

Fig. 3.23 (a) Application of an unbalanced load at t=0.5 s (I_a=5.82 A, I_b= 5.90 A and I_c=5.86 A) for α=0 (b) before and after the application of unbalanced load for one cycle each

3.7.2 Simulation results for rectifier fed RL load at α=30°

The simulated results with at α=30° are given below under different conditions:

3.7.2.1 Active filter is enabled

Fig. 3.24 (a) shows the waveforms of load current (1 kVA load), compensating current, source current and source voltage at α=30° with fuzzy logic controller. The APF is initially disabled from t=0 to t=0.5 s. The compensating current is zero and source current is same as

the load current. The source current is non sinusoidal with harmonics and is found to have THD of 37.57%. At t=0.5 s when the APF is enabled, the compensating current is applied at point of common coupling which makes the source current nearly sinusoidal unlike the load current. The THD of source current is now reduced to 2.88%. These waveforms show that after enabling, the shunt APF compensates the reactive power and reduces the harmonic content in the source current. Fig. 3.24 (b) shows the waveforms of source current and source voltage from t=0.44 s to t=0.46 s and from t=0.54 s to t=0.56 s i.e. the response of the system for one cycle before and after the enabling of APF.

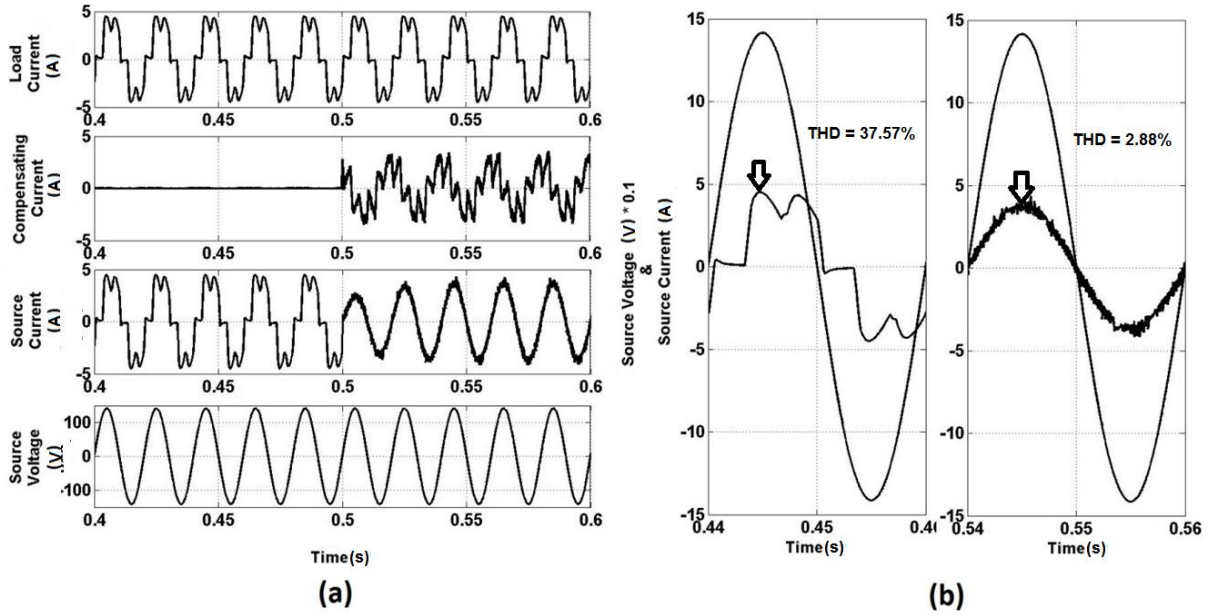

Fig. 3.24 (a) Response of active power filter at α=30° (b) Source voltage and current waveforms for one cycle before and after the enabling of active filter

3.7.2.2 Step change in load

Fig. 3.25 (a) shows the waveforms of load current, compensating current, source current and source voltage at α=30° with fuzzy logic controller. Here, initially the load is 1 kVA up to t=0.5 s and at t=0.5 s the load is suddenly increased to 2 kVA and then, the load is brought back to 1kVA at t=0.7 s. The amplitude of load current, compensating current and source current also increases in response to the increase in load up to t=0.7 s, then they return to previous values. The source current is again found to be nearly sinusoidal. The quality of source current is measured in terms of its THD under these loading conditions. From the FFT analysis of source current waveforms at 1 kVA and 2 kVA, the THD is 2.88% and 2.79% respectively. These waveforms show that after increment in load also, the shunt APF compensates the reactive power and reduces the harmonic content in the source current. Fig. 3.25 (b) shows the waveforms of source current and source voltage from t=0.44 s to t=0.46 s and from t=0.54 s to t=0.56 s i.e. the response of the system for one cycle

before and after the step change in load of APF. Transient is completed in about two cycles without any overshoot.

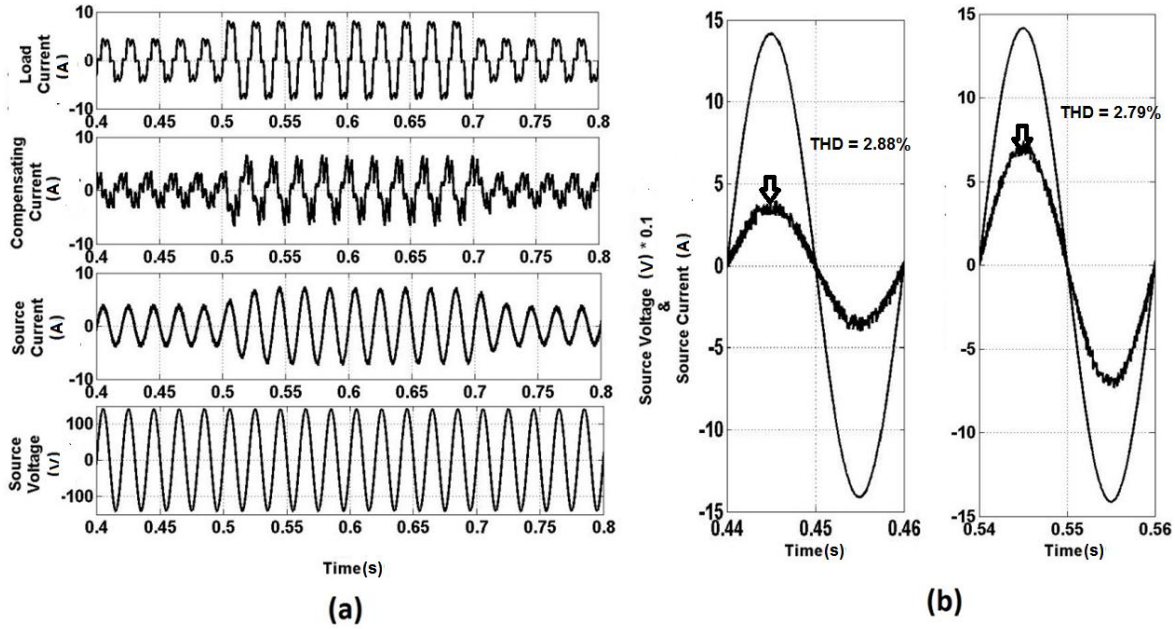

Fig. 3.25 (a) Step change in Load of active power filter at α=30° (b) before and after the step change in load for one cycle each

3.7.2.3 Unbalanced load

Fig. 3.26 (a) shows the waveforms of load current, compensating current, source current and source voltage at α=30° with fuzzy logic controller. Here, initially the load is balanced up to t=0.5 s and at t=0.5 s. Unbalance is introduced by applying a linear star connected load in parallel to existing 1kVA load, with Ra=40 Ω, Rb=60 Ω and Rc=20 Ω. The amplitude of load current, and compensating current are also changed by applying the unbalanced load. The source current is again found to be nearly sinusoidal. The quality of source current is measured in terms of its THD under these loading conditions. From the FFT analysis of source current waveforms at balanced load and unbalanced load, the THD is 2.88% and 2.82% respectively. These waveforms show that even with unbalanced load, the shunt APF compensates the reactive power and reduces the harmonic content in the source current. Fig. 3.26 (b) shows the waveforms of source current and source voltage from t=0.44 s to t=0.46 s and from t=0.54 s to t=0.56 s i.e. the response of the system for one cycle before and after the application of unbalanced load of APF. The source current becomes balanced after enabling APF even though the load is unbalanced.

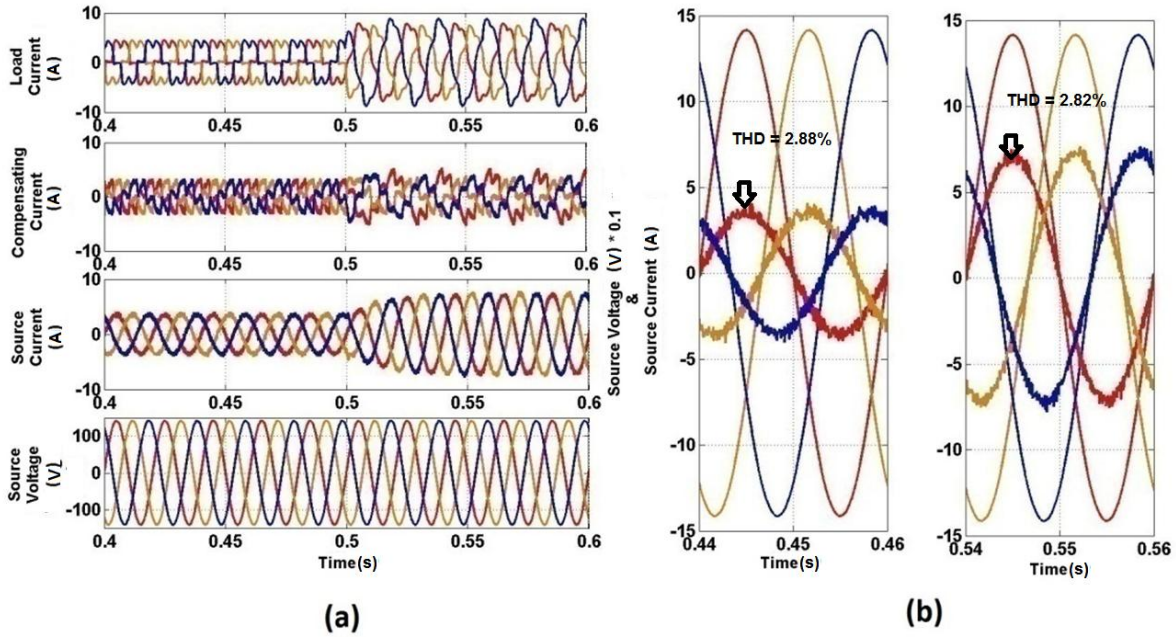

Fig. 3.26 (a) Application of an unbalanced load at t=0.5 s (I_a=4.86 A, I_b= 4.94 A and I_c=4.91 A) for α=30° (b) before and after the application of unbalanced load for one cycle each

3.7.3 Simulation results for rectifier fed RL load at α=60°

The simulated results with at α=60° are given below under different conditions:

3.7.3.1 Active filter is enabled

Fig. 3.27 (a) shows the waveforms of load current (1 kVA load), compensating current, source current and source voltage at α=60° with fuzzy logic controller. The APF is initially disabled from t=0 to t=0.5 s. The compensating current is zero and source current is same as the load current. The source current is non sinusoidal with harmonics and is found to have THD of 64.36%. At t=0.5 s when the APF is enabled, the compensating current is applied at point of common coupling which makes the source current nearly sinusoidal unlike the load current. The THD of source current is now reduced to 3.45%. These waveforms show that after enabling, the shunt APF compensates the reactive power and reduces the harmonic content in the source current. Fig. 3.27 (b) shows the waveforms of source current and source voltage from t=0.44 s to t=0.46 s and from t=0.54 s to t=0.56 s i.e. the response of the system for one cycle before and after the enabling of APF.

3.7.3.2 Step change in load

Fig. 3.28 (a) shows the waveforms of load current, compensating current, source current and source voltage at α=60° with fuzzy logic controller. Here, initially the load is 1 kVA up to t=0.5 s and at t=0.5 s the load is suddenly increased to 2 kVA and then, the load is brought back to 1kVA at t=0.7 s. The amplitude of load current, compensating current and source current also increases in response to the increase in load up to t=0.7 s, then they

return to previous values. The source current is again found to be nearly sinusoidal. The quality of source current is measured in terms of its THD under these loading conditions. From the FFT analysis of source current waveforms at 1 kVA and 2 kVA, the THD is 3.45% and 3.33% respectively. These waveforms show that after increment in load also, the shunt APF compensates the reactive power and reduces the harmonic content in the source current. Fig. 3.28 (b) shows the waveforms of source current and source voltage from t=0.44 s to t=0.46 s and from t=0.54 s to t=0.56 s i.e. the response of the system for one cycle before and after the step change in load of APF. Transient is completed in about two cycles without any overshoot.

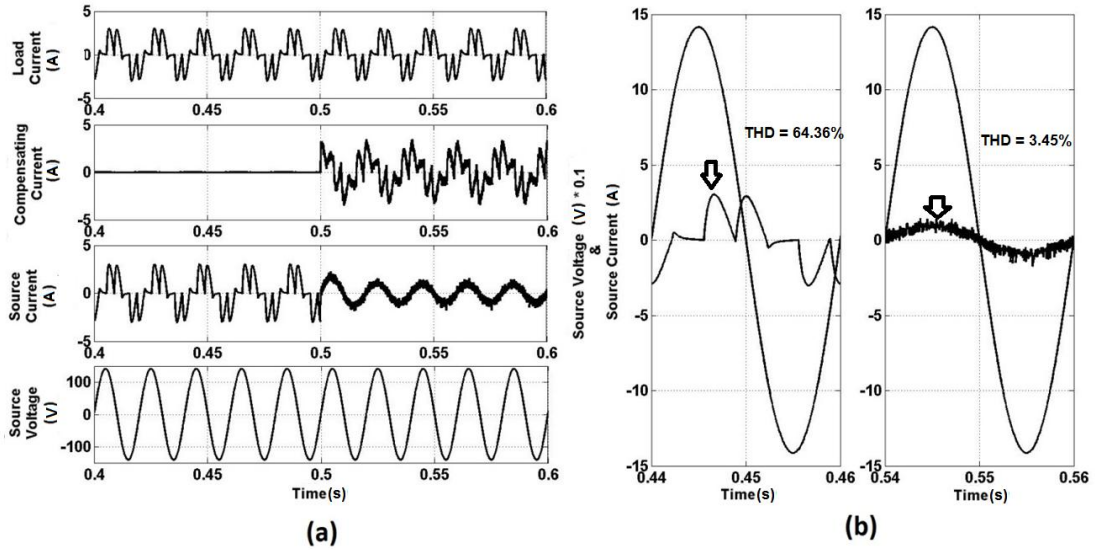

Fig. 3.27 (a) Response of active power filter at α=60° (b) Source voltage and current waveforms for one cycle before and after the enabling of active filter

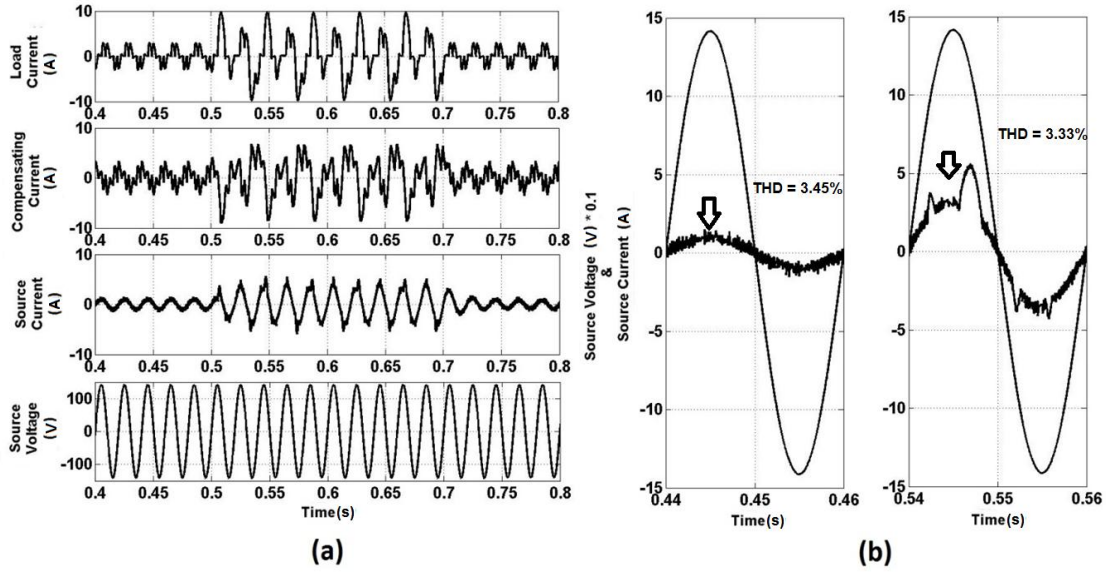

Fig. 3.28 (a)Step change in Load of active power filter at α=60° (b) before and after the step change in load for one cycle each

3.7.3.3 Unbalanced load

Fig. 3.29 (a) shows the waveforms of load current, compensating current, source current and source voltage at α=60° with fuzzy logic controller. Here, initially the load is balanced up to t=0.5 s and at t=0.5 s. Unbalance is introduced by applying a linear star connected load in parallel to existing 1kVA load, with Ra=40 Ω, Rb=60 Ω and Rc=20 Ω. The amplitude of load current and compensating current are also changed by applying the unbalanced load. The source current is again found to be nearly sinusoidal. The quality of source current is measured in terms of its THD under these loading conditions. From the FFT analysis of source current waveforms at balanced load and unbalanced load, the THD is 3.45% and 3.38% respectively. These waveforms show that even with unbalanced load, the shunt APF compensates the reactive power and reduces the harmonic content in the source current. Fig. 3.29 (b) shows the waveforms of source current and source voltage from t=0.44 s to t=0.46 s and from t=0.54 s to t=0.56 s i.e. the response of the system for one cycle before and after the application of unbalanced load of APF. The source current becomes balanced after enabling APF even though the load is unbalanced.

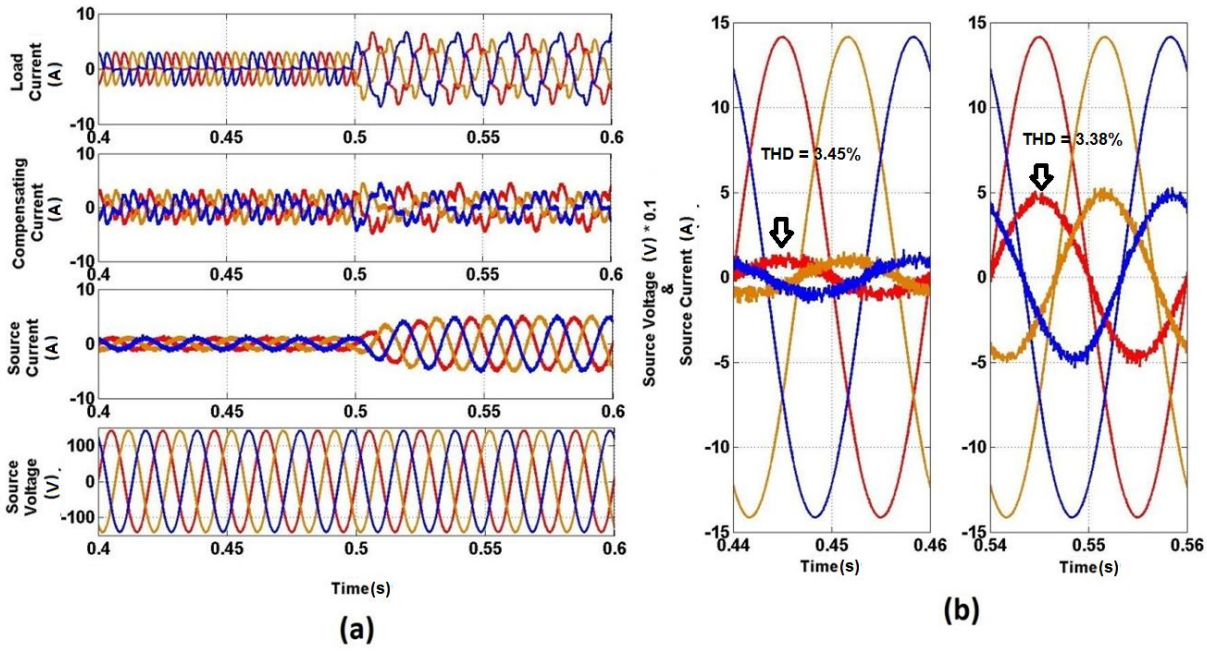

Fig. 3.29 (a) Application of an unbalanced load at t=0.5 s for (I_a=3.64 A, I_b= 3.70 A and I_c=3.68 A) α=60° (b) before and after the application of unbalanced load for one cycle each

3.8 Comparison of Simulation Response

The total harmonic distortion in source current after applying the APF is shown in Table 3.2. THDs found at α=15º and 45º have also been included. As per IEEE std. 519 [226], the source current THD should be lesser than 5%. The soft computing techniques are

introduced to get the lesser value of the source current THD which was permissible by IEEE std. 519. The detailed comparison of all the sourcecurrent THDs with various parameters will be discussed in Chapter 7. The corresponding graph showing the change of total harminic distortion with respect to the firing angle is reported in Fig. 3.30. As the firing angle increses the source current total harmonic distortion also increases.

Table 3.2 Total Harmonic Distortion for various firing angles with fuzzy logic controller

S.No.	Firing angle (α in °)	Total Harmonic Distortion (THD in %)
1	0	2.71
2	15	2.82
3	30	2.88
4	45	3.25
5	60	3.45

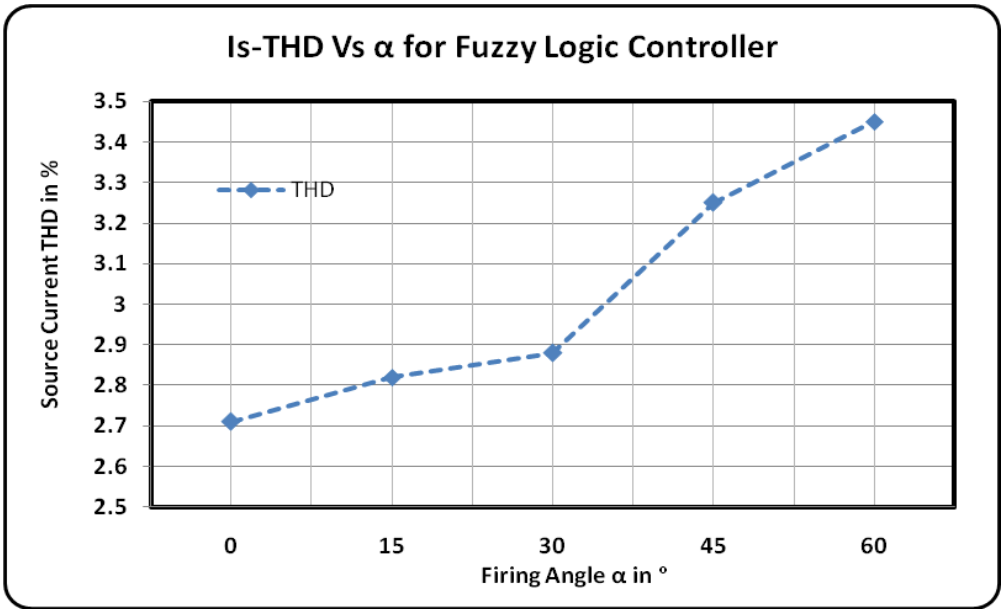

Fig. 3.30 Source Current THD in percentage with respect to Firing angle α in degree for fuzzy logic Controller

3.9 Conclusion

This chapter explained the basics of fuzzy logic controller, simulation system of shunt APF and simulation response of the fuzzy logic controller based shunt APF. By seeing the all the results for different loads with various firing angles we can conclude that the fuzzy logic controller based shunt APF is effective in mitigating the harmonics and compensating the reactive power. It's response is better even at higher firing angles as the source current total harmonic distortion does not cross 5% which is permissible according to IEEE-std. 519. For any firing angles this method will be applicable for getting the permissible source current total harmonic distortion.

4.1 Introduction

Neural Networks (NN) are simplified models of the biological nervous system and therefore have drawn their motivation from the kind of computing performed by a human brain. A NN, in general, is a highly inter connected network of a large number of processing elements called neurons in an architecture inspired by the brain. Neural networks exhibit characteristics such as mapping capabilities or pattern association, generalization, robustness, fault tolerance, and parallel and high speed information processing. Neural networks learn by examples. They can therefore be trained with known examples of a problem to acquire knowledge of it. Once appropriately trained, the network can be put to effective use in solving unknown or untrained instances of the problem.

This chapter explains the basics of neural network, Back-Propagation Algorithm used to train the neurons, implementation of neural network in MATLAB Simulink and the simulation results related to the present work.

4.2 Neural Networks

Neural networks are inspired from the biological nervous system. Fig. 4.1 shows two-input and one-output neural network. It comprises of the following parts:

1. Weights (w_1 and w_2)
2. Bias (b)
3. Activation Function (f(x))

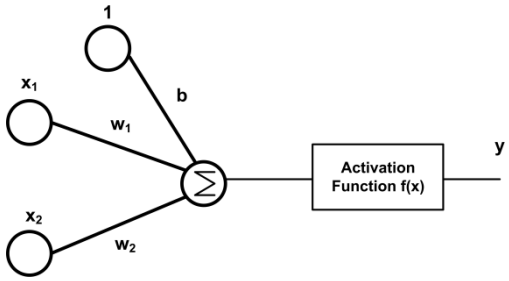

Fig. 4.1 A simple neural network

The net output becomes

$$y = f(b+x_1w_1+x_2w_2)$$

4.2.1 Weights

Fig. 4.1 shows the set of inputs x_1 and x_2, associated weights w_1 and w_2 respectively and the output y. The net output value y can be calculated by the activation of the net input which is sum of the product of each input and the weight raised by the corresponding inputs and the bias.

$$\text{Net input} = b+x_1w_1+x_2w_2$$

4.2.2 Bias

A bias is a weight on a connection from a unit whose input value is always unity. Increasing the bias increases the net input to the unit.

4.2.3 Activation Functions

The activation function is used to calculate the output response of the neuron. For the neurons of the same layer, same activation function is used. There are linear and non-linear activation functions as shown in Fig. 4.2. Non linear activation functions are used in multilayer networks.

Here are some of the commonly used activation functions

1) Identity Function

   $f(x)=x \; \forall \; x$

2) Binary Step Function

   $f(x)=1$; if $f(x) \geq \theta$

   $f(x)=0$; if $f(x) < \theta$ where θ is the threshold

3) Sigmoid Function

   $f(x)=\frac{1}{1+e^{-\sigma x}}$, where σ is steepness parameter

4) Bipolar Sigmoid Function

   $f(x)=\frac{1- e^{-\sigma x}}{1+e^{-\sigma x}}$

4.3 Classification of Data

The implementation of the neural networks depends on the previous or the current data of the system. The perfect utilization of the neural network depends on the perfect usage of the data. The data has to be used for the three purposes viz.

1. Training
2. Validating
3. Testing

4.4 Training Methods

Out of the available training methods, back propagation method has been chosen in this work. Back-Propagation is a multi layer forward network using extended gradient descent based delta learning rule, commonly known as Back-Propagation rule. The aim of this network is to train the net to achieve the balance between the ability to respond correctly to the input patterns that are used for training and the ability to provide target outputs.

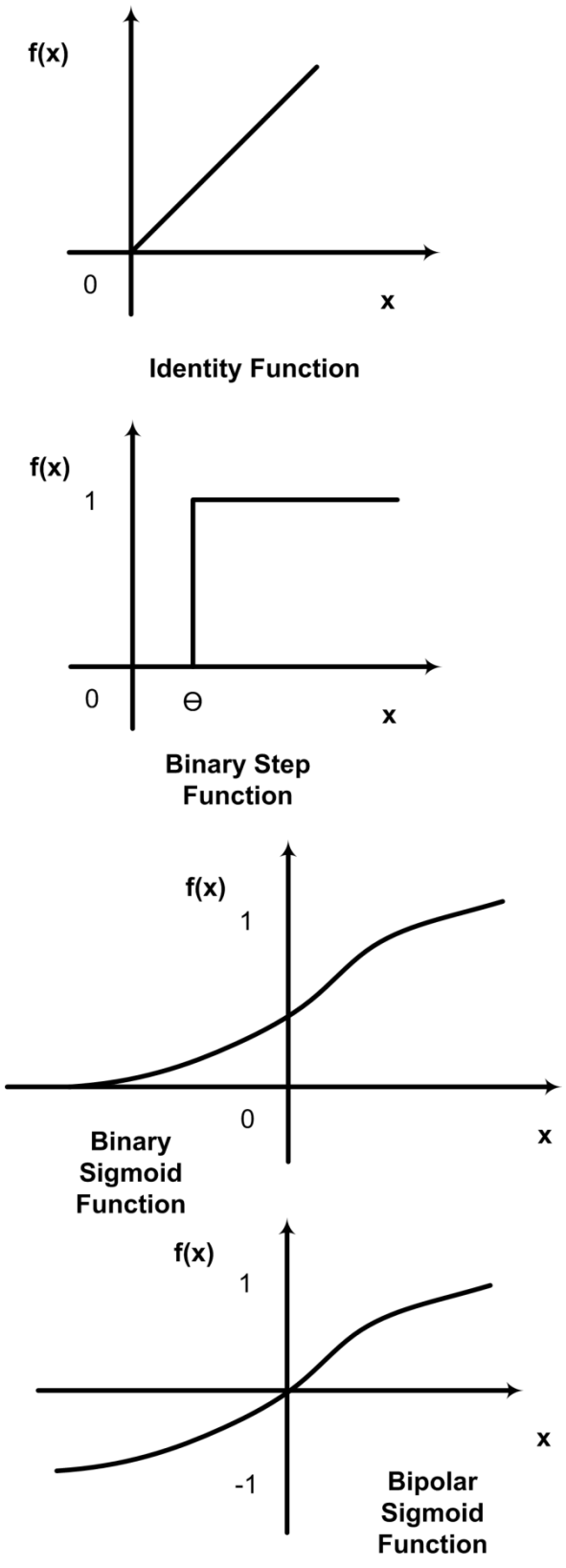

Fig. 4.2 Different Activation Functions

4.4.1 Back-Propagation Algorithm

The architecture of Back-Propagation network is shown in Fig. 4.3, having three layers named as Input Layer, Hidden Layer and Output Layer. Input Layer is x_1, x_2,....., x_i, ..., x_n. It starts from x_1, x_2, the generalized term x_i and the last term x_n.

Input Vector X = [x_1,x_2,.....,x_i,.....,x_n]

Hidden Layer Z = [z_1,z_2,.....,z_j,……,z_p]

Output Layer Y = [y_1,y_2,.....,y_k,……,y_m]

Hidden Layer Weights are

$$V=\begin{bmatrix} V_{11} & V_{12} & . & . & V_{1j} & . & . & V_{1p} \\ V_{21} & V_{22} & . & . & V_{2j} & . & . & V_{2p} \\ . & . & . & . & . & . & . & . \\ . & . & . & . & . & . & . & . \\ V_{i1} & V_{i2} & . & . & V_{ij} & . & . & V_{ip} \\ . & . & . & . & . & . & . & . \\ . & . & . & . & . & . & . & . \\ V_{n1} & V_{n2} & . & . & V_{nj} & . & . & V_{np} \end{bmatrix}$$

Output Layer Weights are

$$W=\begin{bmatrix} W_{11} & W_{12} & . & . & W_{1k} & . & . & W_{1m} \\ W_{21} & W_{22} & . & . & W_{2k} & . & . & W_{2m} \\ . & . & . & . & . & . & . & . \\ . & . & . & . & . & . & . & . \\ W_{j1} & W_{j2} & . & . & W_{jk} & . & . & W_{jm} \\ . & . & . & . & . & . & . & . \\ . & . & . & . & . & . & . & . \\ W_{p1} & W_{p2} & . & . & W_{pk} & . & . & W_{pm} \end{bmatrix}$$

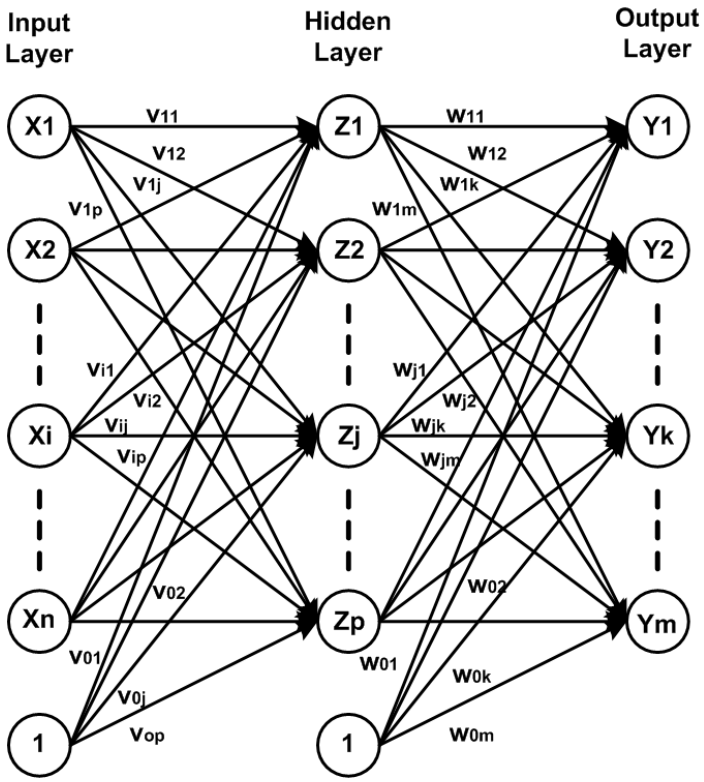

Fig. 4.3 Architecture of Back-Propagation Network

Bias on the hidden unit j

$$V_0 = [v_{01}, v_{02}, \ldots\ldots, v_{0j}, \ldots\ldots, v_{0p}]$$

Bias on the output unit k

$$W_0 = [w_{01}, w_{02}, \ldots\ldots, w_{0k}, \ldots\ldots, w_{0m}]$$

Target Vector $T = [t_1, t_2, \ldots\ldots, t_k, \ldots\ldots, t_m]$

The activation function considered is binary sigmoid function

This process is implemented in following seven steps:

Step: 1

Initialize the weight to random values.

Step: 2

While stopping condition is false, do step 3-7

Step: 3

Obtain the hidden layer values by multiplying the input values with corresponding weights and sum it up with bias. The corresponding equation is as follows

$$z_{-inj} = v_{0j} + \sum_{i=1}^{n} x_i v_{ij}$$

Applying activation function

$$Z_j = f(z_{-inj})$$

This can be sent to the next higher layer (output layer in this case)

Step: 4

Obtain the output layer values by multiplying the input values with corresponding weights and sum it up with bias. The corresponding equation is as follows

$$y_{-ink} = w_{0k} + \sum_{j=1}^{p} z_j w_{jk}$$

Applying activation function

$$Y_k = f(y_{-ink})$$

Step: 5

The error information term is calculated at the output unit k as follows

$$\delta_k = (t_k - Y_k) f'(y_{-ink})$$

$$\delta_k = (t_k - Y_k) f(y_{-ink})(1 - f(y_{-ink}))$$

$$\delta_k = (t_k - Y_k)(Y_k)(1 - Y_k)$$

Where δ_k denotes error at output unit k

Error back propagated to hidden layer is

$$\delta_{-inj} = \sum_{k=1}^{m} \delta_k w_{jk}$$

The error information term is calculated at the hidden unit j as follows

$$\delta_j = (\delta_{-inj}) f'(z_{-inj})$$

$$\delta_j = (\delta_{-inj}) f(z_{-inj})(1-f(z_{-inj}))$$

$$\delta_j = (\delta_{-inj})(Z_j)(1-Z_j)$$

Where δ_j denotes error at hidden unit j

Step: 6

Change in weight of the output layer is given by

$\Delta w_{jk} = \alpha \delta_k Z_j$, where α denotes learning rate.

Change in bias in the output layer is given by

$$\Delta w_{0k} = \alpha \delta_k$$

Therefore, the new weight and bias at output layer are as follow

$$w_{jk}(new) = w_{jk}(old) + \Delta w_{jk}$$

$$w_{0k}(new) = w_{0k}(old) + \Delta w_{0k}$$

Change in weight of the hidden layer is given by

$$\Delta v_{ij} = \alpha \delta_j x_i$$

Change in bias in the hidden layer is given by

$$\Delta v_{0j} = \alpha \delta_j$$

Therefore, the new weight and bias at output layer are as follow

$$v_{ij}(new) = v_{ij}(old) + \Delta v_{ij}$$

$$v_{0j}(new) = v_{0j}(old) + \Delta v_{0j}$$

Step: 7

Test the stopping condition and go to step 2 if necessary. The entire procedure of implementing the Back-Propagation algorithm is explained step by step as a flow chart in Fig. 4.4.

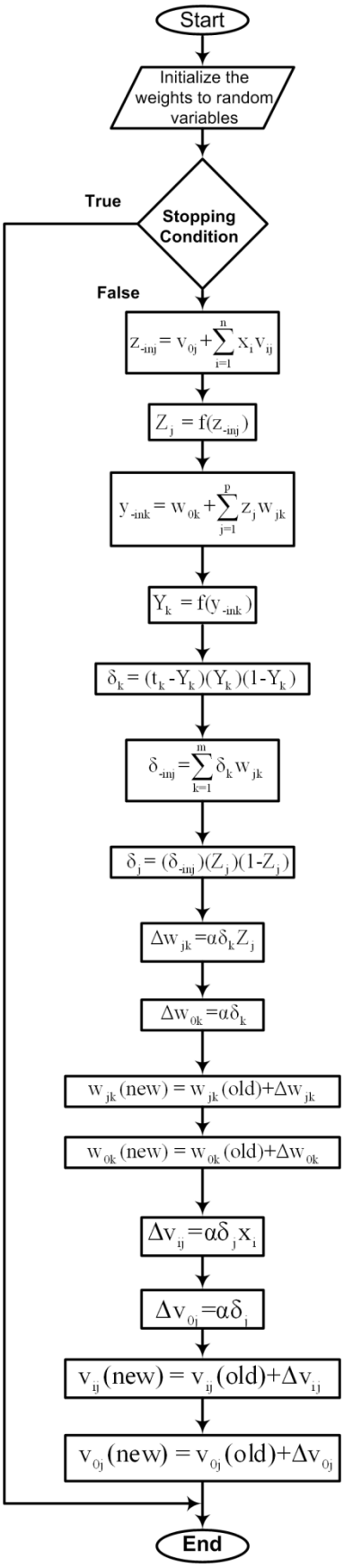

Fig. 4.4 Flow chart of Back-Propagation network

4.5 Implementation of Neural Network based Active Power Filter

This section deals with the application of NN in the APF. Following steps are used to develop neural network in MATLAB NFTOOL environment (Neural Network fitting tool)

1. Select a Network
2. Select Data
3. Classify the data into training data, validation data and test data
4. Network Size
5. Train the Network
6. Evaluate the Network
7. Save the Results

In the step 1 the feed-forward neural network is selected with two layers. This network is mapped between a data set of numeric inputs and a set of numeric targets. A two-layer feed-forward network consists of a set of sigmoid hidden neurons and linear output neurons, which can fit multi-dimensional mapping problem, given that there is enough training data and enough neurons in its hidden layer as in Fig. 4.6.

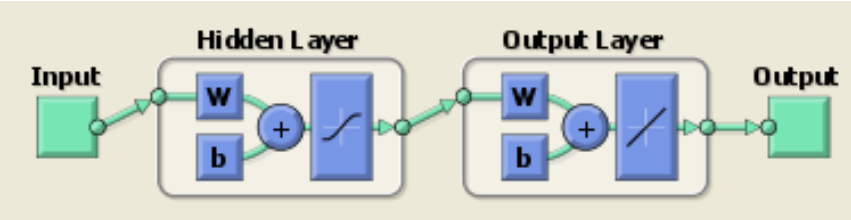

Fig. 4.5 Structure of two layered neural network

In step 2, the input and target data are given to the network from the files saved in workspace or in a computer. In step 3, the complete data is divided into three kinds of samples viz. Training, Validating and Testing Data. In step 4, the number of hidden neurons has to be specified to get the required training. If the training is unsatisfactory then the number of hidden neurons should be changed in this step.

In step 5, the network is trained with Leven Berg-Marquardt Back-Propagation algorithm. Training automatically stops when generalization stops improving, as indicated by an increase in the mean square error of the validation samples. In step 6, the network is evaluated. In this step, the network is optionally tested for the correctness of the target data.

The above steps are repeated for selecting more data (step 2), changing size of network (step 4) and training the network (step 5). In step7, the results which are generated by the network can be saved, can generate an M-file or can generate a simulink diagram.

Fig. 4.6 shows the first step of the process to indicate the layers and their structures of the neural network.

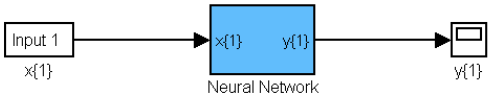

Fig. 4.6 Generated Block with Input and Target

4.6 Simulation Results

The simulated results of the neural network based shunt APF are studied in this section. The load is a three-phase thyristorised controlled rectifier feeding a series R-L load. Three settings of firing angle α is considered as 0, 30º and 60º. In each case, The response is obtained for following conditions:

- Active filter is enabled with fixed and balanced load
- Step change in load with active filter enabled
- Unbalanced load with active filter enabled

4.6.1 Simulation results for rectifier fed RL load at α=0

The simulated results with at α=0 are given below under different conditions:

4.6.1.1 Active filter is enabled

Fig. 4.7 (a) shows the waveforms of load current (1 kVA load), compensating current, source current and source voltage at α=0 with neural network controller. The APF is initially disabled from t=0 to t=0.5 s. The compensating current is zero and source current is same as the load current. The source current is non sinusoidal with harmonics and is found to have THD of 30.64%. At t=0.5 s when the APF is enabled, the compensating current is applied at point of common coupling which makes the source current nearly sinusoidal unlike the load current. The THD of source current is now reduced to 2.43%. These waveforms show that after enabling, the shunt APF compensates for the reactive power demand and reduces the harmonic content in the source current. Fig. 4.7 (b) shows the waveforms of source current and source voltage from t=0.44 s to t=0.46 s and from t=0.54 s to t=0.56 s i.e. the response of the system for one cycle before and after the enabling of APF.

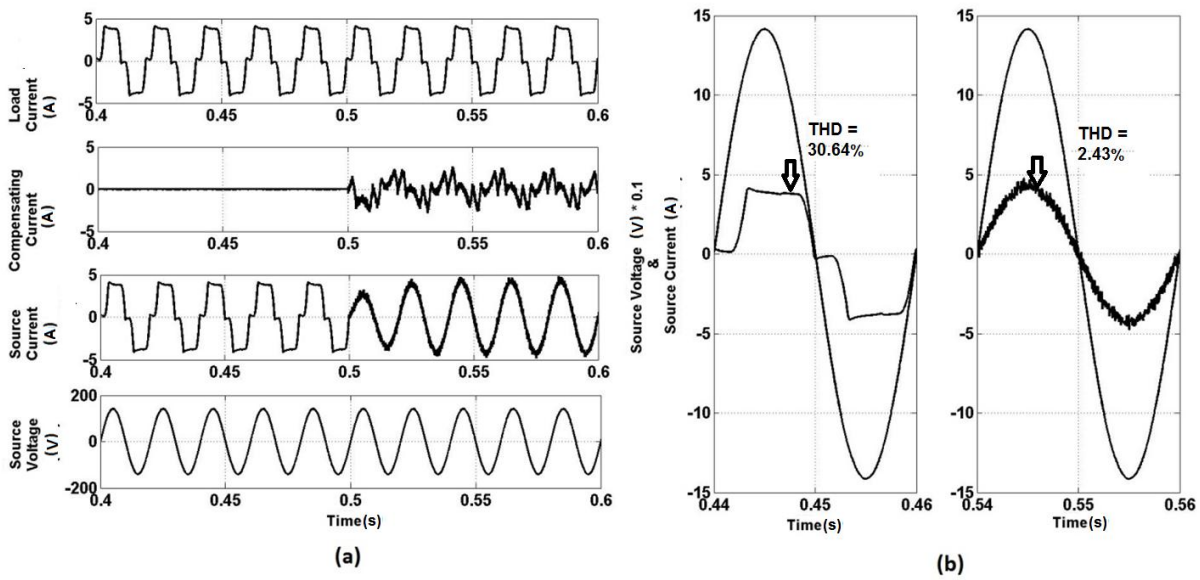

Fig. 4.7 (a) Response of active power filter at α=0 (b) Source voltage and current waveforms for one cycle before and after the enabling of active filter

4.6.1.2 Step change in load

Fig. 4.8 (a) shows the waveforms of load current, compensating current, source current and source voltage at α=0° with neural network controller. Here, initially the load is 1 kVA up to t=0.5 s and at t=0.5 s the load is suddenly increased to 2 kVA and then, the load is brought back to 1kVA at t=0.7 s. The amplitude of load current, compensating current and source current also increase in response to the increase in load up to t=0.7 s, then they return to previous values. The source current is again found to be nearly sinusoidal. The quality of source current is measured in terms of its THD under these loading conditions. From the FFT analysis of source current waveforms at 1 kVA and 2 kVA, the THD is 2.43% and 2.33% respectively. These waveforms show that after increment in load, the shunt APF continues to compensate the reactive power and reduces the harmonic content in the source current. Fig. 4.8 (b) shows the waveforms of source current and source voltage from t=0.44 s to t=0.46 s and from t=0.54 s to t=0.56 s i.e. the response of the system for one cycle before and after the step change in load of APF. The transient is completed in about two cycles without any overshoot.

4.6.1.3 Unbalanced load

Fig. 4.9 (a) shows the waveforms of load current, compensating current, source current and source voltage at α=0 with neural network controller. Here, initially the load is balanced up to t=0.5 s and at t=0.5 s. Unbalance is introduced by applying a linear star connected load in parallel to existing load, with Ra=40 Ω, Rb=60 Ω and Rc=20 Ω. The amplitude of load current, and compensating current change by applying the unbalanced load. The source

current is again found to become nearly sinusoidal. The quality of source current is measured in terms of its THD under these loading conditions. From the FFT analysis of source current waveforms at balanced load and unbalanced load, the THD is 2.43% and 2.35% respectively. These waveforms show that even with unbalanced load, the shunt APF compensates the reactive power and reduces the harmonic content in the source current. Fig. 4.9 (b) shows the waveforms of source current and source voltage from t=0.44 s to t=0.46 s and from t=0.54 s to t=0.56 s i.e. the response of the system for one cycle before and after the application of unbalanced load of APF. The source current becomes balanced after enabling APF even though the load is unbalanced.

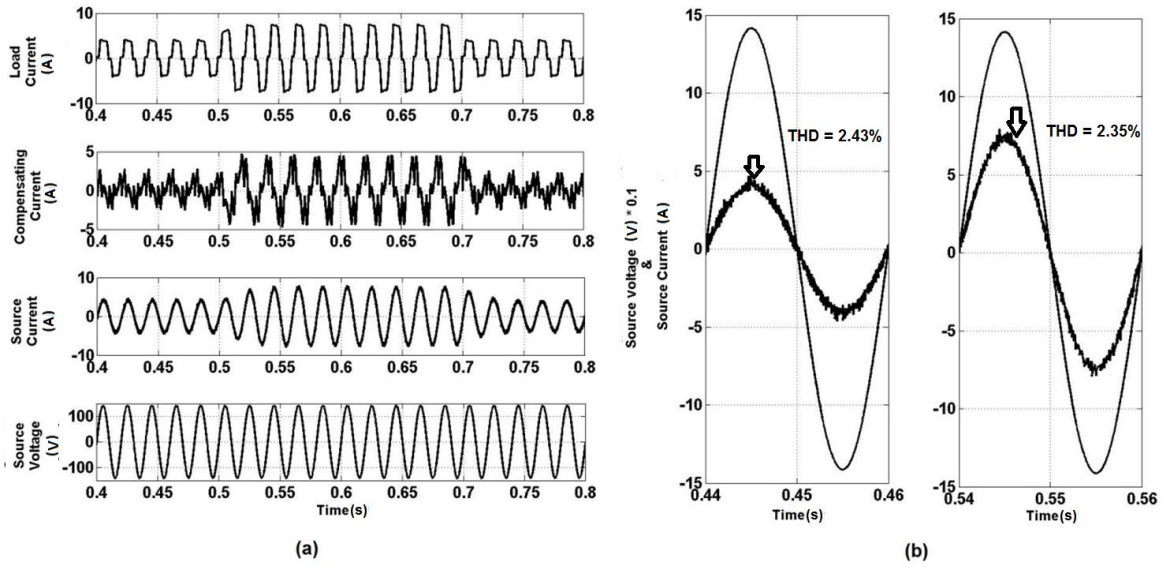

Fig. 4.8 (a) Step change in Load of active power filter at α=0 (b) before and after the step change in load for one cycle each

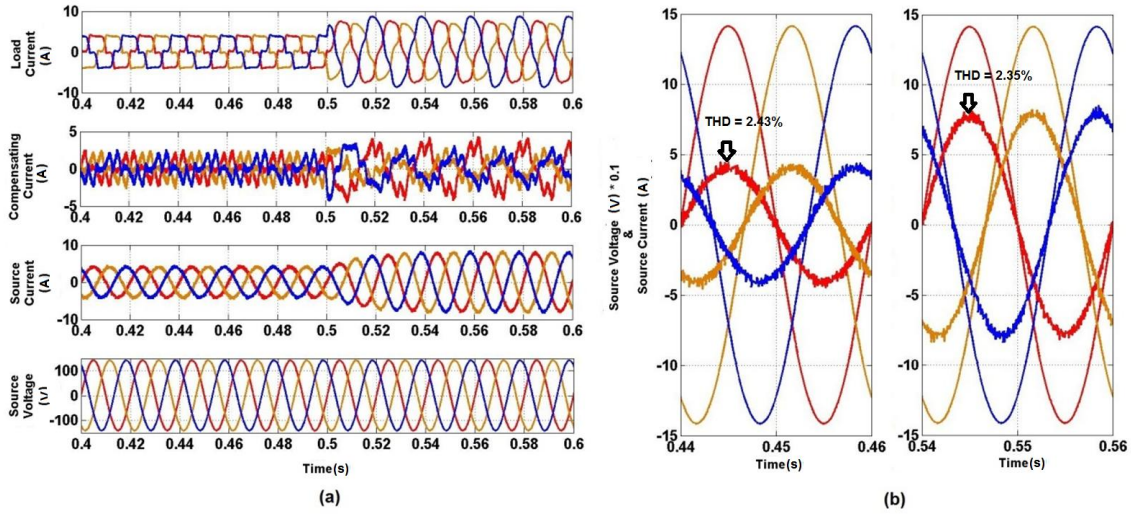

Fig. 4.9 (a) Application of an unbalanced load at t=0.5 s (I_a=5.81 A, I_b= 5.89 A and I_c=5.85 A) for α=0° (b) before and after the application of unbalanced load for one cycle each

4.6.2 Simulation results for rectifier fed RL load at α=30°

The simulated results with at α=30° are given below under different conditions. The reactive power demand of load increases as compared to the case at α=0.

4.6.2.1 Active filter is enabled

Fig. 4.10 shows the waveforms of load current (1 kVA load), compensating current, source current and source voltage at α=30° with neural network controller. The active power filter is initially disabled from t=0 to t=0.5 s. The compensating current is zero and source current is same as the load current. The source current is non sinusoidal with harmonics and is found to have THD of 37.57%. At t=0.5 s when the APF is enabled, the compensating current is applied at point of common coupling which makes the source current nearly sinusoidal unlike the load current. The THD of source current is now reduced to 2.85%. These waveforms show that after enabling, the shunt APF compensates for the reactive power demand and reduces the harmonic content in the source current. Fig. 4.10 (b) shows the waveforms of source current and source voltage from t=0.44 s to t=0.46 s and from t=0.54 s to t=0.56 s i.e. the response of the system for one cycle before and after the enabling of APF.

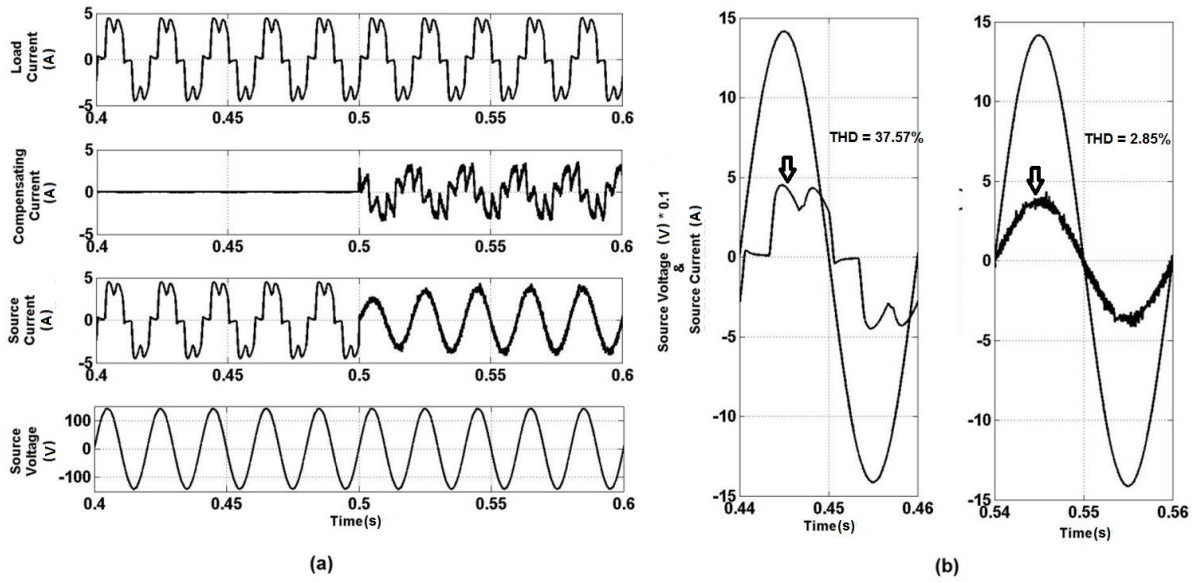

Fig. 4.10 (a) Response of active power filter at α=30° (b) Source voltage and current waveforms for one cycle before and after the enabling of active filter

4.6.2.2 Step change in load

Fig. 4.11 (a) shows the waveforms of load current, compensating current, source current and source voltage at α=30° with neural network controller. Here, initially the load is 1 kVA up to t=0.5 s and at t=0.5 s the load is suddenly increased to 2 kVA and then, the load is brought back to 1kVA at t=0.7 s. The amplitude of load current, compensating current and

source current also increase in response to the increase in load up to t=0.7 s, then they return to previous values. The source current is again found to be nearly sinusoidal. The quality of source current is measured in terms of its THD under these loading conditions. From the FFT analysis of source current waveforms at 1 kVA and 2 kVA, the THD is 2.85% and 2.78% respectively. These waveforms show that after increment in load, the shunt APF continues to compensate the reactive power and reduces the harmonic content in the source current. Fig. 4.11 (b) shows the waveforms of source current and source voltage from t=0.44 s to t=0.46 s and from t=0.54 s to t=0.56 s i.e. the response of the system for one cycle before and after the step change in load of APF. The transient is completed in about two cycles without any overshoot.

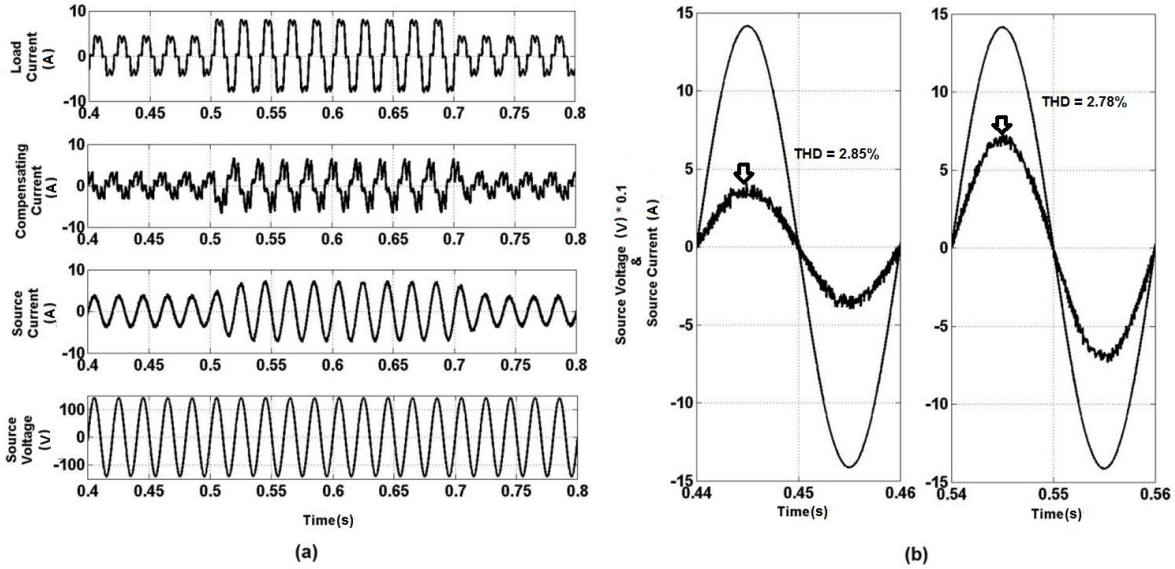

Fig. 4.11 (a) Step change in Load of active power filter at α=30° (b) before and after the step change in load for one cycle each

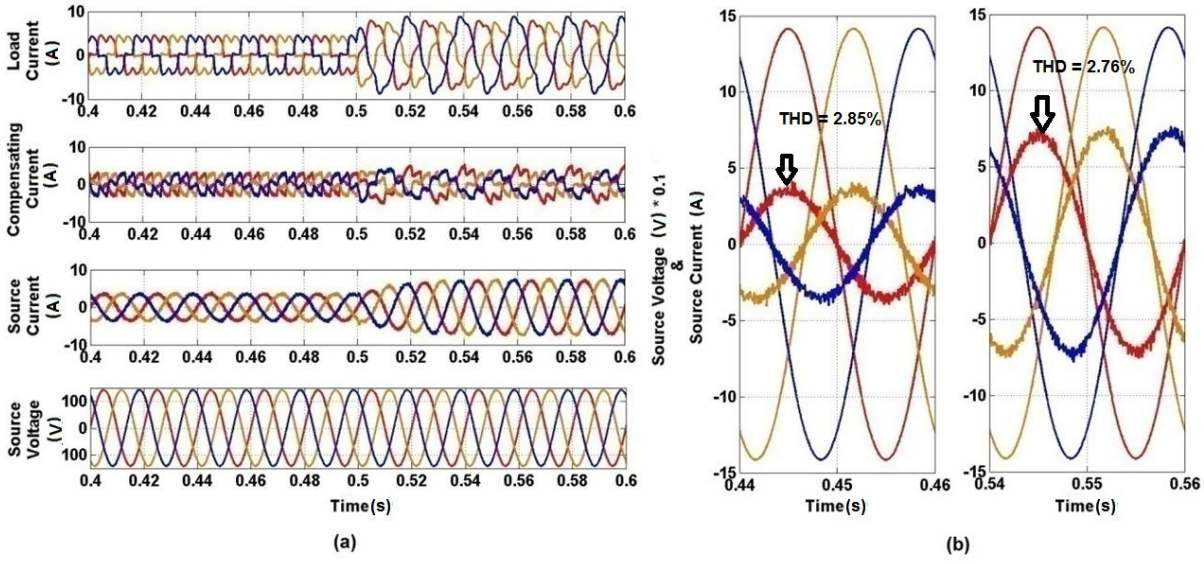

Fig. 4.12. (a) Application of an unbalanced load at t=0.5 s (I_a=4.85 A, I_b=4.93 A and I_c=4.90 A) for α=30° (b) before and after the application of unbalanced load for one cycle each

4.6.2.3 Unbalanced load

Fig. 4.12 (a) shows the waveforms of load current, compensating current, source current and source voltage at α=30° with neural network controller. Here, initially the load is balanced up to t=0.5 s and at t=0.5 s. Unbalance is introduced by applying a linear star connected load in parallel to existing load with Ra=40 Ω, Rb=60 Ω and Rc=20 Ω. The amplitude of load current, and compensating current change by applying the unbalanced load. The source current is again found to become nearly sinusoidal. The quality of source current is measured in terms of its THD under these loading conditions. From the FFT analysis of source current waveforms at balanced load and unbalanced load, the THD is 2.85% and 2.76% respectively. These waveforms show that even with unbalanced load, the shunt APF compensates the reactive power and reduces the harmonic content in the source current. Fig. 4.12 (b) shows the waveforms of source current and source voltage from t=0.44 s to t=0.46 s and from t=0.54 s to t=0.56 s i.e. the response of the system for one cycle before and after the application of unbalanced load of APF. The source current becomes balanced after enabling APF even though the load is unbalanced.

4.6.3 Simulation results for rectifier fed RL load at α=60°

The simulated results with at α=60° are given below under different conditions. The reactive power demand of the load further increases as compared to the previous case of α=30º.

4.6.3.1 Active filter is enabled

Fig. 4.13 (a) shows the waveforms of load current (1 kVA load), compensating current, source current and source voltage at α=60° with neural network controller. The APF is initially disabled from t=0 to t=0.5 s. The compensating current is zero and source current is same as the load current. The source current is non sinusoidal with harmonics and is found to have THD of 64.36%. At t=0.5 s when the APF is enabled, the compensating current is applied at point of common coupling which makes the source current nearly sinusoidal unlike the load current. The THD of source current is now reduced to 3.21%. These waveforms show that after enabling, the shunt APF compensates for the reactive power demand and reduces the harmonic content in the source current. Fig. 4.13 (b) shows the waveforms of source current and source voltage from t=0.44 s to t=0.46 s and from t=0.54 s to t=0.56 s i.e. the response of the system for one cycle before and after the enabling of APF.

4.6.3.2 Step change in load

Fig. 4.14 (a) shows the waveforms of load current, compensating current, source current and source voltage at α=60° with neural network controller. Here, initially the load is 1 kVA up to t=0.5 s and at t=0.5 s the load is suddenly increased to 2 kVA and then, the load is

brought back to 1kVA at t=0.7 s. The amplitude of load current, compensating current and source current also increase in response to the increase in load up to t=0.7 s, then they return to previous values. The source current is again found to be nearly sinusoidal. The quality of source current is measured in terms of its THD under these loading conditions. From the FFT analysis of source current waveforms at 1 kVA and 2 kVA, the THD is 3.21% and 3.15% respectively. These waveforms show that after increment in load, the shunt APF continues to compensate the reactive power and reduces the harmonic content in the source current. Fig. 4.14 (b) shows the waveforms of source current and source voltage from t=0.44 s to t=0.46 s and from t=0.54 s to t=0.56 s i.e. the response of the system for one cycle before and after the step change in load of APF. The transient is completed in about two cycles without any overshoot.

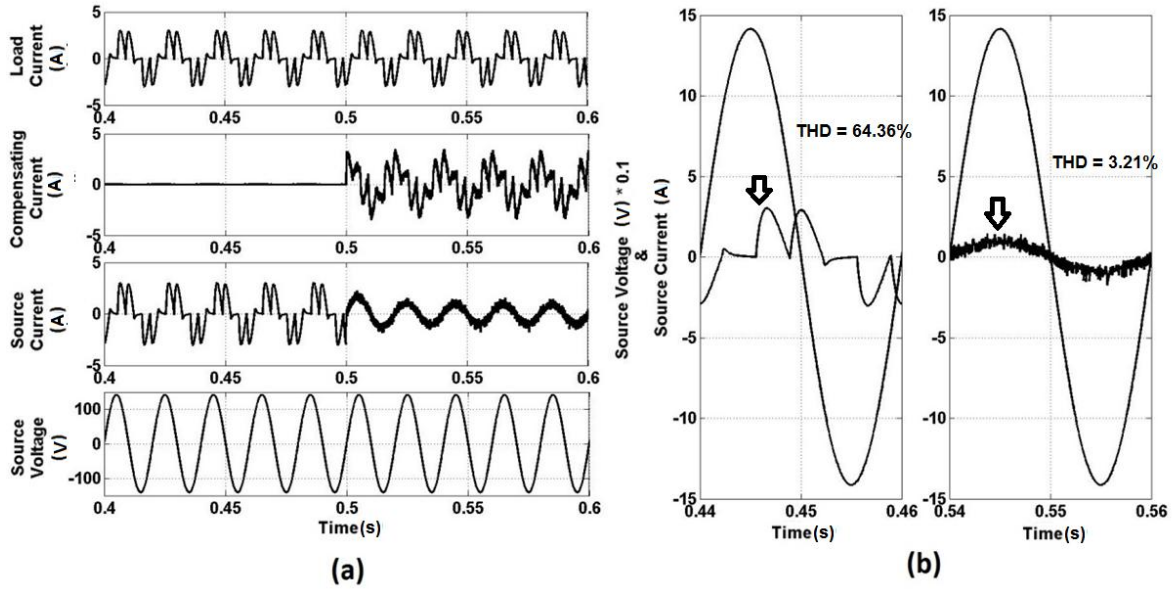

Fig. 4.13 (a) Response of active power filter at α=60° (b) Source voltage and current waveforms for one cycle before and after the enabling of active filter

4.6.3.3 Unbalanced load

Fig. 4.15 (a) shows the waveforms of load current, compensating current, source current and source voltage at α=60° with neural network controller. Here, initially the load is balanced up to t=0.5 s and at t=0.5 s. Unbalance is introduced by applying a linear load in parallel to existing load, with Ra=40 Ω, Rb=60 Ω and Rc=20 Ω. The amplitude of load current, and compensating current change by applying the unbalanced load. The source current is again found to become nearly sinusoidal. The quality of source current is measured in terms of its THD under these loading conditions. From the FFT analysis of source current waveforms at balanced load and unbalanced load, the THD is 3.21% and 3.16% respectively. These waveforms show that even with unbalanced load, the shunt APF compensates the reactive power and reduces the harmonic content in the source current.

Fig. 4.15 (b) shows the waveforms of source current and source voltage from t=0.44 s to t=0.46 s and from t=0.54 s to t=0.56 s i.e. the response of the system for one cycle before and after the application of unbalanced load of APF. The source current becomes balanced after enabling APF even though the load is unbalanced.

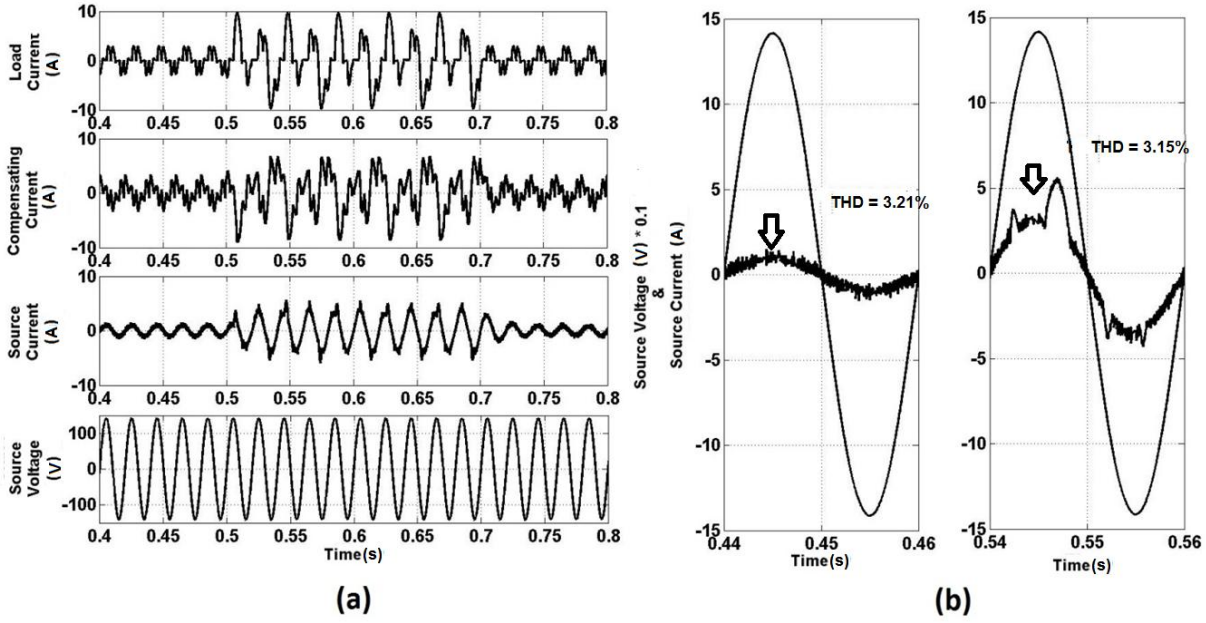

Fig. 4.14 (a) Step change in Load of active power filter at α=60° (b) before and after the step change in load for one cycle each

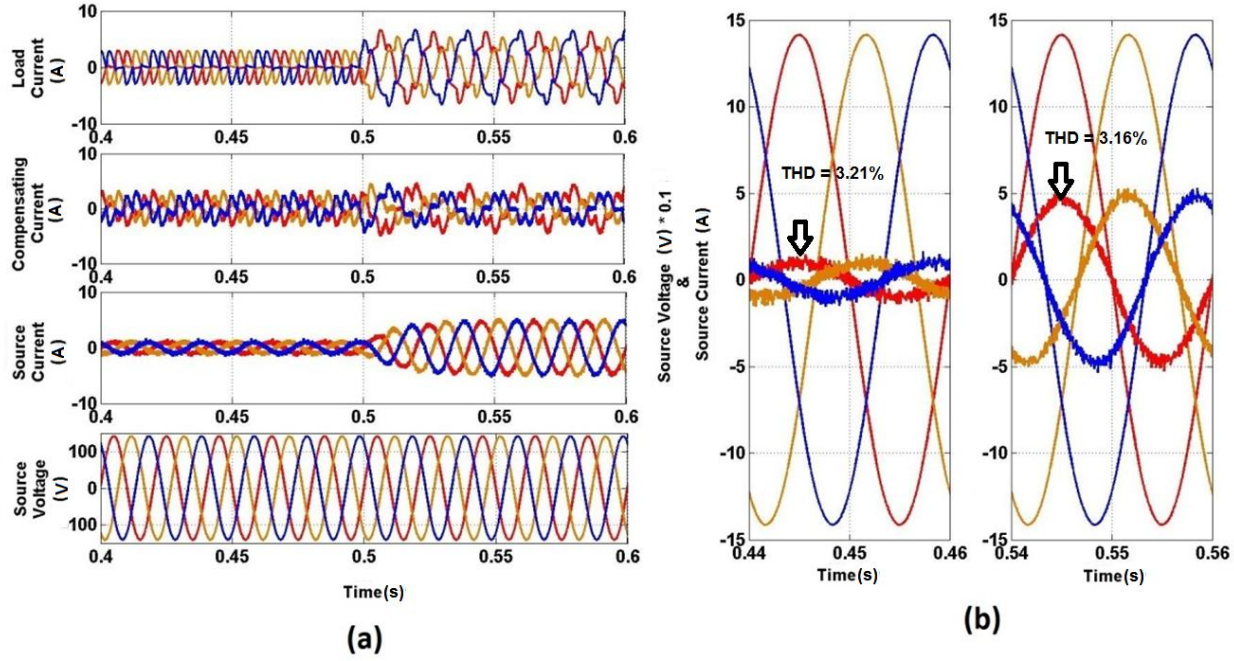

Fig. 4.15 (a) Application of an unbalanced load at t=0.5 s (I_a=3.63 A, I_b=3.69 A and I_c=3.67 A) for α=60° (b) before and after the application of unbalanced load for one cycle each

4.7 Comparison of Simulation Response

The total harmonic distortion in source current after applying the APF is shown in Table 4.1, THDs found at α=15º and 45º have also been included. As per IEEE std. 519 [226], the source current THD should be lesser than 5%. The application of neural network controller are used to get the lesser value of the source current THD which was permissible by IEEE std. 519. The detailed comparison of all the source current THDs with various parameters are discussed in Chapter 7. The corresponding graph showing the change of total harminic distortion with respect to the firing angle is given in Fig. 4.16. As the firing angle increses the source current total harmonic distortion also increases.

Table 4.1 Total Harmonic Distortion for various firing angles with neural network controller

S.No.	Firing angle (α in °)	Total Harmonic Distortion (THD in %)
1	0	2.43
2	15	2.63
3	30	2.85
4	45	3.12
5	60	3.21

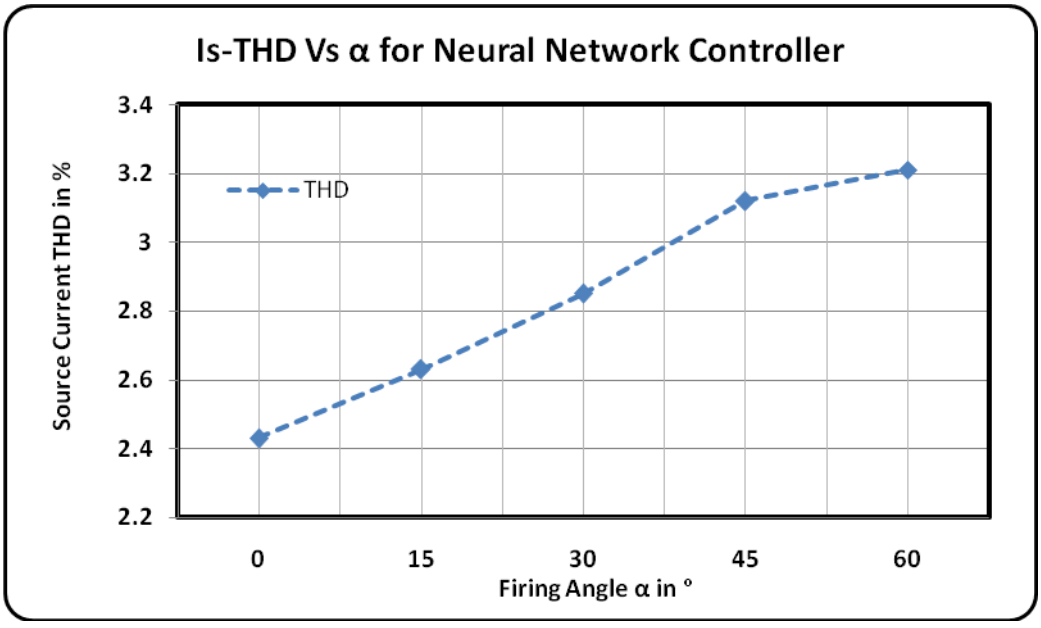

Fig. 4.16 Source Current THD in percentage with respect to Firing angle α in degree for neural network controller

4.8 Conclusion

This chapter explained the basics of neural network controller, simulation diagram of shunt APF and simulation study of the neural network controller based shunt APF. By seeing the all the results for different loads with various firing angles we can conclude that the neural

network controller based shunt APF is effective in mitigating the harmonics and compensating the reactive power. It is good even at higher firing angles as the source current total harmonic distortion is below 5% which is permissible according to IEEE-std. 519.

5.1 Introduction

Neuro Fuzzy is one of the most researched forms of hybrid system in AI applications for various electrical systems. Neural networks and fuzzy logic represent two distinct methodologies to deal with uncertainty. Each of them has its own merits and demerits. Neural networks can model complex non-linear relationships and are suitable for classification phenomenon into predetermined classes. On the other hand, the precision of outputs is quite often limited and does not admit zero error but only minimization of least squares errors. Besides, the training time required for a NN can be substantially large. Also, the training data has to be chosen carefully to cover the entire range over which the different variables are expected to change.

Fuzzy logic systems address the imprecision of inputs and outputs directly by defining them using fuzzy sets and allow for a greater flexibility in formulating system descriptions at the appropriate level of detail. The limitations of fuzzy logic lie in estimating the membership function. There are many ways of interpreting fuzzy rules, combining the outputs of several fuzzy rules and de-fuzzifying the output. Selection of the optimum method is very difficult and time consuming.

Neuro-Fuzzy systems which are an integration of NN and FL have demonstrated the potential to extend the capabilities of systems beyond either of these technologies when applied individually.

5.2 Fuzzy Neuron

The fuzzy neuron is the basic element of fuzzy Back-Propagation model. Fig. 5.1 illustrate the architecture of the fuzzy neuron.

Consider the input vector

$$\bar{I} = (\bar{I}_0, \bar{I}_1, \bar{I}_2 ..... \bar{I}_i ....., \bar{I}_l)$$

Weight vector

$$\bar{W} = (\bar{W}_0, \bar{W}_1, \bar{W}_2 ..... \bar{W}_i ....., \bar{W}_l)$$

Fuzzy Neuron computes the crisp output O is given by

$$O_j = f(NET_j) = f\{CE(\sum_{i=0}^{l} \bar{W}_i . \bar{I}_i)\}$$

Where $\bar{I}_0 = (1,0,0)$ is the bias. Fuzzy weighted summation net is given by

$$net = (\sum_{i=0}^{l} \bar{W}_i . \bar{I}_i)$$

CE = Centroid of triangular fuzzy member treated as defuzzification operation which maps fuzzy weighted summation value to a crisp value.

If $net = (net_m, net_\alpha, net_\beta)$ is fuzzy weighted summation then

$$CE(net) = net_m + \frac{1}{3}(net_\beta - net_\alpha)\} = NET$$

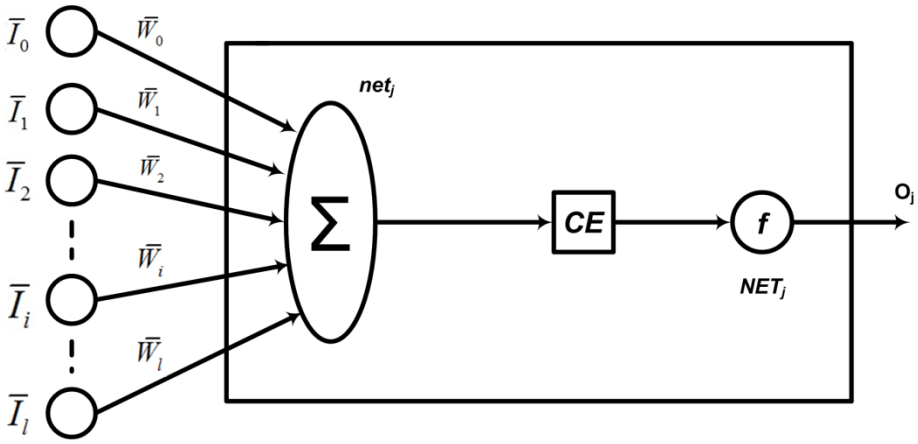

Fuzzy Neuron j

Fig. 5.1 Fuzzy Neuron

f is a sigmoidal function which performs non-linear mapping between input and output and f is defined as

$$f(NET) = \frac{1}{1+e^{-NET}}$$

5.3 Fuzzy Back-Propagation Architecture

Fuzzy Back-Propagation is a three layered feed forward architecture. The three layers are input layer, hidden layer and output layer. As in Back-Propagation Network, the functioning proceeds in two stages, namely

1. Learning or Training and
2. Inference

Consider a configuration of $l-m-n$ (input neuron - hidden neuron - output neuron) for fuzzy Back-Propagation model. Fig. 5.2 illustrates the fuzzy Back-Propagation.

Let $I_p = (I_{p1}, I_{p2}, ..., I_{pi}, ...I_{pl}), p = 1, 2, ...N$ be the pth pattern among N input patterns that fuzzy BP needs to be trained, with $I_0 = (1, 0, 0)$ as the bias.

Here

I_{pi} : ith input component of the input pattern p

O_{pi} : the output value of the ith input neuron

$O`_{pj} and O``_{pj}$: the j[th] and k[th] crisp defuzzification outputs of the hidden and output layer neurons respectively.

$W_{ji} and W_{kj}$: the fuzzy connection weights between the i[th] input neuron and the jth hidden neuron, and the j[th] hidden neuron and k[th] output neuron respectively. In addition,

$CE and f$: sigmoidal and Centroid functions.

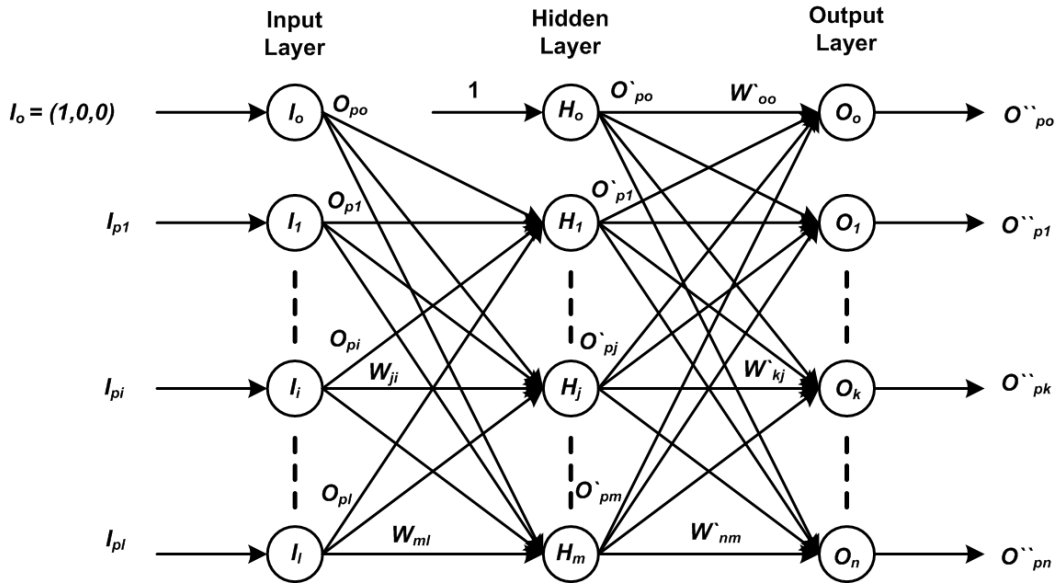

Fig. 5.2 Architecture of Fuzzy Back-Propagation Network

The computations carried out by each neuron are

Input neurons

$$O_{pi} = I_{pi} = 1,2,....l; O_{po} = (1,0,0) \tag{5.1}$$

Hidden neurons

$$O`_{pj} = f(NET_{pj}), j = 1,2,....m; O`_{po} = 1$$

$$NET_{pj} = CE\left(\sum_{i=0}^{l} W_{ji}.O_{pi}\right)$$

Output neurons

$$O``_{pk} = f(NET`_{pk}), k = 1,2,....n-1 \tag{5.2}$$

$$NET`_{pk} = CE\left(\sum_{j=0}^{m} W_{kj}.O_{pj}\right)$$

5.3.1 Learning in Back-Propagation

The learning procedure of fuzzy BP follows the gradient descent method of minimizing error due to the learning. Here, the mean square error function of pattern p is defined as

$$E_p = \sum_{i=1}^{n} \frac{1}{2} \left(D_{pi} - O``_{pi} \right)^2$$

Where D_{pi} : the desire output value of the i[th] output neuron and

$O``_{pi}$: the computed value of the i[th] output neuron.

The overall error of the training pattern

$$E = \sum_{p} E_p$$

The change in weight to minimize error is

$$\Delta W(t) = -\eta E_p(t) + \alpha \Delta W(t-1) \tag{5.3}$$

Where η : the learning rate

α : the constant value

$\alpha \Delta W(t-1)$: Momentum term to be added to speed up the convergence

The term ∇E_p is given by

$$\nabla E_p = \frac{\partial E_p}{\partial W(t)} = \left(\frac{\partial E_p}{\partial W_m(t)}, \frac{\partial E_p}{\partial W_\alpha(t)}, \frac{\partial E_p}{\partial W_\beta(t)} \right)$$

Where $W(t) = (W_m(t), W_\alpha(t), W_\beta(t))$: fuzzy connection weights

$W`_{ji}(t) = (W`_{mji}(t), W`_{\alpha ji}(t), W`_{\beta ji}(t))$ and $W`_{kj}(t) = (W`_{mkj}(t), W`_{\alpha kj}(t), W`_{\beta kj}(t))$: the fuzzy connection weights between the input-hidden and hidden-output layer neurons respectively.

Consider the hidden output layer and applying chain rule,

$$\frac{\partial E_p}{\partial W`_{mkj}} = \frac{\partial E_p}{\partial net`_{pmk}} \frac{\partial net`_{pmk}}{\partial W`_{mkj}}$$

$$= \left(\frac{\partial E_p}{\partial O``_{pk}} \frac{\partial O``_{pk}}{\partial net`_{pmk}} \right) \frac{\partial net`_{pmk}}{\partial W`_{mkj}}$$

$$= -(D_{pk} - O``_{pk}) \left( \frac{\partial O``_{pk}}{\partial NET`_{pk}} \frac{\partial NET`_{pk}}{\partial net`_{pmk}} \right) \frac{\partial net`_{pmk}}{\partial W`_{mkj}}$$

$$= -(D_{pk} - O``_{pk}) O``_{pk} (1 - O``_{pk}).1.O`_{pj}$$

Hence,

$$\frac{\partial E_p}{\partial W`_{mkj}} = -(D_{pk} - O``_{pk}) O``_{pk} (1 - O``_{pk}).1.O`_{pj} \tag{5.4}$$

Again

$$\frac{\partial E_p}{\partial W`_{\alpha kj}} = \frac{\partial E_p}{\partial net`_{p\alpha k}} \frac{\partial net`_{p\alpha k}}{\partial W`_{\alpha kj}}$$

$$= \left(\frac{\partial E_p}{\partial O``_{pk}} \frac{\partial O``_{pk}}{\partial net`_{p\alpha k}} \right) \frac{\partial net`_{p\alpha k}}{\partial W`_{\alpha kj}}$$

$$= -(D_{pk} - O``_{pk}) \left( \frac{\partial O``_{pk}}{\partial NET`_{pk}} \frac{\partial NET`_{pk}}{\partial net`_{p\alpha k}} \right) \frac{\partial net`_{p\alpha k}}{\partial W`_{\alpha kj}}$$

$$= -(D_{pk} - O``_{pk}) O``_{pk} (1 - O``_{pk}) . \left(\frac{-1}{3} \right) . O`_{pj}$$

Hence,

$$\frac{\partial E_p}{\partial W`_{\alpha kj}} = -(D_{pk} - O``_{pk}) O``_{pk} (1 - O``_{pk}) . \left(\frac{-1}{3} \right) . O`_{pj} \qquad (5.5)$$

Similarly,

$$\frac{\partial E_p}{\partial W`_{\beta kj}} = -(D_{pk} - O``_{pk}) O``_{pk} (1 - O``_{pk}) . \left(\frac{1}{3} \right) . O`_{pj} \qquad (5.6)$$

Thus, the eqs. (5.4), (5.5), (5.6) give the $\frac{\partial E_p}{\partial W(t)}$ terms for hidden – output layer. Now, consider the input – hidden layer. Let us define the error values

$$\delta_{pmk} = \frac{\partial E_p}{\partial net`_{pmk}} = -(D_{pk} - O``_{pk}) O``_{pk} (1 - O``_{pk})$$

$$\delta_{p\alpha k} = \frac{\partial E_p}{\partial net`_{p\alpha k}} = -(D_{pk} - O``_{pk}) O``_{pk} (1 - O``_{pk}) . \left(\frac{-1}{3} \right)$$

$$\delta_{p\beta k} = \frac{\partial E_p}{\partial net`_{p\beta k}} = -(D_{pk} - O``_{pk}) O``_{pk} (1 - O``_{pk}) . \left(\frac{1}{3} \right)$$

To obtain,

$$\nabla E_p(t) = \frac{\partial E_p}{\partial W(t)}$$

$$\frac{\partial E_p}{\partial W_{mji}} = \frac{\partial E_p}{\partial O`_{pj}} \frac{\partial O`_{pj}}{\partial W_{mji}}$$

$$= \frac{\partial E_p}{\partial O`_{pj}} \left( \frac{\partial O`_{pj}}{\partial NET_{pj}} \frac{\partial NET_{pj}}{\partial net_{pmj}} \frac{\partial net_{pmj}}{\partial W_{mji}} \right)$$

$$= \frac{\partial E_p}{\partial O`_{pj}} O`_{pj}(1 - O`_{pj}).1.O_{pi}$$

$$= \left(\sum_{k=0}^{n} \frac{\partial E_p}{\partial net`_{pmk}} \frac{\partial net`_{pmk}}{\partial O`_{pj}} \right) O`_{pj}(1 - O`_{pj}).1.O_{pi}$$

Thus,

$$\frac{\partial E_p}{\partial W_{mji}} = \left(\sum_{k=0}^{n} \delta_{pmk} W`_{mkj} \right) O`_{pj}(1 - O`_{pj}).1.O_{pi} \qquad (5.7)$$

Similarly,

$$\frac{\partial E_p}{\partial W_{\alpha ji}} = \left(\sum_{k=0}^{n} \delta_{p\alpha k} W`_{\alpha kj} \right) O`_{pj}(1 - O`_{pj}).\left(\frac{-1}{3} \right).O_{pi} \qquad (5.8)$$

$$\frac{\partial E_p}{\partial W_{\beta ji}} = \left(\sum_{k=0}^{n} \delta_{p\beta k} W`_{\beta kj} \right) O`_{pj}(1 - O`_{pj}).\left(\frac{1}{3} \right).O_{pi} \qquad (5.9)$$

Thus, Eqs. (5.7), (5.8), and (5.9) give the $\nabla E_p(t)$ term for the input-hidden layer weights.

Now change in weights $\Delta W(t)$ for input-hidden layer and $\Delta W`(t)$ for hidden-output layer weights can be obtained using Eq.(5.3).

The updated weights at time t are given by

$W`(t) = W`(t-1) + \Delta W`(t)$, for hidden-output layer

$W(t) = W(t-1) + \Delta W(t)$, for input-hidden layer

5.3.2 Inference

Once the fuzzy BP model has been trained for a given set of input-output patterns a definite number of times, it is ready for inference. Given a set of patters F_p to be inferred, where $F_p = (F_{p1}, F_{p2}, ..., F_{pl})$ .The aim is to obtain O_p , the output corresponding to F_p .

O_p is computed in one pass by allowing F_p to pass through the series of computations illustrated in Eqs.(5.4) and (5.5). The $O``_p$ computed by the output neurons, is the output corresponding to F_p .

5.4 Implementation of Neuro Fuzzy Controller for Active Power Filter

The following steps are performed to develop neuro fuzzy network based SAPF:

1. The input and output data of the PI controller is taken in a matrix and saved in a file.
2. Type anfisedit in MATLAB command prompt to get the GUI.

3. The saved file is called for training data under the heading of load data.
4. In Generate FIS, the number of membership functions, type of membership functions of input and type of membership function of the output are assigned.
5. In Train FIS, the optimization method, error tolerance and no. of epochs are assigned and then train the data.
6. Then Test FIS, view the graph in the GUI. If satisfied proceed otherwise go to step 4 and 5 to change the settings for getting the target value.

5.5 Simulation Results

The simulated results of the neural network based shunt APF are studied in this section. The load is a three phase thyristorised controlled rectifier feeing a series R-L load. Three settings of firing angle α are considered as 0, 30° and 60°. In each case, the response is obtained for following conditions:

- Active Filter is enabled with fixed and balanced load
- Step change in load, with active filter enabled
- Unbalanced load, with active filter enabled

5.5.1 Simulation results for rectifier fed RL load at α=0

The simulated results with at α=0 are given below under different conditions:

5.5.1.1 Active filter is enabled

Fig. 5.3 (a) shows the waveforms of load current (1 kVA load), compensating current, source current and source voltage at α=0 with neuro fuzzy controller. The APF is initially disabled from t=0 to t=0.5 s. The compensating current is zero and source current is same as the load current. The source current is non sinusoidal with harmonics and has 30.64% THD. At t=0.5 s when the APF is enabled, the compensating current is applied at point of common coupling which makes the source current nearly sinusoidal for the same load current. The THD of source current is now reduced to 1.53%. These waveforms show that after enabling, the shunt APF compensates for the reactive power demand and reduces the harmonic content in the source current. Fig. 5.3 (b) shows the waveforms of source current and source voltage from t=0.44 s to t=0.46 s and from t=0.54 s to t=0.56 s i.e. the response of the system for one cycle before and after the enabling of APF.

5.5.1.2 Step change in load

Fig. 5.4 (a) shows the waveforms of load current, compensating current, source current and source voltage at α=0 with neuro fuzzy controller. Here, initially the load is 1 kVA up to t=0.5 s and at t=0.5 s the load is suddenly increased to 2 kVA and then, the load is brought back to 1kVA at t=0.7 s. The amplitude of load current, compensating current and source current also increase in response to the increase in load up to t=0.7 s, then they return to

previous values. The source current is again found to be nearly sinusoidal. The quality of source current is measured in terms of its THD under these loading conditions. From the FFT analysis of source current waveforms at 1 kVA and 2 kVA, the THD is 1.53% and 1.43% respectively. These waveforms show that after increment in load, the shunt APF continues to compensate the reactive power and reduces the harmonic content in the source current. Fig. 5.4 (b) shows the waveforms of source current and source voltage from t=0.44 s to t=0.46 s and from t=0.54 s to t=0.56 s i.e. the response of the system for one cycle before and after the step change in load of APF. The transient is completed in about two cycles without any overshoot.

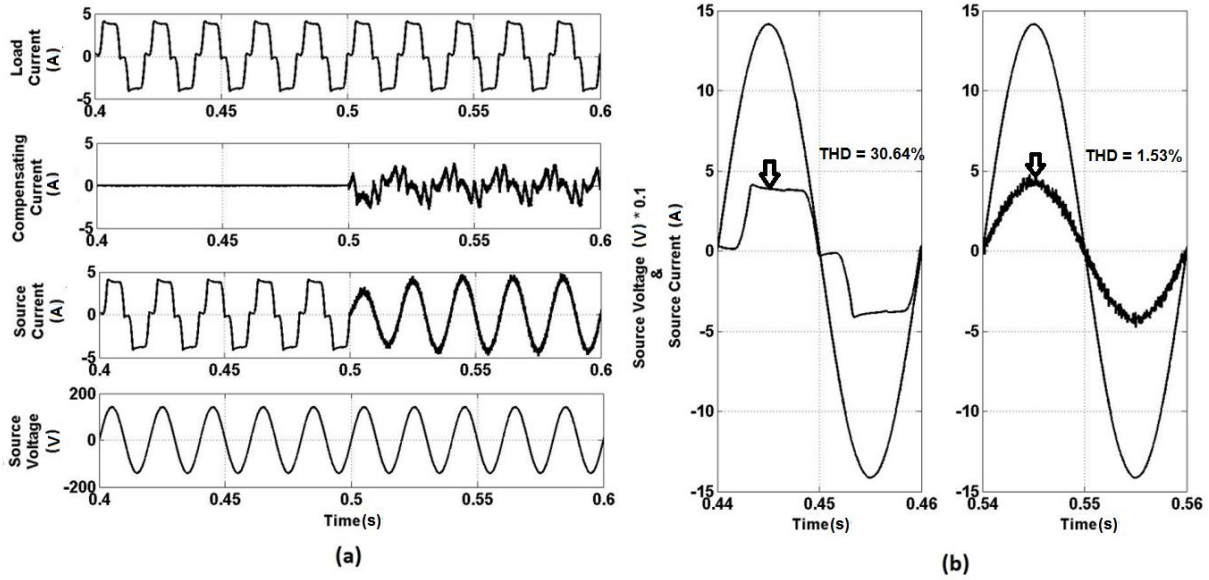

Fig. 5.3 (a) Response of active power filter at α=0 (b) Source voltage and current waveforms for one cycle before and after the enabling of active filter

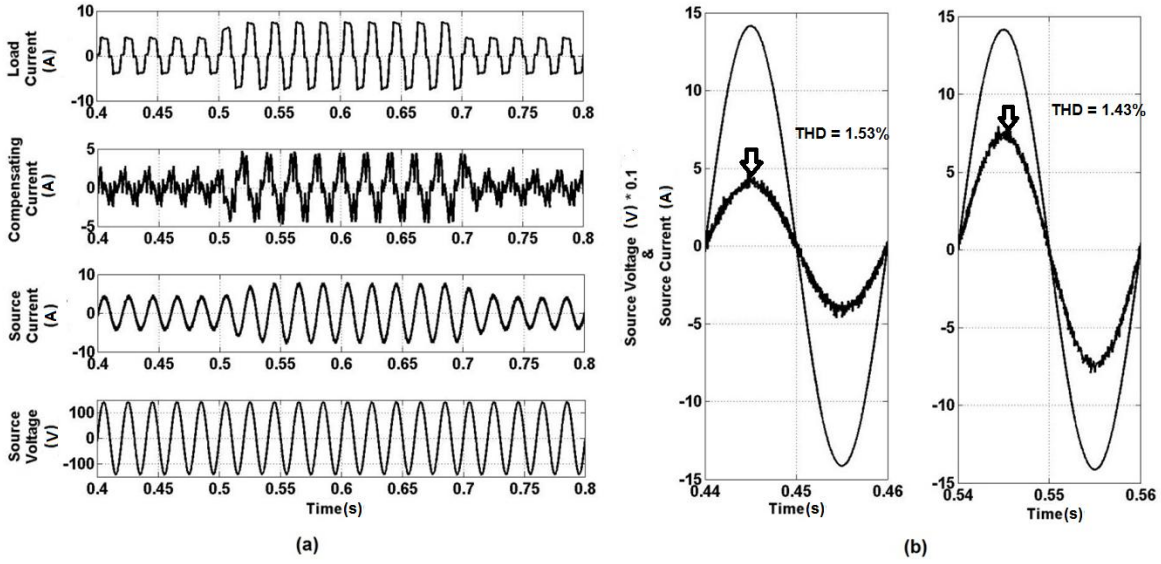

Fig. 5.4 (a) Step change in load of active power filter at α=0 (b) before and after the step change in load for one cycle each

5.5.1.3 Unbalanced load

Fig. 5.5 (a) shows the waveforms of load current, compensating current, source current and source voltage at α=0° with neuro fuzzy controller. Here, initially the load is balanced up to t=0.5 s and at t=0.5 s. Unbalance is introduced by applying a linear star connected load in parallel to existing load, with Ra=40 Ω, Rb=60 Ω and Rc=20 Ω. The amplitude of load current, and compensating current change by applying the unbalanced load. The source current is again found to become nearly sinusoidal. The quality of source current is measured in terms of its THD under these loading conditions. From the FFT analysis of source current waveforms at balanced load and unbalanced load, the THD is 1.53% and 1.48% respectively. These waveforms show that even with unbalanced load, the shunt APF compensates the reactive power and reduces the harmonic content in the source current. Fig. 5.5 (b) shows the waveforms of source current and source voltage from t=0.44 s to t=0.46 s and from t=0.54 s to t=0.56 s i.e. the response of the system for one cycle before and after the application of unbalanced load of APF. The source current becomes balanced after enabling APF even though the load is unbalanced.

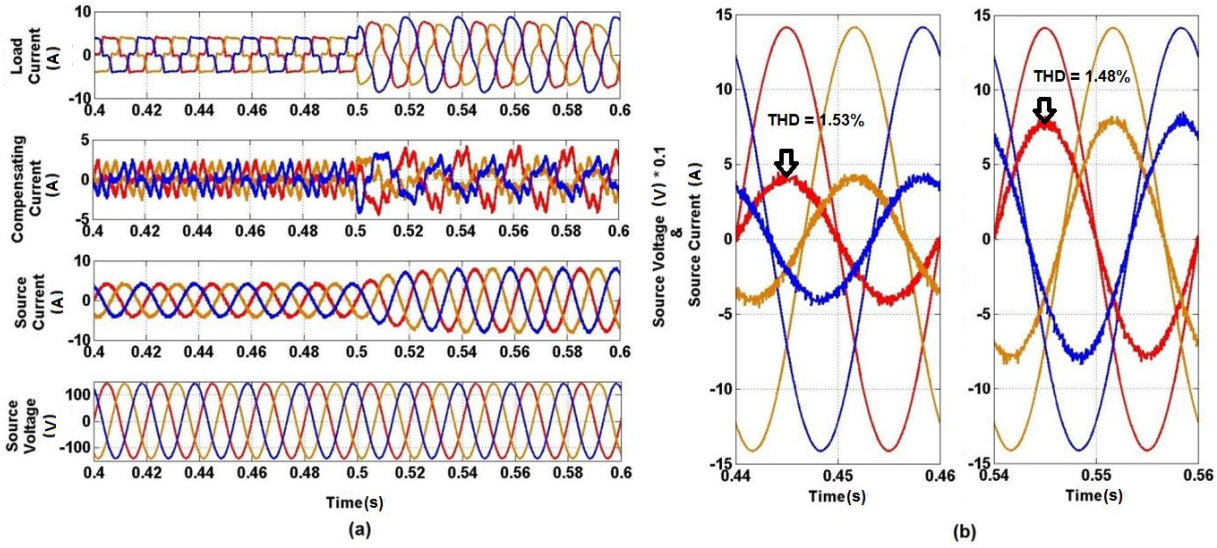

Fig. 5.5 (a) Application of an unbalanced load at t=0.5 s (I_a=5.83 A, I_b= 5.91 A and I_c=5.87 A) for α=0 (b) before and after the application of unbalanced load for one cycle each

5.5.2 Simulation results for rectifier fed RL load at α=30°

The simulated results with at α=30° are given below under different conditions:

5.5.2.1 Active filter is enabled

Fig. 5.6 (a) shows the waveforms of load current (1 kVA load), compensating current, source current and source voltage at α=30° with neuro fuzzy controller. The APF is initially disabled from t=0 to t=0.5 s. The compensating current is zero and source current is same as the load current. The source current is non sinusoidal with harmonics and is found to have

THD of 37.57%. At t=0.5 s when the APF is enabled, the compensating current is applied at point of common coupling which makes the source current nearly sinusoidal unlike the load current. The THD of source current is now reduced to 1.79%. These waveforms show that after enabling, the shunt APF compensates for the reactive power demand and reduces the harmonic content in the source current. Fig. 5.6 (b) shows the waveforms of source current and source voltage from t=0.44 s to t=0.46 s and from t=0.54 s to t=0.56 s i.e. the response of the system for one cycle before and after the enabling of APF.

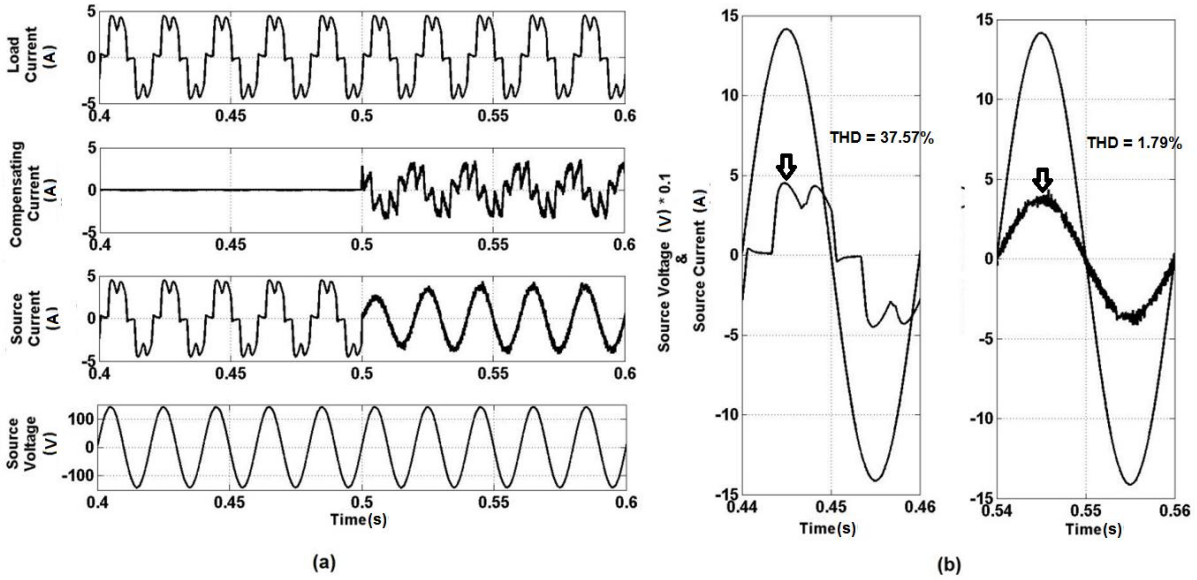

Fig. 5.6 (a) Response of active power filter at α=30° (b) Source voltage and current waveforms for one cycle before and after the enabling of active filter

5.5.2.2 Step change in load

Fig. 5.7 (a) shows the waveforms of load current, compensating current, source current and source voltage at α=30° with neuro fuzzy controller. Here, initially the load is 1 kVA up to t=0.5 s and at t=0.5 s the load is suddenly increased to 2 kVA and then, the load is brought back to 1kVA at t=0.7 s. The amplitude of load current, compensating current and source current also increase in response to the increase in load up to t=0.7s, then they return to previous values. The source current is again found to be nearly sinusoidal. The quality of source current is measured in terms of its THD under these loading conditions. From the FFT analysis of source current waveforms at 1 kVA and 2 kVA, the THD is 1.79% and 1.72% respectively. These waveforms show that after increment in load, the shunt APF continues to compensate the reactive power and reduces the harmonic content in the source current. Fig. 5.7 (b) shows the waveforms of source current and source voltage from t=0.44 s to t=0.46 s and from t=0.54 s to t=0.56 s i.e. the response of the system for one cycle before and after the step change in load of APF. The transient is completed in about two cycles without any overshoot.

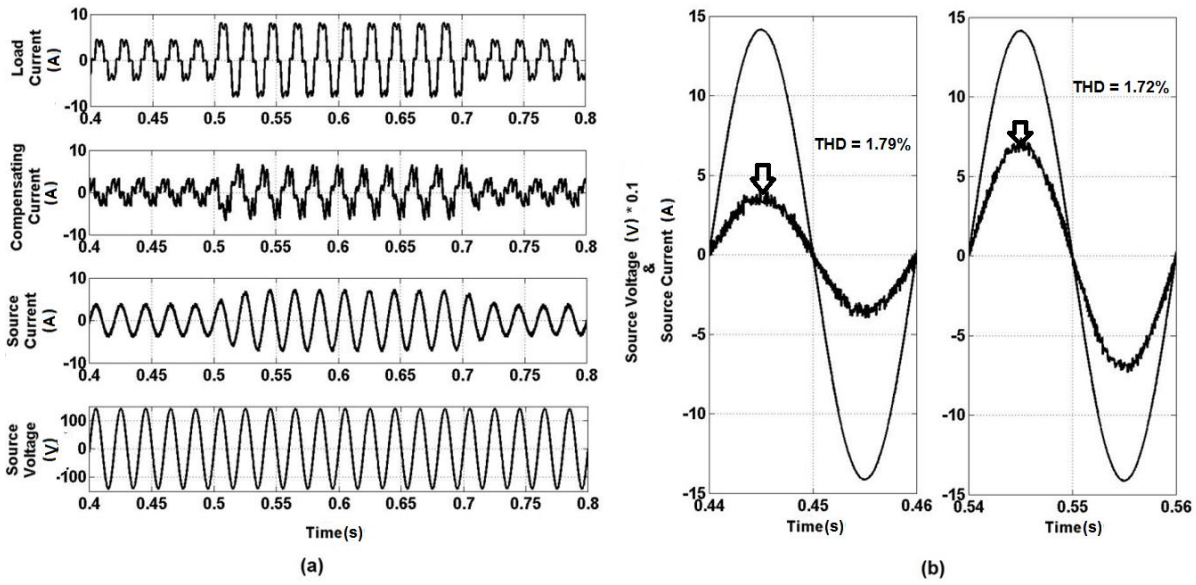

Fig. 5.7 (a) Step change in Load of active power filter at α=30° (b) before and after the step change in load for one cycle each

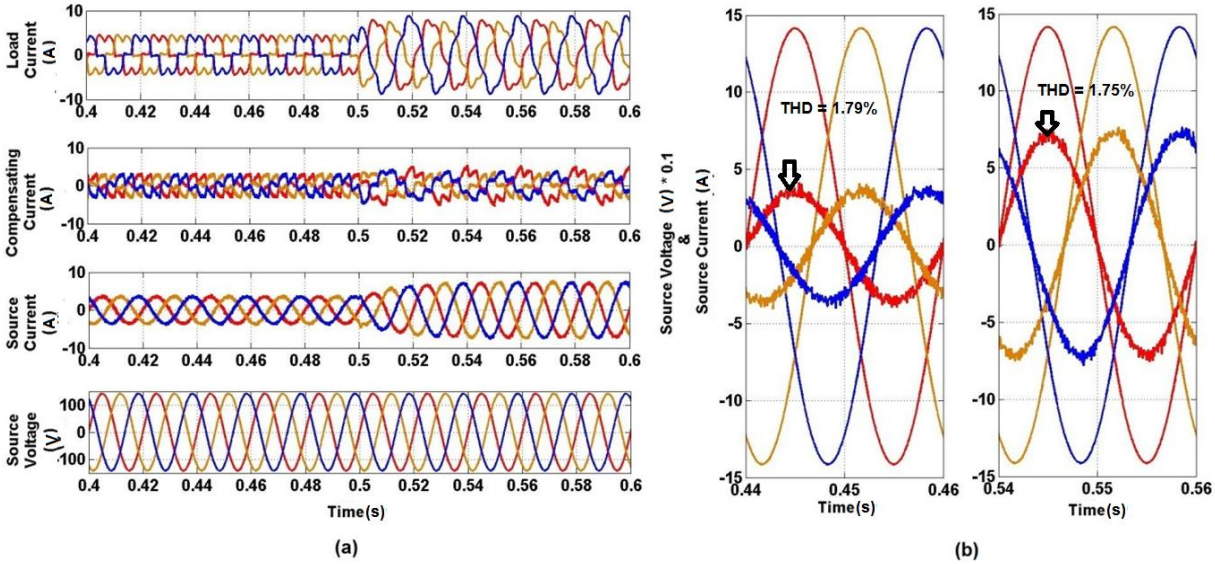

Fig. 5.8 (a) Application of an unbalanced load at t=0.5 s (I_a=4.86 A, I_b=4.95 A and I_c=4.92 A) for α=30° (b) before and after the application of unbalanced load for one cycle each

5.5.2.3 Unbalanced load

Fig. 5.8 (a) shows the waveforms of load current, compensating current, source current and source voltage at α=30° with neuro fuzzy controller. Here, initially the load is balanced up to t=0.5 s and at t=0.5 s. Unbalance is introduced by applying a linear star connected load in parallel to existing load, with Ra=40 Ω, Rb=60 Ω and Rc=20 Ω. The amplitude of load current, and compensating current change by applying the unbalanced load. The source current is again found to become nearly sinusoidal. The quality of source current is measured in terms of its THD under these loading conditions. From the FFT analysis of source current waveforms at balanced load and unbalanced load, the THD is

1.79% and 1.75% respectively. These waveforms show that even with unbalanced load, the shunt APF compensates the reactive power and reduces the harmonic content in the source current. Fig. 5.8 (b) shows the waveforms of source current and source voltage from t=0.44 s to t=0.46 s and from t=0.54 s to t=0.56 s i.e. the response of the system for one cycle before and after the application of unbalanced load of APF. The source current becomes balanced after enabling APF even though the load is unbalanced.

5.5.3 Simulation results for rectifier fed RL load at α=60°

The simulated results with at α=60° are given below under different conditions:

5.5.3.1 Active filter is enabled

Fig. 5.9 shows the waveforms of load current (1 kVA load), compensating current, source current and source voltage at α=60° with neuro fuzzy controller. The APF is initially disabled from t=0 to t=0.5 s. The compensating current is zero and source current is same as the load current. The source current is non sinusoidal with harmonics and is found to have THD of 64.36%. At t=0.5 s when the APF is enabled, the compensating current is applied at point of common coupling which makes the source current nearly sinusoidal unlike the load current. The THD of source current is now reduced to 2.28%. These waveforms show that after enabling, the shunt APF compensates for the reactive power demand and reduces the harmonic content in the source current. Fig. 5.9 (b) shows the waveforms of source current and source voltage from t=0.44 s to t=0.46 s and from t=0.54 s to t=0.56 s i.e. the response of the system for one cycle before and after the enabling of APF.

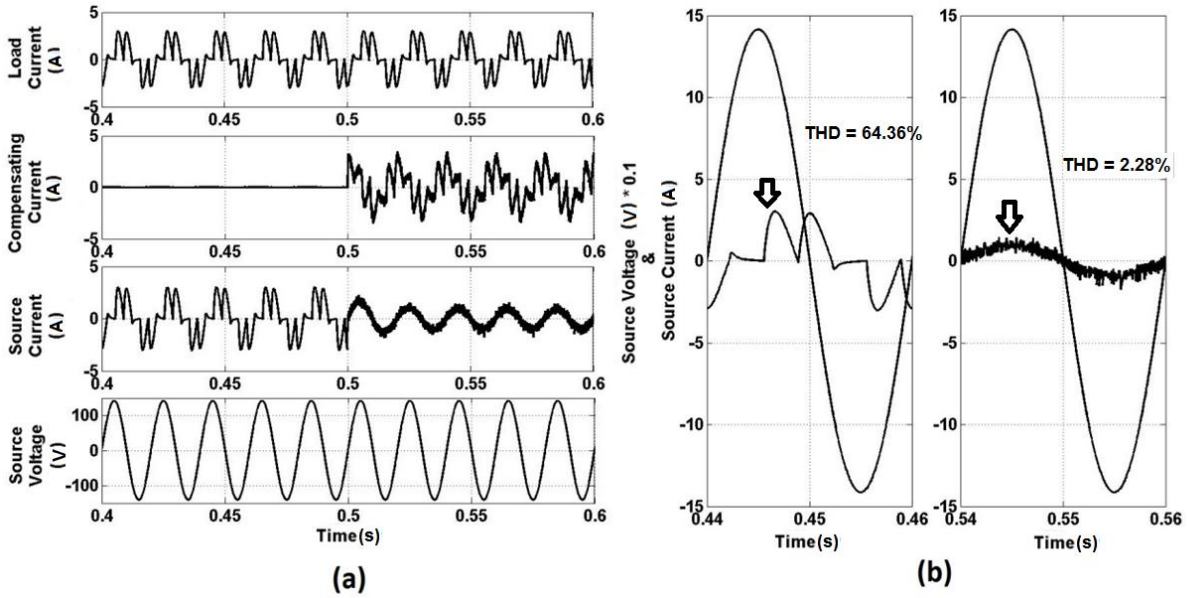

Fig. 5.9 (a) Response of active power filter at α=60° (b) Source voltage and current waveforms for one cycle before and after the enabling of active filter

5.5.3.2 Step change in load

Fig. 5.10 (a) shows the waveforms of load current, compensating current, source current and source voltage at α=60° with neuro fuzzy controller. Here, initially the load is 1 kVA up to t=0.5 s and at t=0.5 s the load is suddenly increased to 2 kVA and then, the load is brought back to 1kVA at t=0.7 s. The amplitude of load current, compensating current and source current also increase in response to the increase in load up to t=0.7 s, then they return to previous values. The source current is again found to be nearly sinusoidal. The quality of source current is measured in terms of its THD under these loading conditions. From the FFT analysis of source current waveforms at 1 kVA and 2 kVA, the THD is 2.28% and 2.22% respectively. These waveforms show that after increment in load, the shunt APF continues to compensate the reactive power and reduces the harmonic content in the source current. Fig. 5.10 (b) shows the waveforms of source current and source voltage from t=0.44 s to t=0.46 s and from t=0.54 s to t=0.56 s i.e. the response of the system for one cycle before and after the step change in load of APF. The transient is completed in about two cycles without any overshoot.

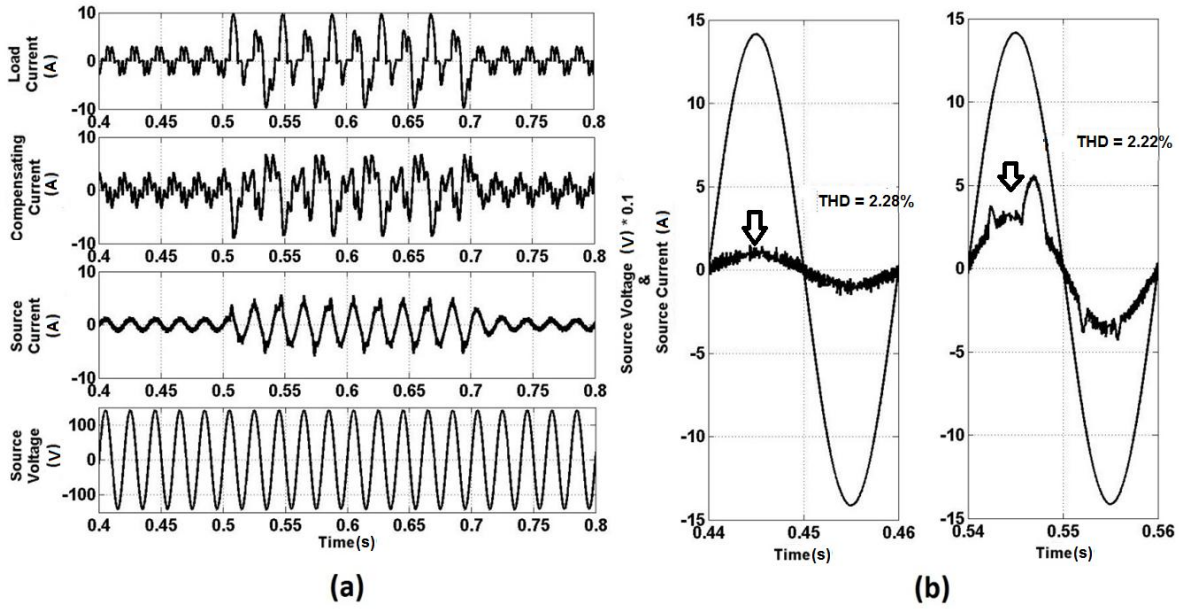

Fig. 5.10 (a) Step change in Load of active power filter at α=60° (b) before and after the step change in load for one cycle each

5.5.3.3 Unbalanced load

Fig. 5.11 (a) shows the waveforms of load current, compensating current, source current and source voltage at α=60° with neuro fuzzy controller. Here, initially the load is balanced up to t=0.5 s and at t=0.5 s. Unbalance is introduced by applying a linear star connected load in parallel to existing load, with Ra=40 Ω, Rb=60 Ω and Rc=20 Ω. The amplitude of load current, and compensating current change by applying the unbalanced

load. The source current is again found to become nearly sinusoidal. The quality of source current is measured in terms of its THD under these loading conditions. From the FFT analysis of source current waveforms at balanced load and unbalanced load, the THD is 2.28% and 2.24% respectively. These waveforms show that even with unbalanced load, the shunt APF compensates the reactive power and reduces the harmonic content in the source current. Fig. 5.11 (b) shows the waveforms of source current and source voltage from t=0.44 s to t=0.46 s and from t=0.54 s to t=0.56 s i.e. the response of the system for one cycle before and after the application of unbalanced load of APF. The source current becomes balanced after enabling APF even though the load is unbalanced.

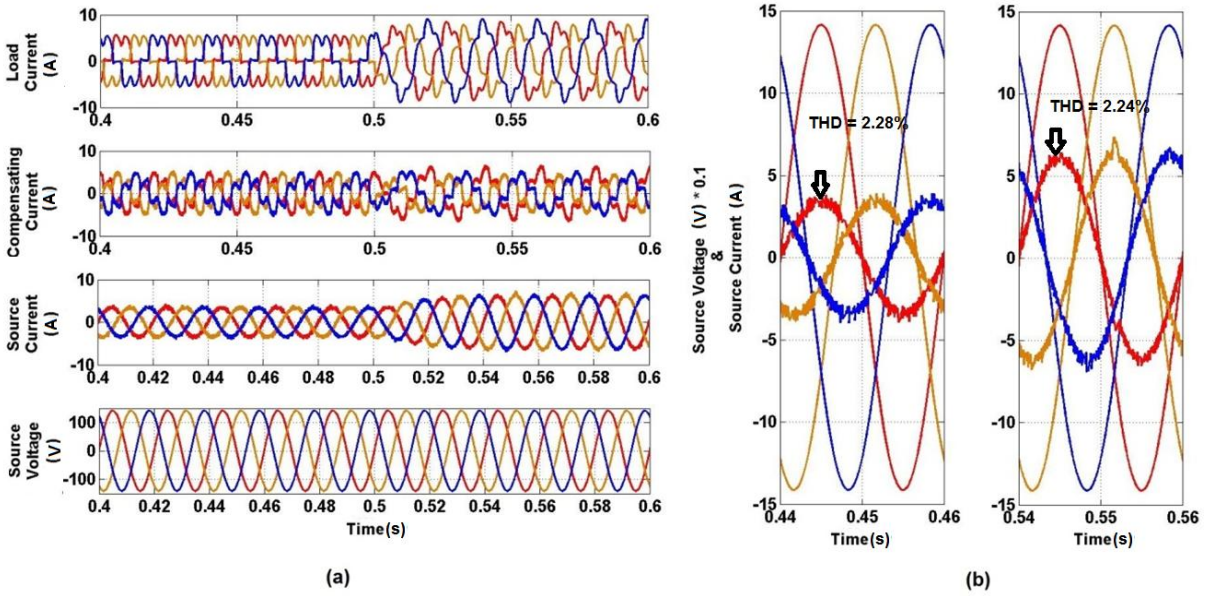

Fig. 5.11 (a) Application of an unbalanced load at t=0.5 s (I_a=3.65 A, I_b=3.71 A and I_c=3.69 A) for α=60° (b) before and after the application of unbalanced load for one cycle each

5.6 Comparision of Simulation Response

The total harmonic distortion in source current after applying the APF is shown in Table 5.1, THDs found at α=15º and 45º have also been included. As per IEEE std. 519 [226], the source current THD should be lesser than 5%. The hybrid soft computing techniques are introduced to get the lesser value of the source current THD which was permissible by IEEE std. 519. The detailed comparison of all the source current THDs with various parameters will be discussed in Chapter 7. The corresponding graph showing the change of total harminic distortion with respect to the firing angle is reported in Fig. 5.15. As the firing angle increses the source current total harmonic distortion also increases.

Table 5.1 Total Harmonic Distortion for various firing angles with neuro fuzzy controller

S.No.	Firing angle (α in °)	Total Harmonic Distortion (THD in %)
1	0	1.53
2	15	1.65
3	30	1.79
4	45	2.05
5	60	2.28

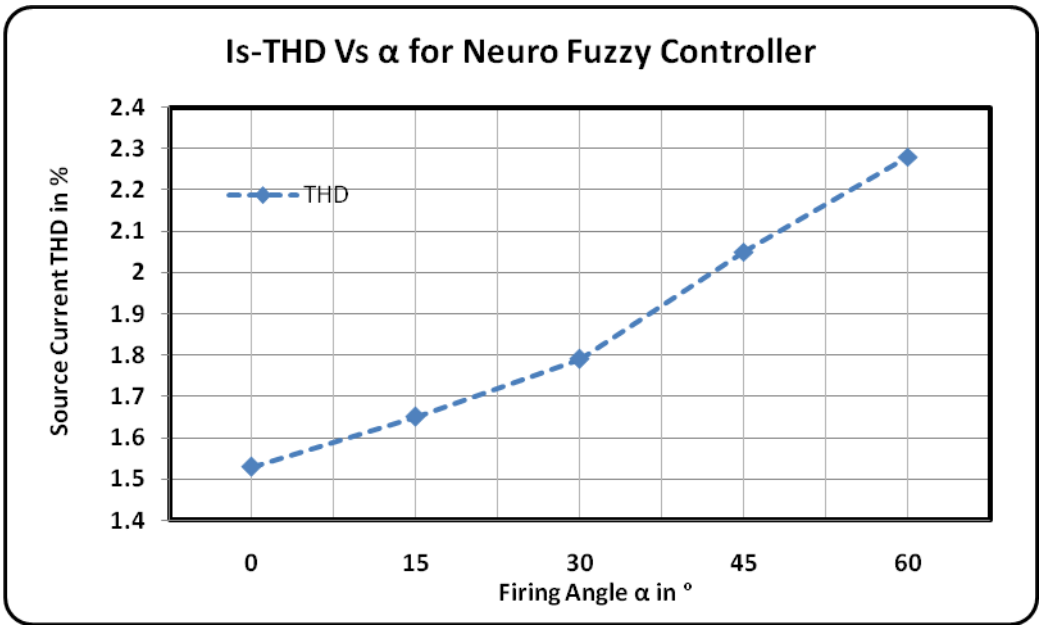

Fig. 5.12 Source Current THD variation with Firing angle (α) for neuro fuzzy Controller

5.7 Conclusion

This chapter explained the basics of neuro fuzzy controller, block diagram of fuzzy Back-Propagation algorithm with flowchart and simulation study of the neuro fuzzy controller based shunt APF. By seeing the all the results for different loads with various firing angles we can conclude that the neuro fuzzy controller based shunt APF is effective in mitigating the harmonics and compensating the reactive power. It is good even at higher firing angles as the source current total harmonic distortion is below 5% which is permissible according to IEEE-std. 519. This controller adopts the benefits of both fuzzy logic and neural network so it is the better out of all these three controllers.

6.1 Introduction

To validate the simulation results of soft computing techniques, a laboratory prototype is developed which includes:

1. Three phase power diode bridge rectifier connected to series R-L load
2. Three phase MOSFETs based inverter with inductors and capacitor as shunt active power filter.
3. dSPACE based controller for effective implementation of SAF control algorithms.

In this set-up, MOSFET (IRPF 460) have been used as the switching devices for realizing inverter which is connected with a capacitor on the DC side and a three phase inductor on the AC side.The other hardware components as required for the operation of the experimental set-up such as dead-band circuit, voltage and current sensor circuits, rectifier fed R-L load as non-linear load have been designed and developed in the laboratory. The schematic diagram for the realization of three phase shunt APF is shown in Fig. 6.1.

A Digital Signal Processor (DSP) DS1104 of dSPACE has been used for the real-time implementation of control algorithm. By using the Real-Time Workshop (RTW) of MATLAB and Real-Time Interface (RTI) feature of dSPACE–DS1104, the Simulink models of the various controllers of the prototypes have been implemented. The control algorithm is first designed in the MATLAB/Simulink software. The RTW of MATLAB generates the optimized C-code for real-time implementation. The interface between MATLAB/Simulink and Digital Signal Processor (DSP, DS1104 of dSPACE) allows the control algorithm to be run on the hardware. The master bit I/O is used to generate the required gate pulses and seven Analog to Digital Converters (ADCs) are used to interface the sensed line currents, supply voltages and dc-bus capacitor voltages. The details of MATLAB based programming for dSPACE controller is given in Appendix-B.

The development of different hardware components as required for the operation of the hardware prototypes are discussed in the next section.

6.2 System Development

To verify the viability and effectiveness of the two level inverter based SAF for harmonic elimination and reactive compensation, experimental investigations have been conducted with non-linear loads. The system is developed mainly in three stages

1. Development of power circuit
2. Sensing of system parameters
3. Development of control hardware

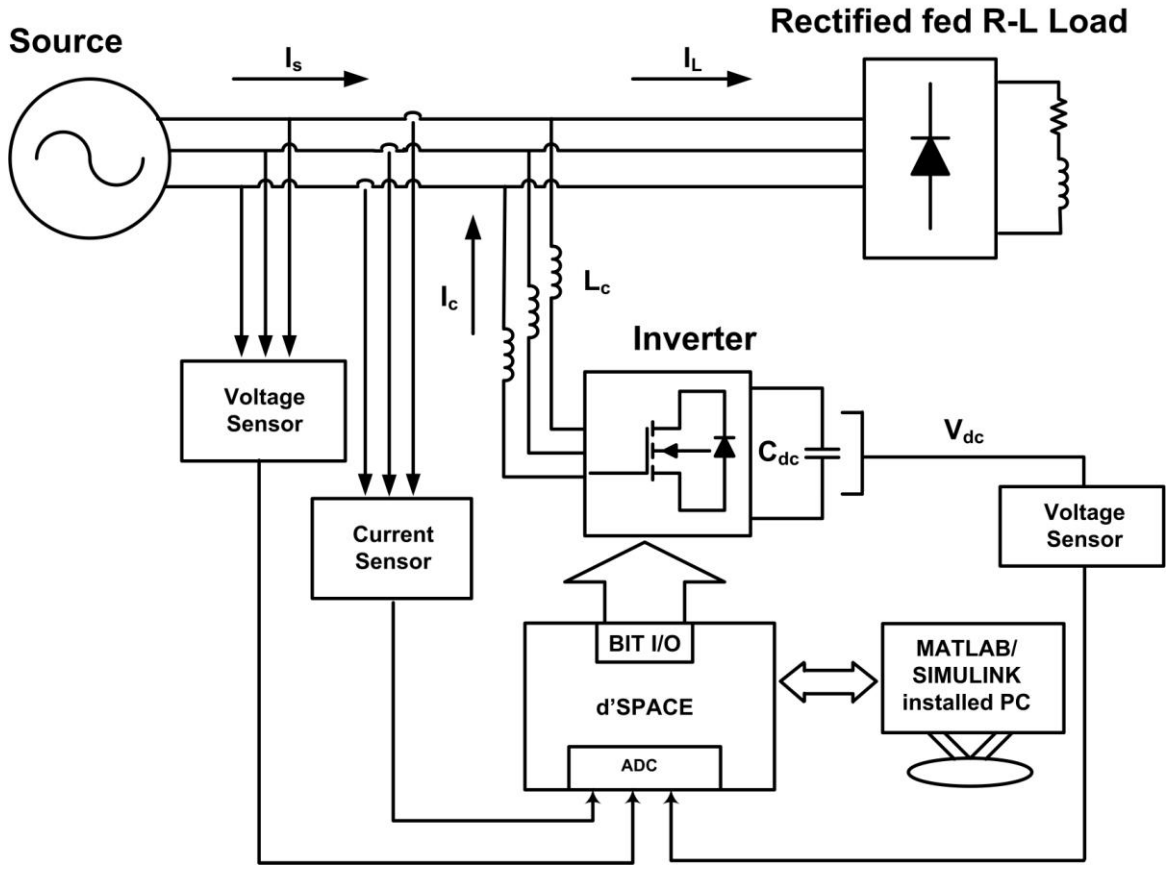

Fig. 6.1 Schematic Diagram of Hardware Implementation of Shunt Active Power Filter

6.2.1 Development of Power Circuit

The development of power circuit of the system is presented in this section.

The Non linear load

The non-linear load used here is the diode rectifier fed R-L load. The AC side is connected to the power supply and R-L load is connected at the DC side.

Fig. 6.2 shows the diode rectifier fed R-L load. The non-linear nature of the rectification produces the harmonics in AC side currents that the APF has to compensate.

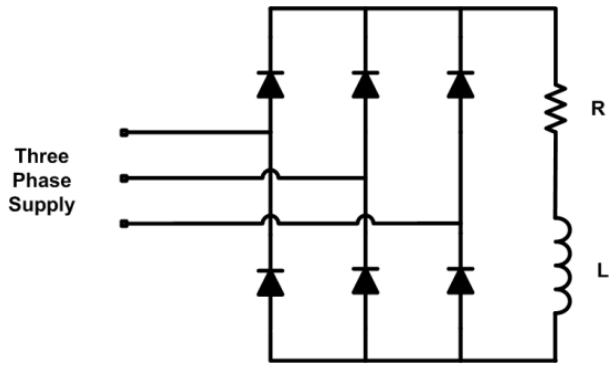

Fig. 6.2 Power Circuit with R-L as the load

Development of the active power filter

The development of APF includes the filter inductor, filter capacitor and the inverter where three inductors are placed on the AC side of the inverter and the capacitor is placed on the DC side.

As shown in Fig. 6.3, the inverter used here is a two level inverter consisting of six MOSFETs with driving circuits connected individually to each gate. The signals coming out from the dSPACE are passed through dead band circuit where each signal is converted into two signals with anti digital logic and small dead band between them. Each signal is going to respective driving circuit. As six switches and six driving circuits are used here, six signals from dead bands are required. The schematic diagram of the dead band circuit will be discussed in the next section.

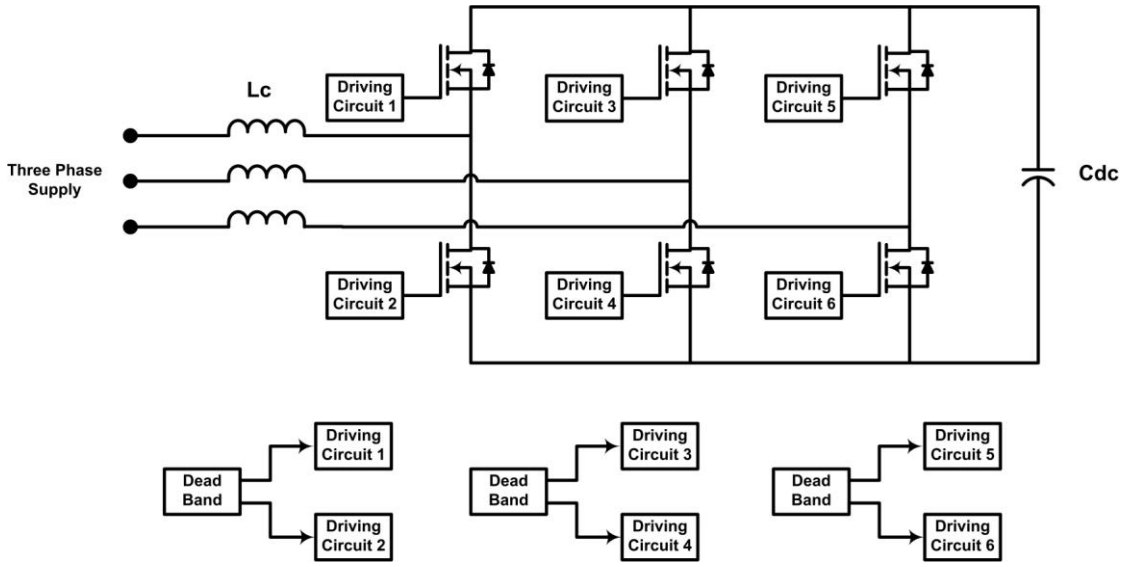

Fig. 6.3 Power circuit of inverter with filter inductors and filter capacitor

6.2.2 Sensing of system parameters

In this section, the system voltage and current measurement is discussed. As in Fig. 6.1, the feedbacks which are required for the dSPACE are seven, out of which three are supply voltages and three are supply currents and one DC voltage at the filter capacitor.

The voltage measurement or voltage sensing circuit for both AC and DC are same. The required circuits are as follows:

6.2.2.1 Voltage sensing circuit

The voltage sensing circuit consists of an isolation amplifier AD202JY with input signal connected at 1 and 2 terminals passing (Fig.6.4) through a potential divider of required values, input power supply to 31 and 32 terminals from +12 V DC supply and the output is taken from 37 and 38 terminals.

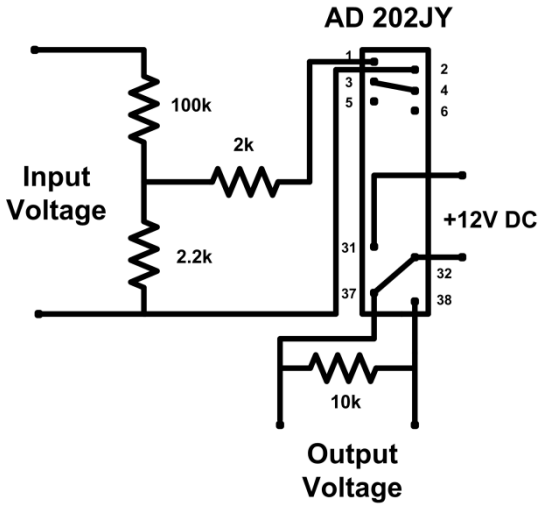

Fig. 6.4 Voltage Sensing Circuit

6.2.2.2 Current sensing circuit

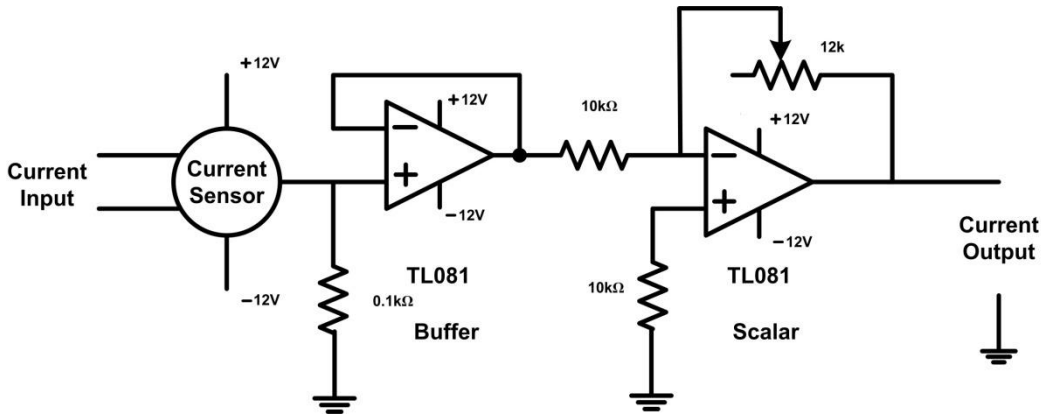

Fig. 6.5 Current Sensing Circuit

The ac source currents have been sensed using the PCB-mounted Hall-effect current sensors (TELCON HTP25). The HTP25 is a closed loop Hall effect current transformer suitable for measuring currents up to 25 A. This device provides an output current into an external load resistance. These current sensors provide the galvanic isolation between the high voltage power circuit and the low voltage control circuit and require a nominal supply voltage of the range ±12V to ±15V. It has a transformation ratio of 1000:1 and thus, its output is scaled properly to obtain the desired value of measurement. The circuit diagram of the current sensing scheme is shown in Fig. 6.5.

6.2.3 Development of Control Hardware

This section include two circuits under control hardware

1. Dead Band Circuit
2. MOSFET Driver Circuit

6.2.3.1 Dead Band Circuit

The dead band circuit is used to provide the two anti phase signals to the upper and lower switches of a leg of the inverter with a small time gap between the switch on and off of the two switches.

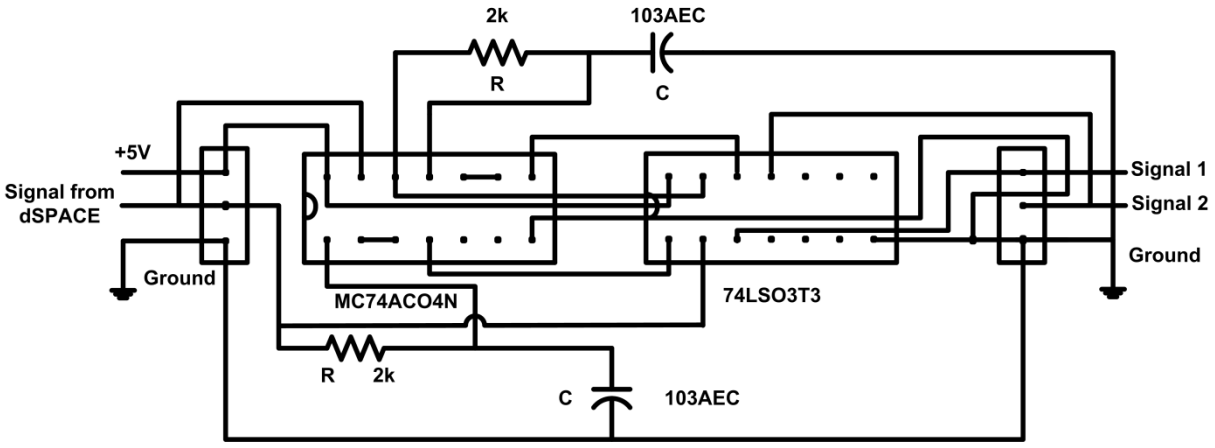

Fig. 6.6 Dead Band Circuit

The circuit diagram of dead band circuit is shown in Fig. 6.6. In the dead band circuit two logic gates NAND and NOT are used. The NAND gate gives signal 1 to the upper switch and the NOT gate gives signal 2 to the lower switch. The signal from dSPACE and +5V DC are used as inputs. The combination of RC will provide the necessary dead band between the signals.

6.2.3.2 MOSFET Driver Circuit

Fig. 6.7 shows the driver circuit and snubber circuit for MOSFET. The driving circuit consists of an opto coupler to isolate the signal from input to the output. The opto coupler MCT2E isolates the signal from dead band to the gate signal. There are two grounds. One is at the input of opto coupler with firing pulses and +5V DC supply and other is at output with gate. There is an individual supply of +12V DC from the rectified AC supply to be given at the output to get the +12V pulses at the gate. The snubber circuit with air cored resistor, power diode, capacitor and MOV is connected to drain and source terminals of the MOSFET. Fig. 6.7 shows the driving circuit and snubber circuit of the MOSFET.

The +12V DC supply can be obtained by rectifying the AC supply. First, the 230V AC supply is transformed to 18V by a 230V/18V transformer and rectified to DC supply by using diodes. The capacitors are used to smoothen the rectified dc and regulator L7812CV and Zener Diodes are used to obtain the DC voltage of +12V.

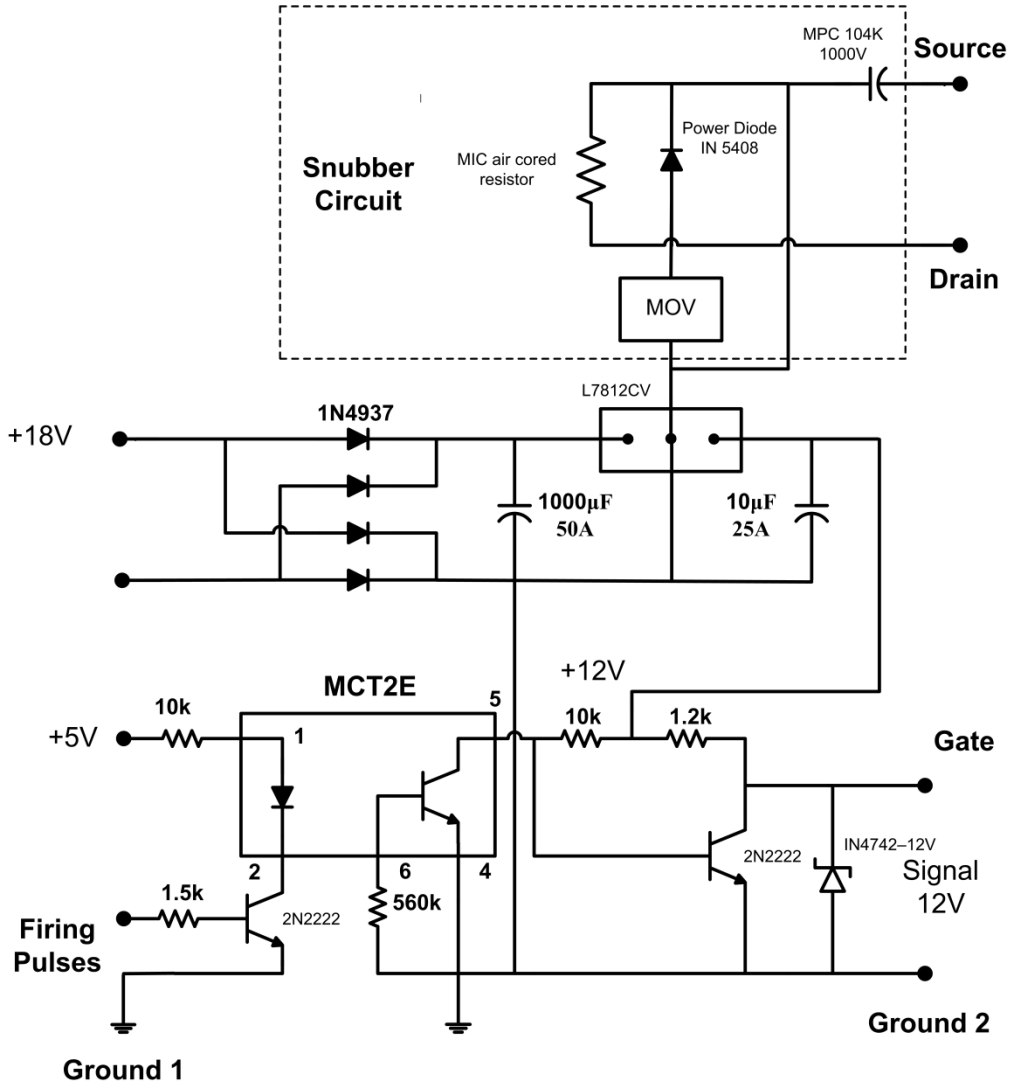

Fig. 6.7 MOSFET Driving Circuit

6.3 Experimental Results

The experimental results are taken for PI and fuzzy logic based controllers. The steady state and transient state responses are recorded in each case. The response of the DC capacitor voltage at variation in load is also captured for these controllers. The results are compared with the corresponding simulation results.

Fig. 6.8 shows the experimental results of the steady state performance of load current, compensating current, source current and source voltage. Fig. 6.8(a) is for PI controller and Fig. 6.8(b) is for fuzzy logic controller. The Fig. 6.8(b) shows the improvement of source current in the fuzzy logic case. The THD of the fuzzy logic case (5.7%) is lower than that of PI controller case (6.3%) is shown in Fig. 6.20.

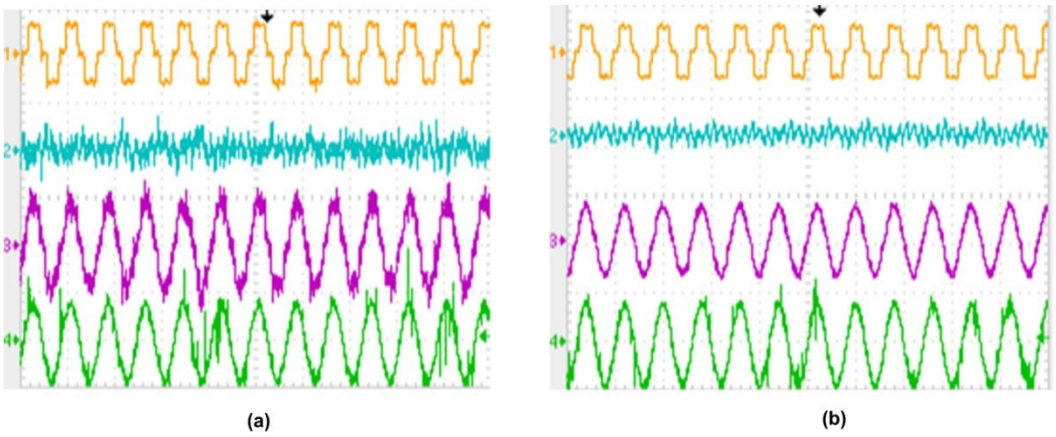

Fig. 6.8 Experimental performance of APF with (a) PIC and (b) FLC : (1) load current (scale: 1 A/div), (2) compensating current (scale: 1 A/div), (3) source current (scale: 1 A/div) and (4) source voltage (scale: 50 V/div)

Fig. 6.9 shows the simulation results of steady state performance of the load current, compensating current, source current and source voltage corresponding to experimental results of Fig. 6.8.

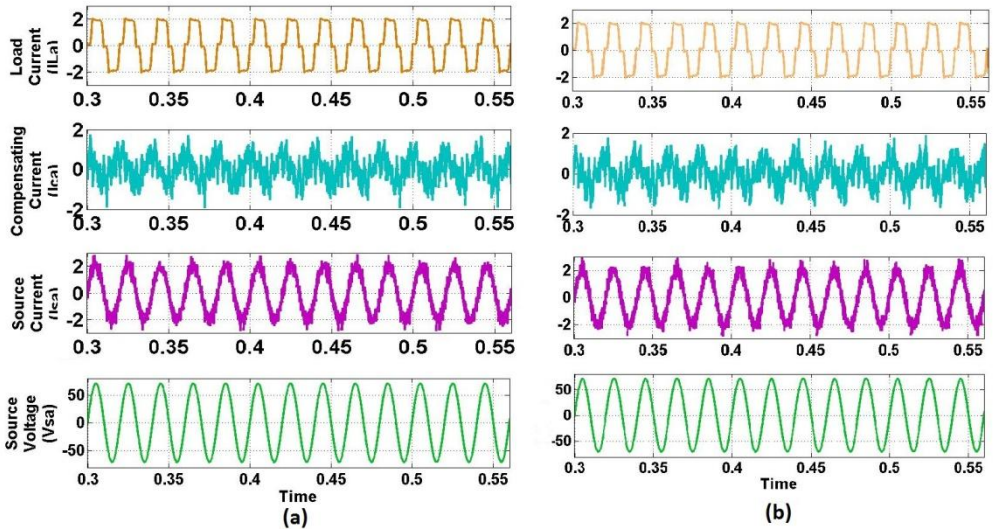

Fig. 6.9 Simulation of Steady State performance of APF (voltage rating brought down to the level of experimental value) with (a) PI and (b) FLC

Fig. 6.10 shows the source current and source voltage of Fig.6.8 on same plane to emphasize that they are also in same phase. As these two waves are aligned properly, the power factor is almost unity. Fig. 6.10(a) is for PI controller and Fig. 6.10(b) is for fuzzy logic controller.

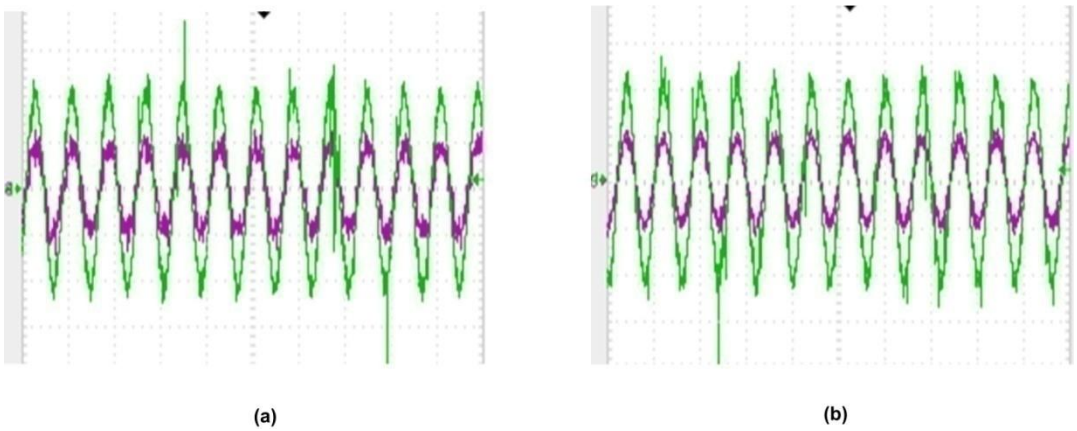

Fig. 6.10 Experimental performance of APF using (a) PI and (b) FLC : (3) source current (scale: 1 A/div) and (4) source voltage (scale: 20 V/div)

Fig. 6.11 shows the simulation results showing the source voltage and source current. The power factor in simulation results is also almost unity. Fig. 6.11(a) is for the PI controller and Fig. 6.11(b) is for fuzzy logic controller. The experimental results of Fig. 6.10 are found similar to the simulation results of Fig. 6.11 under same operating conditions.

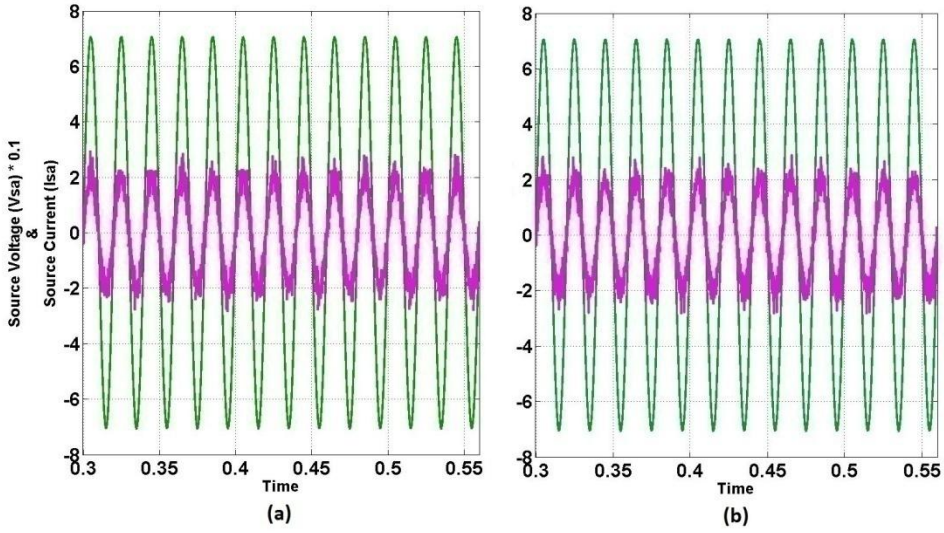

Fig. 6.11 Simulation results of steady state performance of APF using (a) PI and (b) FLC for experimental parameters for source voltage and current

Fig. 6.12 shows the experimental results of the dynamic performance of load current, compensating current, source current and source voltage. The dynamic nature follows due to a step increase in load. Fig. 6.12(a) is for PI controller and Fig. 6.12(b) is for fuzzy logic controller. The Fig. 6.12(b) shows the improvement of source current in the fuzzy logic case. The THD of the fuzzy logic case is better than that of PI controller case as can be seen from Fig. 6.20 and Fig. 6.21. This is the comparison of PI and fuzzy logic controller cases.

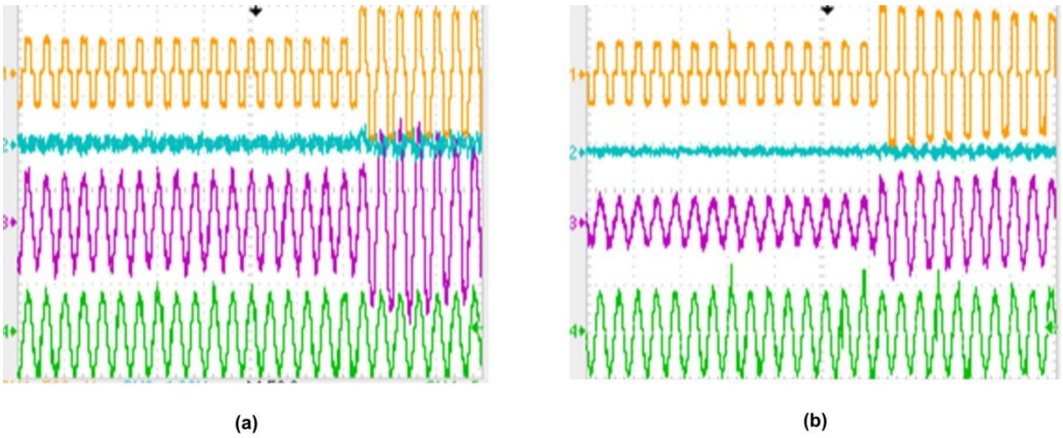

Fig. 6.12 Experimental (Dynamic) performance of APF using (a) PI and (b) FLC for step increase in load: (1) load current (scale: 1 A/div), (2) compensating current (scale: 1 A/div), (3) source current (scale: 1 A/div) and (4) source voltage (scale: 50 V/div)

Fig. 6.13 shows the simulation results of dynamic state performance of the load current, compensating current, source current and source voltage. The simulations are conducted at the operating conditions same as in experimentation to see the comparison with experimental results. Fig. 6.13 is for PI and fuzzy logic controllers. These waveforms for the step increase in load show that compensating current also increases without perceptible delay.

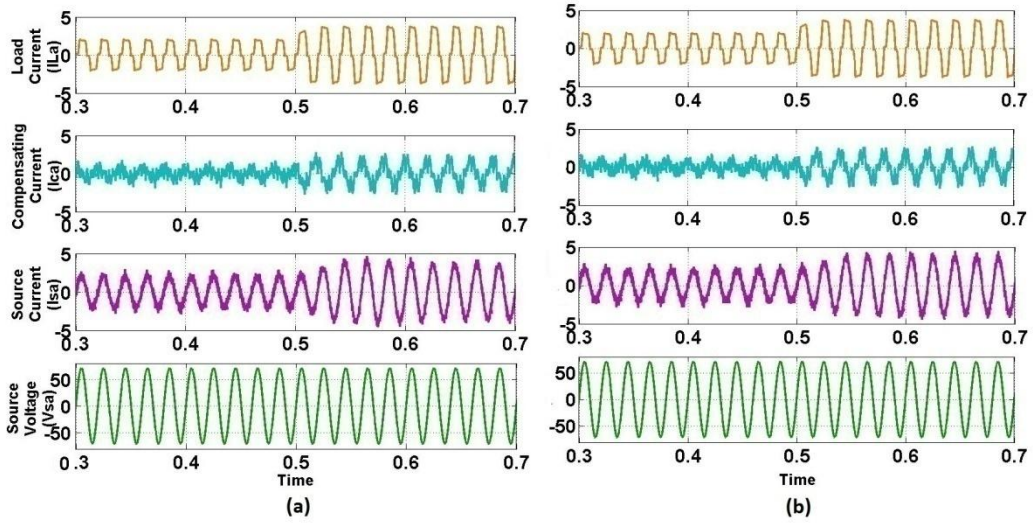

Fig. 6.13 Simulation results of dynamic performance of APF using (a) PI and (b) FLC for step increase in load for experimental parameters

Fig. 6.14 shows the simulation results of dynamic state performance of the load current, compensating current, source current and source voltage. The simulations are conducted at the operating conditions same as in experimentation to see the comparison

with experimental results. Fig. 6.14 is for PI and fuzzy logic controllers. These waves are for the step decrease in load.

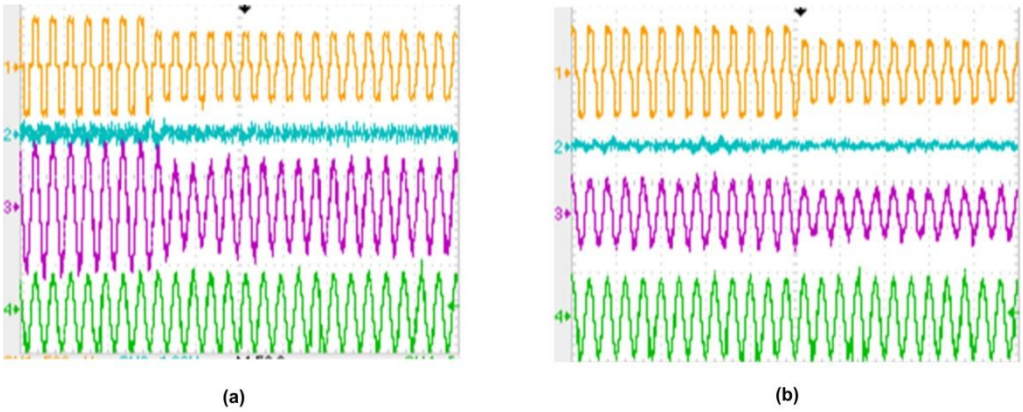

Fig. 6.14 Experimental (Dynamic) performance of APF using (a) PI and (b) FLC for step decrease in load: (1) load current (scale: 1 A/div), (2) compensating current (scale: 1 A/div), (3) source current (scale: 1 A/div) and (4) source voltage (scale: 50 V/div)

Fig. 6.15 shows the simulation results dynamic state performance of the load current, compensating current, source current and source voltage. The Fig.6.15 is for PI and fuzzy logic controllers. So, the comparison between PI and fuzzy logic controller in simulation results of experimental parameters is also shown. These waves are for the step decrease in load.

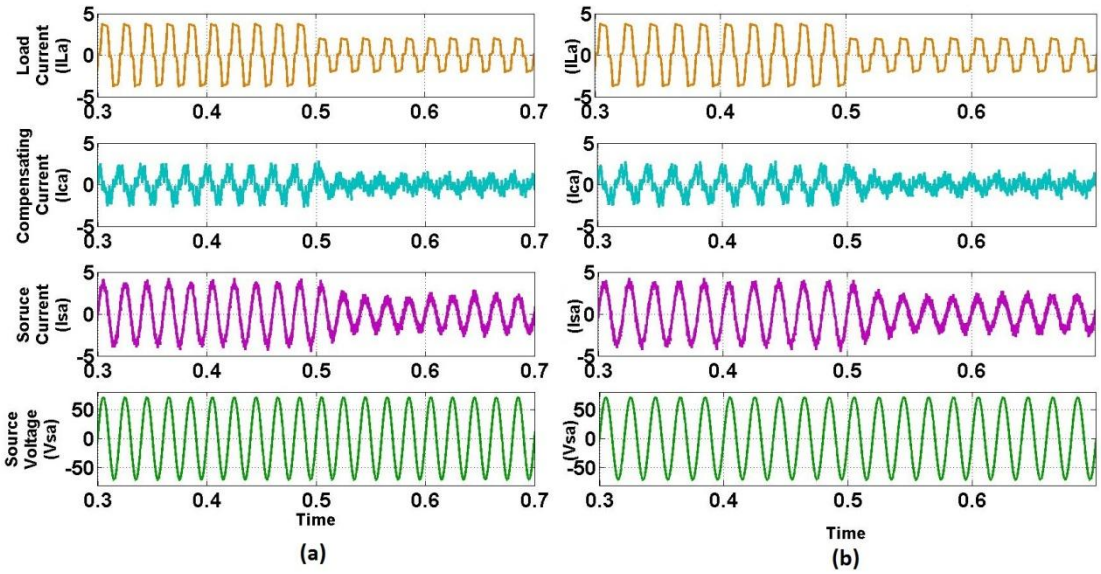

Fig. 6.15 Simulation results of dynamic performance of APF using (a) PI and (b) FLC for step increase in load for experimental parameters

Fig. 6.16 shows the DC capacitor voltage and source current with step increase in load. It shows that the change in DC capacitor voltage with respect to source current and the

change is less in fuzzy logic case (Fig. 6.16(a)) when compared to that of PI controller case (Fig. 6.16(b)). Fig. 6.17 shows the simulation results of the DC capacitor voltage for PI and fuzzy logic cases with same axis. It is clear that the fuzzy logic case attains the steady state early and the change from steady state is less in case of fuzzy logic controller case.

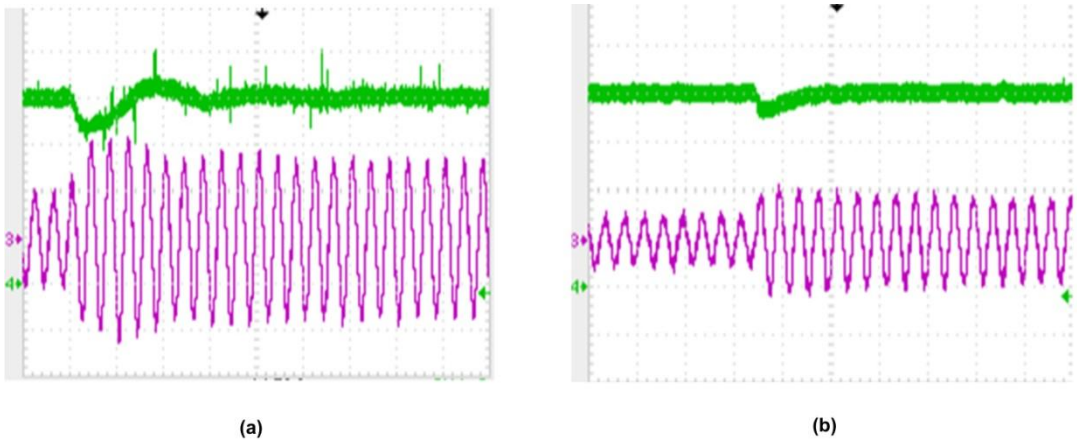

Fig. 6.16 Experimental (Dynamic) performance of APF using (a) PI and (b) FLC for step increase in load: (3) source current (scale: 1 A/div) and (4) DC link voltage (scale: 50 V/div)

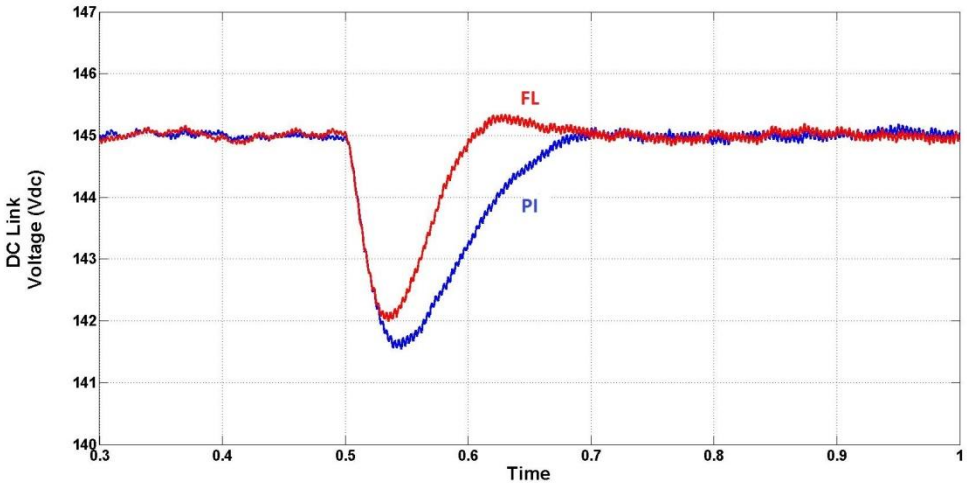

Fig. 6.17 Simulation of step increase in load for DC link voltage

Fig. 6.18 shows the DC capacitor voltage and source current with step decrease in load. It shows that the change in DC capacitor voltage with respect to source current and the change is less in fuzzy logic case (Fig. 6.18(a)) when compared to that of PI controller case (Fig. 6.18(b)). Fig. 6.19 shows the simulation results of the DC capacitor voltage for PI and fuzzy logic cases with same axis. It is clear that in fuzzy logic case the steady state is achieved earlier and the deviation from steady state is less in case of fuzzy logic controller.

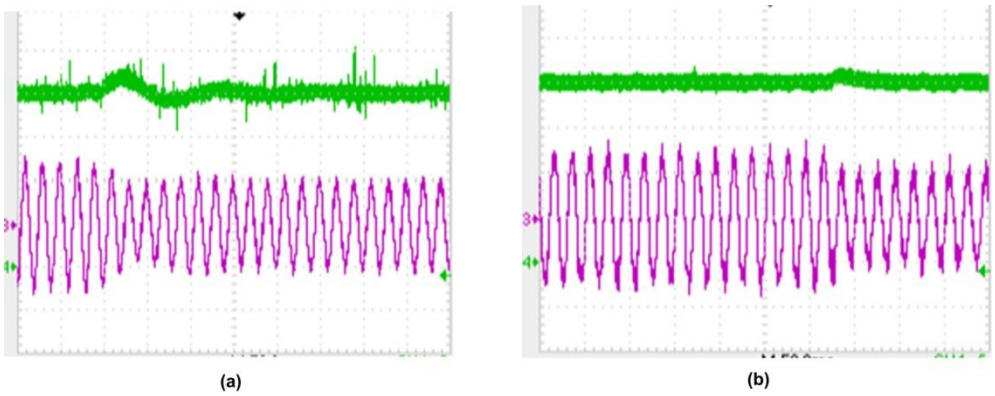

Fig. 6.18 Experimental (Dynamic) performance of APF using (a) PI and (b) FLC for step decrease in load: (3) source current (scale: 1 A/div) and (4) DC link voltage (scale: 50 V/div)

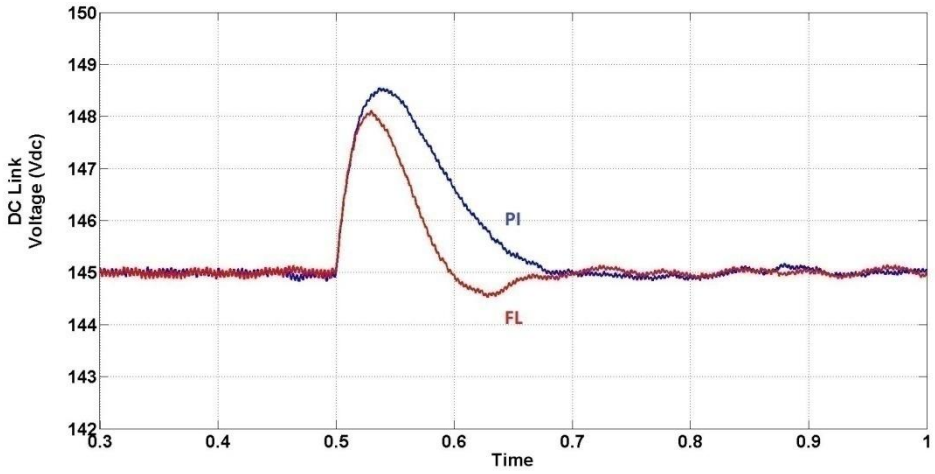

Fig. 6.19 Simulation of step decrease in load for DC link voltage

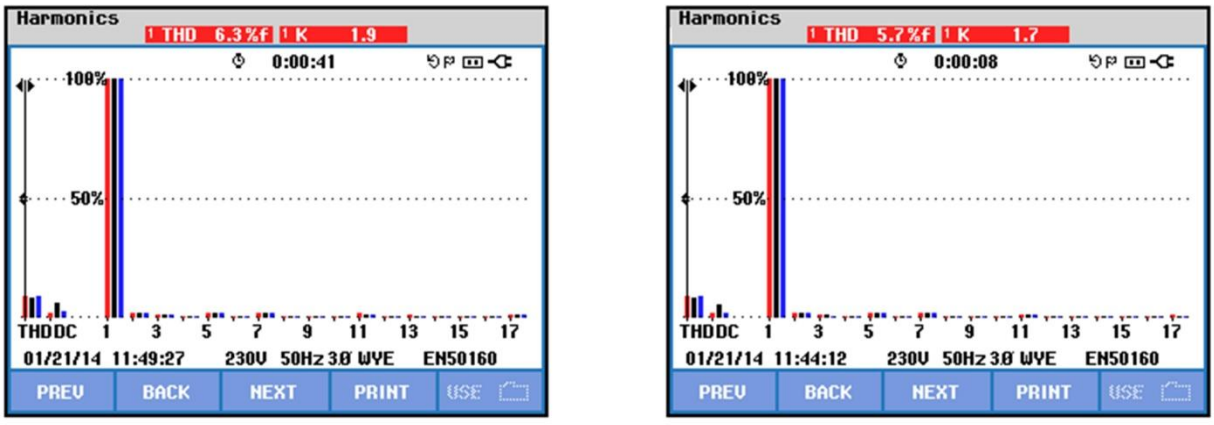

(a) (b)

Fig. 6.20 Experimental spectral analysis for source current in (a) PI controller (b) fuzzy logic controller

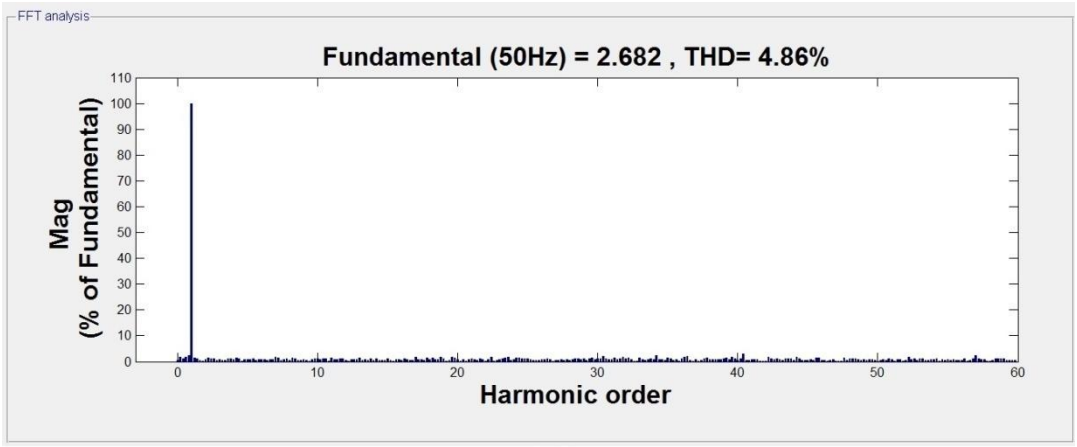

(a)

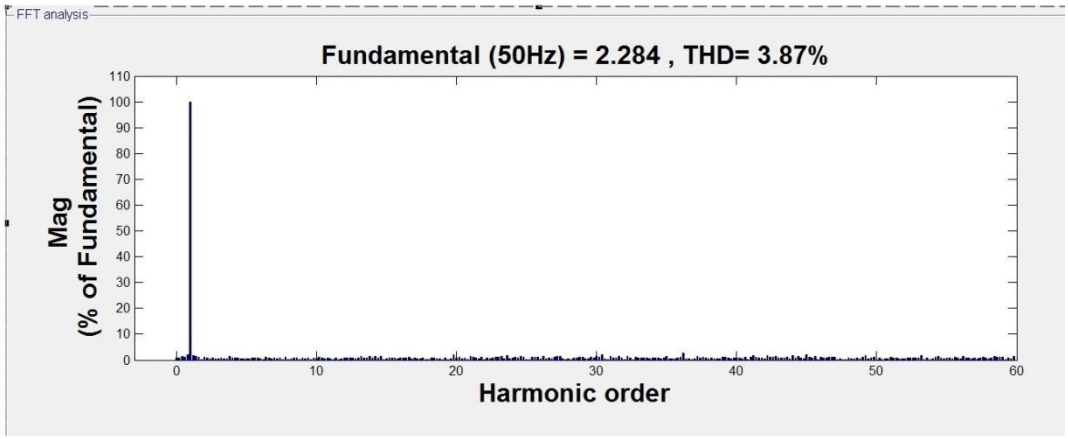

(b)

Fig. 6.21 Simulation results of spectral analysis for source current in (a) PI controller (b) fuzzy logic controller

Fig. 6.20 shows the spectral analysis of the source current in experimentation for PI and fuzzy logic controller cases. Fig. 6.21 shows the spectral analysis for the source current for simulation study with experimental parameters. It is seen that the total harmonic distortion for fuzzy logic case is the least out of the two controllers.

The comparison of experimental and simulation results are almost the same in case of waveforms and total harmonics distrotion of the source current. The same fact is again tabulated in Table 6.1. It shows the total harmonic distortion in PI and fuzzy logic controllers for simulation and experimentation.

Table 6.1 Source current THD (%) for PI and fuzzy logic cases in simulation and experimentation

Source Curent THD (%)	**PI**	**Fuzzy Logic**
Simulation	4.86	3.87
Experimentation	6.30	5.70

6.4 Conclusion

This chapter has given the details of the hardware implementation related to this work. The power and control circuits have been briefly explained with circuit diagrams. The experimental results for all the parameters are given in this chapter. The simulation results for the experimental parameters are also reported for the comparison with experimental results. The comparison of PI and fuzzy logic controller is also given in simulation and experimental results. It is shown that fuzzy logic control gives improved results for both steady state and dynamic conditions as compared to PI controller.

7.1 Introduction

In this chapter, comparison of the simulation and hardware results for different controllers, are presented. Performance results for before and after the compensation with PI controller are presented. After that the performance of soft computing controllers like Fuzzy logic, Neural Network and Neuro Fuzzy over a range of firing angle of the load rectifier are compared.

7.2 Comparison of source current THD and power factor before and after the compensation for PI controller

As in Fig. 2.6, a three phase non-linear load is considered to be supplied from three phase mains. Two values of loading are considered, 1kVA and 2kVA and for this R, L combination is adjusted as the firing angle (α) of rectifier is varied. A star connected R load with Ra=40Ω, Rb=20Ω and Rc=60Ω is connected in parallel to the 1kVA non linear load to study the unbalanced load condition. Table 7.1 shows the THD and power factor for 1 kVA, 2 kVA and for unbalance before compensation. The source voltage and source current before compensation is shown in Fig. 7.1. The THDs and power factors are seen to be increasing as firing angle setting is changed from α=0 to α=60º. As in Fig. 7.1, the source current THD is distorted due to the harmonics. In this case as the firing angle is 0, the reactive power demand is negligible.

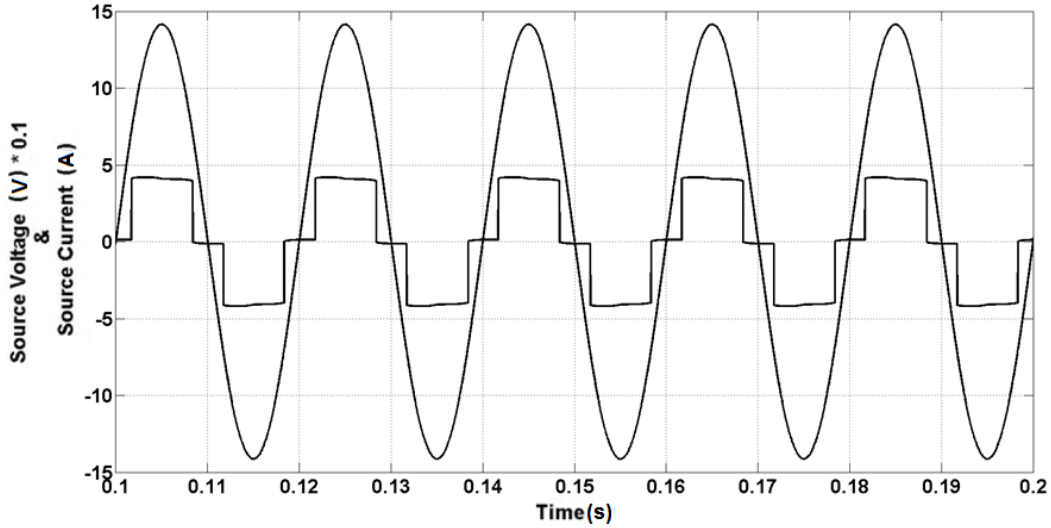

Fig. 7.1 Source voltage and source current before compensation (Balanced non-linear load of 1kVA at α=0)

When the APF is enabled, the source voltage and current corresponding to Fig. 7.1 are shown in Fig. 7.2. The shape of source current is sinusoidal now and also in phase with

the source voltage. The controller used in this set up is PI type of controller and the corresponding THDs and power factors are tabulated in Table 7.2. The THDs are in the permissible limits by IEEE guidelines and they keep on increasing with firing angle. The power factors are almost the same for all the cases showing that the reactive power is almost compensated.

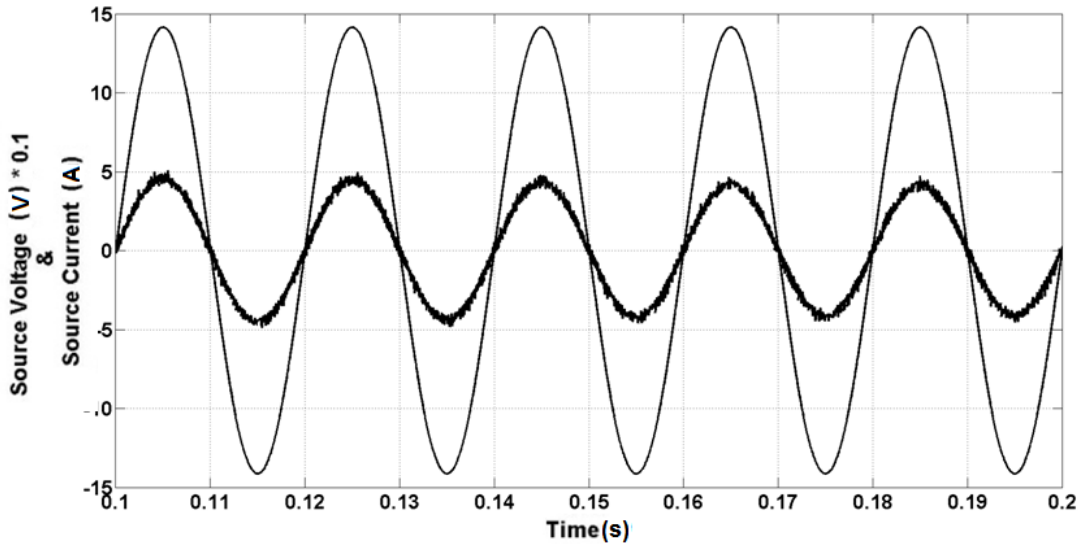

Fig. 7.2 Source voltage and source current after compensation

Table 7.1 Total Harmonic Distortion of source current (%) and Fundamental Power Factor for various firing angles before compensation

Before Compensation						
Firing angle (α)	THD of source current			PF		
	1 kVA	2 kVA	UB	1 kVA	2 kVA	UB
0	30.64	30.88	16.44	0.99	1.00	0.99
15	31.24	31.07	16.53	0.97	0.96	0.96
30	37.57	36.71	19.76	0.91	0.89	0.93
45	46.82	45.27	24.57	0.79	0.78	0.89
60	64.36	62.56	33.43	0.66	0.64	0.84

Table 7.2 Total Harmonic Distortion of source current (%) and Fundamental Power Factor for various firing angles after compensation

After Compensation (PI)						
Firing angle (α)	THD of source current			PF		
	1 kVA	2 kVA	UB	1 kVA	2 kVA	UB
0	2.93	2.88	2.73	1.00	1.00	1.00
15	3.25	3.15	3.12	1.00	1.00	1.00
30	4.00	3.12	3.93	1.00	1.00	1.00
45	4.35	4.26	4.32	1.00	1.00	1.00
60	5.97	4.37	5.38	0.99	0.99	0.99

The comparison of source current THD before and after enabling APF is again shown in Fig. 7.3, Fig. 7.4 and Fig. 7.5 for 1kVA, 2 kVA and unbalance respectively. The THD after compensation in all cases is seen to be much less when compared to that of before compensation case. The THDs increase with firing angle without APF. However, its change is very less when the APF is enabled.

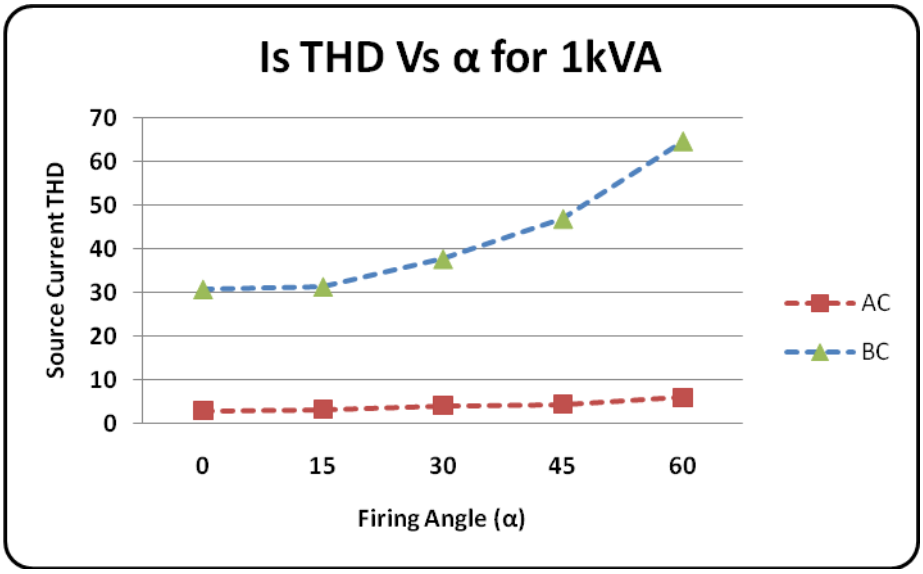

Fig. 7.3 Total Harmonic Distortion with respect to firing angle before and after compensation for 1 kVA

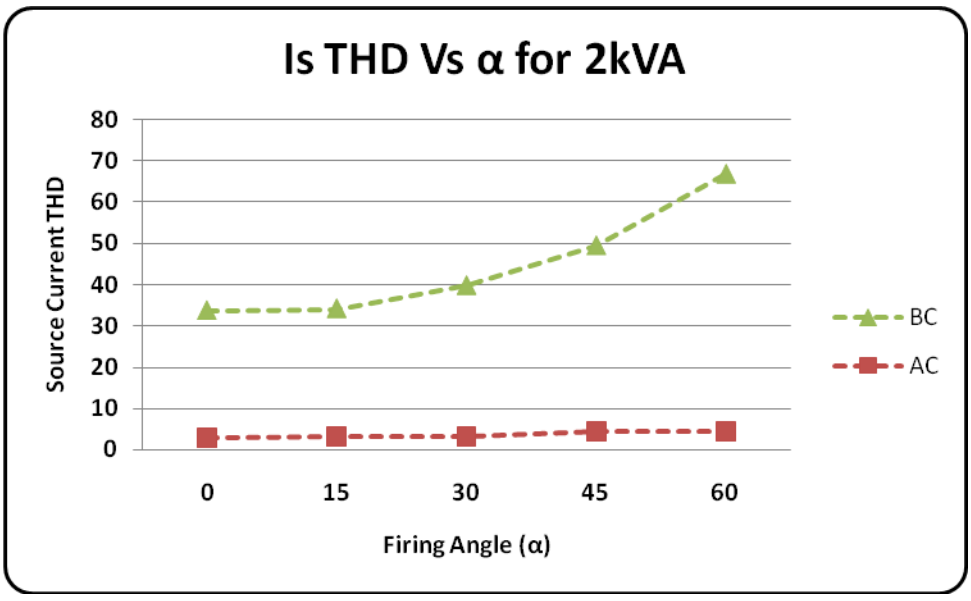

Fig. 7.4 Total Harmonic Distortion with respect to firing angle before and after compensation for 2 kVA

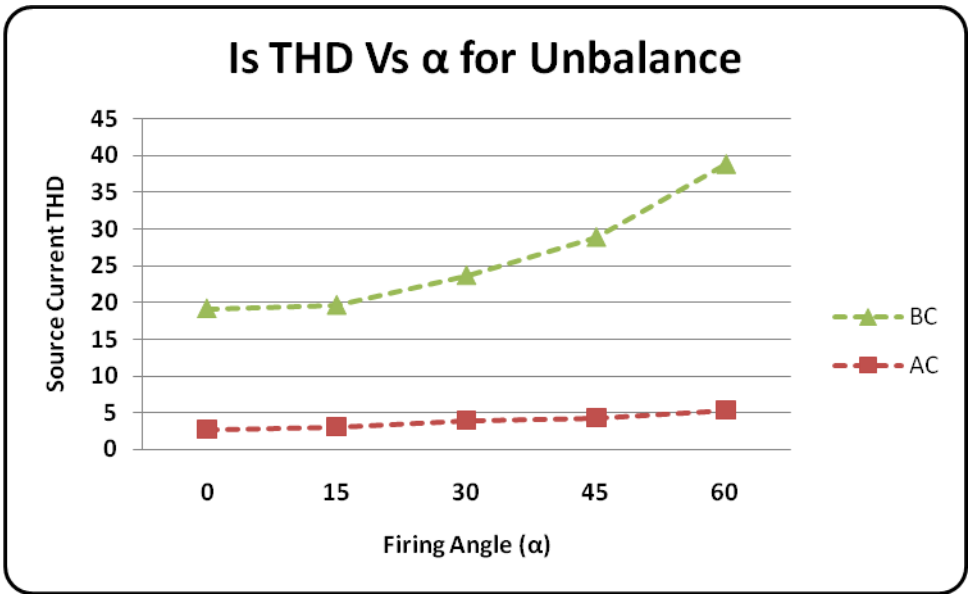

Fig. 7.5 Total Harmonic Distortion with respect to firing angle before and after compensation for unbalance in load

The comparison of power factor before and after enabling the APF is shown in Fig. 7.6, Fig. 7.7 and Fig. 7.8 for 1 kVA, 2 kVA and for unbalance respectively. In all these case the power factor is almost unity showing that the reactive power is perfectly compensated in all the cases.

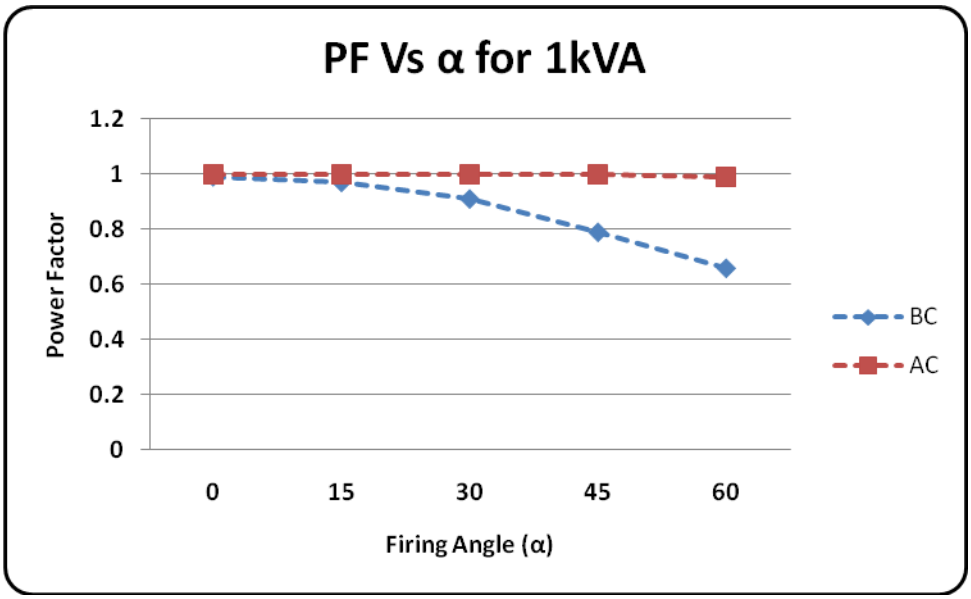

Fig. 7.6 Power Factor with respect to firing angle before and after compensation for 1 kVA

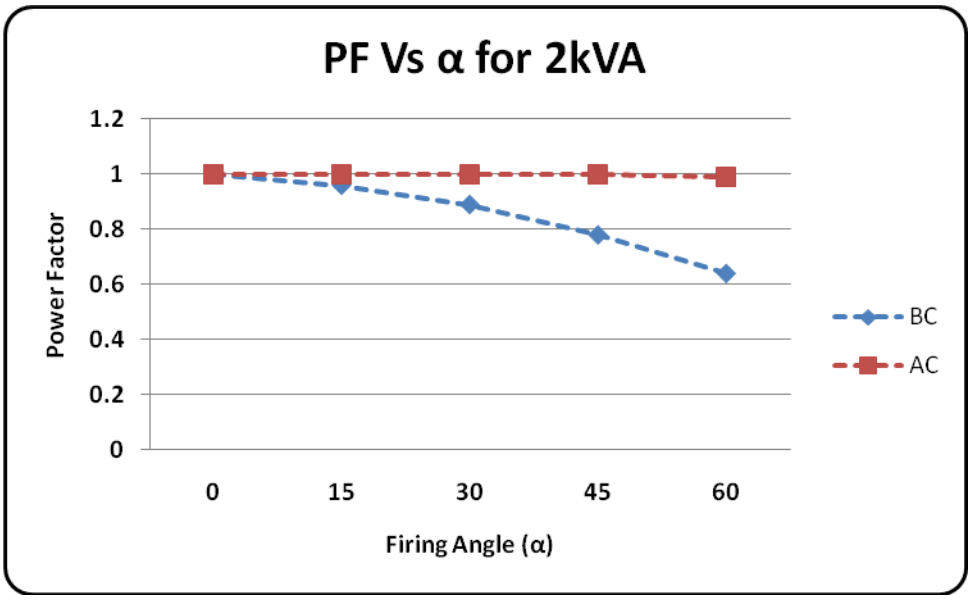

Fig. 7.7 Power Factor with respect to firing angle before and after compensation for 2 kVA

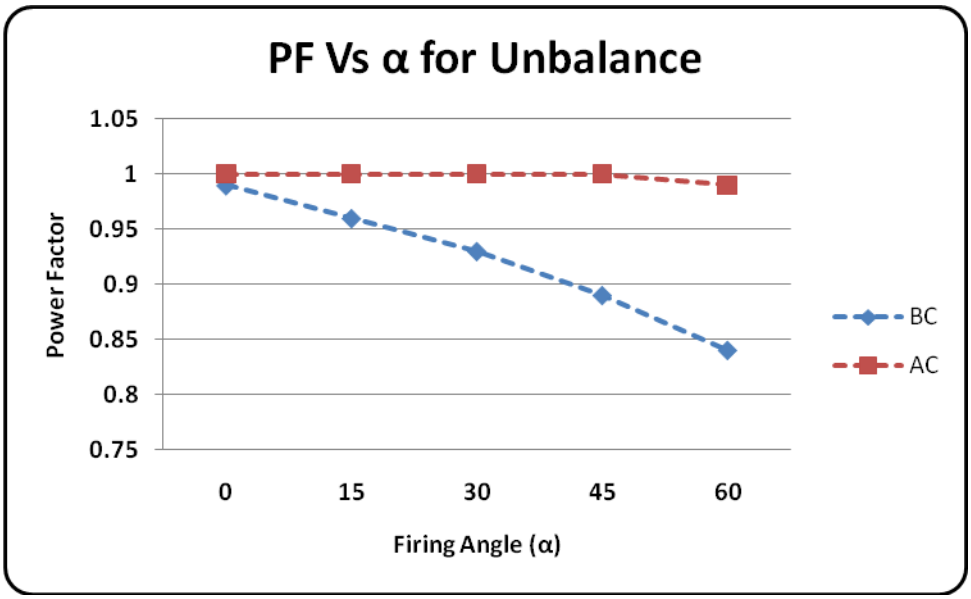

Fig. 7.8 Power Factor with respect to firing angle before and after compensation for unbalance in load

7.3 Performance comparison of all controllers

With PI controller, it is observed in the previous section that the THDs have been fairly low. However, at α=60º setting, the THD becomes 5.97% crossing the permissible limit as can be seen from Table 7.2 for 1 kVA load setting. In general, PI controller offers satisfactory performance for a fixed load. Its parameter need to be retuned for a different load settings. To overcome this problem, soft computing techniques are used in place of PI controller. The soft computing techniques used here are Fuzzy, Neural Network and Neuro

Fuzzy. The THDs offered by all these controllers for 1 kVA load are shown in Table 7.3, that of 2 kVA load is shown in Table 7.4 and for unbalanced load are shown in Table 7.5.

In Table 7.3, the THD of the source current with various controllers namely PI controller, fuzzy and neural network and neuro fuzzy controller are tabulated for various firing angles from α=0 to α=60º for 1kVA load. The neuro fuzzy controller gives improved results when compared to other controllers and the THD at firing angle α=0 is the least in each controller.

Table 7.4 and Table 7.5 present the source current THD with various controllers and various firing angles for 2 kVA and unbalanced load, respectively. Here, again the performance of neuro fuzzy controller is found to be superior to all the types.

Table 7.3 Source current THD (%) with 1kVA load for various firing angles and various controllers

Firing angle (α)	PI	FL	NN	NF
0	2.93	2.71	2.43	1.53
15	3.25	2.82	2.63	1.65
30	4.00	2.88	2.85	1.79
45	4.35	3.25	3.12	2.05
60	5.97	3.45	3.21	2.28

Table 7.4 Source current THD (%) with 2kVA load for various firing angles and various controllers

Firing angle (α)	PI	FL	NN	NF
0	2.88	2.65	2.33	1.43
15	3.15	2.75	2.55	1.58
30	3.12	2.79	2.78	1.72
45	4.26	3.18	3.05	2.01
60	4.37	3.33	3.15	2.22

Table 7.5 Source current THD (%) with unbalance in load for various firing angles and various controllers

Firing angle (α)	PI	FL	NN	NF
0	2.73	2.69	2.35	1.48
15	3.12	2.78	2.57	1.61
30	3.93	2.82	2.76	1.75
45	4.32	3.22	3.08	2.03
60	5.38	3.38	3.16	2.24

The corresponding graph for comparing the all controllers is shown in Fig. 7.9, Fig. 7.10 and Fig. 7.11 for 1 kVA, 2 kVA and for unbalanced load respectively. In all the cases the source current THD is plotted with respect to the firing angle. The neuro fuzzy controller has the least THD in all the cases and while the PI controller has the highest THD.

Table 7.6 Power Factor with 1kVA load for various firing angles and various controllers

Firing angle (α)	PI	FL	NN	NF
0	1.00	1.00	1.00	1.00
15	1.00	1.00	1.00	1.00
30	1.00	1.00	1.00	1.00
45	1.00	1.00	1.00	1.00
60	1.00	1.00	1.00	1.00

Table 7.7 Power Factor with 2kVA load for various firing angles and various controllers

Firing angle (α)	PI	FL	NN	NF
0	1.00	1.00	1.00	1.00
15	1.00	1.00	1.00	1.00
30	1.00	1.00	1.00	1.00
45	1.00	1.00	1.00	1.00
60	1.00	1.00	1.00	1.00

Table 7.8 Power Factor with unbalance in load for various firing angles and various controllers

Firing angle (α)	PI	FL	NN	NF
0	1.00	1.00	1.00	1.00
15	1.00	1.00	1.00	1.00
30	1.00	1.00	1.00	1.00
45	1.00	1.00	1.00	1.00
60	1.00	1.00	1.00	1.00

In Table 7.6, the power factor with various controllers namely PI controller, fuzzy and neural network and neuro fuzzy controller are tabulated for various firing angles from α=0 to α=60º for 1 kVA load. In all the cases, the power factor is unity showing that the control method provides unity power factor with all the controllers. We can conclude that the reactive power is completely compensated in this control method irrespective of type of the controller.

Table 7.7 and Table 7.8 present the power factors with various controllers and various firing angles for 2 kVA and unbalanced load, respectively. Here, again the reactive power is completely compensated.

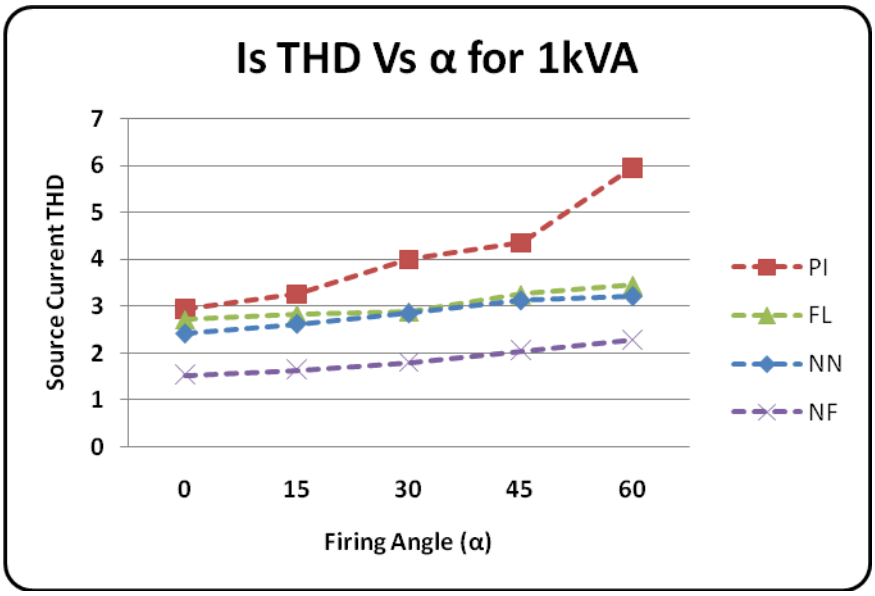

Fig. 7.9 Source current THD (%) with various firing angles for 1kVA load for various controllers

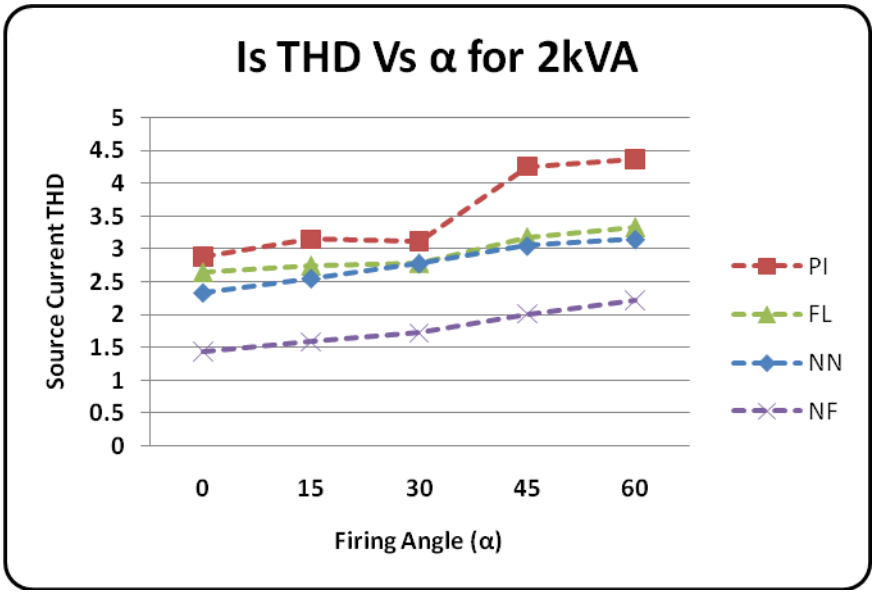

Fig. 7.10 Source current THD (%) with various firing angles for 2kVA load for various controllers

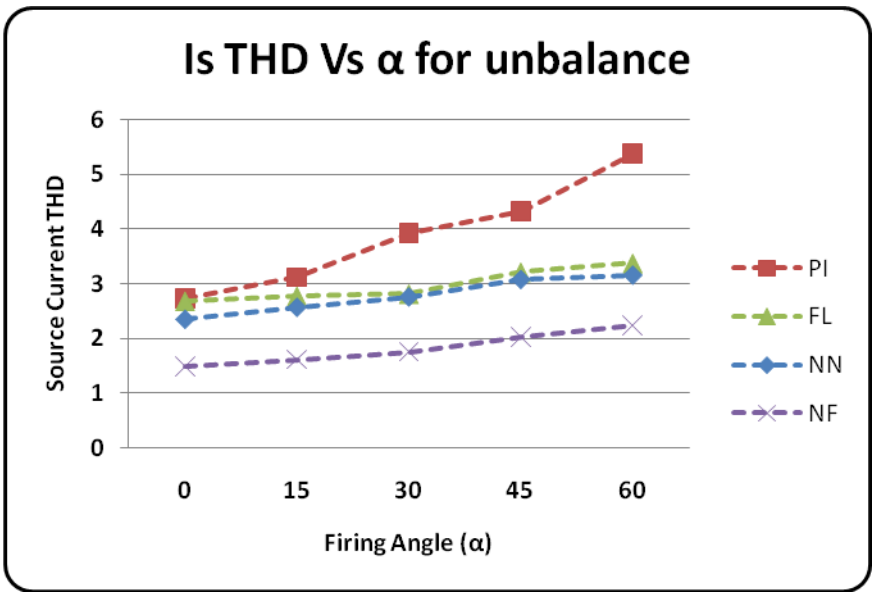

Fig. 7.11 Source current THD (%) with various firing angles for unbalance in load for various controllers

A further insight on the harmonic contents is obtained by spectral analysis. A representative case of neuro fuzzy controller is taken here since this is found to be best among all the controllers considered in this work.The spectral analyses for the neuro fuzzy controller before and after compensation is shown in Fig. 7.12 for firing angle α=0, Fig. 7.13 for firing angle α=30º and Fig.7.14 for firing angle α=60º.

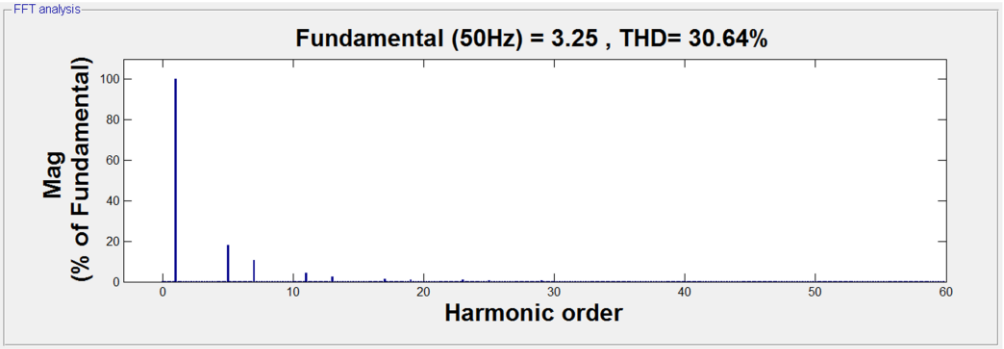

(a)

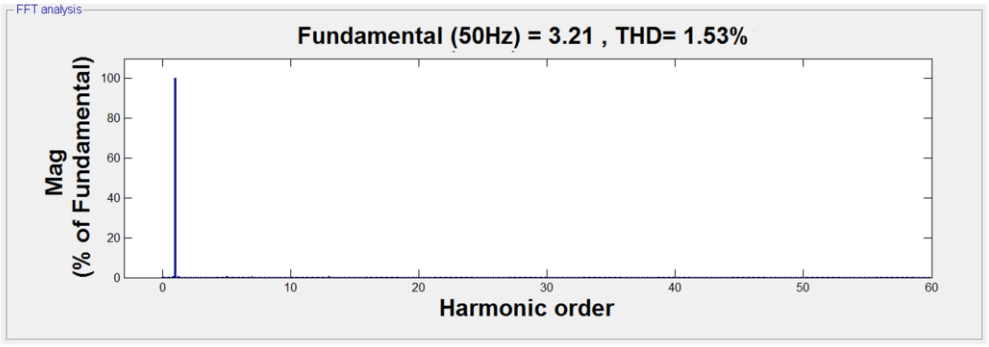

(b)

Fig. 7.12 FFT analysis for source current (a) before and (b) after compensation with 1kVA load for firing angle α=0 and neuro fuzzy controller

Fig. 7.12 shows the FFT analysis of the source current for neuro fuzzy controller at firing angle α=0. In Fig. 7.12 (a) the FFT analysis before the application of the APF is shown and it is 30.64% with some harmonics in the FFT analysis. In Fig. 7.12 (b) the FFT analysis after the application of the APF is shown and it is 1.53% with very less harmonics in the FFT analysis showing that the harmonics are almost mitigated. The corresponding current value is also reduced from 3.25 A to 3.21 A.

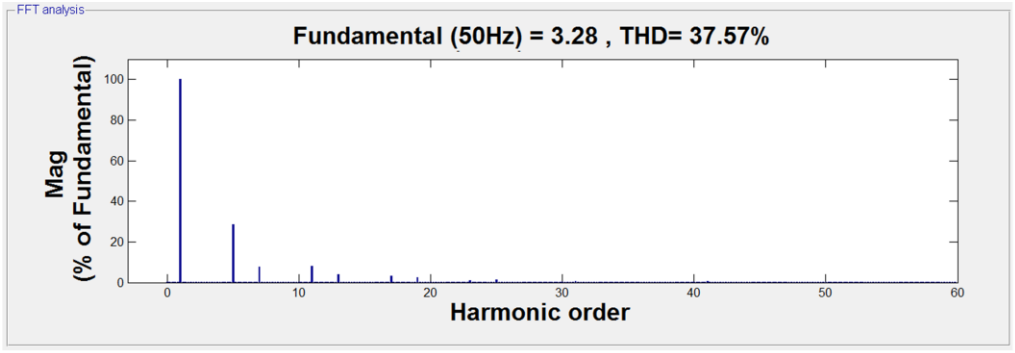

(a)

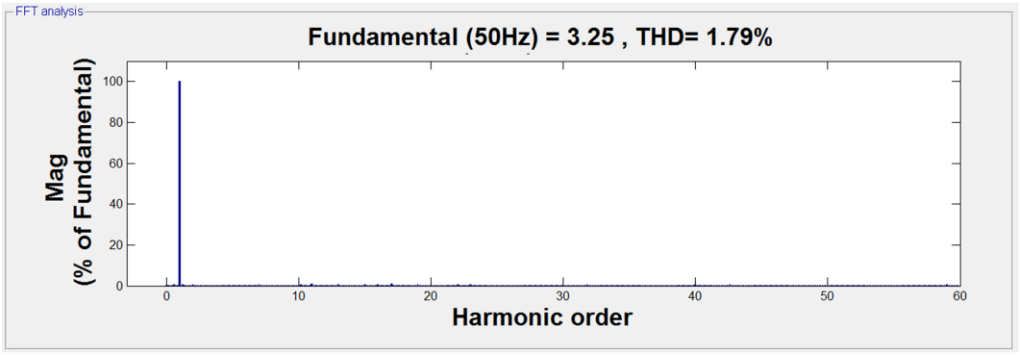

(b)

Fig. 7.13 FFT analysis for source current (a) before and (b) after compensation with 1kVA load for firing angle α=30º and neuro fuzzy controller

Fig. 7.13 shows the FFT analysis of the source current for neuro fuzzy controller at firing angle α=30º. In Fig. 7.13 (a) the FFT analysis before the application of the APF is shown and it is 37.57% with some harmonics in the FFT analysis. In Fig. 7.13 (b) the FFT analysis after the application of the APF is shown and it is 1.79% with very less harmonics in the FFT analysis showing that the harmonics are almost mitigated. The corresponding current value is also reduced from 3.28A to 3.25A.

Fig. 7.14 shows the FFT analysis of the source current for neuro fuzzy controller at firing angle α=60º. In Fig. 7.14 (a) the FFT analysis before the application of the APF is shown and it is 64.36% with some harmonics in the FFT analysis. In Fig. 7.14 (b) the FFT analysis after the application of the APF is shown and it is 2.28% with very less harmonics in

the FFT analysis showing that the harmonics are nearly mitigated. The corresponding current value is also reduced from 3.32 to 3.29.

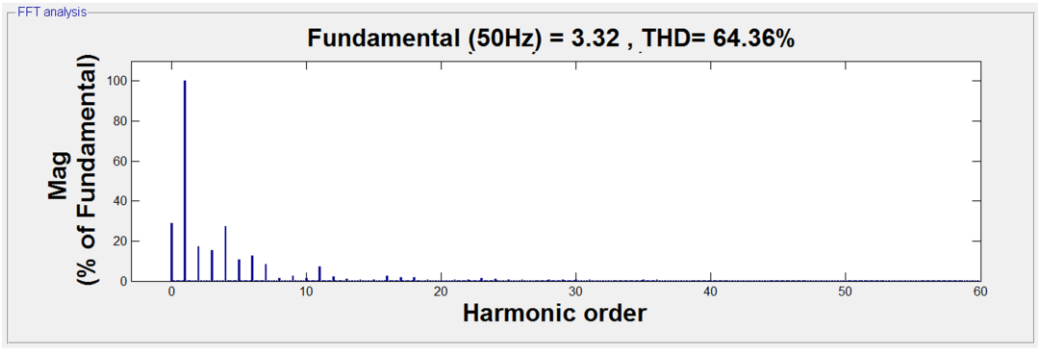

(a)

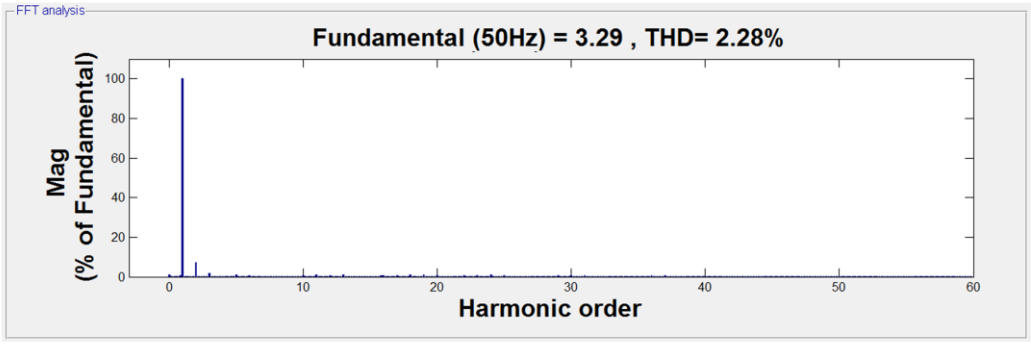

(b)

Fig. 7.14 FFT analysis for source current (a) before and (b) after compensation with 1kVA load for firing angle α=60º and neuro fuzzy controller

7.4 Conclusion

The comparison of the source current THD for shunt APF with different types of controller namely PI, Fuzzy Logic, Neural network and neuro fuzzy is presented. The effectiveness of neuro fuzzy controller is established through the detailed presentation of results. The spectral analyses for neuro fuzzy controller for various firing angles before and after compensation is also presented in this chapter. These analyses show the variation with firing angle for before and after compensation. The firing angle 0 analysis is better than that of other angles.

Chapter 8: CONCLUSIONS AND FURTHER SCOPE OF WORK

8.1 Conclusions

The use of power electronic converters for converting and controlling electrical power is rapidly increasing to achieve high efficiency, improved performance, compactness and power saving. These processes, however, suffer from many power quality problems, mainly related to harmonics and reactive power.

From the available literature, it emerges that the APF is a viable solution for these power quality problems while using power electronic converters. Many topologies are developed to compensate the current and voltage harmonics, reactive power, unbalance etc. The use of voltage source PWM converter based shunt APFs are researched widely due to its high efficiency, light weight, low cost and expandability to multi level and multi-step configurations.

In this thesis, a shunt APF is presented in which issues related to design and control are developed in detail. The developed system is investigated for compensating the harmonics, reactive power and input balancing in three phase three wire system. It is a simple and cost effective solution, especially for low and medium power applications. A current controlled voltage source PWM converter with inductor at ac side and capacitor at dc side is used as a shunt APF. The control technique used here is the unit voltage template method. In this method, the unit voltage templates are generated by dividing each voltage wave with its maximum value. The output of dc capacitor voltage controller is multiplied by these voltage templates to generate the reference currents which are having the magnitude as the output of the controller and the frequency of the source voltage. The error generated between the reference current and actual source current is processed in hysteresis controller to generate the required gating signals for the inverter.

Extensive simulations have been carried out for steady state, transient state and unbalanced load conditions, first using a PI controller. The performance is investigated for (a) balanced load, (b) unbalanced load, (c) step change in load. The firing angle of the rectifier representing a non linear load is varied for achieving the wide variation in harmonic contents and reactive power requirement in non-linear load. The simulation results are obtained in terms of waveforms of load current, compensating current, source current and source voltage under above mentioned loading conditions. The variation of source current THD for various load settings are studied. In order to further verify the simulation results, a prototype is developed in the laboratory with diode rectifier fed RL load as the non linear load. The MOSFET based shunt active power filter is used in this experimentation. Various waveforms are captured in this work like load current, compensating current, source current and source voltage, DC link voltage and spectral analysis for getting total harmonic distortion in both steady state and transient state.

PI controller parameters need to be changed for each load setting to obtain the minimum value of total harmonic distortion. This is not possible when the load is changed suddenly or is frequently varied. So, the artificial intelligent techniques are developed in this thesis to make this action automatic. The artificial intelligent techniques used in this work are fuzzy logic, neural networks and neuro fuzzy.

The fuzzy logic controller is designed based on the mamdani method of fuzzy inference system. In this method, the error, change in error and the output of the controller are designed for the controller with triangular membership functions. In neural network, the Back-Propagation algorithm is used to train the network. In neuro fuzzy controller, the triangular membership function is used for the fuzzy case and the Back-Propagation is used for the neural network case.

In all cases of PI, fuzzy logic, neural network and neuro fuzzy controllers, the harmonic mitigation and the reactive power compensation is achieved. Out of all these methods, neuro fuzzy controller performs the better compared to all the other three methods by utilizing the advantages of both fuzzy logic and neural network methods. The simulation results corresponding to the each controller for steady state and transient, for variation in the firing angle, for balanced, step change in load and unbalanced loads are presented in this thesis. The entire range of work carried out in this thesis is shown in Table 8.1.

Table 8.1 Simulation and Experimental work presented in this thesis

Performance of active power filter in this work	**Controllers**	PI	Fuzzy Logic	Neural Network	Neuro Fuzzy
Simulation Study (α = 0º, 30º and 60º)	Active Filter is enabled	Y	Y	Y	Y
	Step change in load	Y	Y	Y	Y
	Unbalanced load	Y	Y	Y	Y
Experimental Study (α = 0º)	Steady state	Y	Y	N	N
	Transient (increase and decrease in load)	Y	Y	N	N

Y: The work has been included in this work

N: The work has not been included in this work

8.2 Further Scope of the work

After having accomplished this work, the author believes that the following more studies can be done for performance enhancement:

1. A two level inverter is used in this work and there is a possibility to upgrade this work by using a multilevel inverter to get the advantages of the multilevel inverter.
2. Various types of artificial intelligent controller are used as voltage controller. The same step can be extended to change the current control from hysteresis controller to artificial intelligent controllers.
3. There are other types of intelligent controllers based on genetic algorithm, ant colony algorithm, particle swarm algorithm and so on. They can also be tried as voltage or current controllers.
4. The other complex power electronics loads such as matrix converters can also be considered to investigate the performance of artificial intelligent techniques suggested in this work.

PUBLICATIONS FROM THE WORK

International Journals:

1. Kishore Kumar Pedapenki, S. P. Gupta, Mukesh Kumar Pathak, "Shunt Active Power Filter with MATLAB and d'SPACE 1104 Verification", International Journal of Applied Engineering Research, Vol. 11, No. 6, pp. 4085-4090, 2016.
2. Kishore Kumar Pedapenki, S. P. Gupta, Mukesh Kumar Pathak, "Artificial intelligence controller for Power Quality Improvement", Electric Power Components and Systems **(Revised Manuscript Submitted).**
3. Kishore Kumar Pedapenki, S. P. Gupta, Mukesh Kumar Pathak, "Hybrid Artificial Intelligence based solution for Power Quality", Journal of Soft Computing, Springer **(Under Review).**
4. Kishore Kumar Pedapenki, S. P. Gupta, Mukesh Kumar Pathak, " Hybrid Artificial Intelligence based Active Power Filter for balanced and unbalanced loads", International Journal of Electrical Engineering and Informatics **(Under Review).**
5. Kishore Kumar Pedapenki, S. P. Gupta, Mukesh Kumar Pathak, "Comparison among artificial intelligence and hybrid artificial intelligence controllers for Power Quality Improvement", Journal of Power Electronics **(Under Review).**

International Conferences:

1. Kishore Kumar Pedapenki, S. P. Gupta, Mukesh Kumar Pathak, "Comparison of PI & Fuzzy Logic Controller for Shunt Active Power Filter", IEEE - International Conference on Industrial and Information Systems (ICIIS), Sri Lanka, pp. 42-47, 18^{th} - 20^{th} Aug, 2013.
2. Kishore Kumar Pedapenki, S. P. Gupta, Mukesh Kumar Pathak, "Application of Neural Networks in Power Quality", IEEE - International Conference on Soft Computing Techniques & Implementations (ICSCTI), Manav Rachna International University, Faridabad, Haryana, India, 8^{th} -10^{th} October, 2015 (Presented).
3. Kishore Kumar Pedapenki, S. P. Gupta, Mukesh Kumar Pathak, "Soft Control Techniques for Shunt Active Power Filter", IEEE - Power, Communication and Information Technology Conference (PCITC), Siksha O Anusandhan University, Bhubaneswar, Odisha, India, pp. 60-65, 15^{th} - 17^{th} October, 2015.
4. Kishore Kumar Pedapenki, S. P. Gupta, Mukesh Kumar Pathak, "Two Controllers for Shunt Active Power Filter based on Fuzzy Logic", IEEE - International Conference on Research in Computational Intelligence and Communication Networks (ICRCICN),

RCC Institute of Information Technology, Kolkata, West Bengal, India, pp.141-144, 18th -20th Nov, 2015.

5. Kishore Kumar Pedapenki, S. P. Gupta, Mukesh Kumar Pathak, “Neuro Fuzzy based controller for Power Quality Improvement”, IEEE - International Conference on Computational Intelligence and Communication Networks (CICN), MIR Labs, Gyan Ganga Institute of Technology and Sciences Chapter, Jabalpur, Madhya Pradesh, India, 12th -14th Dec, 2015 (Presented).

6. Kishore Kumar Pedapenki, S. P. Gupta, Mukesh Kumar Pathak, “Comparison of Shunt Active Power Filters with Fuzzy and Neuro Fuzzy controllers”, IEEE - International Conference on Computational Intelligence and Communication Networks (CICN), MIR Labs, Gyan Ganga Institute of Technology and Sciences Chapter, Jabalpur, Madhya Pradesh, India, 12th -14th Dec, 2015 (Presented).

7. Kishore Kumar Pedapenki, S. P. Gupta, Mukesh Kumar Pathak, “Shunt Active Power Filter with artificial intelligent controllers”, IEEE - International Conference on Control, Instrumentation, Communication & Computational Technologies (ICCICCT), Noorul Islam University, Nagercoil, Tamil Nadu, India, pp. 74-77, 28th -29th Dec, 2015.

8. Kishore Kumar Pedapenki, S. P. Gupta, Mukesh Kumar Pathak, “Comparison of PI and Neural Network based Controllers for Shunt Active Power Filter”, IEEE - International Conference on Control, Instrumentation, Communication & Computational Technologies (ICCICCT), Noorul Islam University, Nagercoil, Tamil Nadu, India, pp. 214-218, 28th -29th Dec, 2015.

9. Kishore Kumar Pedapenki, S. P. Gupta, Mukesh Kumar Pathak, “Fuzzy membership functions based APF for power quality improvement”, IEEE - International Conference on Control, Instrumentation, Communication & Computational Technologies (ICCICCT), Noorul Islam University, Nagercoil, Tamil Nadu, India, pp. 231-235, 28th - 29th Dec, 2015.

PHOTOGRAPHS OF THE EXPERIMENTAL SETUP

Fig. 1. Front View of the experimental setup

[1] **D. D. Shipp**, “Harmonic analysis and suppression for electrical systems supplying static power converters and other non-linear loads”, IEEE Transaction on Industrial Applications, Vol. IA-15. No. 5, pp. 453-458, 1979.

[2] **Yoshihiko Sumi and Masao Yano**, “New Static VAR Control Using Force-Commutated Inverters”, IEEE Transactions On Power Apparatus And Systems, Vol. PAS-100, No. 9, pp. 4216-4224, 1981.

[3] **L. Gyugyi,** "Reactive power generation and control by thyristor circuits", IEEE Transaction on Industrial Applications, Vol. IA-15, No. 5, pp. 521-532, 1983.

[4] **H. Akagi, Y. Kanazawa, and A. Nabae**, "Instantaneous reactive power compensators comprising switching devices without energy storage components", IEEE Transaction on Industrial Applications, Vol. IA-20, pp. 625-630, 1984.

[5] **H. Akagi, A. Nabae, and S. Atoh**, "Control strategy of active power filters using multiple voltage-source PWM converters", IEEE Transaction on Industrial Applications, Vol. IA-22, pp. 460-468, 1986.

[6] **F. Z. Peng, H. Akagi, and A. Nabae**, "A novel harmonic power filter", Proceedings in IEEE Power Electronics Specialists Conference, pp. 1151-1159, 1988.

[7] **J. S. Subjak Jr. and J. S. Mcquilkin**, "Harmonics-causes, effects, measurements, analysis: An update", IEEE Transaction on Industrial Applications, Vol. 26, pp. 1034-1042,1990.

[8] **T. M. Gruzs**, “A Survey of Neutral Currents in Three-phase Computer Power Systems”, IEEE Transactions On Industry Applications, Vol. 26, No. 4, pp.719-725, 1990.

[9] **K. R. Padiyar and R. K. Varma**, "Damping Torque Analysis of Static VAR System Controllers", IEEE Transactions on Power Systems, Vol. 6, No. 2, pp. 458 - 465, 1991.

[10] **E. H. Watanabe, R. M. Stephan, and M. Aredes**, “New concepts of instantaneous active and reactive powers in electric systems with generic loads”, IEEE Trans. Power Delivery, Vol. 6, pp. 1690–1697, 1991.

[11] **T. Thomas, Hadded Kevork, G. Joos, and A. Jaafari**, “Design and performance of Active Filters”, IEEE Industrial Applications Magazine, Vol.8, pp. 38-46, 1991

[12] **C. A. Quinn and N. Mohan**, "Active filtering of harmonic currents in three-phase, four wire systems with three-phase, single-phase non-linear loads", in Proc. IEEE Applied Power Electronics Conference, pp. 829-836, 1992.

[13] **M. Bou-Rabee, D. Sutanto, F. Barone**, “A New Technique For Three phase Active Power Filter”, IEEE Applied Power Electronics Conference and Exposition, pp. 837-843, 1992.

[14] **W. Shireen, P Enjeti and I Pitel**, “Analysis and design of an active power filter to cancel harmonic currents in low voltage electric power distribution systems”, IEEE-IECON, pp. 368-373, Nov. 1992.

[15] **C. A. Quinn, N. Mohan, and H. Mehta**, "A four-wire, current controlled converter provides harmonic neutralization in three-phase, four-wire systems", IEEE Applied Power Electronics Conference, pp. 841-846, 1993.

[16] **A. Campos, G. Joos, P. D. Ziogas, and J. F. Lindsay**, "Analysis, design of a series voltage unbalance compensator based on a three-phase VSI operating with unbalanced switching functions", IEEE Transaction on Power Electronics, Vol. 9, pp. 269-274, 1994.

[17] **C. L. Chen, C. E. Lin, and C. L. Huang**, "An active filter for unbalanced three-phase system using synchronous detection method", IEEE Power Electronics Specialists Conference, pp. 1451-1455, 1994.

[18] **W. Shireen and M. S. Arefeen**, “A new dc voltage notching scheme for zero voltage switching of PWM inverters”, IEEE-IAS Conference Rec., pp.898-894, 1994.

[19] **W. Shireen, A. Ganesh and P. Enjeti, “**Improved active power factor correction circuit using a zero voltage switching boost converter”, IEEE Power Electronics Specialists Conference, pp. 701- 706, 1995.

[20] **H. Akagi**, "New trends in active filters for improving power quality", in Proc. IEEE Power Electronics, Drives and Energy Systems Conference, pp. 417-425, 1996.

[21] **C. Y. Hsu and H. Y. Wu,** "A new single-phase active power filter with reduced energy storage capacity", Proceeding on Institute of Electrical Engineering - Electrical Power Applications, Vol. 143, No. 1, pp. 25-30, 1996.

[22] **F. Z. Peng and J. S. Lai,** “Generalized instantaneous reactive power theory for three-phase power systems”, IEEE Transactions on Instrumentation and Measurement, Vol. 45, No. 1, pp. 293–297, 1996.

[23] **Subhashish Bhattacharya, Po-Tai Cheng, and M. Deepak Divan**,” Hybrid Solutions for Improving Passive Filter Performance in High Power Applications”, IEEE Transactions on Industry Applications, Vol. 33, No. 3, 1997.

[24] **B. Singh, K. Al-Haddad, and A. Chandra**, “A review of active filters for power quality improvement”, IEEE Transactions on Industrial Electronics, Vol. 46, No. 5, pp. 1–12, 1999.

[25] **B. Singh, K. Al-Haddad, and A. Chandra,** "Computer-Aided Modelling and Simulation of Active Power Filters", Electric Power Components and Systems, Vol. 27, pp.1227-1241, 1999.

[26] **Kishore Chatterjee, B. G. Fernandes, and G. K. Dubey**, “An Instantaneous Reactive Volt–Ampere Compensator and Harmonic Suppressor System”, IEEE Transactions on Power Electronics, Vol. 14, No. 2,pp. 381-392, 1999.

[27] **Shyh-Jier Huang, and Jinn-Chang Wu**, “A Control Algorithm for Three-Phase Three-Wired Active Power Filters Under Non ideal Mains Voltages”, IEEE Transactions on Power Electronics, Vol. 14, No. 4, pp.753-760, 1999.

[28] **A. Chandra, B. Singh, B. N. Singh and K. Al-Haddad**, “An Improved Control Algorithm of Shunt Active Filter for Voltage Regulation, Harmonic Elimination, Power-Factor Correction, and Balancing of Non-linear Loads”, IEEE Transactions on Power Electronics, Vol. 15, No. 3, pp. 495-507, 2000.

[29] **Cheng-Che Chen and Yuan-Yih Hsu**, "A Novel Approach to the Design of a Shunt Active Filter for an Unbalanced Three-Phase Four-Wire System under Non sinusoidal Conditions", IEEE Transactions on Power Delivery, Vol. 15, No. 4, pp.1258-1264, 2000.

[30] **Hideaki Fujita, Y.Watanabe, and Hirofumi Akagi,** “IEEE Transient Analysis of a Unified Power Flow Controller and its Application to Design of the DC-Link Capacitor”, IEEE Transactions on Power Electronics, Vol. 16, No. 5, pp. 735-740, 2001.

[31] **Shailendra Kumar Jain, Pramod Agarwal and H. O. Gupta, "**Design Simulation and Experimental Investigations on a Shunt Active Power Filter for Harmonics and Reactive Power Compensation", Electric Power Components and Systems, Vol. 31, No. 7, pp. 671 - 692, 2003.

[32] **Shailendra Kumar Jain, Pramod Agarwal and H. O. Gupta**, “A Control Algorithm for Compensation of Customer-Generated Harmonics and Reactive Power”, IEEE Transactions on Power Delivery, Vol. 19, No. 1, pp. 357-366, 2004.

[33] **Bo Yin, R. Oruganti, S. K. Panda and A. K. S. Bhat, ”**A novel instantaneous power control strategy for a PWM rectifier under unbalanced input voltage conditions”, 30th Annual Conference of Industrial Electronics Society (IECON), Vol. 1, pp. 251 – 256, 2004.

[34] **M. Routimo, M. Salo and H.Tuusa**, “Comparison of voltage-source and current-source shunt active power filters”, IEEE Annual Power Electronics Specialists Conference, pp. 2571-2577, 2005.

[35] **Ting Qian, Brad Lehman, Anindita Bhattacharya, Herb Ginn,** “Parallel Operation of Shunt Active Power Filters for Damping of Harmonic Propagation in Electric Shipboard Power Systems”, IEEE Electric Ship Technologies Symposium, pp. 248 - 254, 2005.

[36] **Rajesh Gupta, Arindam Ghosh and Avinash Joshi,** “Control of 3-level Shunt Active Power Filter using Harmonic Selective Controller”, IEEE Power India Conference, pp. 15 - 22, 2006.

[37] **Abdelaziz Zouidi, Farhat Fnaiech and Kamal AL-Haddad,** "Voltage source Inverter Based three-phase shunt active Power Filter: Topology, Modeling and Control Strategies", IEEE International Symposium on Industrial Electronics, pp.785-790, 2006.

[38] **Bhim Singh, B. P. Singh and Sanjeet Dwivedi**, "Performance Comparison of High Frequency Isolated AC-DC Converters for Power Quality Improvement at Input AC Mains", International Conference on Power Electronics, Drives and Energy Systems (PEDES '06) , pp.1-6, 12-15 Dec. 2006**.**

[39] **M. K. Mishra and K. Karthikeyan**, "Design and analysis of voltage source inverter for active compensators to compensate unbalanced and non-linear loads", International Power Engineering Conference, pp. 649-654, 2007.

[40] **J. F. Petit, Guillermo Robles and Hortensia Amarís**, "Current Reference Control for Shunt Active Power Filters Under Non sinusoidal Voltage Conditions", IEEE Transactions on Power Delivery, Vol. 22, No. 4, pp. 2254 2261, 2007.

[41] **Lucian Asiminoaei, Cristian Lascu, Frede Blaabjerg and Ion Boldea,** "Performance Improvement of Shunt Active Power Filter With Dual Parallel Topology", IEEE Transactions on Power Electronics, Vol. 22, No. 1, pp. 247 - 259, 2007.

[42] **Maria Isabel Montero, Enrique Romero Cadaval and Fermín Barrero Gonzalez,** "Comparison of Control Strategies for Shunt Active Power Filters in Three-Phase Four-Wire Systems", IEEE Transactions on Power Electronics, Vol. 22, No. 1, pp. 229-236, 2007.

[43] **D. Thukaram and G.Yesuratnam, "**Fuzzy Expert Approach with Curtailed Controllers for improved Reactive Power Dispatch," International Journal of Emerging Electric Power System, Vol. 8, Issue 3, Article7, 2007**.**

[44] **Singh, B., M. Agrawal, and S. Dwivedi,** "Analysis and Design of single-phase power-factor corrected AC-DC Sepic Converter with high frequency isolation." Journal-Institution of Engineers India Part El Electrical Engineering Division, Vol. 87, 2007.

[45] **D. Thukaram and G.Yesuratnam**, **"**Fuzzy Expert Approach with Curtailed Controllers for improved Reactive Power Dispatch,**"** International Journal of Emerging Electric Power System, Vol. 8, Issue3, Article7, 2007.

[46] **Xinhui Wu, Sanjib K. Panda and Jianxin Xu**, "Effect of Pulse-Width Modulation Schemes on the Performance of Three-Phase Voltage Source Converter", 33rd Annual Conference of the IEEE Industrial Electronics Society (IECON), pp. 2026 – 2031, 2007.

[47] **Bhim Singh, P. Jayaprakash, and D. P. Kothari,** "A T-Connected Transformer and Three-leg VSC Based DSTATCOM for Power Quality Improvement", IEEE Transactions on Power Electronics, Vol. 23, No. 6, pp. 2710-2718, 2008.

[48] **Abdelmadjid Chaoui, Jean-Paul Gaubert, Fateh Krim and Laurent Rambault,** "On the Design of Shunt Active Filter for Improving Power Quality", IEEE International Symposium on Industrial Electronics, pp.31-37, 2008.

[49] **Udom Khruathep, Suttichai Premrudeepreechacharn, Yuttana Kumsuwan,** "Implementation of Shunt Active Power Filter Using Source Voltage and Source Current Detection", IEEE Conference on Industrial Electronics and Applications, pp. 2346 - 2351, 2008.

[50] **B. Singh, M. Agrawal, S. Dwivedi**, "Analysis, design, and implementation of a single-phase power-factor corrected AC–DC zeta converter with high frequency isolation", Journal of Electrical Engineering and Technology, Vol. 3, No. 2, pp. 243–253, 2008.

[51] **Peng Xiao, Ganesh Kumar Venayagamoorthy and Keith A. Corzine,** "Seven-Level Shunt Active Power Filter for High-Power Drive Systems", IEEE Transactions on Power Electronics, Vol. 24, No. 1, pp. 6-14, 2009.

[52] **Oleg Vodyakho and Chris C. Mi,** "Three-Level Inverter-Based Shunt Active Power Filter in Three-Phase Three-Wire and Four-Wire Systems", IEEE Transactions on Power Electronics, Vol. 24, No. 5, pp. 1350 - 1363, 2009.

[53] **D. Thukaram and C. Vyjayanthi**, "Relative Electrical Distance Concept for Evaluation of Network Reactive Power and Loss Contributions in a Deregulated System", IET Generation, Transmission, and Distribution, Vol.3, Issue 11, pp. 1000-1019, 2009.

[54] **Singh JG, Tripathy P, Singh SN and Srivastava SC**, " Development of a fuzzy rule based generalized unified power flow controller", European Transactions on Electrical Power, Vol. 19, pp. 702–717, 2009.

[55] **R. K. Varma, Vinod Khadkikar, R. Seethapathy**, "Night-Time Application of PV Solar Farm as STATCOM to Regulate Grid Voltage", IEEE Transactions on Energy Conversion, Vol. 24, No. 4, pp. 983 - 985, 2009.

[56] **C. Patel and R. Mahanty**, " Unified power quality conditioner using a fuzzy controller", International Journal of Emerging Electric Power Systems, Vol. 11, No. 4, pp. 1-17, 2010.

[57] **T. S. Basu, Avik Bhattacharya and Chandan Chakraborty,** "Shunt Active Power Filter/STATCOM Topology for Medium/High Power Applications: Parallel Inverters Operating at Different Switching Frequencies", Annual Conference on Industrial Electronics Society, pp. 2669 - 2674, 2010.

[58] **R. Mahanty**, "Modified static VAR compensator using a large value AC capacitor", Electric Power Systems Research, Vol. 80, No. 2, pp. 240-247, 2010.

[59] **Sanjoy K. Parida, S. C. Srivastava, Sri N. Singh**, "A review on reactive power management in electricity markets", International Journal of Energy Sector Management, Vol. 5, No. 2, pp.201-214, 2011.

[60] **M. Singh, V. Khadkikar, A. Chandra, A, R. K. Varma**, "Grid Interconnection of Renewable Energy Sources at the Distribution Level With Power-Quality Improvement Features", IEEE Transactions on Power Delivery, Vol. 26 , No. 1, pp. 307 - 315, 2011.

[61] **S. Dasgupta, S. N. Mohan, S. K. Sahoo and S. K. Panda**, "Derivation of instantaneous current references for three phase PV inverter connected to grid with active and reactive power flow control", IEEE 8th International Conference on Power Electronics and ECCE Asia (ICPE & ECCE), pp. 1228 – 1235, 2011.

[62] **S. B. Karanki, G. Nagesh, M. K. Mishra and B. K. Kumar**, "A hybrid topology for reducing DC link voltage rating in DSTATCOM applications", IEEE Energy technology, pp. 1-6, 2011.

[63] **M. F. Shousha, S. A. Zaid and O. A. Mahgoub,** "Better Performance for Shunt Active Power Filters", International Conference on Clean Electrical Power, pp. 56-62, 2011.

[64] **Yi Tang, Poh Chiang Loh, Peng Wang, Fook Hoong Choo, Feng Gao and Frede Blaabjerg,** "Generalized Design of High Performance Shunt Active Power Filter With Output LCL Filter", IEEE Transactions on Industrial Electronics, Vol. 59, No. 3, pp. 1443 - 1452, 2012.

[65] **Quoc-Nam Trinh and Hong-Hee Lee,** "An Advanced Current Control Strategy for Three-Phase Shunt Active Power Filters", IEEE Transactions on Industrial Electronics, Vol. 60, No. 12, pp. 5400-5410, 2013.

[66] **Kannan T., Ezhil Reena Joy.T.P., Kumar P.**, "A Fuzzy Based Detuning Control Technology for Contactless Charging System of Electric Vehicles", IEEE International Conference on Advanced Research in Engineering and Technology (ICARET), Paper No. 79, 2013.

[67] **Kannan T., Ezhil Reena Joy.T.P., Kumar P**., "A Novel Fuzzy based Phase Angle Estimation Scheme for Grid Connected Bidirectional Contactless Power Transfer System suitable for EVs and PHEVs", IEEE International Conference on Advanced Research in Engineering and Technology (ICARET), Paper No. 81, 2013.

[68] **R. Mahanty**, "Indirect current controlled shunt active power filter for power quality improvement," International Journal of Electrical Power and Energy Systems, Vol. 62, pp. 441-449, 2014.

[69] **Mostafa S. Hamad, Mahmoud I. Masoud, Khaled H. Ahmed, and Barry W. Williams,** "A Shunt Active Power Filter for a Medium-Voltage 12-Pulse Current Source Converter Using Open Loop Control Compensation", IEEE Transactions on Industrial Electronics, Vol. 61, No. 11, pp. 5840 - 5850, 2014.

[70] **Le Ge, Xiaodong Yuan and Zhong Yang,** "Control System Design of Shunt Active Power Filter Based on Active Disturbance Rejection and Repetitive Control

Techniques", Journal of Mathematical Problems in Engineering, Hindawi Publishing Corporation, pp. 1 - 6, Volume 2014.

[71] **Parag Kanjiya, Vinod Khadkikar, and Hatem H. Zeineldin,** "Optimal Control of Shunt Active Power Filter to Meet IEEE Std. 519 Current Harmonic Constraints Under Non ideal Supply Condition", IEEE Transactions on Industrial Electronics, Vol. 62, No. 2, pp. 724 - 734, 2015.

[72] **Trapti Jain, Sri Niwas Singh and S. C. Srivastava**, "STATCOM Application for Enhancement of Available Power Transfer Capability in Transmission Networks", Static Compensators (STATCOMs) in Power Systems, Part of the series Power Systems, Springer, pp 505-530, 2015.

Fuzzy Logic Controller Papers

[73] **Juan Dixon and Jose Contardo**, "DC Link Fuzzy Control for an Active Power Filter, Sensing the Line Current Only", Annual IEEE Power Electronics Specialists Conference, pp.1109 - 1114, 1997.

[74] **V. S. C. Raviraj and P. C. Sen**, "Comparative Study of Proportional–Integral, Sliding Mode, and Fuzzy Logic Controllers for Power Converters", IEEE Transactions on Industry Applications, Vol. 33, No. 2, pp.518 - 524, 1997.

[75] **Juan W. Dixon, J. M. Contardo, and L. A. Moran**, "A Fuzzy-Controlled Active Front-End Rectifier with Current Harmonic Filtering Characteristics and Minimum Sensing Variables", IEEE Transactions on Power Electronics, Vol. 14, No. 4, pp.724 - 729, 1999.

[76] **A. Dell'Aquila, G. Delvino, M. Liserre, P. Zanchettauan and W. Dixon**, "A New Fuzzy Logic Strategy For Active Power Filter", IEE Power Electronics and Variable Speed Drives Conference, pp. 392 - 397, 2000.

[77] **S. K. Jain, P. Agrawal and H.O. Gupta.**, "Fuzzy logic controlled shunt active power filter for power quality improvement", IEE Proceedings on Electrical Power Applications, Vol.149, No.5, pp. 317 - 328, 2002.

[78] **A. Dell' Aquilla, A. Lecci and V.G. Momopoli,** "Fuzzy Controlled Active Filter Driven by an Innovative Current Reference for Cost Reduction", Proceedings on IEEE International symposium on Industrial Electronics, Vol. 3, pp. 948-952, 2002.

[79] **A. Dell' Aquila, A. Lecci and M. Liserre,** "Microcontroller-Based Fuzzy Logic Active Filter for Selective Harmonic Compensation", IEEE IAS Annual meeting on Industrial Applications Conference, pp. 285 - 292, 2003.

[80] **B. Mazari and F. Mekria,** "Microcontroller-Based Fuzzy Logic Active Filter for Selective Harmonic Compensation", Journal of Information Science and Engineering, Vol. 21, pp.1139-1156, 2005.

[81] **M. Farrokhi, *S.* Jamali and S.A. Mousavi,** "Fuzzy Logic Based Indirect Current Control of the Shunt Active Power Filter", International Universities Power Engineering Conference, pp. 489 – 493, 2004.

[82] **B. Suresh Kumar, K. Ramesh Reddy and V. Lalitha,** "PI, Fuzzy Logic Controlled Shunt Active Power Filter for Three-phase Four-wire Systems with Balanced, Unbalanced and Variable Loads", Journal of Theoretical and Applied Information Technology, Vol. 23, No. 2, pp. 122 - 130, 2003.

[83] **Hocine Benalla and Hind Djeghloud,** "Shunt Active Filter Controlled by Fuzzy Logic", Journal of King Saud University., Vol. 18, Eng. Sci. (2), pp. 231-247, 2005.

[84] **C. N. Bhende, S. Mishra and S. K. Jain,** "TS-Fuzzy-Controlled Active Power Filter for Load Compensation", IEEE Transactions on Power Delivery, Vol. 21, No. 3, pp. 1459 - 1465, 2006.

[85] **Brahim Berbaoui, Chellali Benachaiba, Rachid Dehini and Brahim Ferdic.,** "Optimization of Shunt Active Power Filter System Fuzzy Logic Controller Based on Ant Colony Algorithm", Journal of Theoretical and Applied Information Technology, Vol. 14, No. 2, pp. 117 - 125, 2010.

[86] **G. K. Singh, A. K. Singh and R. Mitra,** "A simple fuzzy logic based robust active power filter for harmonics minimization under random load variation", Electric Power Systems Research, Elsevier, Vol. 77, No. 8, pp.1101–1111, 2007.

[87] **C. Benachaiba and B. Mazari,** " Contribution to the improvement of control strategies of the shunt active filter by a fuzzy PI controller", Technologies Avengers , Vol.18, Issue.1, pp. 23-27, 2007.

[88] **C. Sharmeela, M. R. Mohan, G. Uma and J. Baskaran,** " Fuzzy Logic Controller Based Three-phase Shunt Active Filter for Line Harmonics Reduction", Journal of Computer Science, Vol. 3, No. 2, pp.76-80, 2007.

[89] **Othmane Abdelkhalek, Chellali Benachaiba, Mohammed Haidas and Tarak Benslimane,** " A New Technique Applied To A Fuzzy Regulator To Control The Shunt Active Filter Dc Bus Voltage", Journal of Information Technology and Control, Vol.37, No.3, pp. 227 - 232, 2008.

[90] **M. C. Ben habib, E. Jacquot, S. Saadate,** " An Advanced Control Approach for a Shunt Active Power Filter", International Conference On Renewable Energies and Power Quality, pp. 23 - 29, 2009.

[91] **An Luo, Zhikang Shuai, Wenji Zhu, Ruixiang Fan, and Chunming Tu,** "Development of Hybrid Active Power Filter Based on the Adaptive Fuzzy Dividing

Frequency-Control Method", IEEE Transactions on Power Delivery, Vol. 24, No. 1, pp. 424 - 432, 2009.

[92] **S. Saad and L. Zellouma,** "Fuzzy logic controller for three-level shunt active filter compensating harmonics and reactive power", Electric Power Systems Research, Elsevier, Vol. 79, No. 10, pp.1337–1341, 2009.

[93] **A. A. Helal, N. E. Zakzouk and Y. G. Desouky,** "Fuzzy Logic Controlled Shunt Active Power Filter for Three-phase Four-wire Systems with Balanced and Unbalanced Loads", World Academy of Science, Engineering and Technology, Vol. 58, pp. 597 - 602, 2009.

[94] **Soumia Kerrouche and Fateh Krim,** "Three Phase APF based on Fuzzy logic controller", International Journal of Science and Techniques of Automatic control & computer engineering, Vol. 3, No. 1, pp. 942-955, 2009.

[95] **T. Narasa Reddy and M. V. Subramanyam,** "Fuzzy Logic Controlled Shunt Active Power Filter for Mitigation of Harmonics with Different Membership Functions", International Conference on Advances in Computing, Control, and Telecommunication Technologies, pp. 616 - 620, 2009.

[96] **M. B. B. Sharifian, R. Rahnavard, Y. Ebrahimi,** "Variable Hysteresis Band Current Controller of Shunt Active Filter Based Fuzzy logic Theory under Constant Switching Frequency", International Journal of Computer and Electrical Engineering, Vol. 1, No. 2, pp. 236-244, 2009.

[97] **G. Jayakrishna and K.S.R.Anjaneyulu,** "Fuzzy Logic Control based Three Phase Shunt Active Filter for Voltage Regulation and Harmonic Reduction", International Journal of Computer Applications, Vol.10, No.5, pp. 13 - 19, 2010.

[98] **Karuppanan P and Kamala Kanta Mahapatra,** " PLL with PI, PID and Fuzzy Logic Controllers based Shunt Active Power Line Conditioners", IEEE - International Conference on Power Electronics, Drives and Energy Systems, pp. 1 - 6, 2010.

[99] **Karuppanan P and Kamala Kanta Mahapatra,** " Fuzzy Logic Controlled Active Power Line Conditioners for Power quality Improvements", International Conference on Advances in Energy Conversion Technologies, pp. 7 -15, 2010.

[100] **E. Latha Mercy, R. Karthick and S.Arumugam,** " Fuzzy Controlled Shunt Active Power Filter for Power Quality Improvement", International Journal of Soft Computing, Vol. 5, No. 2, pp. 35-41, 2010.

[101] **D. A. Gadanayak and P. C. Panda,** " A Novel Fuzzy Variable-Band Hysteresis Current Controller For Shunt Active Power Filters", ACEEE Proceedings of International Conference on Control, Communication and Power Engineering, Vol. 2, No. 2, pp. 24 - 28, 2010.

[102] **G. M. Sarhan, A. A. Elkousy, A. A. Hagras and Sh. M. Saad,** " Adaptive Control of Shunt Active Power Filter Using Interval Type-2 Fuzzy Logic Controller", Proceedings of International Middle East Power Systems Conference (MEPCON'10), pp. 19 - 27, 2010.

[103] **P. Rathika and D. Devaraj,** " Artificial Intelligent Controller based Three Phase Shunt Active Filter for Harmonic Reduction and Reactive Power Compensation", Proceedings of the International Multi Conference of Engineers and Computer Scientists, Vol II, pp. 17 - 26, 2010.

[104] **Nadhir Mesbahi and Ahmed Ouari,** " A Fuzzy Logic Control For Three -Level Shunt Active Power Filter", International Conference On Industrial Engineering and Manufacturing, pp. 9 -18, 2010.

[105] **Mikkili Suresh, Anup Kumar Panda and Y. Suresh,** " Fuzzy Controller Based Three Phase Four Wire Shunt Active Filter for Mitigation of Current Harmonics with Combined p-q and Id-Iq Control Strategies", Energy and Power Engineering, Vol. 3, No. 4, pp. 43-52, 2011.

[106] **Karuppanan P and KamalaKanta Mahapatra,** "PLL with Fuzzy Logic Controller based Shunt Active Power Filter for Harmonic and Reactive power Compensation", IEEE - International Conference on Power Electronics, Drives and Energy Systems, pp. 12 - 18, 2011.

[107] **B. Suresh Kumar, K. Ramesh Reddy and V. Lalitha,** "PI, Fuzzy And Neuro Controlled Shunt Active Power Filters For Three Phase Four Wire System With Balanced, Unbalanced And Variable Loads", Journal of Theoretical and Applied Information Technology, Vol. 23, No. 4, pp 26 - 33, 2011.

[108] **Karuppanan PitchaiVijaya and Kamala Kanta Mahapatra,** " Adaptive - Fuzzy Controller Based Shunt Active Filter for Power Line Conditioners", Telecommunications, Computing, Electronics and Control (TELKOMNIKA), Vol.9, No.2, pp. 203 - 210, 2011.

[109] **Hamza Bentria,** " Shunt Active Power Filter Controlled by Fuzzy Logic Controller For Current Harmonic Compensation and Power Factor Improvement", Journal of Theoretical and Applied Information Technology, Vol. 32, No.1, pp. 33 - 39, 2011.

[110] **Suresh Mikkili and Anup Kumar Panda,** " SHAF for Mitigation of Current Harmonics Using p-q Method with PI and Fuzzy Controllers", Engineering, Technology & Applied Science Research (ETASR), Vol. 1, No. 4, pp. 98 - 104, 2011.

[111] **Chennai Salim and Benchouia Mohamed Toufik,** " Intelligent Controllers for Shunt Active Filter to Compensate Current Harmonics Based on SRF and SCR Control Strategies", International Journal on Electrical Engineering and Informatics, Vol. 3, No. 3, pp. 372- 393, 2011.

[112] **K. Sebasthi Rani and K. Porkumaran,** " Performance Evaluation of PI and Fuzzy Controller Based Shunt Active Power Filter", European Journal of Scientific Research Vol. 61, No. 3, pp.381-389, 2011.

[113] **Rathika Ponpandi and Devaraj Durairaj,** "A Novel Fuzzy—Adaptive Hysteresis Controller Based Three Phase Four Wire-Four Leg Shunt Active Filter for Harmonic and Reactive Power Compensation", Energy and Power Engineering, Vol. 3, No. 7, pp. 422 - 435, 2011.

[114] **Karuppanan P, Kamala Kanta Mahapatra**, "PI and fuzzy logic controllers for shunt active power filter — A report", ISA Transactions, Vol. 51, Issue. 5, pp.163-169, 2012.

[115] **Karuppanan P, Kamala Kanta Mahapatra,** "Erratum to “PI and fuzzy logic controllers for shunt active power filter—A report”, [Isa Transactions 51, 163–169], ISA transactions, Vol. 51, No. 5, pp. 667 - 671, 2012.

[116] **H. Kouara, A. Chaghi**, "Three Phase Four Wire Shunt Active Power Filter Based Fuzzy Logic Dc- Bus Voltage Control", ACTA Technica Corviniensis - Bulletin of Engineering, Tome V, Fascicule. 4, pp. 25 - 31, 2012.

[117] **Mikkili, Suresh, and A. K. Panda,** "Real-time implementation of PI and fuzzy logic controllers based shunt active filter control strategies for power quality improvement", International Journal of Electrical Power and Energy Systems, Vol. 43, No. 1, pp. 1114 - 1126, 2012.

[118] **Kouara, H., H. Laib, and A. Chaghi**. "A New Method to Extract Reference Currents for Shunt Active Power Filter in Three Phase Four Wire Systems", International Journal of Advanced Science and Technology, Vol. 46, No. 3, pp. 165 - 174, 2012.

[119] **A. F. Abdel Gawad, Md. A. Farahat**, "Shunt Active Power Filter Simulation Based On Fuzzy Logic Controller And Genetic Algorithm", Journal of Electrical Engineering, pp. 1-9, 2012.

[120] **B. Soujanya Yadav, L. Ramadevi and P. S. R. Murthy**, "Fuzzy Based Cascaded Multilevel Shunt Active Power Filter For Power Line Conditioners", International Journal of Electrical and Electronics Engineering, Vol. 2, No. 2, pp. 45 - 49, 2012.

[121] **Lamchich, Moulay Tahar**. "ANN current controller based on PI-Fuzzy adaptive system for shunt power active filter", Advances in Power Electronics, Hindawi Publications, pp. 1 - 6, 2012.

[122] **Panda, Anup Kumar, and Suresh Mikkili**. "Fuzzy logic controller based shunt active filter control strategies for power quality improvement using different fuzzy MFS", International Journal of Emerging Electric Power Systems, Vol. 13, No. 5, pp. 2012.

[123] **Li Bin and Tong Minyong**, "Control Method of the Three-Phase Four-Leg Shunt Active Power Filter", Energy Procedia, Elsevier Journal, Vol.14, No. 3, pp. 1825 -1830, 2012.

[124] **N. Sentilnathan and T. Manigandan,** "Implementation of a Novel Control Strategy Using Fuzzy Logic Controller to Shunt Active Filter for Line Harmonic Reduction", Journal of Computer Science, Vol. 8, No. 5, pp. 737 - 746, 2012.

[125] **Benaissa, Amar, Boualaga Rabhi, Mohamed Fouad Benkhoris, Ammar Moussi, Jean-Claude Le Claire**, "Fuzzy logic controller for five-level shunt active power filter under distorted voltage conditions", Annual Conference on IEEE Industrial Electronics Society, pp. 4973 - 4978, 2012.

[126] **P. V. Ram Kumar and M. Surya Kalavathi,** "Fuzzy Based Hysteresis Current Controlled Shunt Active Power Filter for Power Conditioning", International Journal of Modern Engineering Research, Vol. 3, No. 1, pp. 477 - 484, 2013.

[127] **Tianhua Li and Juntao Fei,** "Feedback Linearization Control of a Shunt Active Power Filter Using a Fuzzy Controller", International Journal of Advanced Robotic Systems, Vol. 10, pp. 1 - 8, 2013.

[128] **A. M. Gore and D. S. More**, "Performance investigation of Shunt Active Power Filter with PI and fuzzy controllers", IEEE International Conference on Control Applications (CCA), pp. 1159 - 1164, 2013.

[129] **Suresh Dhanavath and Sajjan Pal Singh,** "An Improved Hybrid Active Power Filter For Power Quality Improvement In Three Phase Four Wire System", International Journal of Engineering Science & Advanced Technology, Vol. 3, No. 5, pp. 251 - 258, 2013.

[130] **Bangia Sakshi, P. R. Sharma, and Maneesha Garg,** "Simulation of Fuzzy Logic Based Shunt Hybrid Active Filter for Power Quality Improvement", International Journal of Intelligent Systems and Applications, Vol. 5, No. 2, pp. 96 - 104, 2013.

[131] **K. Sarasvathi and R. Rajalakshmi,** "Performance Analysis Of Shunt Active Filter Using Different Controllers", International Journal of Engineering Trends and Technology, Vol. 4, No. 5, pp. 1815 - 1820, 2013.

[132] **Usman Hamisu, and Suleiman Musa,** "Harmonic Mitigation Using Single Phase Shunt Active Power Filter With Fuzzy Logic Controller for the Improvement of Power Quality", International Journal of Electrical Components & Sustainable Energy, Vol. 1, No. 2, pp. 28 - 33, 2013.

[133] **Fei Juntao Zhang, Weifeng Yan Shenglei and Zhuli Yuan**, "Adaptive current control with PI-fuzzy compound controller for shunt active power filter", Mathematical Problems in Engineering, Hindawi Publications, pp. 1 - 8, 2013.

[134] **Salim, Chennai, and Benchouia Mohamed Toufik**. "Three-level (NPC) Shunt Active Power Filter Performances based on Fuzzy Controller for Harmonic Currents Compensation under Non-Ideal Voltage Conditions", International Journal on Electrical Engineering and Informatics, Vol. 6, No. 2, pp. 342 - 358, 2014.

[135] **Benazir Hajira A, Ramya M, Sathyapriya M, Anju R and Kumar P**, "Fuzzy Logic Controller based 3-Phase Shunt Active Power Filter for Current Harmonic Mitigation", International Journal of Advanced Research in Electrical, Electronics and Instrumentation Engineering, Vol. 3, No. 3, pp. 7789 - 7796, 2014.

[136] **Beny, P. G**. "Power Quality Enhancement Using Shunt Active Filter with Fuzzy Logic Controller", International Journal of Innovative Ideas in Research, Vol. 1, No. 1, pp.1 - 12, 2014.

[137] **Parimala V, Ganeshkumar D, Benazir Hajira A,"** Harmonic reduction using shunt active power filter with PI controller", International Journal of Scientific Engineering and Research, Vol. 2, No. 4, pp. 85 - 90, 2014.

[138] **Aziz Boukadoum1 and Tahar Bahi**, "Fuzzy Logic Controlled Shunt Active Power Filter for Harmonic Compensation and Power Quality Improvement", Journal of Engineering Science and Technology Review, Vol. 7, No. 4, pp.143 - 149, 2014.

[139] **H. Kouara, H. Laib and A. Chaghi**, " Comparative Study of Three Phase Four Wire Shunt Active Power Filter Topologies based Fuzzy Logic DC Bus Voltage Control", International Journal of Energy, Information and Communications Vol.5, No. 3, pp.1 - 12, 2014.

[140] **Karvekar, Sushil**, "Goertzel Algorithm Based Shunt Active Power Filter Using Sliding Mode Controller", Proceedings of the World Congress on Engineering and Computer Science, Vol. 1, pp. 266 - 271, 2014.

[141] **P. Parthasaradhy, Dola Gobinda Padhan and K. A. Chinmaya**, " Regulation of the DC Bus Voltage of a Three Phase Active Power Filter by PI and Fuzzy Logic Controller", The International Journal of Engineering and Science, pp.78-84, 2014.

[142] **Aziz Boukadoum and Tahar Bahi**, "Harmonic Current Suppression By Shunt Active Power Filter Using Fuzzy Logic Controller", Journal of Theoretical and Applied Information Technology, Vol. 68, No. 3, pp. 25 - 35, 2014.

[143] **A. M. Fahmy, A. K. Abdelsalam and A. B. Kotb**. "4-leg shunt active power filter with hybrid predictive fuzzy-logic controller", IEEE International Symposium on Industrial Electronics, pp. 59 - 66, 2014.

[144] **N. Madhuri, , S. R. Doradla, and M. Surya Kalavathi,** "Fuzzy based Fault Tolerant shunt Active Power Filter", IEEE International Conference on Control, Instrumentation, Communication and Computational Technologies (ICCICCT), pp. 78 - 86, 2014.

[145] **K. Sebasthirani and K. Porkumaran,** "Performance Enhancement Of Shunt Active Power Filter With Fuzzy And Hysteresis Controllers", Journal of Theoretical and Applied Information Technology, Vol. 60, No. 2, pp. 64 - 70, 2014.

[146] **S. Musa, M. A. M. Radzi, H. Hisham and N. I. Abdulwahab**, "Fuzzy logic controller based three phase shunt active power filter for harmonics reduction", IEEE Conference on Energy Conversion, pp. 58 - 64, 2014.

[147] **Benaissa, Amar, Boualaga Rabhi, and Ammar Moussi,** "Power quality improvement using fuzzy logic controller for five-level shunt active power filter under distorted voltage conditions", Frontiers in Energy, Vol. 8, No. 2, pp. 212-220, 2014.

[148] **Dipen A. Mistry, Bhupelly Dheeraj, Ravit Gautam, Manmohan Singh Meena and Suresh Mikkili**, "Power Quality Improvement Using PI and Fuzzy Logic Controllers Based Shunt Active Filter", World Academy of Science, Engineering and Technology International Journal of Electrical, Computer, Electronics and Communication Engineering, Vol. 8, No. 4, pp. 82 - 88, 2015.

[149] **Vandana Sharma, and Anurag Singh Tomer,** "Comparative Analysis on Control Methods of Shunt Active Power Filter for Harmonics Mitigation", International Journal of Science and Research, Vol. 3, No. 2, pp. 45 - 62, 2015.

[150] **A. Benazir Hajira, M. Ramya, R. Anju, M. Sathyapriya**, "Power Quality Improvement in Three Phases four Wire System Using Pi and Fuzzy Logic Controller", International Journal of Advanced Research in Computer Science and Software Engineering, Vol. 4, No. 3, pp. 86 - 95, 2015.

[151] **Suresh Mikkili and A. K. Panda**, “Performance analysis and real-time implementation of shunt active filter current control strategy with type-1 and type-2 FLC triangular M.F”, International Transactions on Electrical Energy Systems – John Wiley, Vol. 24, No. 3, pp. 347–362, 2016.

[152] **R. Belaidi, A. Haddouche and H. Guendouz**, “Fuzzy Logic Controller Based Three-Phase Shunt Active Power Filter for Compensating Harmonics and Reactive Power under Unbalanced Mains Voltages”, Energy Procedia, Vol.18, pp. 560 – 570, 2016.

Neural Network Controller Papers

[153] **Dawei Gao Xiaorui Sun,** " A Shunt Active Power Filter with Control Method Based on Neural Network", International Conference on Power System Technology, pp.1619 - 1624, Vol. 3, 2011.

[154] **A. Elmitwally, S. Abdelkader and M. El-Kateb,** " Neural network controlled three-phase four-wire shunt active power filter", IEE Proceedings of Generation, Transmission and Distribution, Vol. 147, No. 2. pp. 52 - 59, 2000.

[155] **M. Rukonuzzaman and M. Nakaoka,** " Single-phase Shunt Active Power Filter with Adaptive Neural Network Method for Determining Compensating Current", Annual Conference of the IEEE Industrial Electronics Society, pp. 121 - 127, 2001.

[156] **M. Rukonuzzaman and M. Nakaoka,** " An Advanced Active Power Filter with Adaptive Neural Network Based Harmonic Detection Scheme", Annual Conference of the IEEE Industrial Electronics Society, pp. 157 - 164, 2001.

[157] **Jesus R. Vazquez, Patricio Salmeron, Jaime Prieto and Alejandro Perez,** " Practical Implementation of a Three-Phase Active Power Line Conditioner with ANNs Technology", Annual Conference of the IEEE Industrial Electronics Society, pp. 101 - 107, 2001.

[158] **J. R. Vazquez, Patricio Selmeron, F. Javier Alcantara and Jaime Prieto,** " A new active power line conditioner for compensation in unbalanced/ distorted electrical power system", Power System Computational Conference, Session 28, Paper 6, pp. 1 - 6, 2002.

[159] **J. R. Vazquez and P. Salmeron,** " Active power filter control using neural network technologies", IEE Proceedings on Electrical Power Applications, Vol. 150, No. 2, pp. 24 - 29, 2003.

[160] **J. L. Flores Garrido and P. Salmeron Revuelta,** " Harmonic detection by using different artificial neural network topologies", International Conference On Renewable Energies And Power Quality, pp. 58 - 64, 2003.

[161] **F. Temurtas, R. Gunturkun, N. Yumusaka and H. Temurtas,** " Harmonic detection using feed forward and recurrent neural networks for active filters", Electric Power Systems Research, Elsevier, Vol. 72, No. 4, pp. 33–40, 2004.

[162] **L. H. Tey, P. L. So and Y. C. Chu,** " Improvement of Power Quality Using Adaptive Shunt Active Filter", IEEE Transactions on Power Delivery, Vol. 20, No. 2, pp. 121 - 128, 2005.

[163] **Satya Prakash Dubey, Pukhraj Singh and H. V. Manjunath,** " DSP Based Neural Network Controlled Parallel Hybrid Active Power Filter", International Journal of Emerging Electric Power Systems, Vol. 4, No. 2, pp. 1 - 7, 2005.

[164] **M. Tarafdar Haque, and A.M. Kashtiban,** " Application of Neural Networks in Power Systems; A Review", World Academy of Science, Engineering and Technology, Vol. 6, pp. 53 - 57, 2005.

[165] **Marcelo G. Villalva and Ernesto Ruppert F,** " Control of a Shunt Active Power Filter with Neural Networks – Theory and Practical Results", IEEJ Transactions, Volume 126, Issue 7, pp. 946 - 953 , 2006.

[166] **N.B.Muthuselvan, Subhransu Sekhar Dash, and P. Somasundaram,** " Artificial Neural Network Controlled Shunt Active Power Filter", IEEE Annual India Conference**,** pp. 1 - 5, 2006.

[167] **Djaffar Ould Abdeslam, Patrice Wira, Jean Mercklé, Damien Flieller and Yves-André Chapuis,** " A Unified Artificial Neural Network Architecture for Active Power Filters", IEEE Transactions on Industrial Electronics, Vol. 54, No. 1, pp. 121 - 128, 2007.

[168] **Yongtao Dai and Wenjin Dai,** " Harmonic and Reactive Power Compensation with Artificial Neural Network Technology", Proceedings of the 7th World Congress on Intelligent Control and Automation, pp. 12 - 18, 2008.

[169] **Maurizio Cirrincione, Marcello Pucci and Gianpaolo Vitale,** " A Single-Phase DG Generation Unit With Shunt Active Power Filter Capability by Adaptive Neural Filtering", IEEE Transactions on Industrial Electronics, Vol. 55, No. 5, pp. 45 - 49, 2008.

[170] **Y. Han, M. M. Khan, L. Xu, G. Yao, L. Zhou and C. Chen,** " A new scheme for power factor correction and active filtering for six-pulse converters loads", Bulletin of the Polish Academy of Sciences Technical Sciences, Vol. 57, No. 2, pp. 157 - 169, 2009.

[171] **Rachid Dehini, Abdesselam Bassou, Brahim Ferdi,** " Artificial Neural Networks Application to Improve Shunt Active Power Filter", International Journal of Computer and Information Engineering, Vol. 3, No. 4, pp. 247 - 254, 2009.

[172] **Ngac Ky Nguyen, Patrice Wira, Djaffar Ould Abdeslam and Damien Flieller,** " Artificial Neural Networks Application to Improve Shunt Active Power Filter", Annual Conference of the IEEE Industrial Electronics Society, pp. 1 - 8, 2009.

[173] **Guiying Liu, Shiping Su, Peng Peng,** "Intelligent Control and Application of All-function Active Power Filter", International Conference on Intelligent Computation Technology and Automation, pp. 58 - 64, 2010.

[174] **Vahid Dargahi, Mohammad Jafar Zandzadeh, Mehdi Salehifar and Abbas Shoulaie,** " Utilization a Flying Capacitor Multicell Converter Based Adaptive Shunt Active Power filter to Enhance Power Quality", **I**nternational Power System Conference, pp. 123 - 129, 2010.

[175] **N. Gupta, S. P. Dubey and S. P. Singh,** " Neural Network Based Active Power Filter for Power Quality Improvement", IEEE Power and Energy Society General Meeting, pp. 1 – 8, 2010.

[176] **Yang Han, Lin Xu, Muhammad Mansoor Khan, Gang Yao, Li-Dan Zhou, Chen Chen,** " Neural Network Based Active Power Filter for Power Quality Improvement", Journal of Electrical Engineering, Springer, Vol. 91, No. 7, pp. 313–325, 2010.

[177] **N. Gupta, S. P. Dubey and S. P. Singh,** "Neural network based shunt active filter for harmonic and reactive power compensation under non-ideal mains voltage", IEEE Conference on Industrial Electronics and Applications, pp. 34 - 40, 2010.

[178] **Chennai Salim and M.T Benchouia,** " An Artificial Neural Network Controller for Three-level Shunt Active Filter to Eliminate the Current Harmonics and Compensate Reactive Power", Majlesi Journal of Electrical Engineering, Vol. 5, No. 3, pp. 24 - 32, 2011.

[179] **Chennai Salim and M.T Benchouia,** " A Fast Detection of Harmonic Compensation Current for Active Power Filters using Adaptive RBF Neural Network and Hysteresis Current Controller", International Conference on Electricity Distribution Frankfurt, pp. 6 - 9, 2011.

[180] **Ngac Ky Nguyen, Patrice Wira, Damien Flieller, Djaffar Ould Abdeslam and Jean Merckle,** " Harmonics Identification with Artificial Neural Networks: Application to Active Power Filtering", International Journal of Emerging Electric Power Systems, Vol. 12, No. 5, Article 1, pp. 1 - 9, 2011.

[181] **Ch. Sujatha, Sravanthi Kusam, K. Chandra Shekar,** " Shunt active filter algorithms for a three phase system fed to adjustable speed drive", International Journal of Engineering Science and Technology, Vol. 3, No. 10, pp. 56 - 64, 2011.

[182] **Chennai Salim, M. T. Benchouia, A. Golea, and S. E. Zouzou,** " Shunt Active Filter based on three–level (NPC) Inverter using Current and DC Voltage Artificial Neural Network Controllers", International Electrical Engineering Journal, Vol. 1, No. 1, pp. 523 - 528, 2011.

[183] **Awan Uji Krismanto, M. Ashari, P. Mauridhy Heri and Takashi Hiyama,** " Shunt Active Power Filter Control using Radial Basis Function Neural Network", International Journal of Advanced Robotic Systems, Vol. 10, No. 258, pp. 33 - 37, 2013.

[184] **Garrido, J. L. Flores, and P. Salmeron Revuelta,** "Control of an active power filter using dynamic neural networks", International Conference on Renewable Energies and Power Quality, pp. 43 - 49, 2006.

[185] **El - Mamlouk, M. Wael, H. E. Mostafa, and M. A. El-Sharkawy,** "Active power filter controller for harmonic suppression in industrial distribution system", Ain Shams Engineering Journal, Vol. 2, No. 3, pp. 161 - 172, 2011.

[186] **R. Zahira, and A. Peer Fathima**, "A technical survey on control strategies of active filter for harmonic suppression", Procedia Engineering, Vol. 30, No. 3, pp. 686-693, 2012.

[187] **S. Janpong, K. L. Areerak and K. N. Areerak**, "A Literature Survey of Neural Network Applications for Shunt Active Power Filters", World Academy of Science, Engineering and Technology, Vol. 5, No. 3, pp. 273 - 279, 2011.

[188] **Sahu, Laxmi Devi and Satya Prakash Dubey,** "ANN based Hybrid Active Power Filter for Harmonics Elimination with Distorted Mains", International Journal of Power Electronics and Drive Systems, Vol. 2, No. 3, pp. 241 - 248, 2012.

[189] **Zeng, Lingquan and Xin Li**, "Research on harmonic suppression in power system based on improved adaptive filter", Energy Procedia, Vol. 16, No. 4, pp. 1479-1486, 2012.

[190] **M. V. V. Appalanaidu, B. Sankaraprasad, and Kotyada Kalyani**, "Neural network based shunt active filter for harmonic reduction: A technological review", International Journal of Engineering Research and Development, Vol. 2, No. 11, pp. 32 - 41, 2012.

[191] **Almaita and K. H. Eyad**, "Adaptive Radial Basis Function Neural Networks-Based Real Time Harmonics Estimation and PWM Control for Active Power Filters", Vol. 2, No. 11, pp. 32 - 41, 2012.

[192] **L. B. G. Campanhol**, "Neural-Networks and Synchronous Reference Frame Applied in the Harmonic Compensation with a Three-Phase Parallel Active Power Filter", International Conference on Renewable Energies and Power Quality, pp. 23 - 38, 2012.

[193] **Ponnusamy, Thirumoorthi, and Yadaiah Narri,** "Control of shunt active power filter using soft computing techniques", Journal of Vibration and Control, Vol. 20, No. 5, pp. 713 - 723, 2014

[194] **Ramchandra, N., and M. Kalyanchakravarthi,** "Neural Network Based Unified Power Quality Conditioner", International Journal of Modern Engineering Research, Vol. 2, No. 1, pp. 359 - 365, 2012.

[195] **Bhattacharya Avik, and Chandan Chakraborty,** "A shunt active power filter with enhanced performance using ANN-based predictive and adaptive controllers", IEEE Transactions on Industrial Electronics, Vol. 58, No. 2, pp. 421-428, 2011.

[196] **Nguyen, Ngac Ky**, "Harmonics Identification with Artificial Neural Networks: Application to Active Power Filtering", International Journal of Emerging Electric Power Systems, Vol. 12, No. 5, pp. 1 - 7, 2011.

[197] **Fei Juntao and Zhe Wang,** "Adaptive RBF Neural Network Control for Three-Phase Active Power Filter", International Journal of Advanced Robotic Systems, Vol. 10, No. 258, pp. 1 - 9, 2014.

[198] **Fei, Juntao, and Zhe Wang**, "Adaptive control of active power filter using RBF neural network", IEEE International Conference on Mechatronics and Automation (ICMA), pp. 123 - 128, 2014

[199] **Qasim, Mohammed, Parag Kanjiya, and Vinod Khadkikar,** "Artificial-neural-network-based phase-locking scheme for active power filters", IEEE Transactions on Industrial Electronics, Vol. 61, No. 8, pp. 3857-3866, 2015.

[200] **Geetha Mathiyalagan, Sivanandam Venkatesh, K. Ramkumar and Rengarajan Amirtharajan**, "Modelling and Simulation of Shunt Active Filter for Non Linear Load", Research Journal of Information Technology, Vol. 6, No. 3, pp. 216 - 222, 2015.

[201] **Mohammed Qasim and Vinod Khadkikar**, "Application of Artificial Neural Networks for Shunt Active Power Filter Control", IEEE Transactions On Industrial Informatics, Vol. 10, No. 3, pp. 1765 - 1774, 2016.

[202] **Mahajan Vasundhara, Pramod Agarwal, and Hari Om Gupta,** "An artificial intelligence based controller for multilevel harmonic filter", International Journal of Electrical Power & Energy Systems, Vol. 58, No. 5, pp. 170-180, 2016.

Neuro Fuzzy Controller Papers

[203] **Bayindir, K. Cagatay, M. Ugras Cuma, and Mehmet Tumay,** "Hierarchical neuro-fuzzy current control for a shunt active power filter", Neural Computing & Applications Vol. 15, No. 3, pp. 223 - 238, 2006.

[204] **Husev Oleksandr, Sergey Ivanets and Dmitri Vinnikov,** "Neuro-fuzzy control system for active filter with load adaptation", IEEE International Conference on Compatibility and Power electronics, pp. 145 - 152, 2011.

[205] **Jha Mridul, and S. P. Dubey,** "Neuro-Fuzzy based Controller for a Three-Phase Four-Wire Shunt Active Power Filter", International Journal of Power Electronics and Drive Systems, Vol. 1, No. 2, pp. 148 - 155, 2011.

[206] **G. Nageswara Rao, K. Chandra Sekhar, and P. Sangameswara Raju,** "Neuro-Fuzzy Five-level Cascaded Multilevel Inverter for Active Power Filter", International Journal on Electrical & Power Engineering, Vol. 3, No. 1, pp. 12 - 19, 2012.

[207] **N. K. Bett, J. N. Nderu, and P. K. Hinga,** "Adaptive Neuro-fuzzy Inference system based control of three-phase hybrid power filter for harmonic mitigation", International Journal of Emerging Technology and Advanced Engineering, Vol. 2, No. 8, pp. 34 -39, 2012.

[208] **R. Zahira and A. Peer Fathima,** "A technical survey on control strategies of active filter for harmonic suppression", Procedia Engineering, Vol. 30, No. 3, pp. 686 - 693, 2012.

[209] **M. Vishnuvardhan, , and P. Sangameswararaju,** "Neuro-Fuzzy Controller and Bias Voltage Generator Aided UPQC for Power Quality Maintenance", International Journal of Computer Theory and Engineering, Vol. 4, No. 1, pp. 59 - 66, 2012.

[210] **Rao, G. Nageswara, K. Chandra Sekhar, and P. Sangameswara Raju,** "Multilevel inverter for power quality improvement using intelligent systems", IEEE International Conference on Advances in Engineering, Science and Management, pp. 41 - 48, 2012.

[211] **C. B. Jayakumar, K. S. Venkatramanan,** "Comparison of PI Fuzzy and Neuro fuzzy Controller for Shunt Active Power Filter for Enhancement of Power Quality", International Journal of Electrical Engineering, Vol. 5, No. 4, pp. 367 - 382, 2012.

[212] **B. Rajani and P. Sangameswara Raju,** "Neuro-Fuzzy Controller Based Multi Converter Unified Power Quality Conditioner with PQ Theory", International Electrical Engineering Journal, Vol. 4, No. 4, pp. 926 - 938, 2013.

[213] **N. Karthik, , M. Surya Kalavathi, and Shaik Abdul Gafoor,** "Shunt active power filter based on cascaded multilevel converters using ANFIS", International Conference on Computational Intelligence and Information Technology, pp. 551 - 559, 2013.

[214] **Thulasiraman, Sundar Rajan Giri, and Christober Asir Rajan**, "Fuzzy Inference System Based Power Factor Correction Of Three Phase Diode Rectifier Using Field Programable Gate Array", American Journal of Applied Sciences, Vol. 10, No. 9, pp. 986 - 995, 2014.

[215] **Weike, Yuan, Liu Bin, and Xue Yong,** "Fuzzy Neural Networks and GA Based Predictive Control for Active Power Filter", IEEE International Conference on Measuring Technology and Mechatronics Automation, pp. 598 - 605, 2015.

[216] **M. N. Dharmik, and N. N. Kasat**, "Neuro-Fuzzy based Inverter Implement with FPGA", International Journal of Advanced Research in Computer and Communication Engineering, Vol. 3, No. 1, pp. 56 - 66, 2016.

[217] **Rajan, G. T. Sundar,** "Power Factor Correction of Three Phase Diode Rectifier at Input Stage using Artificial Intelligent Techniques for DC Drive Applications", International Journal of Innovative Research in Science, Engineering and Technology, Vol. 3, No. 6, pp. 458 - 466, 2016.

[218] **B. Venkata siva, B. Mahesh babu, L. Ravi Srinivas and S. S. Tulasiram**, "Design of Shunt Active Power Filter for Improvement of Power Quality with Artificial Intelligence Techniques", International Journal of Advanced Research in Electrical, Electronics and Instrumentation Engineering, Vol. 3, No. 8, pp. 67 - 74, 2016.

Books

[219] **S. Rajasekaran and G. A. Vijaya Lakshmi Pai,"** Neural Networks, Fuzzy Logic and Generic Algorithm, Synthesis and Applications**",** Prentice-Hall of India Private Limited, New Delhi- 110001, 2004.

[220] **S. N. Sivanandam, S. Sumathi and S. N. Deepa,"** Introduction to Fuzzy Logic using MATLAB**",** Springer, 2007.

[221] **S. N. Sivanandam, S. Sumathi and S. N. Deepa,"** Introduction to Neural Networks using MATLAB 6.0**",** Tata McGraw Hill Education Private Limited, New Delhi, 11th reprint, 2010.

[222] **J. Arrillaga, N. R. Watson,"** Power System Harmonics", 2nd ed., John Wiley & Sons Ltd., Chichester, U.K., 2003.

[223] **R. C. Dugan, M. F. McGranaghan, H. W. Beaty,"** Electric Power Systems Quality", 2nd ed., McGraw-Hill, New York, 2006

[224] **IEEE Recommended** Practices and Requirements for Harmonics Control in Electric Power Systems, IEEE Std. 519, 1992.

[225] **Ned Mohan, T. M. Undeland, W. P. Robbins**, **"**Power Electronics Converters Applications and Design", 3rd edition, John Willey & Sons,1995.

[226] **IEEE Guide** for Harmonic Control and Reactive Compensation of Static Power Converters, IEEE Standard 519, 1981.

[227] **Zoran Vukic, Ognjen Kuljaca, "Lectures on PID Controllers", April - 2002 http://www.thetoppersway.com/wp-content/uploads/2016/01/PID CONTROLLERS.pdf**

[228] **K. R. Padiyar, "**HVDC Power Transmission Systems, Technology and System Interactions", New Age International (P) Limited Publishers, 1990**.**

[229] **Narain G. Hingorani, Laszlo Gyugyi**, **"**Understanding Facts: Concepts and Technology of Flexible AC Transmission Systems", Wiley-IEEE Press, 1999.

APPENDIX – A

In this appendix, the selection of PI controller parameters (proportional and integral constants) is explained. The method used is the trial and error method. In this method, the integral constant is taken as small as possible and keeps on changing the proportional constant. After reaching the best proportional constant according to the best total harmonic distortion, the proportional constant is kept constant and then the integral constant keeps on increasing to get the best integral constant according to total harmonic distortion.

These two values are set as the proportional and integral constants for the PI controller. These two values are different for different loads. So, the artificial controller comes into picture. These two values set for PI controller in this work is for 1kVA load by taking the number of samples of proportional and integral constants as explained above and is shown in a Table below.

Table A1. Selection of the best proportional and integral constants

Changing k_p by keeping k_i constant at one			
Load	**k_p**	**k_i**	**THD**
1kVA	0.51	1	3.18
	0.52	1	3.21
	0.53	1	3.29
	0.54	1	3.11
	0.55	1	3.08
	0.56	1	**2.99**
	0.57	1	3.04
	0.58	1	3.24
	0.59	1	3.31
	0.6	1	3.35
Changing k_i by keeping k_p at adjusted value			
Load	**k_p**	**k_i**	**THD**
1kVA	0.56	2	3.45
	0.56	3	3.15
	0.56	4	3.22
	0.56	5	3.27
	0.56	6	3.19
	0.56	7	3.16
	0.56	8	3.12
	0.56	9	3.00
	0.56	**10**	**2.93**
	0.56	11	2.97
	0.56	12	3.06
	0.56	13	3.17
	0.56	14	3.22
	0.56	15	3.34

Hence, proportional constant and integral constant are selected as 0.56 and 10 respectively

In this appendix-B, the MATLAB simulink program used in the experimentation is shown in Fig. B1. The ADC signals C5, C6 and C7 are the sensed currents of phase A, phase B and phase C respectively. The Mux ADC signals are the sensed voltages of phase A, phase B and phase C. The ADC signal C8 is the sensed voltage at DC link capacitor. The signals g1, g3 and g5 of Control Circuit block are taken from the input output channel in LED panel to generate signals to the dead bands which are discussed in chapter 6 as shown in Fig.6.6. Finally, seven inputs (ADC C5, C6, C7, C8 and Mux ADC) and three outputs g1, g2 and g3 are associated in this work.

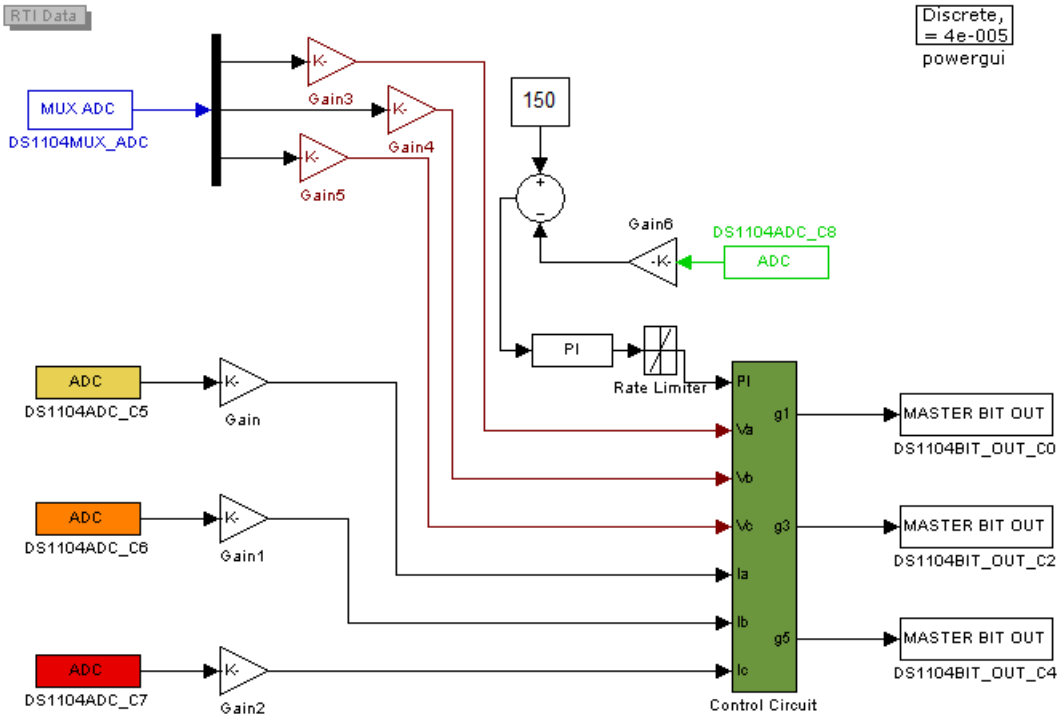

Fig. B1. MATLAB Simulink diagram for performing the experimental validation for active power filter using d'SPACE

Fig. B2 is the Control Circuit block of Fig. B1. The unit voltage template method is used in this work. The function block, Fcn, generates the maximum value of each phase and each voltage wave is divided by this maximum value to get the unit voltage template. Multiplication of this wave with output of controller gives the reference current wave form. Comparing each current with this reference current and sending this error though hysteresis controller and data type conversion provide the required signals to dead bands g1, g3 and g5.

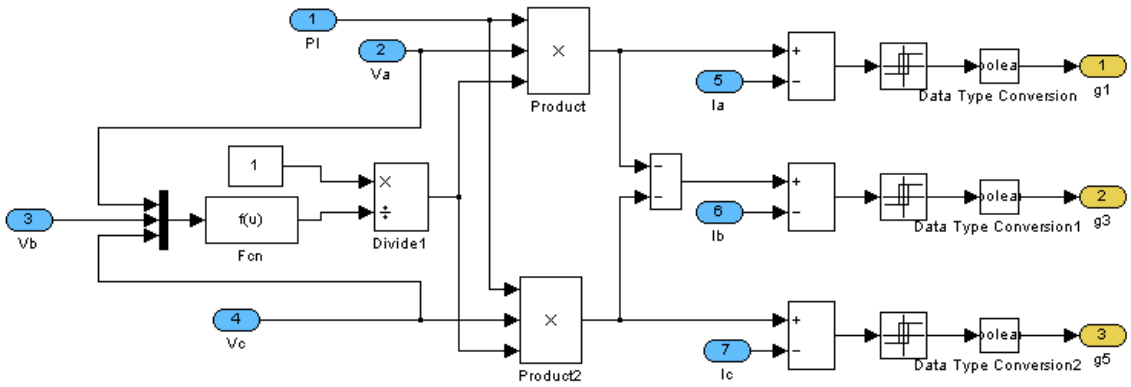

Fig. B2. Control Circuit of Fig. B1